international conference

FT 2019

conference proceedings

dr. Darko Lovrec
dr. Vito Tič

University of Maribor Press

Fluid Power 2019
Fluidna Tehnika 2019

University of Maribor

Faculty of Mechanical Engineering

International conference
Fluid Power 2019

Conference Proceedings

Editors
Darko Lovrec
Vito Tič

September 2019

University of Maribor Press

Fluid Power 2019

DARKO LOVREC & VITO TIČ

Abstract The International Fluid Power Conference is a two day event, intended for all those professionally-involved with hydraulic or pneumatic power devices and for all those, wishing to be informed about the 'state of the art', new discoveries and innovations within the field of hydraulics and pneumatics. The gathering of experts at this conference in Maribor has been a tradition since 1995, and is organised by the Faculty of Mechanical Engineering at the University of Maribor, in Slovenia. Fluid Power conferences are organised every second year and cover those principal technical events within the field of fluid power technologies in Slovenia, and throughout this region of Europe. This year's conference is taking place on the 19th and 20th September in Maribor.

Keywords: • fluid power technology • components and systems • control systems • fluids • maintenance and condition monitoring •

CORRESPONDENCE ADDRESS: Darko Lovrec, University of Maribor, Faculty of Mechanical Engineering, Maribor, Slovenia, e-mail: darko.lovrec@um.si. Vito Tič, University of Maribor, Faculty of Mechanical Engineering, Maribor, Slovenia, e-mail: vito.tic@um.si.

University of Maribor Press

Table of Contents

University of Maribor Press

Plenary speak

Fluid Power Innovations – On track for Future Challenges

OLIVIER REINERTZ & KATHARINA SCHMITZ

Abstract Without additional measures, the growing population, limited resources and rising pollution of our planet would lead to significant reductions of living standard in future. Therefore, in the field of drive technology, product development of the next decades needs to focus on sustainability, clean energy and mobility, connectivity, and health – the global future challenges. Nowadays, fluid power is a leading drive technology. Nevertheless, to assure and widen its market share, the branch needs to contribute to the aforementioned efforts. The paper focuses on future fields of applications, their specific requirements and actual weaknesses of fluid power. Furthermore, selected attempts to cope with these actual technical issues from academia and industry are discussed. The paper concludes with opportunities for future technical developments by known concepts and missing technologies to solve our future challenges, which may lead to unique selling points.

Keywords: • future challenges • sustainability • clean energy • connectivity • health •

CORRESPONDENCE ADDRESS: Olivier Reinertz, RWTH Aachen University, Institute for Fluid Power Drives and Systems (ifas), Aachen, Germany, e-mail: Olivier.Reinertz@ifas.rwth-aachen.de. Katharina Schmitz, RWTH Aachen University, Institute for Fluid Power Drives and Systems (ifas), Aachen, Germany, e-mail: Katharina.Schmitz@ifas.rwth-aachen.de.

1   Introduction

At present, the world faces different challenges resulting from increasing world population and the ambition of rising living standards. According to the UN World Population Prospects 2019, the world population is growing since decades and, despite the declining curse, it will continue to grow in future. This will lead to a total population of approx. 9.7 billion people in 2050, a growth of two billion in the next three decades. Two thirds of this strong growth are not due to high fertility but result from current age structures, a high share of young people in some developing countries, and growing life expectancies. Thus, it will occur even if childbearing in high-fertility countries today were to fall immediately to around two births per woman over a lifetime. Therefore, a fast reduction in population growth rate is not expected. Moreover, the global share of population aged 65 years or older will increase from today's nine to sixteen percent in 2050 [1].

Meanwhile, the per capita energy consumption continuously increases since begin of the 20th century. Despite a forced usage of renewable energy, a limitation of global warming below 2 °C seems to be illusory, as it would require 50% of the used energy being supplied by regenerative sources in one decade. Despite this, usage of different sources of renewable energy must be forced to the highest extend, as it is the long-term solution for covering the rising energy demand without nuclear power taking the limited resources of carbon-based technologies into account [2].

Therefore, measures to cope with a fast growing and ageing population, the linked climate changes due to carbon dioxide emissions, and limitations in resources as well as for reducing pollution of the environment are required. Thereof, in the field of drive technology, four global future challenges arise: sustainability, clean energy and mobility, connectivity, and health.

Nowadays, fluid power is one of the world's leading drive technologies. To assure and widen its market share, the branch needs to contribute to the aforementioned efforts. The following sections focus on the future challenges and a selection of resulting future fields of applications as well as actual weaknesses and mitigation strategies of fluid power to point out opportunities for future technical developments, which may lead to unique selling points.

2 How Fluid Power Copes with its Future Challenges

2.1 Sustainability

Limited resources and the environmental impact resulting from production, operation and decommissioning at the end of lifetime or unexpected failures during operation of all kinds of technical goods and machines will force product developers to rethink technology decisions and design rules.

Diverse strategies for optimizing sustainability exist. Nevertheless, due to the high-power density of fluid power, efficiency is the most significant parameter in sustainability assessments [3].

2.1.1 Energy Efficiency

On a system level, avoiding throttling losses and/or using hydraulic units in their optimal operational range by changing system architectures and control schemes is in focus. Commercial examples of such optimizations are the increased use of pump-controlled presses and compact actuators, avoiding throttling losses of control valves. The elevated efficiency leads to reduced cooling power demands enabling additional benefits in efficiency and convective cooling of selected electro-hydraulic systems [4], [5]. The following figure 1 gives an exemplary overview on achievable energy savings and reductions in oil volume.
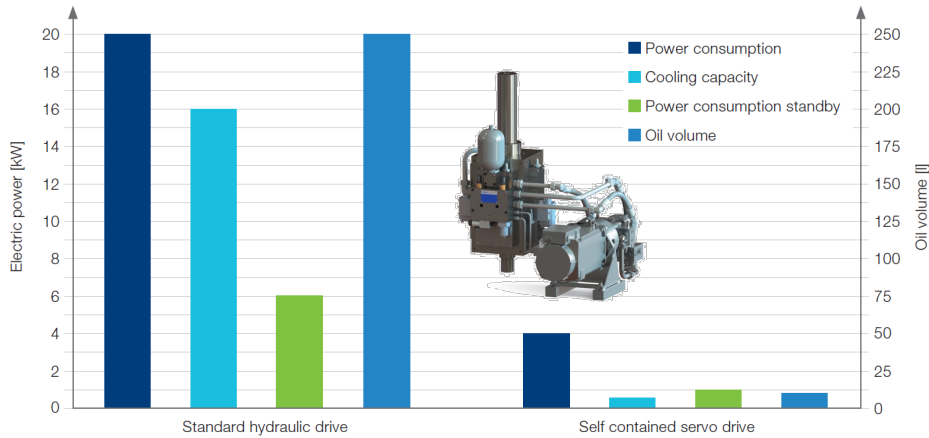
Figure 1: Comparison of standard hydraulics and compact drive.
Source: [4]

Despite these examples of existing industrial solutions, there is still need for improvements. Especially in the field of the used pumps, their ability for high rotational speeds enabling more compact designs and resource effective electric drives as well as their performance at low speed and high pressure possess significant optimization potential.

In contrast to the results in figure 1, the highest efficiency is not necessarily achieved by pump-controlled systems. Especially in mobile machinery, the internal combustion machine drives all installed pumps at its speed. The usage of variable displacement pumps is possible, but churning losses of the required number of continuously rotating machines limit the overall efficiency. Economical aspects emphasize that especially for complex machines with a high number of drives, as, e.g., wheel excavators, the number of positive displacement machines needs to be reduced by valve logics to a realistic number.

Another example for the attempt to commercialise a revolutionary efficient hydraulic system is based on the STEAM system developed at ifas of RWTH Aachen University [6]. The system uses three quasi-constant pressure levels to supply the actuators of an excavator Figure 2.
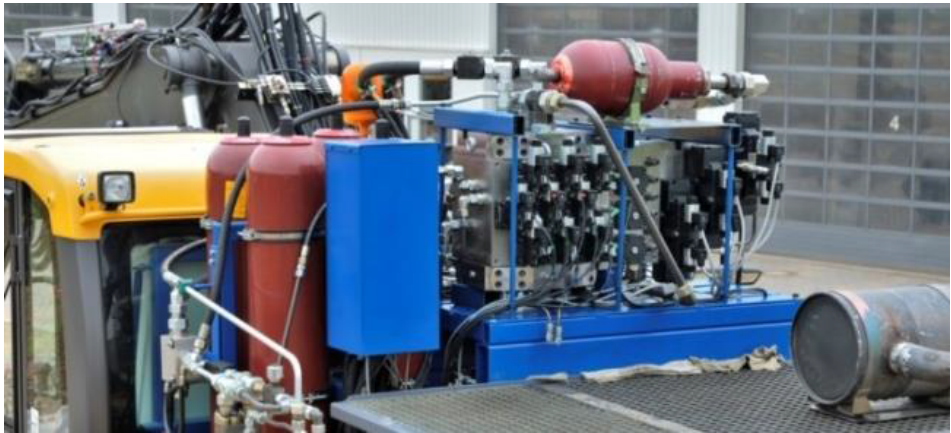
Figure 2: STEAM system prototype installed on top of the test excavator.
Source: [6]

Connecting pressure accumulators to the pressure rails enables hybridization and thus recuperation. A prototype realisation saved up to 30 % of primary energy during typical operation cycles. At first, unavailability of the required components for an industrial implementation hindered a transfer of the technology into the market. Recently, Bosch Rexroth announced the development of a novel valve system for mobile applications being able to implement key aspects of this STEAM architecture [7]. This will enable a promising way for system optimization of mobile machines in near future.

Efficiency optimizations of components aim for higher peak efficiencies of pumps and motors and reduced avoidable flow losses in lines and ducts to expand their optimal operational range.

A recent development in the field of pump and motor technology are the AX series of company Bucher bringing the floating cup principle for the first time on the market. Due to its 24 pistons, pulsation and noise are very low, while the unit withstands operation at lowest speeds and high pressures due to a higher amount of hydrostatic balancing compared to state of the art axial piston machines. Moreover, according to first announcements, the novel unit achieves higher total efficiencies compared to state of the art devices [8]. Furthermore, in 2018 the Danish company Danfoss, which acquired Artemis Intelligent Power, a Scottish pioneer in digital displacement pump technology, announced the construction and build-up of a digital displacement pump manufacturing for mobile machinery [9].

Besides Pump optimization, flow loss reduction can also contribute to significant energy savings. In many applications, building space and economic constraints are hindering the implementation of bigger sized components. One possible solution was presented by Parker Hannifin on this year's Hannover trade fair by means of a flow optimized cartridge of a 2/2-way FTP servo-proportional valve [10]. In addition, flow optimization of fittings and hoses gets into focus of industrial research. Moreover, different suppliers and research institutes have presented the use of additional manufacturing for flow optimization of housings and manifolds. Unfortunately, economically viable products are not achieved without generating additional benefits by function integration or by weight reduction in mass-sensitive applications. This is enforced by the rough surface structure of additively manufactured metal parts reducing the effect of flow optimization by additional losses.

2.1.2   Component Lifetime

Another measure for sustainability improvement is an increased lifetime of systems and their components to reduce the impact of production and decommissioning on the total balance. In this field lies an essential system immanent strength of correctly designed fluid power components and systems, which are well known for their robustness and long service life. These benefits in comparison to other drive technologies as, e.g., mechanical drives, result from energy conversion by means of well lubricating fluids, simple overload protections by means of pressure relief valves and the use of compensated tribological contacts lowering wear intensive solid friction. Moreover, an increase in use-time can be achieved by means of predictive maintenance leading to a condition-based replacement of components instead of a time or cycle based approach. This aspect will be further discussed in the connectivity section.

2.1.3   Fluids and Materials

As mineral oil-based fluids have huge potential to pollute landscape careful decommissioning is required and a risk for contamination exists. Required resources and the risk for contamination of the environment can be reduced by using smaller reservoir sizes. This requires reservoir and filter architecture optimization and fluids withstanding the higher loads due to shorter cycle times. Sophisticated pressure media can improve fluid and component lifetime and system efficiency in parallel, e.g. by lowering friction and optimizing machine behaviour over the operational temperature

span by increasing the viscosity index [11]. Herein, a trend towards ash- and zinc-free cleaner mineral oil based fluids is observed.

An additional solution is the usage of biodegradable fluids, which can possess advantageous tribological properties and lifetimes. Biologically based biodegradable fluids further improve sustainability, as long as the biological feed stock is sustainably produced and not in direct concurrence to food production. A national study on the usage of renewable resources in Germany came to the result, that in 2011, 55 % of all biological lubricants with more than 50 % renewable sources went into hydraulic applications, while only 13 % of the lubricant market consisted of hydraulic fluids. Hence, the market share of biological fluids in hydraulics was significantly higher than in all other fields. The study further forecasts slightly increased use of biological fluids [12]. Nevertheless, the general market share of biological fluids remains rather small.

Furthermore, first attempts for sustainable fluids in form of water-based dispersions with biologically based and degradable thickeners and additives arise. These were initially developed for cooling and lubrication in machine tools and are actually tested for hydraulic applications [13].

Fluid additives and special bronze of hydrostatic units containing heavy metals improve sustainability of the components by enhancing their lifetime and efficiency while leading to additional environmental impacts during recycling and uncontrolled leakages. It is evident, that also biologically degradable pressure fluid formulations absorb heavy metals from the bronze during operation reducing biologic degradability. This effect even amplifies in case water enters the system and hydrolysis occurs [14].

Therefore, an additional field of research for improving sustainability in fluid power is special bronze substitution in hydrostatic units by using surface coatings and optimized contact geometries. Figure 2 shows some exemplary results of studies at ifas.
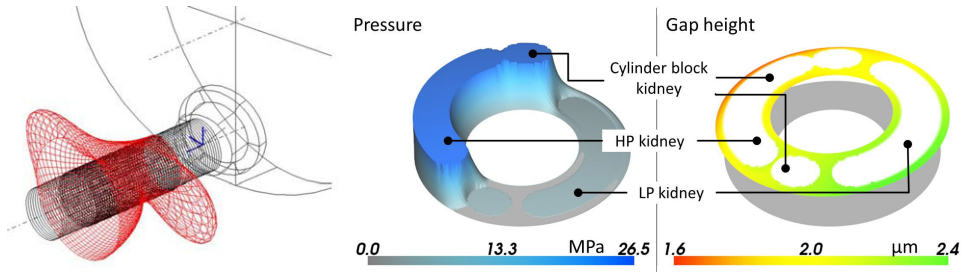
Figure 3: Exemplary results of tribological optimization tools at ifas.
Sources: [14], [15]

The left part depicts the gap height in the piston bushing contact [15]. The tool enables optimization of micro-contoured pistons to withstand the loads without necessity for wear during running in procedure. Therefore, coated hard/hard pairings become realizable and bronze can be substituted. The second picture shows an exemplary simulation result for the even more challenging interface between valve plate and cylinder block [16]. The tool is still under development and solutions for a bronze free contact are not available to date.

2.2   Clean Energy and Mobility

Clean Energy and Mobility play the outstanding role in carbon dioxide mitigation and global warming reduction. In long term, battery and fuel cell powered electrical drives or e-fuel based combustion engines will power individual mobility. Thus, the electric energy sector delivers the power not only for industrial and private use but also for the whole mobility sector. In the following, selected promising renewable energy sources with hydraulic innovation potentials are analysed.

2.2.1   Wind Energy

In the scope of the last decades, wind industry developed very fast by means of public funding initiatives enabling now one of the cheapest forms of electricity in many markets [17]. Herein, the actual role of fluid power is limited on pitch adjustment, hydraulic actuated brakes and comparable partly safety related auxiliary functions. Moreover, lubrication systems of the mechanical gearboxes use hydraulic pumps and filters. The technical feasibility and the systematic advantages of the lower stiffness and enhanced damping of a hydrostatic drivetrain for wind turbines of several megawatts

was already proven by simulation and measurement [18]. Two prototypes aiming for realisation of a digital hydraulic drivetrain of a 7 MW wind turbine have been build up and tested in laboratory and field testing by Mitsubishi using the Artemis Digital Displacement Technology [19]. Despite these prototypes and results, a commercial product of such a wind turbine with variable hydrostatic transmission still waits to come on the market. Actually, a consortium named Hydrautrans develops a novel hydrostatic transmission for wind turbines based on the floating cup principle aiming at reducing the energy costs by 0.6 ct/kWh compared to actual systems [19].

The introduction of wind power plants with continuously variable transmissions and constant speed synchronous generators would give a boost to the fluid power branch, as a high number of big-sized components would be required. Unfortunately, despite the proven technical feasibility, installation costs and durability concerns are still hindering this revolutionary concept from being commercially used.

2.2.2   Wave Energy

The enormous peak power of high waves challenges mechanical structures and drivetrains of wave energy converters. Additionally, the input power is strongly oscillating requiring rectification and smoothing. The majority of concepts takes off the power from linear movements (buoy converters, e.g., Carnegie CETO, AWS Waveswing, etc.) or swivelling movements with limited angular strokes (Pelamis, Oyster, Mocean Energy, etc.). Due to the robustness and high-power density of hydraulic cylinders and accumulators compared to electrical direct drives and capacitors, especially for large-scale devices hydraulic power take offs (PTO) are widely used.

The activities in the field of wave energy converters with hydraulic PTO strongly decreased with the liquidation of the two Scottish companies Pelamis Wave Power and Aquamarine Power. Actually, the most successful large-scale wave energy converter with hydrostatic PTO is the CETO design from Carnegie Clean Energy. Unfortunately, also this company is actually under restructuring and recapitalisation [21].

Some of the typical limiting factors of hydraulic PTOs are hard deposits on submerged cylinder rods forming subsea and destroying the rod sealings, wear of the cylinder sealings due to long distances of cyclic movement, required measures against entrained water and costs of the PTO. In general, the resulting energy costs of WECs are still far

too high for commercialisation and funding programs as used for wind energy are missing.

2.3   Connectivity

In future, modularisation, digitalisation and connectivity of components towards cyber physical systems are going to enable seamless communication between human, different devices and cloud services for, e.g., authentication, optimization of the commissioning and production processes, increasing lifetime and predictive maintenance. The concept of the Industrial Internet of Thinks (IIoT) focuses four different aspects shown in figure 4:

- Vertical integration: Continuous communication across the entire Automation Pyramid from the Device and Sensor Level to realize production tasks in a machine, up to the ERP-systems for managing the entire company processes.
- Horizontal Integration: Integrated communication between different manufacturing instances, e.g., different machines, client and different suppliers, Logistics, Cloud etc.
- Digital product lifecycle: enabling, e.g., integrated engineering by using data from the whole life cycle.
- Flexible integration of the human into the relevant processes. Support by means of intelligent tools supplying all relevant data and toolchains for the task.

Thus, intelligent features, as, e.g., lifetime estimation of a CPS, can be encapsulated directly in a component or calculated in the cloud and deliver data for, e.g., supply chain management. During the digital product lifecycle, data of the CPS is collected and can be used, e.g., by machine learning to optimize the product and its lifetime calculation. In case of required maintenance work, the system instructs the worker.

Actually, a definition of the realisation of the IIoT is still unclear. Due to the complex nature and many uncertainties concerning realisation and benefits, expensive implementation strategies are not followed by all small and medium enterprises. These will be challenged in the future by the emerging technologies leading to new requirements on their components and customer models.
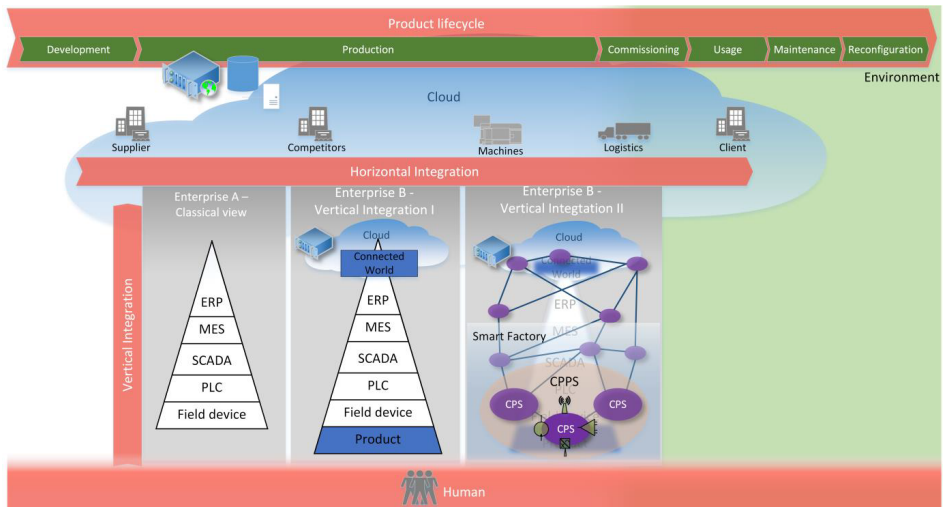
Figure 4: Four dimensions of IoT in the industrial environment.
Source: [22]

To make this disruptive technology accessible to small and medium enterprises, first demonstration projects are ongoing at ifas, showing the automated commissioning of hydraulic and pneumatic drives based on the development of fluid power cyber physical systems. This includes the interoperability of different drive technologies due to the encapsulated technology specific functions and the availability of standardised procedures. The project focus lies on the build-up of demonstration platforms, generic examples for implementation and the definition of requirements for such systems [22].

Additionally, an increased use of autonomous self-organizing construction machines results from an integrated design and construction process for buildings making the required information accessible. Actual driver oriented machine concepts will therefore be adopted to the needs and possibilities of autonomous machines. This comes along with new requirements on and opportunities for the branch. Actually, this new concepts are still to be developed. The Center for Mobile Machinery (CMM) at RWTH Aachen focuses amongst others this field of research [23].

Furthermore, connectivity of fluid power systems and components includes the hydraulic and mechanical interfaces as well. A trend towards modularised systems as, e.g., compact drives, can be observed. This enables compact systems without failure prone connections, building space reductions and the outsourcing of all hydraulic

control and design work to the drive supplier. The drive's controller encapsulates all functions and, from a command side, the drive behaves comparable to, e.g., an electromechanical drive. Therefore, this compact drives can be implemented without a deeper understanding of fluid power.

Individualisation is another key aspect of IIoT solutions. Due to the integrated design process, exact specifications for components are accessible from the system model while methods to customize a product to these specific demands emerge from its own design process. This allows automated customization of products challenging actual production processes. One possible solution is the production by additive manufacturing. First demonstrators for such hydraulic components are available and the first additively manufactured component for aerospace applications is just going into production [24]. Nowadays, additively manufactured hydraulic components are only economically viable when additional requirements, as, e.g., weight reduction, are important aspects.

2.4   Health

The last of our four categories is widespread. On the one hand side, there is healthy and sustainable food production for the rising population, where hydraulic machines play an important role. Actual challenges lie in the field of precision farming, optimizing sustainability by reducing the required amount of seeds, pesticides and fertilizers. Disruptive concepts, as, e.g., farming in glasshouses under controlled conditions, will gain in importance due to the climate change and limited ground capacities and require new machine concepts for automation.

Focusing new machine concepts with quiet electric motors, noise emissions of hydraulics are getting into focus. Especially the pump noise and high frequent emissions of turbulent flows passing resistances put hydraulics in a negative light. Available measures to reduce noise emissions are the reduction of the pressure losses on resistances and the implementation of pumps with optimized commutation and reduced outflow oscillations by means of, e.g., customized gear geometries [25] or a high number of pistons [8].

The forecasted ageing of the population will lead to a need for higher degree of automation and assisting devices in health and geriatric care. This field could be an interesting application of pneumatic soft robotics, especially in exoskeletons, when a portable and lightweight solution for pneumatic power supply would be available. Several studies on unconventional pneumatic power sources exist, but a viable solution still needs to be found [26]. Also for micro-hydraulics interesting applications in the field of mobile robotics, e.g., for rescue operations, arise. Unfortunately, only few sufficiently miniaturised hydraulic components are available, hindering the further development of such devices [27].

Finally, to achieve the forecasted grows in life expectancy and decrease in child and maternal mortality, further improvements of medical devices are required. While the field of medical devices using fluid power components for gas and fluid control is already well established, it is emphasized, that a new interesting field of such fluid power driven devices could result from attempts to realise real-time imaging by means of MRI devices during a medical intervention by means of an MRI compatible robot. As in the environment of an MRI usage of ferromagnetic materials is hazardous, fluid power systems from plastic materials can be a promising solution. Examples of hydraulic and pneumatic prototype realisations can be found in [28] and [29].

3 Conclusion

From an actual perspective, the major future challenges of fluid power lie in the fields of sustainability, clean energy and mobility, connectivity and health. In the scope of this paper, the status quo, actual issues and arising opportunities in these fields have been analysed.

Efficiency is the dominant sustainability parameter of hydraulic systems and in focus of component manufacturers, systems designers and clients. Many solutions to enhance efficiency are on the market, but overall efficiency of machines still bears strong potential for optimization. Especially in the field of mobile machinery, the low efficiency of internal combustion engines strongly affects the energy requirements of today's systems despite hydraulic improvements. Moreover, heavy metal containing bronze and selected fluids affect sustainability. Unfortunately, a commercially viable solution for bronze substitution is still to be developed and stays a critical point for staying on track. Furthermore, biologically based and/or high-performance fluids improving efficiency and lifetime are available and can optimize sustainability of

selected existing systems without additional changes. A future wider usage of such fluids is expected.

The field of clean energy is the enabler for all technical developments in future. Wind energy will play a continuously important role in the energy market and the fluid power branch has an interest in being involved in the development at the highest possible extend. Unfortunately, hydraulic drivetrains for wind turbines have not found the way to market today. In the field of wave energy, many hydraulic solutions have been tested, but the expected energy costs are still too expensive. In addition, there are unsolved technical issues of the devices and drive trains. Both fields would extremely profit from big-sized hydraulic components being produced in higher numbers and thus economically more attractive. But it's a chicken-and-egg question.

In the field of connectivity, some bigger companies and research institutes are on a good way to demonstrate their vision and abilities in the field. Unfortunately, this is not the case for all small and medium enterprises. It is evident that shaping the understanding and definitions of IIoT during development to the needs of fluid power is much easier than adopting the products later onto a system, which is primarily developed by a concurring drive technology. Therefore, a deeper debate of IIoT and a common understanding of its possibilities and opportunities in the branch is necessary.

Finally, the limited potential for food production will force efficiency increases in farming leading to novel approaches and unpredictable requirements on machines and fluid power components. Service robotics and human assist devices will gain in importance and bear portfolio diversification potentials for component manufacturers, as the components need to be customized to the miniaturised systems. The same applies for customized components for MRI compatible robotics.

In conclusion, the arising challenges with their specific demands on drive technology bear big potentials for the fluid power branch. These encourage not only the further optimization of the existing technology, but also the emergence and commercialisation of revolutionary approaches and fields of applications, which give us the chance to further develop our markets.

References

[1]   United Nations (2019). World Population Prospects 2019: Highlights. Department of Economic and Social Affairs, Population Division, New York, ISBN: 978-92-1-148316-1

[2]   Jones, G. A., Warner, K. J. (2016). The 21st century population-energy-climate nexus. *Energy Policy, 93*, 206-212. doi: 10.1016/j.enpol.2016.02.044

[3]   Waerder, M., Merkelbach, S., Schmitz, K. (2019). Carbon Footprint Determination of an electro-hydraulic compact axle (EHA) based on DIN EN ISO 14067. *Proceedings of the 16th Scandinavian International Conference on Fluid Power*, 22. – 24. May 2019, Tampere, Finnland

[4]   Voith Turbo H + L Hydraulic (2019). Self contained press drive PDSC. Technical data sheet

[5]   Moog Inc. (2017). Electrohydrostatic Actuation System (EAS). Case Study

[6]   Vukovic, M. (2017). Hydraulic Hybrid Systems for Excavators. Dissertation, RWTH Aachen University, Shaker edition, Aachen, ISBN: 978-3-8440-5312-8

[7]   Heemskerk, E., Burgis, S., Hörner, F. (2019). A Multi Pressure Network System for Mobile Applications. *Proceedings of the 16th Scandinavian International Conference on Fluid Power*, 22. – 24. May 2019, Tampere, Finnland

[8]   Bucher Hydraulics (2019). AX Series Piston Pumps and Motors - Fixed Displacement from 18 to 76 cc/rev. Technical data sheet

[9]   Artemis Intellgent Power Ltd. (2018). Danfoss to build low-carbon global manufacturing facility for Artemis technology. Press Release, 9th November 2018

[10]   Parker Hannifin Corp. (2019). Hannover 2019: Partnering with Customers to Increase Productivity and Profitability through Engineering Innovation, Press Release, 16th May 2019

[11]   Bock, W., Dornacher, G., Schürmann, T. (2018). Hydraulic Fluids – Solutions of Complex Requirements, *Proceedings of the 11th International Fluid Power Conference (11. IFK), Vol 3,* pp. 404-410, Aachen, 19th – 21st March 2018

[12]   N.N. (2014). Marktanalyse Nachwachsende Rohstoffe. *Schriftenreihe Nachwachsende Rohstoffe,* Fachagentur Nachwachsende Rohstoffe e. V. (FNR), Vol. 34. ISBN 978-3-942147-18-7 (in German)

[13]   Otto, N. (2019). Experimentelle Untersuchung nachhaltiger Hydraulikfluide auf Ester- und Wasserbasis, Dissertation, RWTH Aachen University, Shaker Edition, Aachen, ISBN 978-3-8440-6427-8 (in German)

[14]   Göhler, O.-C. (2007). Alterungsuntersuchungen und Methoden zur Alterungsvorhersage für umweltverträgliche Schmierstoffe in neu gestalteten Tribosystemen. Dissertation, RWTH Aachen University, Shaker Edition, Aachen, ISBN 978-3-8322-7020-9 (in German)

[15]   Gels, S., Murrenhoff, H. (2010). Simulation of the Lubricating Film between Contoured Piston and Cylinder. *International Journal of Fluid Power, 11*, No. 2, 15-24, doi:10.1080/14399776.2010.10781003

[16]   Wegner, S., Löschner, F., Gels, S., Murrenhoff, H. (2016). Validation of the physical effect implementation in a simulation model for the cylinder block/valve plate contact supported by experimental investigations. *Proceedings of the 10th International Fluid Power Conference, Vol.1*, 269-281, Dresden, 8th-10th March 2016

[17]   Global Wind Energy Council (2019). GWEC – Global Wind Report 2018. Brussels, Belgium, April 2019

[18]   Schmitz, J. (2015). Konzipierung und Vermessung hydrostatischer Windkraftgetriebe. Dissertation, RWTH Aachen University, Shaker Edition, Aachen, ISBN: 978-3-8440-3654-1 (in German)

[19]   Sasaki, M., Yuge, A., Hayashi, T., Nishino, H., Uchida, M., Noguchi, T. (2014). Large Capacity Hydrostatic Transmission with Variable Displacement. *Proceedings of the 9th International Fluid Power Conference, Vol. 2*, pp. 226-236, Aachen, 24th-26th March 2014

[20]   Hydrautrans (2019). Webpage www. hydrautrans.com, visited 19th July 2019

[21]   Carnegie Clean Energy (2019). Webpage www.carnegiece.com, visited 19th July 2019

[22]   Alt, R., Murrenhoff, H., Schmitz, K. (2018). A survey of "Industrie 4.0" in the field of Fluid Power – challenges and opportunities by the example of field device integration. *Proceedings of the 11th International Fluid Power Conference (11. IFK), Vol 2,* pp. 14-25, Aachen, 19th – 21st March 2018

[23]   CMM (2019). Webpage www.mobile-machinery.de, visited 24th July 2019

[24]   Liebherr-Aerospace & Transportation SAS (2019). Liebherr-Aerospace Starts Serial Production of 3D Printed Components. Press Release, 17th Jan 2019

[25]   Casoli, P., Vacca, A., Berta, G. L. (2008). Optimization of Relevant Design Parameters of External Gear Pumps. *Proceedings of the 7th JFPS International Symposium on Fluid Power,* 277-282, Toyama, 15th - 18th Sep. 2008, ISBN: 4-931070-07-X

[26]   Wu, H., Kitagawa, A., Tsukagoshi, H. (2005). Development of a Portable Pneumatic Power Source Using Phase Transition at the Triple Point, *Proceedings of the 6th JFPS International Symposium on Fluid Power,* 310-315, Tsukuba, 7th - 10th Nov. 2005, ISBN: 4-931070-06-X

[27]   Saunders, A. (2018). Building the World's Most Dynamic Humanoid Robot, *Plenary Lecture at the 11th International Fluid Power Conference (11. IFK),* Aachen, 19th – 21st March 2018

[28]   Gassert, R., Moser, R., Burdet, E., Bleuler, H. (2006). MRI/fMRI-Compatible Robotic System with Force Feedback for Interaction with Human Motion. *IEEE/ASME Transactions on Mechatronics, Vol. 11 (2)*, 216-224, doi:10.1109/TMECH.2006.871897

[29]   Groenhuis, V., Siepel, F. J., Veltman, J., van Zandwijk, J. K., Stramigioli, S. (2018). Stormram 4: An MR Safe Robotic System for Breast Biopsy. *Annals of Biomedical Engineering, Vol. 46 (10),* pp. 1686–1696. doi: 10.1007/s10439-018-2051-5

University of Maribor Press

Plenary speak

Programmable Mechatronic Pneumatics and Robotics with the Festo Motion Terminal

DAVID RAGER, MATTHIAS DOLL, RÜDIGER NEUMANN & ELIAS KNUBBEN

Abstract The Festo Motion Terminal is a programmable servo valve terminal con-sisting of proportional valves, integrated sensors and a processor unit for software functions. This enables pneumatics for modern flexible automa-tion as well as for new concepts like the BionicCobot – a pneumatic robot for human-robot collaboration. In both applications, the valve terminal is placed in a central control cabinet, so that tubes are required between the valve and actuator. The paper presents a compact physical tube model that is applicable for both system simulation and controller design. With the tube model and integrated sensors, external pressure and position sensors at the drive are substituted by observer-based estimations. The estimations are used for a pneumatic operation mode, where travel time, impact velocity and holding force can be controlled by software. The combination of pro-grammable valve terminal, physical modelling and advanced control is the basis for mechatronic pneumatics.

Keywords: • Festo Motion Terminal • mechatronic pneumatics • tube model • position estimation • robotics •

CORRESPONDENCE ADDRESS: David Rager, Festo AG & Co. KG, Esslingen, Germany, e-mail: david.rager@festo.com. Matthias Doll, Festo AG & Co. KG, Esslingen, Germany, e-mail: matthias.doll@festo.com. Rüdiger Neumann, Festo AG & Co. KG, Esslingen, Germany, e-mail: ruediger.neumann@festo.com. Elias Knubben, Festo AG & Co. KG, Esslingen, Germany, e-mail: elias.knubben@festo.com

1   Introduction

The Festo Motion Terminal in Figure 1 is a valve terminal with configurable proportional valves, integrated sensors, bus connection and a controller with software-based pneumatic functions [1], [2]. Each valve consists of four proportional 2/2-way main stage valves in bridge circuit. One main stage valve is pneumatically piloted by two piezo pre-stage valves. In addition to position sensors for the main stage valves, integrated pressure and temperature sensors are available for each valve port. External sensors can be integrated via the analog and digital input module.
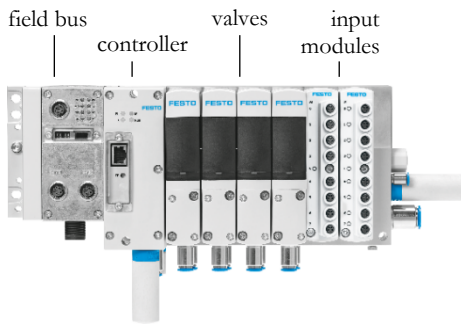
Figure 1: Festo Motion Terminal.
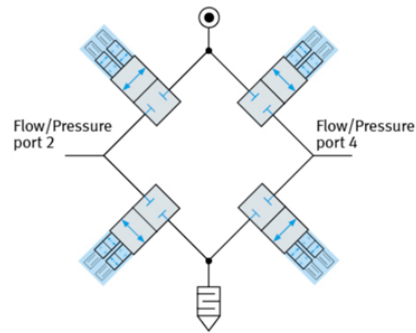
Figure 2: Valve principle.

The four main stage valves are arranged in a bridge circuit as shown in Figure 2. With this valve structure, many basic pneumatic functions can be realized without additional mechanical components. The proportional control behavior allows the mapping of specific sizes or flow rates as well as supply or exhaust air throttles for cylinder drives. This enables pneumatics for modern flexible automation as well as for new concepts like the BionicCobot.

The BionicCobot in Figure 3 is a pneumatic lightweight robot with seven degrees of freedom [3]. In its kinematics, the robot is modelled after the human arm, consisting of shoulder, upper arm, elbow, ulna and radius as well as gripping hand. Each joint is actuated by a pneumatic rotary drive with an absolute position encoder and two pressure sensors. The rotary drives operate according to the agonist antagonist principle, which allows motion dynamics and stiffness to be variably adjusted.

D. Rager, M. Doll, R. Neumann & E. Knubben:
Programmable Mechatronic Pneumatics and Robotics with the Festo Motion Terminal

19

Figure 3: BionicCobot – a pneumatic lightweight robot with human motion dynamics.

The rotary drives are controlled by the Festo Motion Terminal, that is placed separate from the arm. The tubes between the valve terminal and the drives are up to 120 cm long and run inside the arm. Due to pressure loss and air vibrations in the tube, the pressures measured at the valve differ from those at the drive. In a control loop, this can lead to unstable system behavior or low performance.

The following questions combine both the BionicCobot as well as classical automation: How to consider tubes in pneumatic control applications with valve terminal structure? Are sensors required on the actuator, if already present in the valve? How can mechanical functions in pneumatics be replaced by software? The solution proposed in this paper consists of modelling air dynamics in the tube, replacing position and pressure sensors at the cylinder by observer-based estimations with valve-integrated sensors and a new mechatronic pneumatics concept.

2 Tube Modelling

The tube is the connecting element between pneumatic components. Depending on diameter, length and wall material, the tube significantly influences a pneumatic drive. This is illustrated in Figure 4, where pressure and flow at the inlet and outlet of a tube is shown while pressurizing a constant volume. Dependent on the diameter either the pressures at inlet and outlet or the mass flows deviate from each other. This comes from the tube's flow resistance or volume respectively.

tube with 8 mm diameter   tube with 4 mm diameter
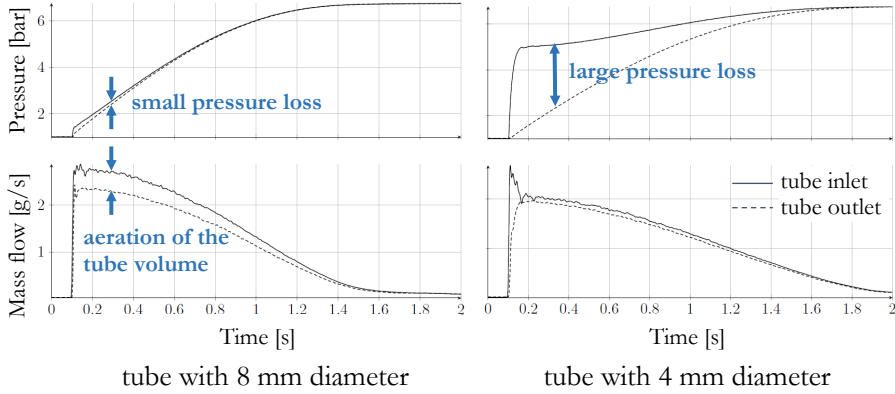
Figure 4: Influence of the tube when pressurizing a constant volume.

The pressure sensors of the Festo Motion Terminal are placed in the valve and measure the pressure at the tube inlet. Even with short tubes, the valve pressure can differ significantly from the pressure at the cylinder. This is considered in the following with a control tube model. The requirements for the control tube model are an exact reproduction of the relevant frequency range, a low model order in the state space domain, a physical structure with physical parameters and good agreement with measurements.

2.1   Dynamics

The control tube model is based on the one-dimensional linear resistance compressible model [4], in short: linear resistance model. The linear resistance model describes the behavior of air in the tube in form of the partial differential equations

$$
\begin{aligned}
\frac{\partial p(x,t)}{\partial x} &= -\frac{1}{A}\frac{\partial q(x,t)}{\partial t} - R_{\text{fric}}q(x,t), \\
\frac{\partial q(x,t)}{\partial x} &= -\frac{A}{c^2}\frac{\partial p(x,t)}{\partial t}.
\end{aligned}
\tag{1}
$$

D. Rager, M. Doll, R. Neumann & E. Knubben:
Programmable Mechatronic Pneumatics and Robotics with the Festo Motion Terminal

21

The pressure p and mass flow q depend on time t and location x in the tube. The constant parameters are the cross-sectional area A, the speed of sound c and the laminar friction coefficient R_{fric}. Due to the distributed parametric structure, the linear resistance model is not well suited for controller development and position estimation. Therefore, it is approximated in the following.

The partial differential equations are converted into ordinary differential equations by spatial discretization with the finite difference method [4], [5]. The tube length l is divided into N elements of the length $\Delta x = l/N$. Then the partial position derivatives of pressure and mass flow $\partial p/\partial x$ and $\partial q/\partial x$ are approximated at discrete grid points by finite differences.

In the simplest case the Euler method is used, and the model is approximated with only one element ($N = 1$). Two ordinary differential equations are obtained which describe pressure and mass flow at the inlet (index i) and outlet (index o) of the tube:

$$
\begin{aligned}
\frac{\mathrm{d}q_{\text{o}}}{\mathrm{d}t} &= \frac{A}{l}(p_{\text{i}} - p_{\text{o}} - R_{\text{fric}}lq_{\text{o}}), \\
\frac{\mathrm{d}p_{\text{i}}}{\mathrm{d}t} &= \frac{c^2}{Al}(q_{\text{i}} - q_{\text{o}}).
\end{aligned}
\tag{2}
$$

This second-order model is derived from Rager et al. [5] [6] and is used for pressure control in a constant volume with tube. The model quality is high for a large constant volume but decreases for small volumes significantly. Since the chamber volume of pneumatic cylinder drives can become smaller or larger than the tube volume depending on the position, the quality of this model is not sufficient.

Therefore, the linear resistance model is approximated at two discrete grid points ($N = 2$). The resulting fourth-order model:

$$\frac{\mathrm{d}q_o}{\mathrm{d}t} = \frac{2A}{l}\left(p_\mathrm{m} - p_\mathrm{o} - R_\mathrm{fric}\frac{l}{2}q_\mathrm{o}\right),$$

$$\frac{\mathrm{d}p_\mathrm{m}}{\mathrm{d}t} = \frac{2c^2}{Al}(q_\mathrm{m} - q_\mathrm{o}),$$

$$\frac{\mathrm{d}q_\mathrm{m}}{\mathrm{d}t} = \frac{2A}{l}\left(p_\mathrm{i} - p_\mathrm{m} - R_\mathrm{fric}\frac{l}{2}q_\mathrm{m}\right),$$ (3)

$$\frac{\mathrm{d}p_\mathrm{i}}{\mathrm{d}t} = \frac{2c^2}{Al}(q_\mathrm{i} - q_\mathrm{m}),$$

consists of two tube elements and additionally describes pressure and mass flow in the middle of the tube.
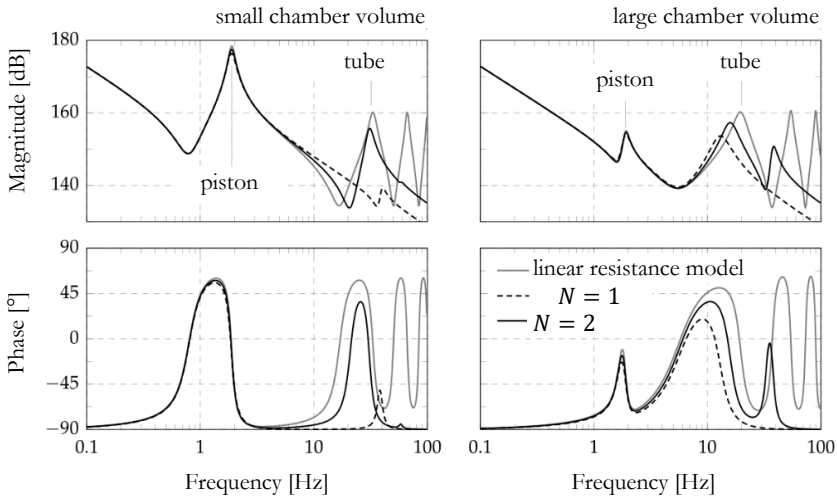
Figure 5: Frequency response from valve mass flow to valve pressure of the cylinder model with the tube model of order two and four.

Figure 5 shows the frequency response of the second- and fourth-order tube models compared to the linear resistance model on a pneumatic cylinder. On the left side the piston is retracted (small chamber volume) on the right side it is extended (large chamber volume). The first resonance corresponds to the motion dynamics of the piston. Up to about 6 Hz the frequency responses hardly differ from each other. The difference between the models is visible in the tube resonance. With small chamber volume, the tube resonance of the linear resistance model is much better reproduced by the fourth-order model. With a large chamber volume, the fourth-order model is closer to the linear resistance model, too.

D. Rager, M. Doll, R. Neumann & E. Knubben:
Programmable Mechatronic Pneumatics and Robotics with the Festo Motion Terminal

23

In Figure 6 the tube model is compared to measurements, where a constant volume is pressurized through a tube. The model's output is the pressure at the valve. The pressure oscillations at 0.6 s are well reproduced by the model. However, while the air is flowing, the vibration is too weakly damped and the pressure loss too small. This leads to a deviation of almost 2 bar between measured and simulated valve pressure. While exhausting, the pressure loss is smaller, but the behavior is basically the same.
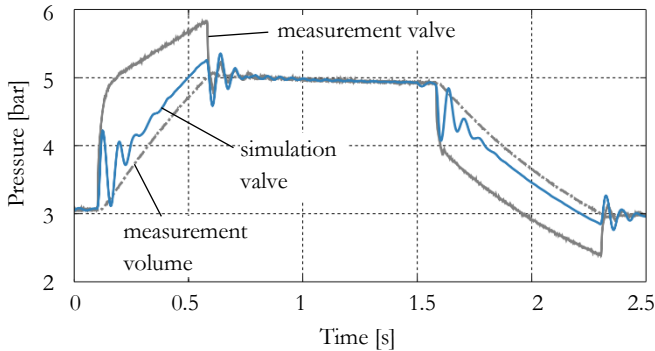
Figure 6: Validation of the linear tube model with laminar flow.

The large deviation is caused by the neglect of turbulent flow in the tube model. Since high mass flows occur mainly for short periods in pneumatic applications, this is an essential phenomenon for high model quality. In the following, the control tube model is extended by the pressure loss due to turbulent flow.

2.1   Pressure loss

The pressure loss in the tube is caused by friction between the individual air molecules respectively the air molecules and the tube wall. The friction depends on the type of flow - laminar or turbulent. Up to now, the control tube model is only valid for laminar flow. In turbulent flow, the pressure loss is significantly higher, and the oscillations more strongly damped (see Figure 6). This represents an essential phenomenon for a high model quality.

2.1.1 Cb method

In pneumatics, the tube is often simplified as concentrated pneumatic resistance and described by conductance C_t and critical pressure ration b_t (Cb value) [7], [8]. The pressure loss thus corresponds to an equivalent narrowing of the cross-section through which the flow passes. The mass flow

$$\dot{m} = C_t \rho \Psi \left(\frac{p_o}{p_i}, b_t \right) p_i \tag{4}$$

in the tube depends on the pressures p_i and p_o at the inlet and outlet of the tube and the air density ρ. Eckersten and Bala ([7], [9]) propose the empirical formulae

$$C_t = \frac{0.029 d^2}{\sqrt{l d^{-5/4} + 510}}, \qquad b_t = \frac{474 C_t}{d^2} \tag{5}$$

for the Cb values in dependence of tube length l and diameter d. To integrate the Cb method into the tube model, equation (4) must be solved for pressure and the flow function must be approximated [5]. The resulting pressure loss

$$\Delta p = \Phi(\dot{m}, p_o) \tag{6}$$

depends on mass flow and outlet pressure and substitutes the laminar pressure loss $R_{\mathrm{fric}} l q_E$ in equations (2) and (3).

2.1.2 Fanno flow

The Cb method described above models the tube as a concentrated pneumatic resistance, neglecting the effects of frictional flow and the tube's spatial expansion. Both aspects are considered in Fanno flow theory. The underlying nonlinear equations however require numerical solvers [10]. To reduce the computational effort and to illustrate the connection with existing methods, Chabane et al. [11] have converted the underlying equations into the mass flow dependent Cb values

$$C_t(\dot{m}) = \frac{A \alpha_f(\dot{m})}{\rho \sqrt{s_c(\dot{m}) R T}}, \qquad b_t(\dot{m}) = 1 - \frac{1}{s_c(\dot{m})}. \tag{7}$$

D. Rager, M. Doll, R. Neumann & E. Knubben:
Programmable Mechatronic Pneumatics and Robotics with the Festo Motion Terminal

25

The flow and compressibility coefficient a_f and s_c are calculated from tube length, diameter, pipe friction coefficient, mass flow and isentropic exponent. The variables R and T are the specific gas constant of air and the air temperature.

To illustrate the difference to the pneumatic resistance with a constant Cb value, the product $C_t \Psi$ of conductance and flow function is plotted over the pressure ratio in Figure 7. The solid line shows a simulated flow measurement made at constant primary pressure. To obtain different pressure ratios, the secondary pressure is varied (see top right). With the resulting flow conditions, the Cb values from equation (7) are almost constant and the curve closely approximates the known characteristic of the quarter ellipse. If the same flow measurement is carried out at variable primary pressure and constant secondary pressure, the curve changes significantly. The Cb values are no longer constant here. They strongly depend on the pressure ratio respectively the flow rate and thus differ from the model of the pneumatic resistance.
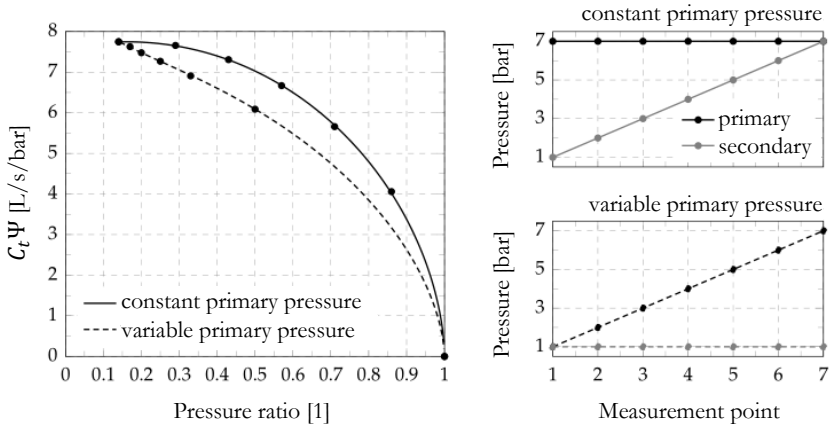
Figure 7: Flow function for constant and variable primary pressure at a tube.

Figure 8 shows the same measurement from section 2.1 now with pressure loss calculated by the Cb method and Fanno flow. While aerating, both models are very close to the measurement. Both the pressure loss and the pressure oscillation are very accurately reproduced. In the deaeration phase, a difference between the two models is visible. Here, the decreasing volume pressure is the variable primary pressure and the pressure loss is better reproduced by the more accurate Fanno flow.
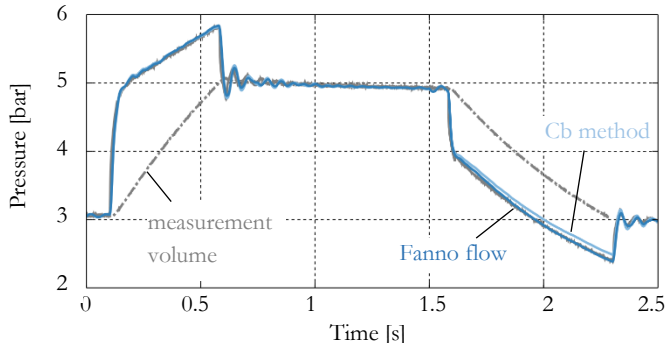
Figure 8: Validation of the tube model with turbulent flow.

3   Programmable mechatronic pneumatics

With programmable mechatronic pneumatics, a concept is presented that converts standard pneumatic drives into mechatronic pneumatic drives. The drive is to perform a point-to-point movement from one end position to the other, but motion parameters such as travel time, impact speed and holding force can be parameterized via software. This avoids mechanical throttles and pneumatic or hydraulic cushioning systems that must be adjusted mechanically.

3.1   Position estimation

For standard pneumatic drives, it is common to mount proximity switches at the cylinder. They detect when the piston arrives at the end position. This information is used for sequence programming and basic error diagnostic of the plant. For mechatronic pneumatics, continuous information about the piston's position is crucial. However, mounting position transmitters on the cylinder increases the cost, reducing the price advantage of standard pneumatic drives.

With the presented tube model, position and velocity of the drive can be reconstructed by using integrated sensors in the valve and proximity switches [10]. The complete plant model consists of the mechanic cylinder model, the pressure dynamics of both chambers, two tube models and the valve model.

D. Rager, M. Doll, R. Neumann & E. Knubben:
Programmable Mechatronic Pneumatics and Robotics with the Festo Motion Terminal

27
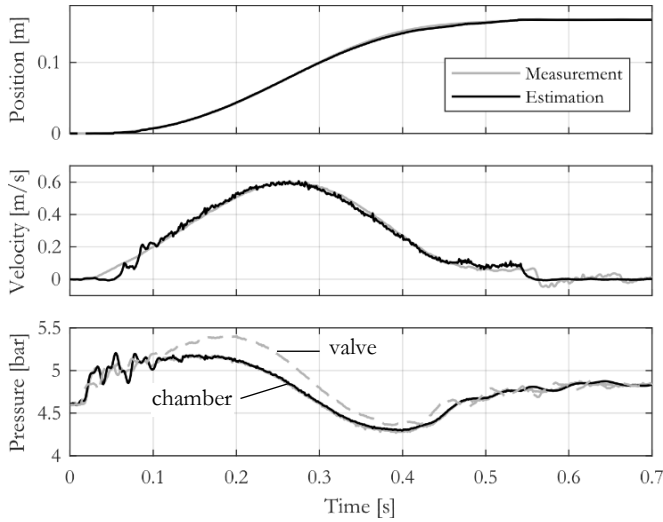
Figure 9: Position estimation for a pneumatic cylinder with 3-meter-long tubes.

The resulting twelfth-order model is highly nonlinear and unobservable at standstill. An unscented Kalman filter is used to estimate the complete system's state, e.g. position, velocity and chamber pressures. At standstill, the piston will be in the end position, where its position is detected by the proximity switches.

Figure 9 shows the position estimation for a Festo DSNU-40-160 cylinder with 3-meter-long tubes. With a maximum position error of about 3 mm, the estimation quality is very high. The velocity deviations at the beginning of the stroke come from observer convergence and model uncertainties. At stroke end, the piston position is determined by the proximity switch and fed to the observer. The small oscillations of the piston are therefore not reproduced in the estimation.

3.2 Adaptive open-loop control with active cushioning

Although the position estimation is good, its quality does not reach that of a measurement system. Therefore, the well-known servo pneumatic control algorithms based on speed and acceleration feedback cannot be applied to this problem. Instead the concept of iterative learning control is applied.

Iterative learning control is suitable for control tasks in which the same target trajectory is to be run repeatedly. The control error from the previous iteration is used in the next run to reduce the deviation from the target trajectory. Thus, the control error converges over the individual iterations towards zero. Compared to a non-learning controller, a large part of the control variable is realized by the feedforward component learned in this way and a good tracking behavior can be achieved.

The desired trajectory is derived from a time optimal control of a servo pneumatic cylinder drive [12] and extended by a constant low velocity movement near the end position. The constant low velocity at stroke end makes sure that the permissible impact velocity is not exceeded in presence of control errors. An additional parameter is the force in the end position. By adapting the force specifically to the application, air consumption can be reduced compared to standard pneumatics [13].

Figure 10 illustrates the automatic learning process realized with the position estimation. The measurement on the right is shown for reference. The first stroke is carried out with reduced velocity. From stroke to stroke, the movement becomes faster and converges after sixteen strokes to the setpoint trajectory. Throughout the whole learning process, the end velocity is not exceeded. In the case of a drop in supply pressure or an increase in friction, for example, the process adapts to the changed environmental conditions.
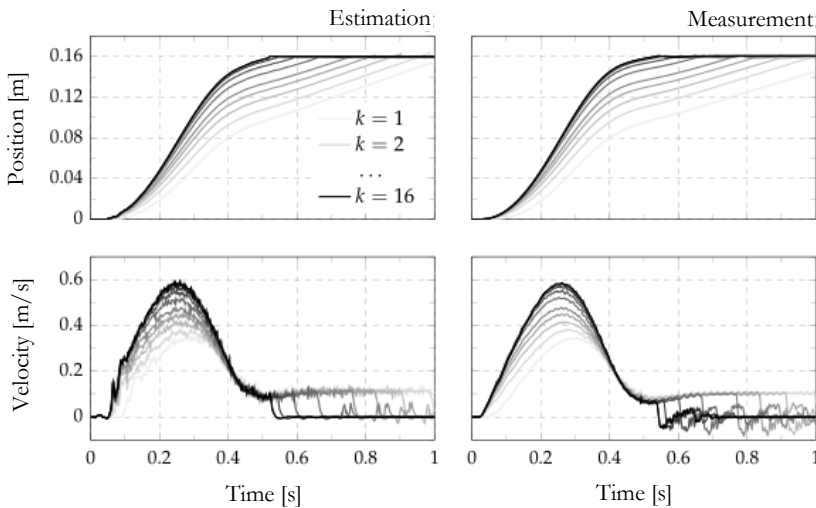
Figure 10: Learning process of the adaptive control concept.

D. Rager, M. Doll, R. Neumann & E. Knubben:
Programmable Mechatronic Pneumatics and Robotics with the Festo Motion Terminal

29

3.3 Comparison to standard pneumatics

In standard pneumatics, end position cushioning is usually achieved by mechanical cushioning systems. Festo mainly offers two systems – the adjustable cushioning PPV and the self-adjusting cushioning PPS [12]. With the PPV, the throttle must be adjusted with a screw on the actuator depending on piston speed, supply pressure and load mass. The PPS is designed for a wide range of applications. Compared to an optimally adjusted PPV, the cushioning performance is lower.
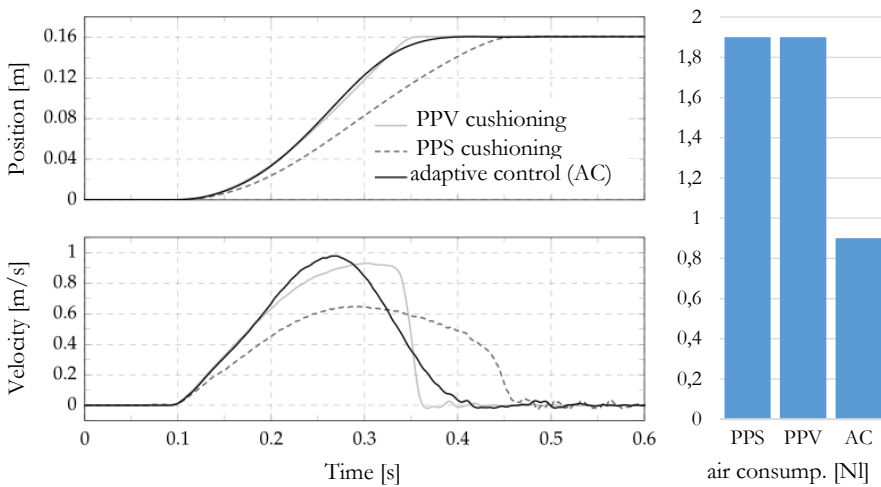
Figure 11: Comparison to standard pneumatics.

Figure 11 shows a comparison between the adaptive control and conventional pneumatics with pneumatic cushioning systems. The measurement with the conventional cushioning systems was carried out in exhaust air throttled operation. The drive is always moved at the maximum speed without exceeding the permissible impact energy or the piston oscillating back in the end position.

The shortest travel time is achieved with the PPV. It is not possible to change the speed during operation, as the screw of the cushioning throttle would have to be readjusted. The lower performance of the PPS leads to a longer travel time. However, the travel time can be changed during operation since the self-adjusting cushioning works at different speeds. The adaptive control does not depend on fixed cushioning lengths, so that in this case the deceleration phase starts from half the cylinder stroke. This makes

higher speeds possible so that the resulting travel time is only slightly lower compared to the PPV. Travel time and cushioning can be adjusted at any time by electronic interfaces.

The air consumption of the standard pneumatic operation depends solely on the cylinder and the supply pressure. The forward stroke requires 1.9 norm liters. Due to the adjusted holding force (here 50 newton) of the adaptive control, the air consumption is 0.9 norm liter.

## 4	Conclusion

In this paper, a concept for mechatronic pneumatics with the Festo Motion Terminal is presented. A compact physical tube model for controller design was derived that models air oscillation and pressure loss in a tube. With the tube model and valve-integrated sensors, position and velocity of the piston and the chamber pressures were estimated. The estimated quantities are used for an adaptive open-loop control of a pneumatic drive, based on an iterative learning control scheme. In this operating mode, travel time and impact velocity can be set by software. In comparison to standard pneumatic drives with conventional cushioning systems, the achieved travel time was shorter while no mechanical adjustments were needed. Due to the adjustable holding force it is possible to reduce the air consumption in comparison to standard pneumatics. The combination of programmable valve terminal, physical modelling and advanced control empowers pneumatics for industry 4.0 and upcoming challenges regarding climate change.

References

[1]	Rager, D., Neumann, R., Post, P., Murrenhoff, H. (2017). Pneumatische Antriebe für Industrie 4.0. *Fachtagung Mechatronik 2017*

[2]	Festo AG & Co. KG. (2017). Weltneuheit Festo Motion Terminal VTEM.

[3]	Festo AG & Co. KG. (2017). BionicCobot - Sensitive helper for human-robot collaboration

[4]	Stecki, J. S., Davis, D. C. (1986). Fluid transmission lines - distributed parameter models part 1: A review of the state of the art, *Proc. Inst. Mech. Eng., Part A: J. Power Energy*, Bd. 200, pp. 215-228

[5]	Krichel, S. V., Sawodny, O. (2011). Dynamic modeling of pneumatic transmission lines in Matlab/Simulink, *Fluid Power and Mechatronics (FPM), 2011 International Conference.*

D. Rager, M. Doll, R. Neumann & E. Knubben:
Programmable Mechatronic Pneumatics and Robotics with the Festo Motion Terminal

31

[6]   Rager, D., Neumann, R., Murrenhoff, H. (2015). Simplified Fluid Transmission Line Model for Pneumatic Control Applications, *Proceedings of the Fourteenth Scandinavian International Conference on Fluid Power, SICFP15, Tampere, Finland*

[7]   Rager, D., Neumann, R., Murrenhoff, H. (2016), Remote Pressure Control - Considering Pneumatic Tubes in Controller Design, *10th International Fluid Power Conference (10. IFK).*

[8]   Eckersten, J. (1977). Vereinfachte Strömungsberechnung für pneumatische Elemente," Atlas Copco Deutschland GmbH, pp. 62-65

[9]   ISO6358-1. (2013). Pneumatic fluid power - Determination of flow-rate characteristics of components using compressible fluids - Part 1: General rules and test methods for steady-state flow, Geneva

[10]   Bala, H. P. (1985). Durchflussmessungen und strömungstechnische Kenngrößen, *O+P Ölhydraulik und Pneumatik*, Bd. 29, pp. 541-544

[11]   Rager, D., Doll, M., Neumann, R., Berner, H. (2018). New programmable valve terminal enables flexible and energy-efficient pneumatics for Industry 4.0, *11th International Fluid Power Conference (11. IFK)*

[12]   Hildebrandt, A. (2009). Regelung und Auslegung servopneumatischer Aktuatorsysteme, Shaker

[13]   Doll, M. (2015). Optimierungsbasierte Strategien zur Steigerung der Energieeffizienz pneumatischer Antriebe.

[14]   Festo AG & Co. KG. (2013). Mehr Produktivität durch optimal gedämpfte Pneumatikzylinder

[15]   Oertel, H. jr., Böhle, M., (2006). Dohrmann, Strömungsmechanik, 4 Hrsg., Vieweg-Verlag

[16]   White, F. M. (2011). Fluid Mechanics, 7 Hrsg., McGraw-Hill, New York

[17]   Chabane, S., Sesmat, S., Hubert, D., Gautier, D., Wartelle, C., Bideaux, E. (2015). Reynolds number-dependent mass flow rate calculation for pneumatic pipes, *Proceedings of the Institution of Mechanical Engineers, Part I: Journal of Systems and Control Engineering*, pp. 419-428

University of Maribor Press

Modelling, Optimal Design and Simulation of Hydraulic Oil Reservoir

ALMIR OSMANOVIĆ, ADIS EFENDIĆ & ELVEDIN TRAKIĆ

Abstract Nowadays, hydraulics is present in all branches of industry and transportation. The reservoir as main part of hydraulic system serves primarily as a storage space and supply point for the hydraulic system fluid. The reservoir design contributes to the proper functioning of the entire system and reduces normal maintenance requirements. It keeps the fluid clean, separates air and contaminants from the fluid. The reservoirs also dissipate the heat of the fluid to the outside atmosphere, and in this paper is present hydraulic reservoir in which the heat is transferred with natural convection. In order to get the optimal construction for the hydraulic fluids reservoir, the estimation is carried out on the hydraulic reservoir with ribbed surfaces, as in this way the surface is extended, which allows better transfer of the heat and enhances the efficiency of the system. Additionally, a CFD and a thermal analysis of an optimized hydraulic reservoir of an Apkant press is represented.

Keywords: • hydraulic system • hydraulic reservoir • modelling • simulation • hydraulic press •

CORRESPONDENCE ADDRESS: Almir Osmanović, University of Tuzla, Faculty of Mechanical Engineering, Tuzla, Bosnia and Herzegovina, e-mail: almir.osmanovic@untz.ba. Adis Efendić, University of Tuzla, Faculty of Mechanical Engineering, Tuzla, Bosnia and Herzegovina, e-mail: adis_efendic@hotmail.com. Elvedin Trakić, University of Tuzla, Faculty of Mechanical Engineering, Tuzla, Bosnia and Herzegovina, e-mail: elvedin.trakic@untz.ba.

1   Introduction

Hydraulic reservoirs are components of a hydraulic system whose main purpose are the storage of working fluid. Usually in the reservoir are placed: filter, refrigerator and heater of fluid and often pump. An electric motor, pump and measurement device can be installed on the reservoir. Hydraulic reservoir is usually prismatic or cylindrical. The construction and its position should allow easy filling and control of the working fluid level, easy maintenance and good heat removal. The suction line is placed 2 to 5 cm above the bottom of the reservoirs and usually has a filter. The return line is placed 2 to 5 cm below the minimum level of oil, which prevents the appearance of the foam and vortexing. The return line should be placed far away from the suction cup to prevent mutual interference. The inner surface of the reservoirs should be smooth and protected from corrosion, shock and high temperature. Inside the reservoir there are barriers. The air vent with the air filter is mounted on the upper side of the reservoirs and should allow the outlet of air and vapor from the reservoirs and prevents the entry of mechanical particles and water vapor from the air. The bottom of the prismatic reservoir is usually slightly tilted in relation to the horizontal. The drain hole is placed on the lowest part of the bottom of the reservoirs so that the reservoirs is completely drained when the fluid is replaced. The drain plug is often magnetized to collect metal particles. In prismatic reservoirs, the cleaning hole is placed on the side, and at the cylindrical tops. A level indicator is installed to control the working fluid level. The level indicator should have a maximum and minimum level of working fluid. About 15 % of the volume should be left in the reservoir due to air extraction. All outside surfaces of the reservoirs should be free to dissipate heat.
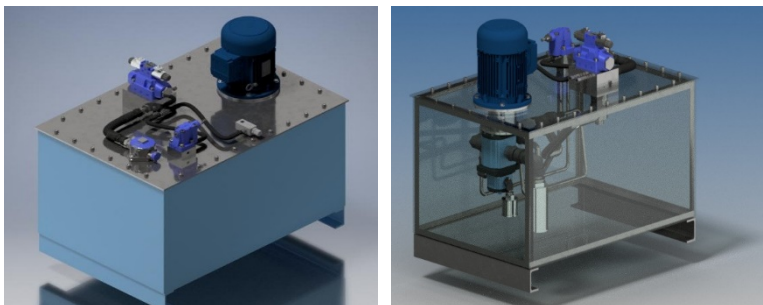
Figure 1: Hydraulic reservoir.

2 Construction and dimension of hydraulic reservoirs

Construction and dimension of the hydraulic reservoir is very important for the proper functioning of the hydraulic system and maintenance of the working fluid -oil. Important functions of the reservoirs are: accumulation of the required amount of fluid, extraction of water and mechanical impurities from the working fluid, inside the reservoir working fluid is heated or cooled. In order to perform all the above functions while retaining the oil in the reservoir, it is necessary to properly dimension and construct reservoir. Reservoirs are made of steel sheet by welding, cast iron or aluminium. Reservoirs of larger dimensions are made by welding, and smaller dimensions by moulding [1]. The size of the reservoir is defined according to the type of plant on which the hydraulic system is installed and the pump capacity:

$$V_R = z \cdot Q_p \tag{1}$$

For mobile machine, the volume of the reservoir is defined in relation to the total volume of all actuators (V_C) installed. The values of volume for reservoir are given in Table 1.

Table 1: Guidelines for selecting the volume of the reservoir [1].

Type of plant	Volume of the reservoir	Minimum oil quantity in relation to the largest volume
Mobile machine	$1,5\ V_c$	$0,5\ V_c$
Stationary plants		
When the pump is switched off during operation	$3\ Q_p$	$0,5\ Q_p$
With the pump unloading	$(4-5)\ Q_p$	$(2-3)\ Q_p$
Permanent work with intense warming	$(4-10)\ Q_p$	$(3-5)\ Q_p$

In addition to the criteria for dimensioning the volume of the reservoirs specified in Table 1, it is also necessary to take into account the characteristics of the oil in terms of air separation speed. The volume of the reservoir must be such a size that it will ensure the retention of the oil in the reservoir, at least as long as the amount of air extraction time from the oil is. The retention time of the oil can be extended by the installation of

the barriers, which, once or more times, change the direction of oil flow from the return to the suction part of the reservoir. In addition, these barriers accelerate the process of extracting water and impurities from the oil [1].
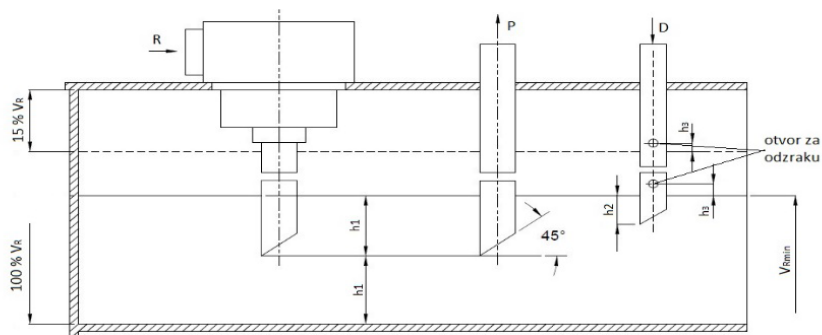
Figure 2: Section of the reservoir [1].

With standards are defines the shapes and dimensions of the hydraulic reservoirs. Figure 3 shows a square reservoir with indicated basic dimensions. Figure 3a shows a reservoir with square shape, a volume of up to 1000 l, according to DIN 24339. Figure 3b shows a reservoir of square shape, volume up to 25000 l. For this type of reservoir, due to large surfaces, the inner sides are made of ribbed sheet.
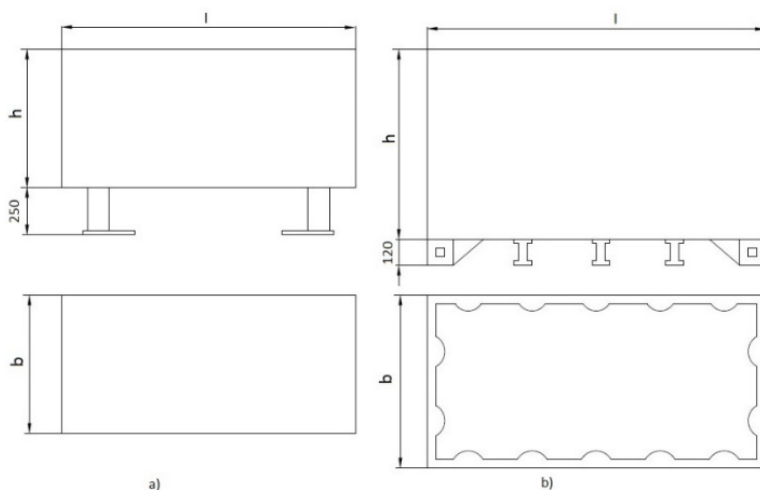
Figure 3: Simplified look of a square-shaped reservoir [3].

2.1 Ribbed surface of the reservoirs

In order to intensify the transfer of heat from the heating surface to the environment, metal elements of various shapes are added to the surface, thus increasing the contact area with the surrounding air. These are called ribs or fins [2].
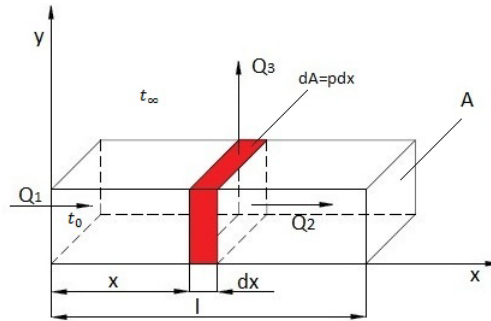
Figure 4: A rectangular rib.

The heat delivered by the rib $dA = pdx$ to the environment is obtained from the energy balance:

$$Q_3 = Q_1 - Q_2 \tag{2}$$

The amount of heat that enters through the root of the rib is determined by the expression:

$$Q_1 = -\lambda \left(\frac{\partial t}{\partial x}\right) Adx \tag{3}$$

The amount of heat exiting the control surface in the x-axis is:

$$Q_2 = -\lambda \left(\frac{\partial t}{\partial x} + \frac{\partial^2 t}{\partial^2 x}\right) Adx \tag{4}$$

The heat that the rib gives to the environment by convection over the surface $dA = pdx$ where P is the circumference/volume of the rib are:

$$Q_3 = \alpha(t - t_\infty)Pdx \tag{5}$$

After arranging and introducing the shift: $\theta = t - t_\infty \implies d\theta = dt$, $m^2 = \frac{P\alpha}{\lambda A}$ it gets the differential form of the equation:

$$\frac{\partial^2 \theta}{\partial^2 x} - m^2\theta = 0 \tag{6}$$

To solve the differential equation, introduce the following shift:

$$X^{''} - m^2 X = 0 \tag{7}$$

wherein:

$$X = e^{rx} \implies X' = re^{rx} \implies X^{''} = r^2 e^{rx} \tag{8}$$

After solving the differential form of equation (6), the final form is obtained:

$$\theta = C_1 e^{-mx} + C_2 e^{mx} \tag{9}$$

3   Model and optimization of hydraulic reservoir

The hydraulic reservoir of Apkant press Type AP-100/30 is taken as an example for modelling and analysis. The hydraulic reservoir itself is an integral part of the press structure. The hydraulic reservoir is located 2.2 m from the bottom of the press. The shape of the hydraulic reservoir is rectangular, as shown in Figure 5. The total volume of the reservoir is V = 0.31768 m³. There are suction and return pipe openings on the front. On the lower side of the reservoirs there is an oil drain hole, while on the upper side there is three openings ports for inspection and cleaning of the reservoirs. Inside the reservoir there is a suction filter, which is connected to the suction line. The amount of oil inside the reservoir is 150 l.
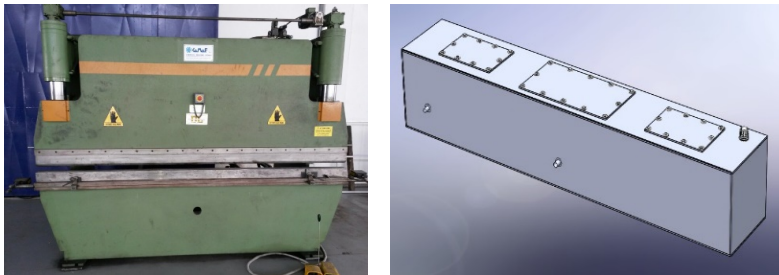
Figure 5: Apkant press and 3D model of hydraulic reservoir.

Hydraulic oil parameters

Hydraulic oil VG 32 is used for the hydraulic system for Apkant press. The basic characteristics of the VG32 hydraulic oil for different temperatures are shown in Table 2.

Table 2: VG32 hydraulic oil.

	Temperature °C				
	0	20	40	60	80
Viscosity [mm²/s]	300	79	32	14,4	8,1
Density [kg/m³]	880	867	854	841	828
Thermal conductivity [W/mK]	0,135	0,133	0,132	0,131	0,129
Specific heat capacity [kJ/m³K]	1663,20	1708,2	1750,7	1799,7	1838,2
Actual specific heat capacity [kJ/kgK]	1,890	1,970	2,050	2,140	2,220

Hydraulic reservoir dimension

The dimensions of the hydraulic reservoir (length, width and height) are determined by the amount of oil inside the reservoir (V = 150 l). The dimensions of the hydraulic reservoir and its calculation are shown in Table 3.

Table 3: Basic dimensions of a hydraulic reservoir.

Formula	Value	Unit	Description
$l = \dfrac{V - V_1}{V_2 - V_1} \cdot (l_2 - l_1) + l_1$	790	mm	Length of reservoir
$b = \dfrac{V - V_1}{V_2 - V_1} \cdot (b_2 - b_1) + b_1$	585	mm	The width of the reservoir
$h = \dfrac{V - V_1}{V_2 - V_1} \cdot (h_2 - h_1) + h_1$	410	mm	Reservoir height
$V = l \cdot b \cdot h$	0,1846	m³	The volume of the reservoir
$V_Z = V - V_U$	0,00364	m³	The volume of air in the reservoir
$h = \dfrac{V_U}{l \cdot b}$	333,11	mm	Height of oil in reservoir

We adopt that the thickness of the sheet wall of the hydraulic reservoir is 3 mm. Acceptance of sheet thickness of hydraulic reservoir was performed on the basis of analysis of existing reservoir at Apkant press. The thickness of the sheet wall on the existing reservoir is 6 mm, since the existing reservoir has the role of preventing static deformation on the lateral sides of the press, it can be concluded that the optimized hydraulic reservoirs does not have to have the same sheet thickness, but can be made of thinner sheet thickness. When selecting the material from which the hydraulic reservoir will be made, care must be taken of its strength and its thermal properties in order to satisfy all the aspects required for the reservoir. The thermal property of the material is very important for the calculation of the amount of heat which, through conduction through the thickness of the reservoir, is drained from the oil inside the reservoir and transmitted to the surrounding air by natural or forced convection. Material for reservoir is AISI 1020 steel.

Rib area calculation

Table 4 and 5 show the fluid parameters, geometric characteristics and ribbed parameters.

Table 4: Fluid and ribbed surface parameters.

Surrounding fluid (air)	Ribbed surface
$t_f = 20$ [°C]	$t_o = 20$ [°C]
Air characteristics for: $t_{sr} = \dfrac{41+20}{2} = 30,5[°C]$ $C_p = 1,005$ [kJ/kgK] $v = 16,00 \cdot 10^{-6}$ [m²/s] $\lambda_f = 2,67 \cdot 10^{-2}$[W/mK] $Pr_f = 0,701$	Geometric characteristics of the ribbed surface $l_{uku} = 2,75$ [m] $b = 0,380$ [m] $L = 0,050$ [m] $B = 0,0195$ [m] $\delta = 0,003$ [m] $\lambda = 47$ [W/mK]

Optimization of the hydraulic reservoir for the Apkant press must be carried out due to the inaccessibility of the existing hydraulic reservoir, during the elimination of failures occurring on the electric Motor, hydraulic parts, and for inspection of the reservoir and cleaning.

In addition to the above reasons, the optimization (improvement) of the hydraulic reservoir should also be carried out for better heat removal from the hydraulic oil. The solution will be a new construction of the hydraulic reservoir, which will be located on the ground next to the side of the hydraulic Abkant press.

Table 5: Rib surface calculation.

Formula	Value	Unit	Description
$t_{sr} = t_{un} = \dfrac{t_{ul} + t_{izl}}{2}$	40,50	°C	Internal wall surface temperatures
$t_{va} = t_0 = t_{un} - \dfrac{Q \cdot \delta}{\lambda}$	40,45	°C	Reservoirs wall outer surface temperatures
$Ra = \left(\dfrac{g\beta B^3 \Delta t}{v^2} Pr\right)_f$	$19,8316 \cdot 10^3$		Rayleihg-ov number
$N_u = \left[\dfrac{576}{\left(R_a \cdot \frac{B}{b}\right)^2} + \dfrac{2,87}{\left(R_a \cdot \frac{B}{b}\right)^{1/2}}\right]^{-0,5}$	3,532371		Nuseltov number
$\alpha = \dfrac{\lambda_f}{B} \cdot N_u$	4,7983	$\dfrac{W}{m^2 K}$	Heat transfer coefficient
$m = \sqrt{\dfrac{\alpha}{\lambda\delta}}$	5,8335	m^{-1}	Coefficient
Condition: $x = l \; ; \; t_\infty = t_f \; ; \; l = L \Longrightarrow$ $t_l = t_f + (t_0 - t_f)\dfrac{1}{\cosh(ml)}$	39,609	°C	Temperature at end of rib
$\eta = \dfrac{th(ml)}{ml}$	97,25	%	Dagree of rectangular rib utilization
$Q_{reb} = \alpha \cdot [(2 \cdot b \cdot L + 2 \cdot \delta \cdot L) \cdot \eta]$ $\cdot (t_0 - t_f) \cdot n$	460,518	W	The total amount of heat emitted by the ribs

On the upper side of the hydraulic reservoir there will be an electric motor, a hydraulic distribution valve, pump, a suction and return pipeline, and an oil inlet to the reservoir. A drainage hole will be located on the underside of the reservoirs, while rectangular ribs will be placed on the rest of the reservoir to increase the surface for better heat convection during natural convection. Inside the reservoir will be barrier, which will have the task of directing the hydraulic oil from the return to the suction section and preventing the hydraulic oil from whirling.
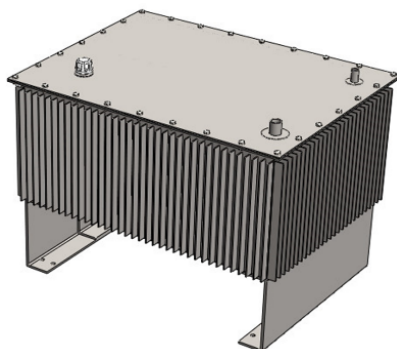
Figure 6: Model of optimized hydraulic reservoir.

4   Thermal and CFD analysis of optimized hydraulic reservoir

For optimized hydraulic reservoir is used numerical methods and data structures to solve and analyse fluid flow problems - Computational fluid dynamics (CFD). Thermal analysis of the ribbed surface of the hydraulic reservoir are also presented. Figure 7 shows the hydraulic reservoir network obtained in the computer program. A denser mesh was used for the simulation to obtain more accurate results, while the figure shows a slightly larger mesh for better visibility.

a)   b)
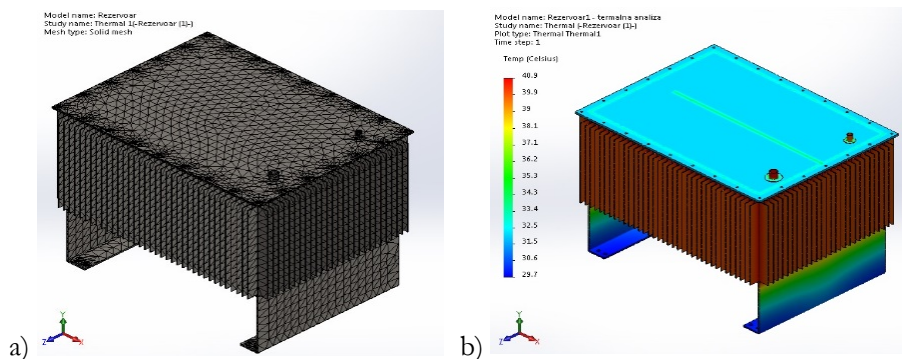
Figure 7: a) Hydraulic reservoir mash network; b) Thermal analysis of hydraulic reservoir.
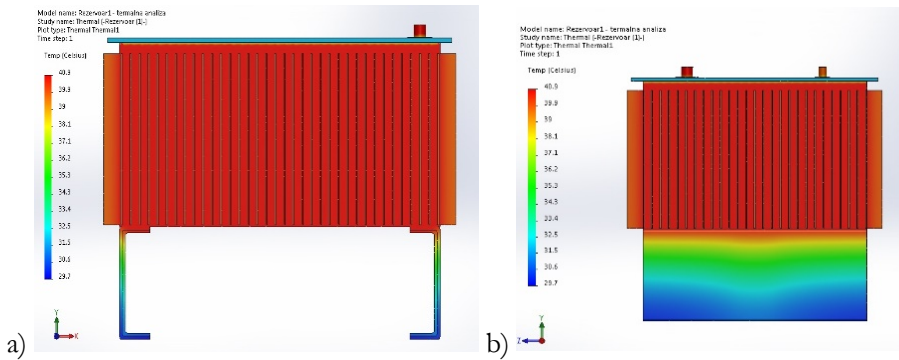
Figure 8: Hydraulic reservoir thermal analysis – a) side; b) front view.
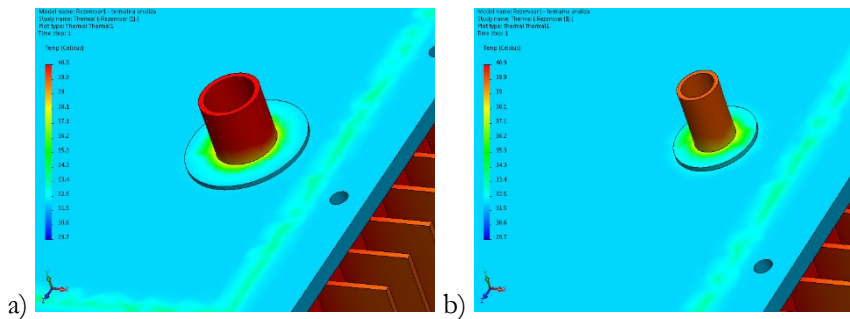
**Figure 9: Thermal analysis of hydraulic reservoir
a) return pipeline, b) suction pipeline.**

Figures 7, 8 and 9 show a thermal analysis of a hydraulic reservoir. The figures show that the temperature of all the sides and even the bottom of the hydraulic reservoir. It can be observed a change in temperature by the height of the support of the hydraulic reservoir, which is transmitted to the surface of the support by conduction from the bottom of the reservoir, which is further transmitted by conduction over the entire height of the support.

The conduction of heat by conduction through the support of a hydraulic reservoir is accompanied by the convection of heat by convection to the surrounding air. The value of these temperatures is in the function of the coefficient of heat conduction of the material and the coefficient of heat transfer from the surface to the surrounding air.
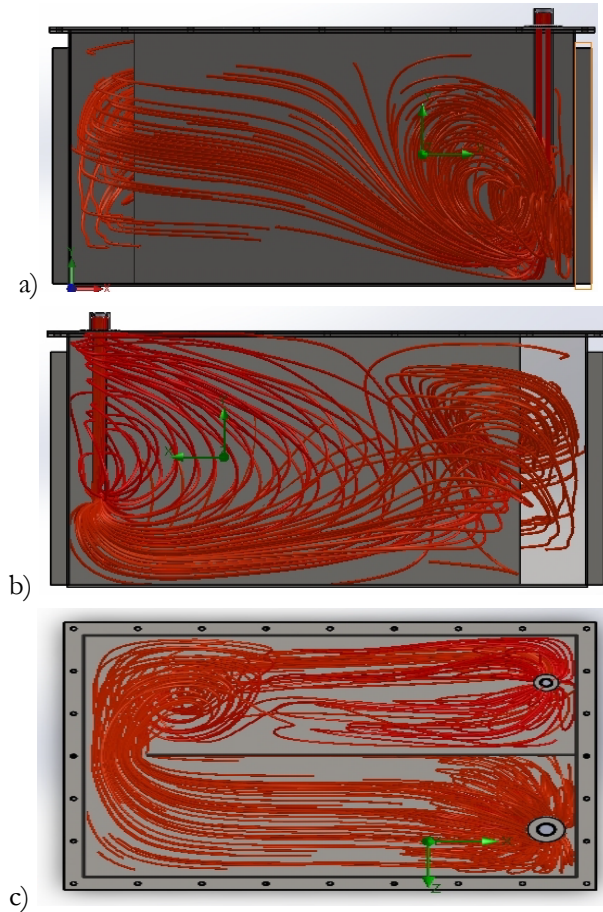
Figure 10: Fluid movement inside the hydraulic reservoir
a) back side, b) suction side, c) top view.

Figures 10 show the fluid (oil) flow in the hydraulic reservoir from the inlet (return side) to the outlet (suction side). It can be noticed that the fluid has turbulent motion on the back side, after leaving the return pipe.

5   Conclusion

A hydraulic reservoir is an integral part of a hydraulic unit, which has the task of storing a certain amount of hydraulic oil required for the operation of the hydraulic system. Today, hydraulic reservoirs are made of materials that have good thermal properties, to increase better heat dissipation from hydraulic oil. The normal operating temperature

of the working fluid in the hydraulic system is about 50 °C. Usually, the working fluid during work is heated to a higher temperature, so it needs to be cooled. The simplest way to cool is to place a fan in front of the reservoir, but it has the minimal efficient rate. Placing copper tubes in a reservoir through which cold water flows has a higher efficient rate, but since the system is open, the water consumption is high. Special closed systems with heat exchanger have the best cooling effect. In practice, free air-cooled systems are also used, but they are large in size, complex in construction and expensive. Based on the results of thermal analysis present in this paper, it can be concluded that by using a finned surface, a higher efficiency of the hydraulic reservoir is achieved, by increasing the surface from which heat is released to the surrounding fluid (air). The amount of heat discharged from the hydraulic oil depends on the thermal characteristics of the hydraulic oil and also on the actual value of the heat transfer coefficient.

References

[1]   Savić, V. (1990). Uljna hidraulika i hidraulične komponente i sistemi, Zenica.
[2]   Ari, V., Janne, P., Timo, H. (2011). Fundamentals of heat transfer, Faculty of technology, lut energy, lecture note 7.
[3]   Watton, J. (2009). Fundamentals of Fluid Power Control. Cambridge: Cambridge University Press.
[4]   Cundiff, J. S. (2002). Fluid power circuits and controls: fundamentals and applications. Boca Raton: CRC Press LLC
[5]   Dieter, W., Norbert, G. (2011): Hydraulik Grundlagen, Komponenten, Schaltungen, Heidelberg: Springer-Verlag.
[6]   Tič, V., Lovrec, D. (2012). Design of modern hydraulic tank using fluid flow simulation. International Journal of Simulation Modelling (IJSIMM); Jun2012, Vol. 11 Issue 2, p77.
[7]   Cristescu, C., Kedzia, K., Dumitrescu, C., Radoi, R. (2018). Maintenance of fluid power equipments. International Conference of Hydraulics and Pneumatics – HERVEX. 7 - 9 November, Calimanesti-Caciulata, Romania, pp. 68-76.
[9]   Priyatosh, B. (2000). Computional Fluid Dynamics (CFD) Analysis and Optimization Hydraulic Control Valves, 48th National Conference on Fluid Power, Milwaukee, USA
[10]   Hydraulic oil - http://www.nisotec.eu/sr-lat/hidraulicna-ulja

Evaluation of Flow-induced Forces in Hydraulic Valves

ANŽE ČELIK, BLAŽ BOBNAR & FRANC MAJDIČ

Abstract Flow-induced forces, a consequence of fluid flow passing narrow passages, play critical role in determining performance of hydraulic directional control valves. The appropriate determination and evaluation of such forces is of importance early in a design stage because their operation directly affect the necessary force of electro-actuators. The paper shows and explains evaluation of flow-induced forces on directional control valve, by means of experimental and numerical approach. Such a valve is designed for flow rates up to 80 l/min and pressures up to 350 bar. Measurement of (axial) flow forces was performed through two independent approaches. It was found out that experimental approach matches with simulation approach. Further, the discrepancies were also presented, whose origin was recognized and explained. Validity of numerical model could be confirmed based on the agreement between experimental and simulation approach. By using the appropriate numerical model, it is possible to reduce development costs, because experimental approach is usually time-consuming and expensive.

Keywords: • directional control valve • CFD analysis • LVDT sensor • voice coil • flow force •

CORRESPONDENCE ADDRESS: Anže Čelik, Poclain Hydraulics d.o.o., Žiri, Slovenia, e-mail: anze.celik@poclain.com. Blaž Bobnar, University of Ljubljana, Faculty of Mechanical Engineering, Ljubljana, Slovenia, e-mail: blazbobnar288@gmail.com. Franc Majdič, PhD, University of Ljubljana, Faculty of Mechanical Engineering, Ljubljana, Slovenia, e-mail: franc.majdic@fs.uni-lj.si.

1   Introduction

Flow-induced forces are one of the most important factor to consider in hydraulic component development process. This is especially true for proportional hydraulic valves but also for conventional on-off valve, actuated by electromagnet. Flow forces directly affect valve performance criteria, such as power envelope (see Figure 1), spool stability, dynamic response and others [1].
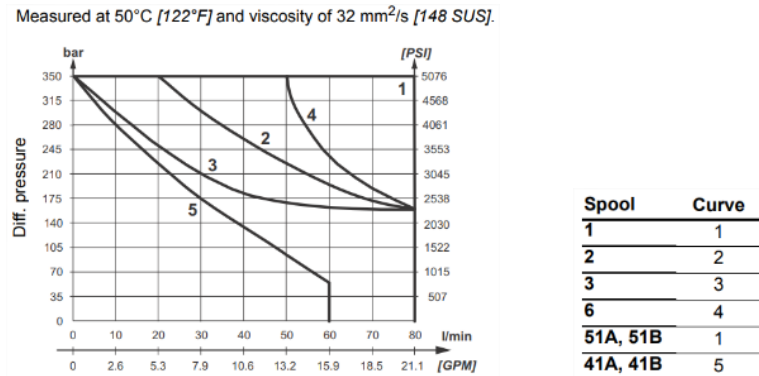
Figure 1: Typical p-Q characteristic for hydraulic valve [16].

In the field of flow forces in hydraulic valves, a significant number research has been done. Already in the 1950's various authors studied the possibilities of reduction or compensation of flow forces (e.g. Beackon et al. [2], Blackburn et al. [3] and Clark et al. [4]). Backe et al. [5] was the first to propose methods to compensate flow forces. Additionally, Lugowski [7] proposed compensation profile in upstream meter-in orifice.

In recent studies, the problem of flow forces was studied by two ways: by **numerical approach** where computational fluid dynamics (CFD) analysis is performed and by **experimental approach** (e.g. E. Lisowski et al. [6], Herakovič [8], Bordovsky et al. [9], Yuan et al. [10]). The latter (if performed adequately) is the most accurate method because it measure directly the flow force for given design and boundary conditions. However, it is not practical to validate all designs only by means of experiment. This old-traditional method is expensive in terms of time (and money) and gives limited insight into the product behavior and performance.

The main goal of this investigation is to perform experimental research of (steady) flow forces on directional control valve (produced by Poclain) as well as validation of corresponding numerical tool (CFD).

1.1 On flow-induced forces

In a hydraulic valve, the so-called disturbance forces appear that work against solenoid or control forces. Flow forces can be understood as forces that appear with a change of direction and/or velocity of the flow stream. The forces acting on a sliding spool are divided into radial (F_r) and axial forces (F_a).

1.1.1 Axial flow forces

Flow force exists due to non-uniform pressure field on the spool area. Static pressure field on the left side of the spool (see Figure 2) is uniform whereas the one on right side of the spool is affected by the conversion of the potential energy (static pressure) into kinetic energy – a negative pressure occurs at vena contracta. A net force is produced in a direction that always closes the spool. In such case, flow force acts in a way to stabilize the spool [11].
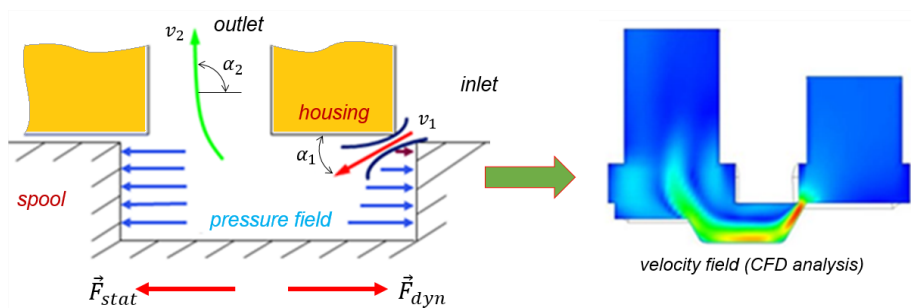
Figure 2: Spool pressure and velocity profile.

Flow forces can be classified as steady or transient flow force [12]. Steady flow forces are those exerted by the fluid on the spool during steady flow conditions; transient forces are the additional forces due to the time variation of the flow condition.

$$\sum \vec{F} = \vec{F}_{stat} + \vec{F}_{dyn} = \frac{d(m \cdot \vec{U})}{dt} \tag{1}$$

The stationary part of the flow force for the inlet edge can be calculated from the axial momentum component. Here, the following equation usually appears:

$$\vec{F}_{stat} = \rho \cdot Q \cdot \vec{U} = \rho \cdot Q \cdot (v_2 \cdot \cos \alpha_2 - v_1 \cdot \cos \alpha_1) \tag{2}$$

The non-stationary part of the flow force can be calculated using the length L of the accelerated fluid in the control volume of the sliding-spool chamber:

$$\vec{F}_{dyn} = -\rho \cdot L \cdot \frac{d\vec{Q}}{dt} \tag{3}$$

2   Numerical approach

Flow force evaluation has been performed by the commercial 3D CFD tool Simcenter STAR-CCM+ (v11.04). The primary goal of the CFD simulations is to compare results with experimental approach as well as to get the appropriate CFD simulation models for further optimization and development of new hydraulic valves.

This part of study refers to static conditions. This means that spool is fixed at given position during the analysis; therefore, induced flow forces are resultant forces of static conditions.

2.1   Pre-processing steps

2.1.1   Valve geometry

As declared by the valve nomenclature, the 4-ports, 3-position valve and the spool of type "1" are used. It is important that 3D CAD model represent actual geometry, used for experimental purposes (so, to have representative digital twin). Here, using hydraulic fittings on inlet/outlet ports is of importance because they locally effect flow patterns and consequently pressure distribution. CFD simulation of directional control valve takes into account flow passage in "b" position (i.e. P➔A and B➔T) and "a" position (i.e. P➔B and A➔T) of the spool. Both spool positions are also depicted on Figure 3.
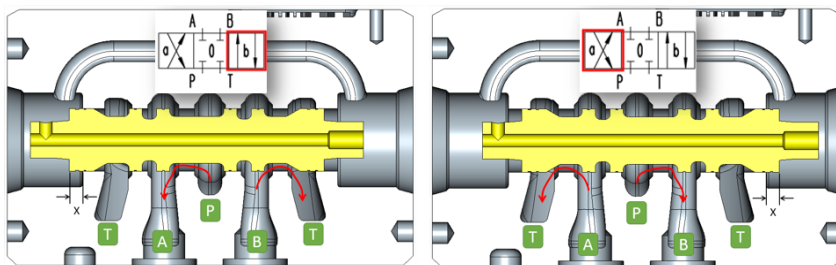
Figure 3: Flow passages - "b" side activated (left); "a" side activated (right).

2.1.2 Mesh parameters

In the core mesh, polyhedral mesh has been used (basic size of ~1,4 mm) and local mesh refinement has been applied in various regions. In order to accurately capture near-wall phenomenon, 6 boundary (prism) layers were used. Sensitivity analyses has shown that 8 or even 12 boundary layers do not bring noticeable improvement in terms of results. Figure 4 depicts cross section view on P-A chamber of finite volume mesh. Mesh setting criteria has been adjusted in order to assure (at least) 6 prism layers in entire wetted volume.
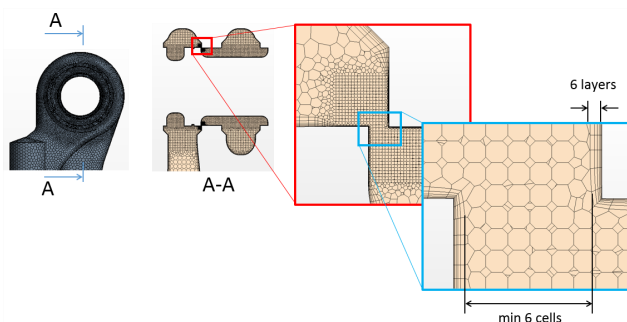
Figure 4: Cross section view of FV mesh.

2.1.2 Boundary conditions and fluid properties

On the inlet ports (P and A or B), various different mass flow rates have been prescribed (10, 30, 50 and 80 l/min). On the outlet ports (A or B and T), environmental pressure of 5 bar has been prescribed. For simulation of (static) flow force, the assumption of incompressibility has been taken into account. In this case, parameters of oil ISO VG46

at 50 °C has been used. In particular, constant density of 855,5 kg/m³ and dynamic viscosity of 0,0249 Pa s were used.

2.2 Processing steps

2.2.1 Turbulence model

In this particular case, two industry widely used turbulence models have been used: realizable k-ɛ and SST k-ω. These models have been applied in order to evaluate their impact on results.
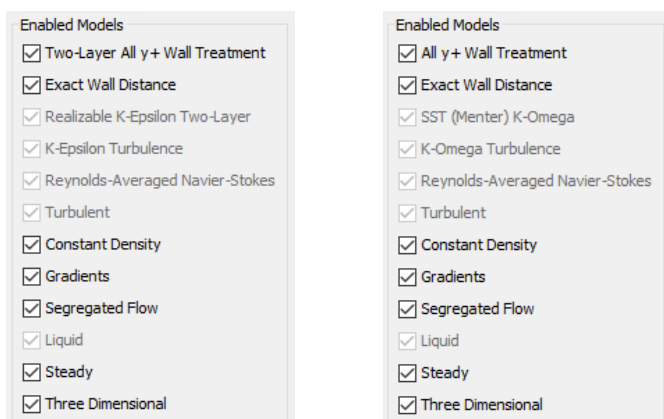
Figure 5: Selected physical models (left: k-ɛ, right: k-ω).

It is worth to mention that default values of parameters in RANS equation have been used. Their values could be easily observed in corresponding literature (e.g. [13]).

2.2.2 Convergence (stopping criteria)

Stopping criteria allows specifying how long the solution runs for and under what conditions it stops iterating and/or marching in time. For all simulation tasks, residuals and physical quantities (i.e. pressure drop and flow forces) were observed.

2.3 Post-processing steps

For comparison purposes, results of flow forces from CFD analyses are shown next to the experimental results in chapter 3.3. Hereafter, only some fundamental observations from numerical simulation are shown and explained. Simulation results are presented for two different turbulence models (i.e. k-ε and k-ω).

2.3.1 Pressure losses

Pressure losses for flow direction P➔A as a function of spool opening (i.e. spool underlap) are depicted on Figure 6 (normalized values). It is clearly seen that the bigger the spool opening, the lower the pressure loss.
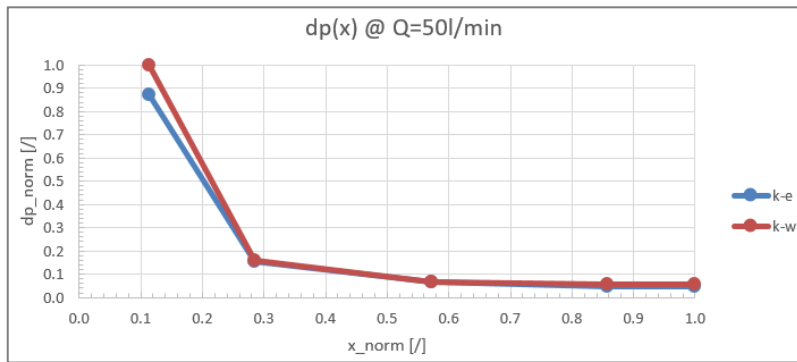
Figure 6: Pressure losses for P➔A.

2.3.2 Flow forces

Figure 7 depicts flow forces for flow direction P➔A as a function of spool opening (normalized values). The trends of flow forces are the same as seen for pressure losses - the bigger the spool opening, the lower the flow forces. Both turbulence models predict similar results.
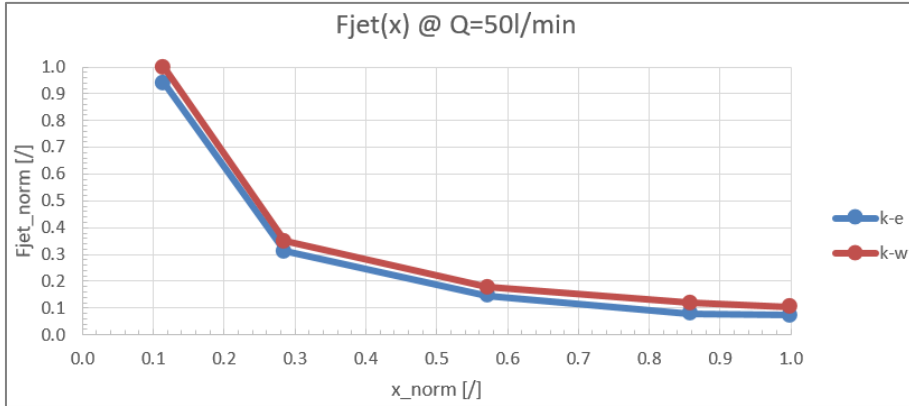
Figure 7: Flow forces for P→A.

2.3.3   Flow coefficient

Figure 8 depicts flow coefficient (Cq) for flow direction P→A as a function of spool opening (the latter is given in normalized values). It can be seen that the smaller the spool opening, the higher the flow coefficient. Maximal value of Cq is achieved at smallest spool opening, where flow is (fully) turbulent and flow number (λ) or Reynold number (Re) becomes high. In general, the parameter Cq depends flow regime and geometry [11], [14].
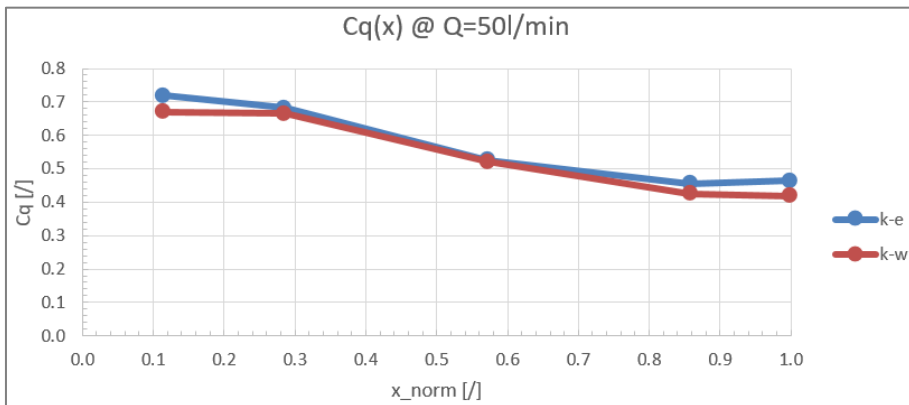
Figure 8: Flow coefficient for P→A.

3 Experimental approach

Experimental approach was performed at Laboratory for Fluid Power and Controls (LFT) from the Faculty of Mechanical Engineering in Ljubljana.

3.1 Development of test device

3.1.1 Measuring system with force sensor

Measuring system includes stroke sensor (LVDT), flow meter, pressure sensors and temperature sensor. For spool stroke setting, a micrometer screw was used because it enables relatively precise adjustment of the spool position. In order to prevent additional radial forces, internal components were connected by axial joints. The measuring system with corresponding sensors is shown on Figure 9.
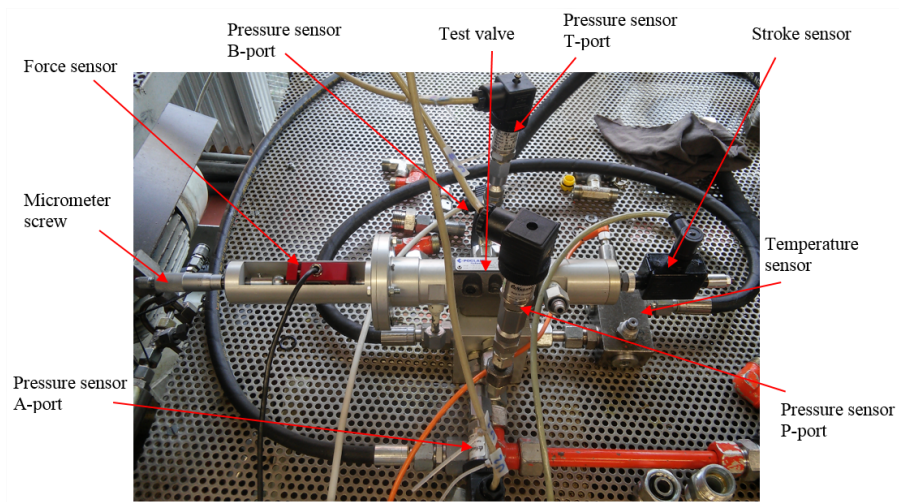
Figure 9: Measuring system with force sensor.

3.1.2 Measuring system with voice coil actuator

Voice coil or electrodynamic actuator consists of a moving coil whose winding is perpendicular to a fixed magnetic flux and a permanent magnet in the core [15]. Measurement of flow force with a voice coil actuator is indirect because measured force is obtained via electric current required to keep the actuator in a given position.
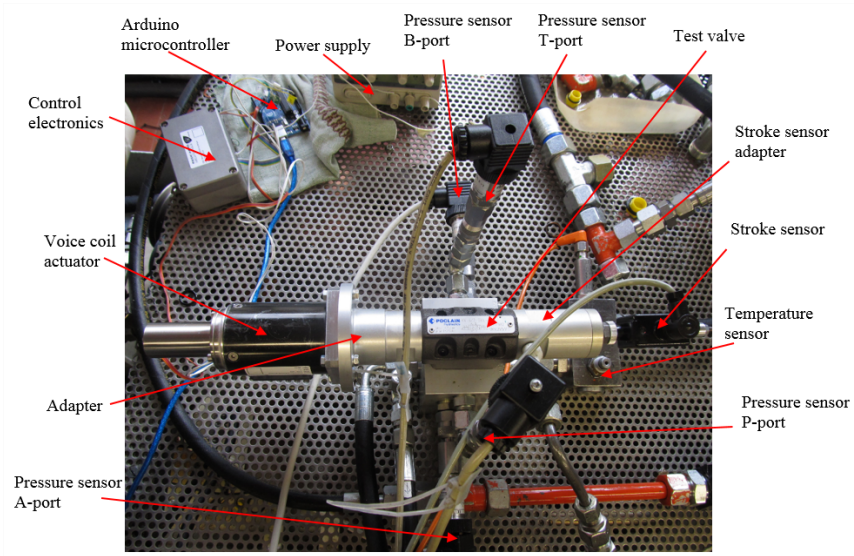
Figure 10: Measuring system with voice coil actuator.

The actuator contains also a Hall Effect sensor, which acts as a stroke sensor. The voice coil actuator was controlled by Arduino microcontroller and the control electronics. Measuring system with voice coil actuator and corresponding sensors is shown on Figure 10.

3.2   Experiment

The existing hydraulic test device was used for test purposes (scheme is shown on Figure 11). Hydraulic pump from Hydro Leduc with a displacement of 130 cm^3 and maximum flow rate of 170 l/min at 65 bar were used.
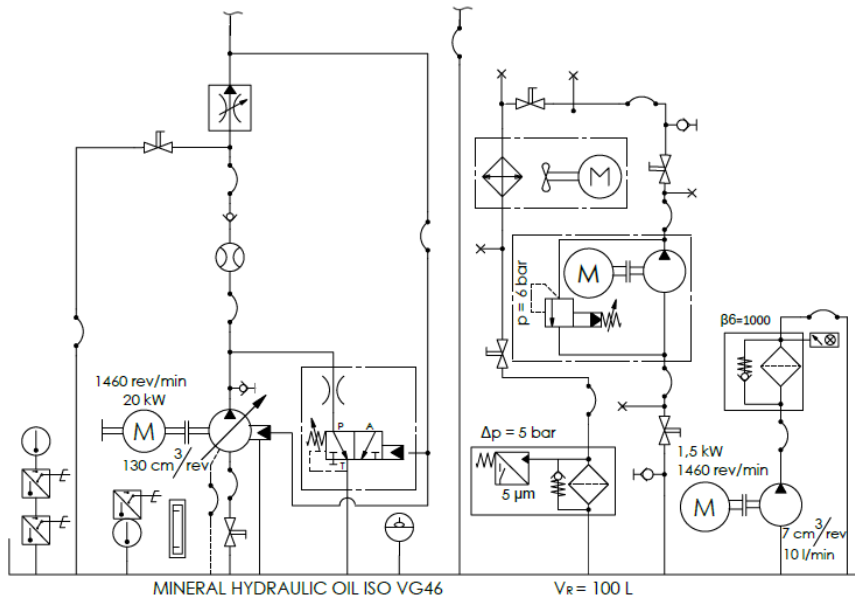
Figure 11: Hydraulic scheme of aggregate.

Hydraulic oil ISO VG46 was used in the specified filtration range – 19/17/14 according to standard ISO 4406:1999 [16] and kept in the temperature range of T = 45 ±5 °C. In order to ensure the sensor accuracy, they were calibrated before starting the measurements.

Measured data were captured by LabVIEW software, except measurements with a voice coil actuator, where flow force and the spool stroke were acquired with the Arduino software. All measured signals were transmitted to the computer via DAQ device National Instruments. For each test sequence, three consecutive measurements were made and then the mean value and standard deviation of flow force was calculated (using Microsoft Excel). Mean values of flow forces were used for post-processing (i.e. plotting) purposes.

3.3 Results

Measured values of flow force were compared with corresponding CFD simulations, which took into account two different models of turbulence. The results are shown as normalized flow force vs. normalized spool opening for each flow rate given in the measurement protocol.

3.3.1   Symmetrical flow conditions

Results for symmetrical flow conditions are depicted on Figure 12. The graph represents normalized values of flow force $F_{jet,norm}$ as a function of spool opening x_{norm} (i.e. spool underlap) for various flow rates. It makes sense to provide some explanations that refer to the results for each flow rate:

- Values on vertical axes are normalized by the maximal value of F_{jet} from k-ε model of particular test sequence.
- $Q = 10$ l/min: measured values of flow force using force sensor match with values obtained by the CFD analysis. In addition, some deviation are also observed on the measurements using voice coil actuator. Main reason for deviation is the instability of voice coil actuator. For this particular flow rate, values of flow forces are relatively small (in the range of few newton), which means that disturbance effects (e.g. friction, noise on data acquisition...) have important contribution.
- $Q = 30$ l/min: measured curves have the same trend as seen for the smallest flow rate (except that magnitude of flow force is higher). Further, due to the test bench power limitation, it was not possible to assure nominal flow rate at smallest spool opening (this is why results are not plotted).
- $Q = 50$-80 l/min: it can be seen that measured flow forces (especially for load cell) demonstrate independence with respect to the spool opening. This is even more obvious at maximal flow rate. It is assumed that radial (lateral) flow forces play important role and that influence of radial force increases with increasing flow rate. Further, radial forces depend on size of radial clearance between the spool and the valve housing. It can be seen that values measured using the voice coil actuator are higher compare to force sensor. Reason could be that voice coil actuator constantly corrects the position of spool according to the load; therefore, lateral forces are less affected as the spool moves constantly (no stick-slip effect).
- Influence of higher pressure on T-port on flow force has also been discovered. It has been found out that tank pressure (up to 150 bar) has no impact on flow forces.
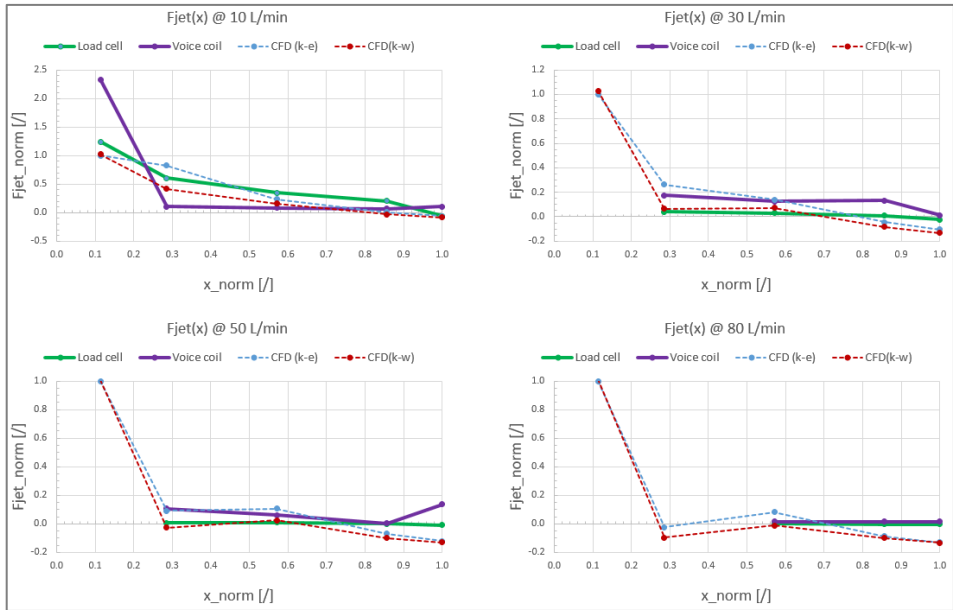
Figure 12: Flow force comparison (symmetrical flow conditions).

In order to evaluate the influence of radial clearance on lateral forces, additional investigations have been performed by means of standard spool modification. As can be seen on Figure 13, influence of lateral forces is greatly reduced by increasing the radial clearance (note that gap clearance is decreasing by increasing spool index); on the other hand, internal valve leakage is greatly increased as well.
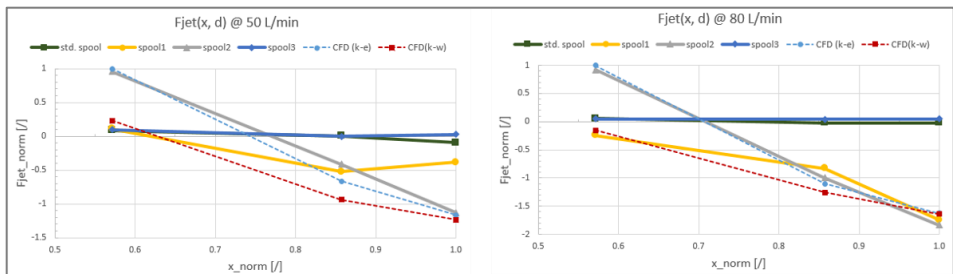
Figure 13: Flow force for different flow rates and gap clearances.

Spools with the biggest gap clearance (i.e. spool1 and spool2) exhibit similar trends as the results from CFD analysis. However, some deviation is observed for spool1 at flow rate of 50 l/min. It is assumed that flow force reduction appear due to geometrical imperfection (i.e. circularity, which have been found to be slightly increased on some metering edges).

3.3.2 Non-symmetrical flow conditions

Results for non-symmetrical flow conditions are depicted on Figure 14. Some complementary explanations that refer to the results for each flow rate are given hereafter:

- Q = 10 l/min: measured values match with the CFD analysis. Values of flow forces are relatively small (in the range of few newton); therefore, disturbance effects (e.g. friction, noise on data acquisition...) in this case have important contribution.
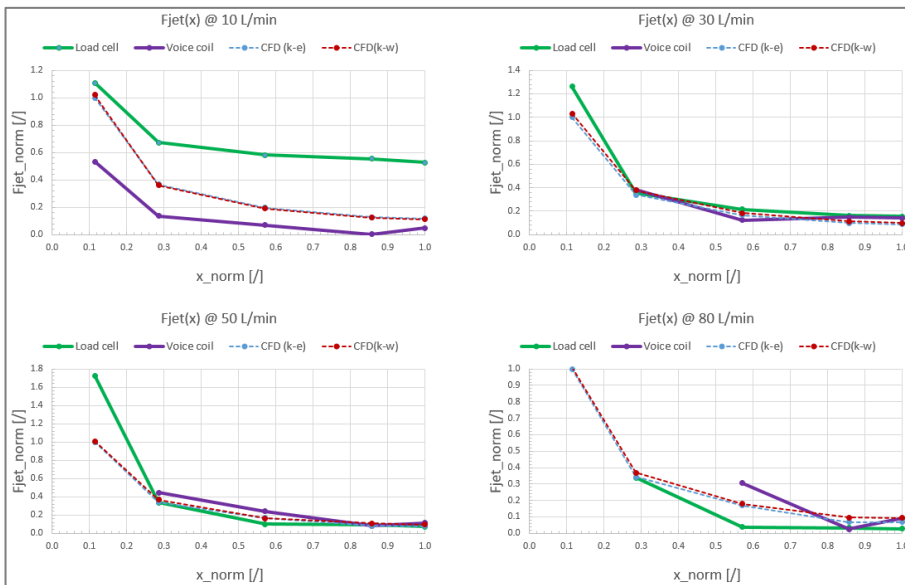
Figure 14: Flow force comparison (non-symmetrical flow conditions).

- Q = 30 l/min: in absolute manner, values of flow forces increase and are therefore less impacted by disturbance effects. Deviation could be observed at minimal spool

opening, using force sensor. The reason is inaccurate position of the spool due to limitation of test equipment and impact of spool dimensional tolerances (stack-up).

– Q = 50 l/min: although there is a good agreement between experiment and CFD analysis, deviation at smallest spool opening becomes even more evident. As proved by additional CFD investigations, position inaccuracy plays important role on flow force evaluation. Sensitivity analysis on spool position accuracy at Q = 50 l/min is depicted on Figure 15. It can be seen that 4 % tolerance[1] on spool position (at smallest spool opening) greatly affects the magnitude of flow force. Based on experimental results, the actual position of the spool during the measurement was closer to lower tolerance.However, as already mentioned, it was not possible to set the spool position more precisely with existing test equipment

- Q = 80 l/min: it can be seen that lateral forces (measured by load cell) greatly affect flow forces, similarly as found in symmetrical conditions at flow rate 80 l/min (see Figure 12). In this particular case, there is a significant deviation of flow forces, measured by voice coil. The reason for this issue is a poor accuracy of the voice coil actuator at given values of flow forces (i.e. actuator works on its limit).

- Influence of higher pressure on B-port (up to 150 bar) has no impact on flow forces.
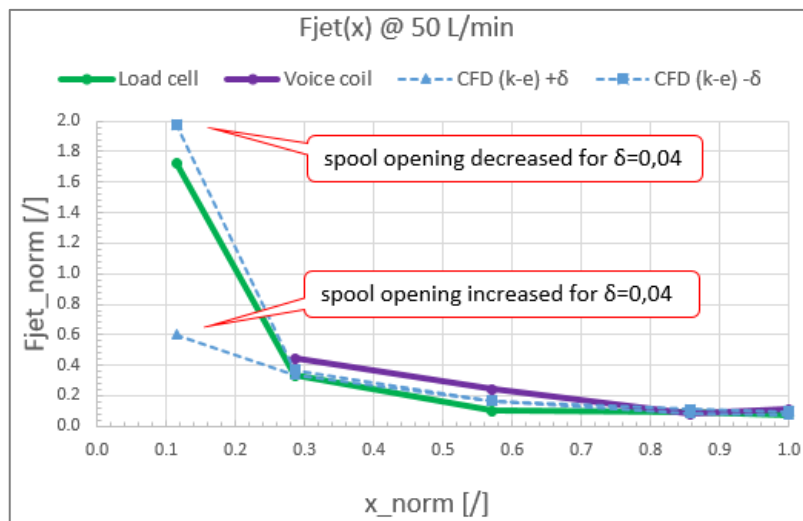
Figure 15: Sensitivity analysis on spool position accuracy at 50 l/min.

---

[1] With respect to the full spool stroke

4   Conclusion

The main goal of investigation is to perform experimental research on (steady) flow forces and validation of numerical tool (CFD) for predicting flow forces in hydraulic valves. Therefore, numerical and experimental approaches have been performed under the same conditions in order to allow for direct results comparison. Based on comparison of experimental and numerical approach, it is possible to conclude that CFD tool (if user respects guidelines and best practices) provide acceptable results from engineering point of view. The tool can be effectively used in the future for development of new valve products or for evaluation of existing components.

4.1   Numerical approach

Computational fluid dynamics (CFD) analysis have been used to perform steady-state flow analysis. For simulation of (static) flow force, the assumption of incompressibility has been taken into account. In this particular case, parameters of oil ISO VG46 at 50 °C has been used. Boundary conditions refers to the inlet flow rate and atmospheric flow rate on the outlet ports. Polyhedral mesh has been used in the core regions along with local mesh refinement. In order to accurately capture near-wall phenomenon, boundary (prism) layers were used. In this particular case, two industry widely used (2-equations) turbulence models have been used: realizable k-ε and SST k-ω. These models have been applied in order to evaluate their impact on results. Default values of parameters in RANS equation have been used. For all simulation tasks, residuals and physical quantities (i.e. pressure drop and flow forces) were taken into account for stopping criteria.

Finally, pressure drop, (axial) flow forces and flow coefficient have been extracted (post-processed) from CFD results. All three post-processing variables show the same trend: the bigger the spool opening, the lower the output values (pressure drop, flow force, flow coefficient, respectively).

4.2   Experimental approach

Two types of measuring devices were developed and manufactured, namely a measuring device with a force sensor and a measuring device with a voice coil actuator. Measurements of flow forces were made on both measuring devices for symmetrical and for non-symmetrical flow conditions. Agreement with CFD analysis is on

acceptable level; for symmetrical flow conditions, flow forces are small and disturbance effects become more pronounced compare to non-symmetrical flow conditions. For the latter, flow forces are much higher. It has also been observed that in general, the experimental results are in agreement with CFD analysis irrespective which turbulent model was used.

By comparing experimental results with a force sensor and voice coil actuator, one can figure out that the results using force sensor are in a better agreement with CFD analysis. The results using voice coil actuator deviated at certain points, especially where values are on the power limit of voice coil actuator. It is worth mention here that more skills would be needed on usage of voice coil actuator in order to ensure better control and output results.

With regard to the spool position accuracy, limitation of the available measuring equipment (and financial resources on projects) did not allow to be more precise.
The problem of lateral (radial) forces was partially solved by applying bigger gap clearance (i.e. using spools with smaller diameters). As a result, higher internal leakage appears which does not meet catalogue data.

4.3   Future work

This project initiate several topics, which need to be discovered more deeply in the future. Namely, special consideration should be devoted to lateral (radial) flow forces, which play an important role of hydraulic component power limit. Correlation between clearance in gap, spool geometry (e.g. cilindricity, circularity) and number of balancing grooves needs to be investigated more deeply.

Further, test equipment represent an important factor for correct and accurate flow force evaluation. Here, accurate spool position is the primary matter of interest. When using voice coil actuator, which has been found to be less accurate compare to load cell, it is essentially to properly control the input and subtract the noise-related phenomena from results. With all those improvements, it is then feasible to perform evaluation of dynamic flow forces (i.e. due to spool/fluid inertia).

References

[1] Yuan, Q. (2014). Flow Forces Investigation through Computational Fluid Dynamics and Experimental Study, Proceedings of the 9th International Fluid Power Conference. Aachen. Germany

[2] Beackon, T. E. (1957). Hydrodynamic Forces on Hydraulic Piston Valves, Engineering, Nov.

[3] Blackburn, J. F., LEE, S. Y. (1952). Contribution Hydraulic Control, Steady state axial forces on control-valve pistons ASME

[4] Clark, R. N. (1957). Compensation of steady-state flow forces in spool type hydraulic valves, ASME

[5] Backe, W. (1961): Möglichkeiten zur Kompensation von Reaktionskräften an Steuerelementen hydraulischer Kreis-läufe, Industrie-Anzeiger, Feb.

[6] Lisowski, E., Czyzycki, W., Rajda, J.(2013).Three dimensional CFD analysis and experimental test of flow force acting on the spool of solenoid operated directional control valve. Energy Conversion and Management

[7] Lugowski, J. (2013). Steady state flow force compensation in a hydraulic spool valve, arXiv.org – Physics – arXiv:1312.1310

[8] Herakovič, N. (2009). Flow force analysis in a hydraulic sliding spool valve. Strojarstvo 51, pp. 555-564

[9] Bordovsky, P., Schmitz, K., Murrenhoff, H. (2016). CFD Simulation and Measurement of Flow Forces Acting on a Spool Valve. 10th International Fluid Power Conference, Dresden

[10] Yuan, Q., Singh, S., Kulkarni, A., Kulkarni, M., Nalgirkar, P., Navale, R. (2014). Flow forces investigation through computational fluid dynamics and experimental study. 9th International Fluid Power Conference, Aachen

[11] Merrit, H. E. (1967). Hydraulic control system, John Wiley and Sons, New York

[12] Yuan, Q., Li, P. Y. (2005). Using Steady Flow Force for Unstable Valve Design: Modeling and Experiments; Journal of Dynamic Systems, Measurement, and Control

[13] Simcenter STAR-CCM+ Documentation 2019.2

[14] Simcenter Amesim Help, rev. 2019.1

[15] Pack Aero (2015): Technical catalogue of voice coil actuator

[16] https://www.poclain-hydraulics.com/_upload/ressources/media/pdf/A52142B.pdf; last visited on 3.7.2019

University of Maribor Press

Hydraulics for a Smart-grapple Attachment

MATEJ LUHENI, RAFKO VOJE & FRANC MAJDIČ

Abstract Modern mobile-hydraulic machines with a hydraulic arm manipulator are operated with in-cab control joysticks. In this study we focused on a hydraulic grapple attachment. Despite its usefulness, operating a hydraulic arm with a grapple attachment can be challenging for novices - and even for experts. This is especially important when working with fragile materials, for example, pipes. Therefore, with these machines it is sensible to install a gripping-force control-assist system. We developed an electro-hydraulic control system with an in-cab touch-display controller based on a Raspberry Pi microcomputer. The system allows different operating modes, depending on the installed attachment, which the user can choose. The electro-hydraulic system allows us to use attachments such as a universal grapple arm, a tree shear grapple arm or a biomass grapple with a saw unit, grapple for bulk materials, etc.

Keywords: • mobile hydraulics • grapple • smart system • graphical interface • wireless connection •

1   Introduction

To operate a hydraulic grapple that is connected to the manipulating arm of a mobile machine, the operator must have a great deal of experience, especially when handling fragile objects [1]. The operator uses a joystick to determine the force with which the object is gripped [2] to [10]. Therefore, in order to prevent damage to fragile objects, such as the drainage pipe in Figure 1, we have developed a hydraulic control system with an adjustable gripping force.

Figure 1: Manipulation of a fragile object.

The construction of the present hydraulic grapple is modular. There is no need to change the whole attachment to provide various work functions, but only to replace the arms and grip units with a quick-locking screw (Figure 2). A large number of different arms can thus be used on one universal unit. In this way a universal grapple with the best grip, a biomass grapple, a log grapple and many others can be obtained and used.

A chainsaw can also be mounted on the main drive unit in combination with a biomass grapple, for example. These attachments require different operating parameters in order to operate properly. The assist-control system we have designed allows for the selection and adjustment of the operating parameters for various attachments via an in-cab touchscreen.

Figure 2: Quick replacement of the arms.

2 Smart-grapple development

2.1 Construction of the grapple

The modular construction of the grapple is shown in Figure 3. The grabber arm is secured to the manipulator arm via a connecting joint. The rotation of the predator is controlled by a gerotor hydraulic motor, which drives the rotary joint that is connected to the main drive unit. For larger predator models, two or more motors are installed. The working arms are fixed to the drive unit via a quick lock.
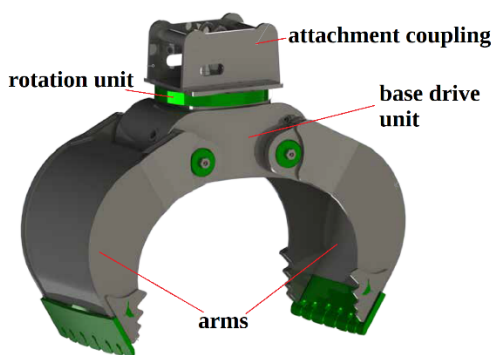
Figure 3: The main subparts of the Modularis-Drive grapple.

Compared to other grapples that use only one hydraulic cylinder, our system uses two (Figure 4), which provide twice the gripping force. In addition, this construction allows the arms to adjust to the shape of the load and thus provide a better grip. With proper settings for the built-in valves, it is possible to choose between synchronous and asynchronous motion.
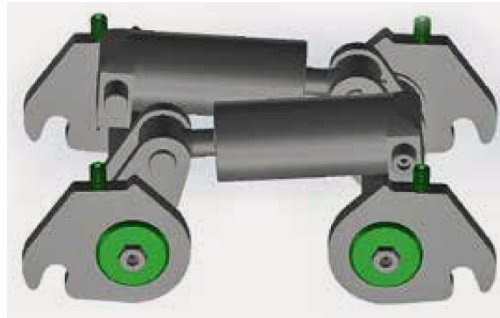
Figure 4: Mechanism for closing and opening the grapple with two hydraulic cylinders.

3.1 Hydraulic system

Figure 5 shows a schematic of the hydraulic system for the designed smart grapple. A proportional two-stage pressure-reducing valve (pos. 6.1) was used to adjust the pressure in the grapple's hydraulic cylinders. In order to monitor the working pressure in real time, a pressure sensor was installed in one of the cylinders (pos. 1a). In this way the operator can always monitor the force acting on the object during use.

The measured value is checked during the operation by the controller, and if there are any overloads an alarm is sounded. The chainsaw is activated with a 2/2-way directional control valve (pos. 6.2), which is activated when the hydraulic motor brake is turned on (pos. 5.2), and which is actuated by a 3/2-way directional valve (pos. 6.5). The hydraulic block described above was installed in the grapple coupling. The oil flow is driven to the hydraulic cylinders via a rotating joint (pos. 4). By adjusting the sequential valves (pos. 2a and 2b) it is possible to choose between synchronous and asynchronous arm movements.
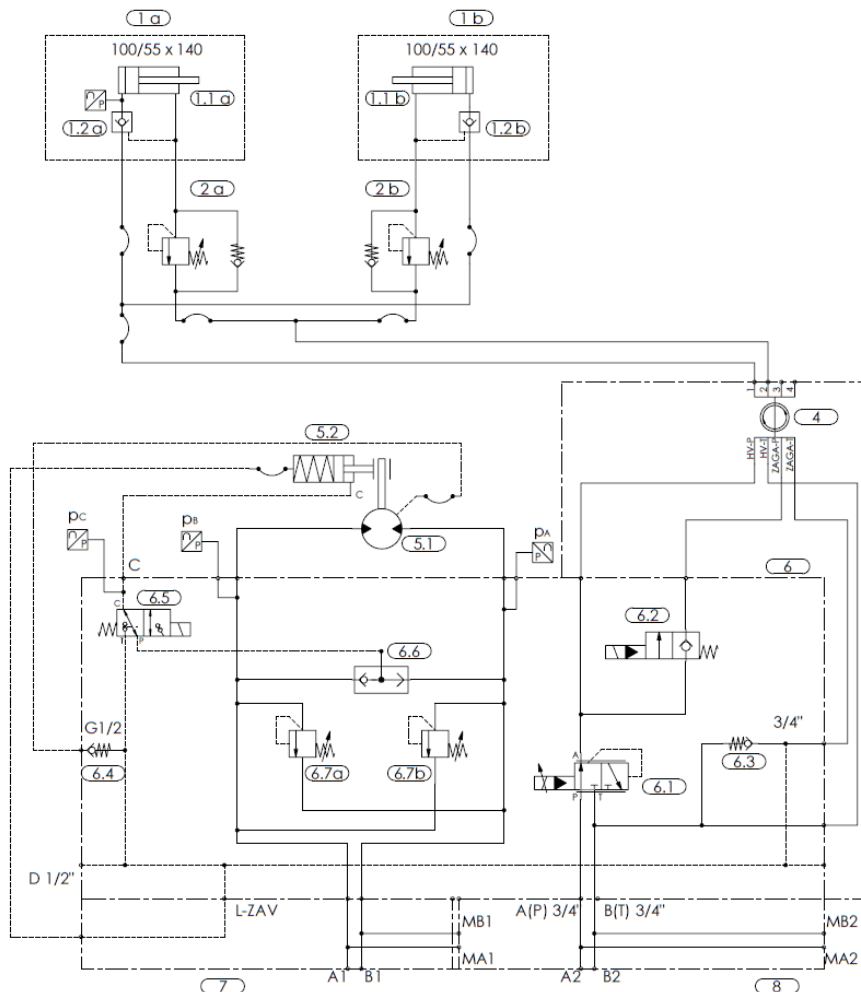
Figure 5: Hydraulic scheme of the designed smart-grapple system.

3.2 Control system

The control system is designed in such a way that the user can choose the operating parameters according to the kind of attachment to be used. Because the grapple is designed so that it can rotate by any number of turns, we had to transmit the signal from the pressure sensor to the controller via a wireless connection. For this purpose we designed the wireless module shown in Figure 6. The module has one analogue voltage input channel for the signal acquisition from 0 to 5 V. The Wi-Fi module ESP-

WROOM-02 is in charge of the signal transmission. The module is powered by a battery that is built into the grapple housing.

Figure 6: Electronic circuit with a ESP-WROOM-02 wireless module

For the main control unit, we used a CM3-Panel touchscreen with a Raspberry Pi computing module as the computer unit. The graphical user interface (GUI), see Figure 7, was created in the Python software environment.
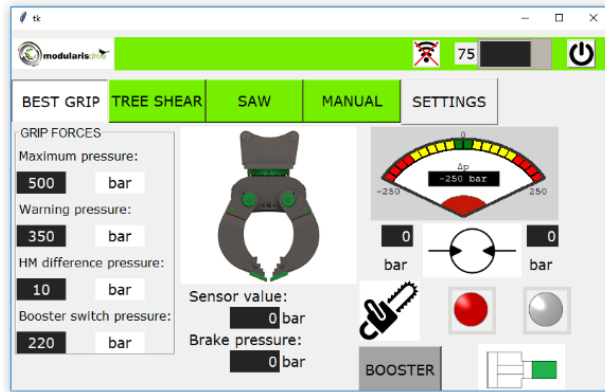
Figure 7: The main menu of the GUI

The interface allows us to select the operating mode and to set the desired parameters for the chosen attachment. The animation between closing and opening of the arms is shown in the middle; below are the values of the cylinder-pressure sensor and the brake sensor. On the right is an animation of the pressure difference for the hydraulic motor connections. To operate the saw, the pressure difference must be small enough for the

operator to switch it on. If the difference is not small enough, the brake must be switched on, after which the green signal light is illuminated. We also predicted the installation of a pressure amplifier, which, due to the limited space in the grapple housing, could not be installed at this stage. The amplifier could be activated via the BOOSTER button through the application.

4   Measurements and validation

In the present initial phase of development we tested the system in the laboratory. We verified the rotation of the grapple, the operation of the brake, and the opening and closing functions of the arms. The control system was also validated in this set. The graph in Figure 8 shows the pressure parameters at the inlet and outlet ports of the designed hydraulic block. The flowmeter was installed directly into the pump, before the mobile hydraulic directional valve, which has a built-in pressure-relief valve with a spring setting pressure of 70 bar. Therefore, in Phase 1, when the valve is closed, oil flows over the relief valve. Phases 2 and 4 are rotation stages, while the intermediate stages are pressure states with the directional valve in the closed position. Due to the limitations of the test facility, we did not reach the operating pressures of the mobile machine, but the results show that the system is working properly.
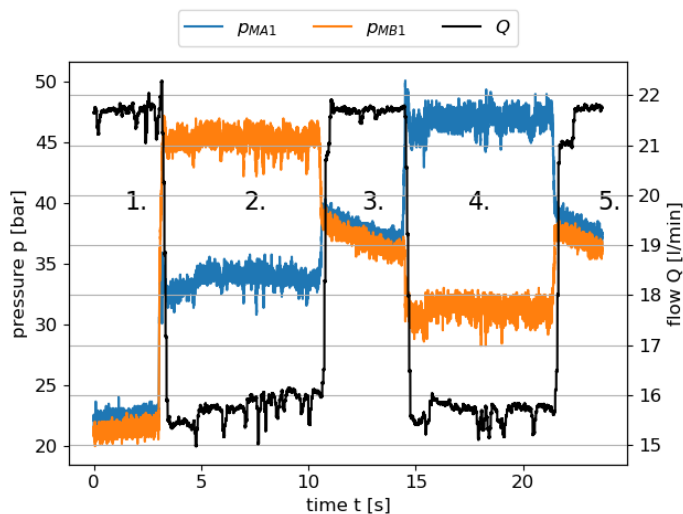
Figure 8: Results of measurements with the rotating grapple in both directions.

The graph in Figure 9 shows a test of the brake's performance that was activated in Phase 3 during the rotation of the grapple. The increase in pressure proves that the brake is working properly and that the operator can use a chainsaw at this stage.
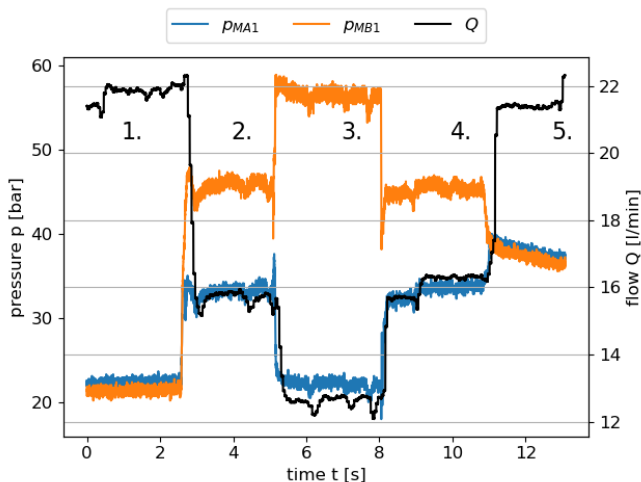
Figure 9: Pressure measurements with hydraulic-brake test.

5   Conclusion

We have designed and built the hydraulic system of a grapple with a control-assist system for installation in the cab of a working machine. Due to the limitations of the test site, at this stage we were unable to test the operation of the pressure-reducing valve to adjust the gripping force, which will be tested in the next phase of the project. The designed system is suitable for pressures up to 350 bar (using a 500 bar pressure amplifier) and hydraulic oil flow rates up to 60 litres/min. The test on the first prototype showed the proper functioning of the device, as well as the correct functioning of the control-assist system.

References

[1]   Chacko, V., Yu, H., Cang, S., Vladareanu, L. (2014). State of the art in excavators. V: Proceedings of the 2014 International Conference on Advanced Mechatronic Systems, ISSN 2325-0690 pp. 481–488 doi:10.1109/ICAMechS.2014.6911593

[2]   Fodor, S., V´azquez, C., Freidovich, L. (2015). Automation of slewing motions for forestry cranes. 15th International Conference on Control, Automation and Systems (ICCAS). IEEE, 2015, pp. 796–801

[3]   Kanan, R., Elhassan, O., Bensalem, R. (2018). An IoT-based autonomous system for workers' safety in construction sites with real-time alarming, monitoring, and positioning strategies. Automation in Construction 88, pp. 73–86

[4]   Akyeampong, J., Udoka, S., Caruso, G., Bordegoni, M. (2014). Evaluation of hydraulic excavator Human–Machine Interface concepts using NASA TLX. International Journal of Industrial Ergonomics 44:3, pp. 374–382

[5]   Teizer, J., Allread, B. S., Fullerton, C. E., Hinze, J. (2010). Autonomous pro-active realtime construction worker and equipment operator proximity safety alert system. Automation in construction 19:5, pp. 630–640

[6]   Parker, R., Bayne, K., Clinton, P. (2016). Robotics in forestry. New Zealand Journal of Forestry 60, pp. 8–14

[7]   Huang, L., Kawamura, T., Yamada, H. (2012). Master-slave control method with force feedback for grasping soft objects using a teleoperation construction robot. International Journal of Fluid Power 13:2, pp. 41–49

[8]   Cheng, P., Oelmann, B., Linnarsson, F. (2011). A local positioning system for loader cranes based on wireless sensors - A feasibility study. IEEE Transactions on Instrumentation and Measurement 60:8, pp. 2881–2893

[9]   Azar, E. R., Kamat, V. R. (2017). Earthmoving equipment automation: A review of technical advances and future outlook. Journal of Information Technology in Construction (ITcon) 22:13, pp. 247–265

[10]   Shimano, Y., Kami, Y., Shimokaze, K. (2014). Development of PC210LCi-10/PC200i-10 machine control hydraulic excavator Technical Report Komatsu Technical Report 2014

University of Maribor Press

Advanced Spool Materials for Friction Reduction in Pneumatic Valves

MARKO ŠIMIC & NIKO HERAKOVIČ

Abstract High-dynamics and low energy consumption of pneumatic and hydraulic valves can be reached if the new light-weight and low-friction spools are used. The main part of the paper presents the thorough experimental study of the tribological conditions inside a pneumatic valve. Within experimental study the friction behaviour of new pneumatic valve spools made of advanced composite materials is analysed in detail. More and more fluid components, such as pneumatic valves, are intended to be used without any lubricant; therefore experimental tests are carried out in dry working conditions. On the basis of the measured actuation force the static and dynamic friction forces are determined. The measured actuation forces of composite spools are compared with the actuation force of conventional aluminium spool. Finally, the new composite spools are validated and the spool material with best friction characteristics, the minimal actuation force, is defined.

Keywords: • pneumatic valve • composite spool • tribology • friction forces • actuation force •

CORRESPONDENCE ADDRESS: Marko Šimic, University of Ljubljana, Faculty of Mechanical Engineering, Ljubljana, Slovenia, e-mail: marko.simic@fs.uni-lj.si. Niko Herakovič, University of Ljubljana, Faculty of Mechanical Engineering, Ljubljana, Slovenia, e-mail: niko.herakovic@fs.uni-lj.si.

1   Introduction

In newer high performance industry applications such as high-response, accurate and energy efficient hydraulic and pneumatic drives, new advanced control components with better characteristics are required. Here, the step response of the valve has a major impact on the improvement of the non-linear behaviour of the drive. The new systems also require low energy consumption control components such as hydraulic and pneumatic valves. These valve characteristics can be improved by using new materials and new sophisticated valve actuators [1]. In many environments, especially in pneumatics, neither grease nor oil particles are permissible. Therefore, a thorough analysis of the interaction between the seal and the sliding counterface in lubricated and dry conditions is required when designing pneumatic valves.

Author in [2] describe the methodology how to design an air-lubricated seals for pneumatic cylinders, which can significantly reduce the friction forces. The importance of seal geometry, material, and roughness of the counterpart (cylinder bore) was investigated in [3] and [4] by means of experimental friction measurements on pneumatic piston seals. In [5] and [6], friction force measurements were carried out on commercial pneumatic cylinders and seals by means of experimental tests and numerical approach; the findings made it possible to develop new low-friction seal geometries. A detailed analysis of the seal–counterface contact provided information on seal behaviour in terms of sealing capability, friction, and wear are presented in [7]. Surface treatment of elastomers and surface texturing as a means of improving tribological properties by reducing friction, wear, and the noise of sliding sealing systems were addressed in [8] and [9], where elastomer surface conditioning with thin-film or thick-film coating and solid lubricant embedded in thermoplastic polyurethane seals and flat samples was investigated. In [10], the cross-section of hydraulic and pneumatic elastomer seals was redesigned and optimized on the basis of a numerical analysis and experimental tests, reducing friction to improve performance.

On the basis of the above cited literature it can be seen that most studies are focused on the development of new sealing components in pneumatic cylinders. Some of the authors analysed the friction behaviour of pneumatic valves, but again, the seals represent the main focus of the studies. There is no paper describing in detail the spools made of different materials and their characteristics, which might also influence the friction behaviour inside the pneumatic valves and consequently the dynamic performance of the valve. Therefore, the study presented in this paper focuses on the

much more important role of the pneumatic valve spool in order to characterise the friction behaviour inside the pneumatic valves and to show how much the actuation force can be reduced.

2   Pneumatic valve

2.1   Design of pneumatic valve

Pneumatic valve treated in this study is shown in the photo of Figure 1. It is a directional spool valve ISO 3 5/3 BCC (5 ports, 3 stages) which is controlled by two on/off pilot stage valves activated with solenoid actuators (Sol_1 and Sol_2).
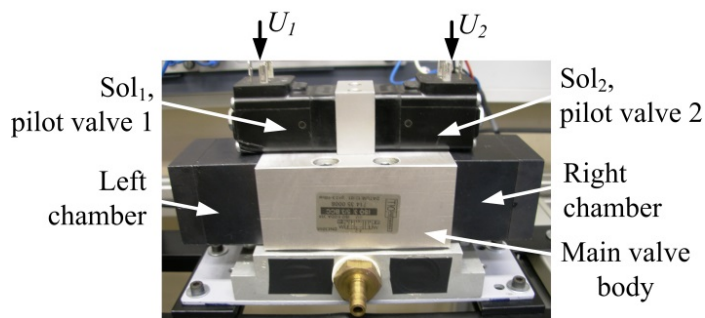
Figure 1: Pneumatic valve ISO 3 5/3 BCC.

The pneumatic valve has two main parts which is analysed and have major effects on the tribological behaviour: the cartridge assembly inserted into the main pneumatic valve body and the valve spool (Figure 2).

The cartridge assembly consists of six NBR (Nitrile Butadiene Rubber) seals, five spacers made of trademark material Lexan 3262R (Polycarbonate-PC with 20 % of glass fibres) and two end aluminium covers (Al cover). The spacers assure the exact position of the seals along the valve body to achieve the valve functionality and to prevent the valve internal leakage between control valve chambers. Arrows, shown in Figure 2 from 1 to 5, presents the valve ports: 1-inlet, 2 and 4- working ports, 3 and 5-air exhaust.
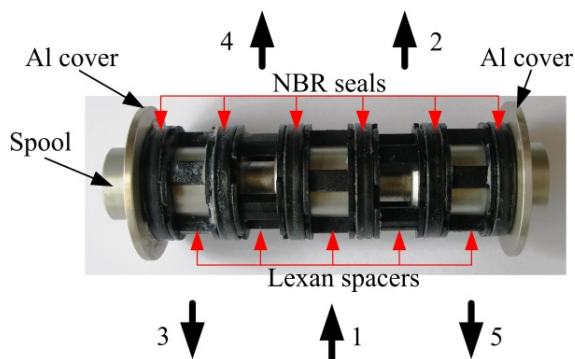
Figure 2: Cartridge-spool assembly.

The functionality of the valve without air leakage is assured with the proper dimensions and tolerances of the seals and the pneumatic spool. The manufacturer provides the inner and outer diameter tolerance for the NBR seals. Material characteristics and the type of the seal are: hardness of 80 Shore, tensile strength of 25 MPa, type PNA 28-2 80NBR878.

2.2   Spools made of advanced material
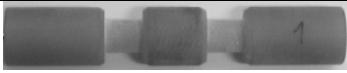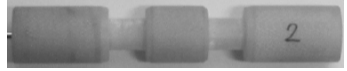
The spools analysed in the experimental study are presented in Table 1. A conventional spool, made of aluminium (Al), is treated as the reference spool while the other spools can be divided into three main groups according to the material classification and manufacturing process [11]:

- 1-FWC (filament-wound composites, spools number 3, 4, 9 and 10),
- 2-ET (engineering thermoplastics, spools number 6 and 8) and
- 3-LC (laminated composites, spools number 1, 2, 5 and 7).

The raw materials used for the spool manufacturing process are epoxy and phenolic resins for the FWC and LC composites. Dicyandiamide is used as hardener and BDMA (benzyl dimethylamine) as accelerator.

For reinforcements, several different fabrics are used: glass fabric, woven roving fabric and cotton fabric for the laminating process, and glass, carbon, PES (Polyester) and aramid for the filament winding process.

Table 1: Pneumatic spools made of different materials.

1		7	
2		8	
3		9	
4		10	
5		Al	
6			

2.3 Friction in a pneumatic valve

The friction forces appear in the contact areas between the pneumatic spool and the seals. The exact contact locations and the friction forces, $F_{tr,i}$, for a single contact can be presented with the cross-sectional view of the 3D model as shown in Figure 3b. The resultant of the friction forces can be calculated by using equation (1) where $F_{n,i}$ represents the normal component of the force produced by the spool mass and the pretension of the seals. The coefficient, μ_i, represents the friction coefficient at a given contact.
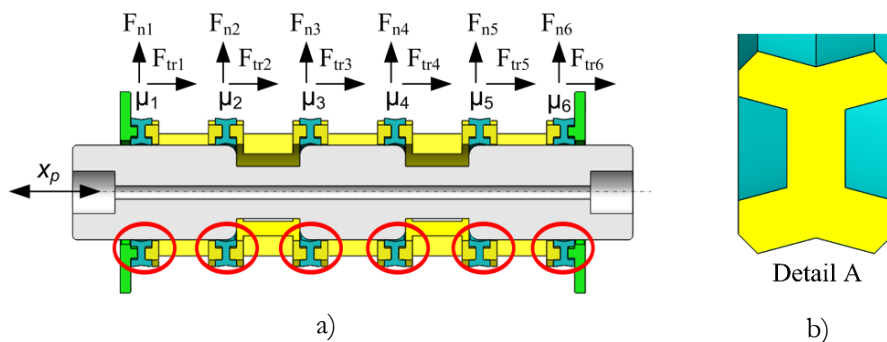
Figure 3: a) location of the spool/cartridge contacts and b) cross-section of the seal.

$$F_{tr} = \sum_{i=1}^{6} F_{tr,i} = \sum_{i=1}^{6} F_{n,i} \cdot \mu_i \tag{1}$$

The cross-section view of a non-deformed seal before the installation is presented in Figure 3b as Detail A. The inner and outer surfaces have a conical shape. The inner conical surface of the seal is deformed when the spool is inserted into the cartridge assembly. That causes the elastic deformation of the seal and the internal compressive stress of the seal which results in the increase of the normal component of the friction force, $F_{n,i}$.

The exact deformation of the seals is very hard to define due to the non-linear deformation of the seal material and the uncertainty of the seal diameter measurement. Therefore, the tolerances of the inner and outer seal diameter provided by the manufacturers represent the only information on which we can rely. Otherwise, the FEM numerical calculation of the seals can be performed to analyse the deformation of the seals during the installation and during the spool movement. As this research focuses on the experimental determination of the actuation forces (friction forces) of spools made of different materials, the tribological phenomena of viscoelastic friction was not studied in detail.

4   Experimental test rig and the measurement method

The test rig for the measurement of the friction force, $F_{tr\,(t)}$, was developed on the basis of the systems described in [12]. The scheme of the experimental setup is shown in Figure 4.

The tested pneumatic valve is placed in a horizontal position to achieve the most common used orientation of the valve in industrial applications. The valve is not under pressure which is different from the normal use. We have to be aware that friction forces increase with the inlet pressure increase due to seal deformation. In this paper the influence of the inlet pressure on friction forces is not considered and will be investigate in further research work.
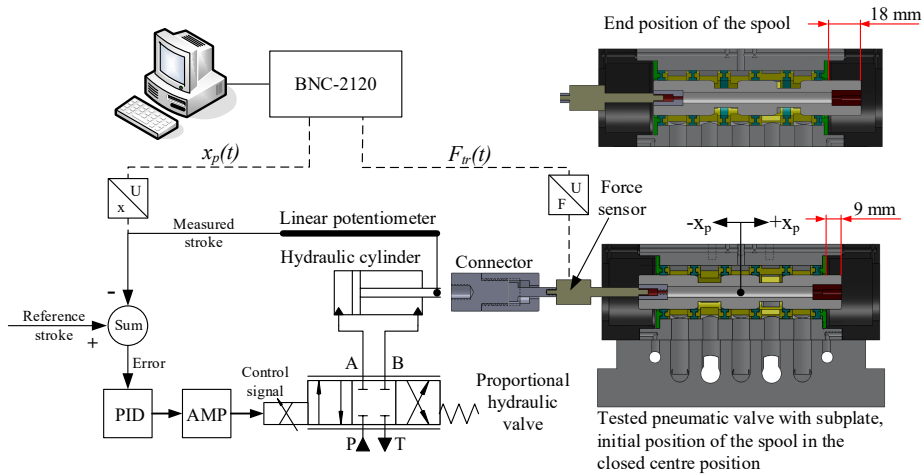
Figure 4: Scheme of the experimental setup.

The hydraulic drive unit and the closed-loop control is used to perform desired stroke and spool velocity cycle. The test rig was developed to ensure the concentric position of the hydraulic cylinder and the pneumatic spool. The connector fixed between hydraulic cylinder and force sensor eliminates the torsion loads.

The spool stroke was measured by linear potentiometer with stroke resolution of 0.05 mm and linearity tolerance below 0.5 %. The force was measured by force sensor HBM KMZ26z with the measuring range from 0 to 500 N and linearity error below 0.2 %. The measuring parameters, the spool stroke, x_p *(t)*, and the friction force, F_{tr} *(t)*, were monitored and saved by using the data acquisition unit BNC-2120 and NI LabVIEW software. The measuring cycle for the determination of the friction force consists of one forward (+x_p) spool stroke. Backward stroke (-x_p) can be neglected due to valve symmetry as well as symetry of the measured results (Figure 5). Five measuring cycles are carried out for a single spool velocity, $\dot{x}_p$.
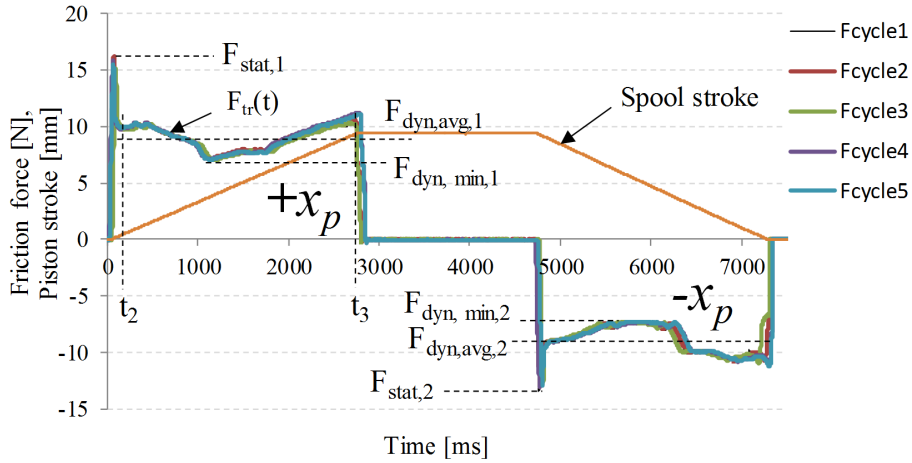
Figure 5: Test cycle and friction characteristic variables for the aluminium spool.

The static friction force, $F_{stat,i}$, is determined at low spool velocity cycle ($\dot{x}_p = 0.2$ mm/s). In this way the inertia force due to spool mass can be neglected. The dynamic friction force represents the measured friction force while the spool is moving with constant velocity. It is calculated as twom main parameters, the average dynamic friction force $F_{dyn,avg,i}$ and the minimal friction force during the cycle $F_{dyn,min,i}$.

5   Experimental results and discussions

The friction force characteristics of pneumatic spools are determined by using the graphical analyses described in Figure 6 and 7. Each measured friction force curve, F_{tr} (t), is analysed in detail where the main parameters, such as static friction force, $F_{stat,i}$ and average dynamic friction force, $F_{dyn,avg,i}$ are determined. The friction force curves as a function of time are presented only for +x direction of the spool stroke due to the valve symmetry. Figure 6 shows the measured friction force curve for Al spool at spool velocity $\dot{x}_p = 30$ mm/s. Results show the unique distribution of the measured friction forces, $F_{tr,m}$ (t), during the spool movement. On the basis of the constant overall contact area between the seals and the spool we expected the typical curve represented with the dotted line, F_{tr} (t). The reason for the deviation can be explained with the non-homogenous surface structure of the spool and the seals material. The tribological behaviour of the contact areas changes during the spool movement, which results in the dynamic friction force deviation. The static friction force is determined at minimal spool velocity, $\dot{x}_p = 0.2$ mm/s (Figure 7). The dynamic friction force curves show that

the increasing of the spool velocity results in a non-linear increasing of the dynamic friction force. Also the shape of the friction curve changes with the change of spool velocity, which can be seen at three different friction curves at spool velocities $\dot{x}_p = 0.2$, 60 and 100 mm/s shown in Figure 7.
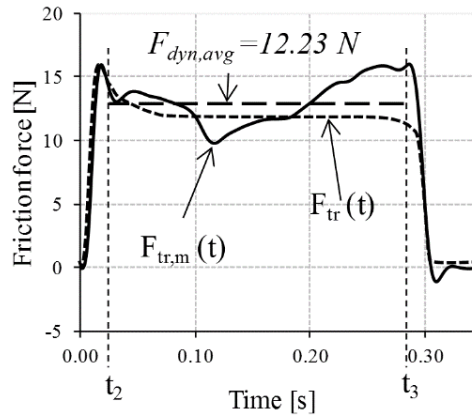
Figure 6: Measured friction force curve, $F_{tr,m}$ (t), of aluminium spool ($\dot{x}_p$ = 30 mm/s).
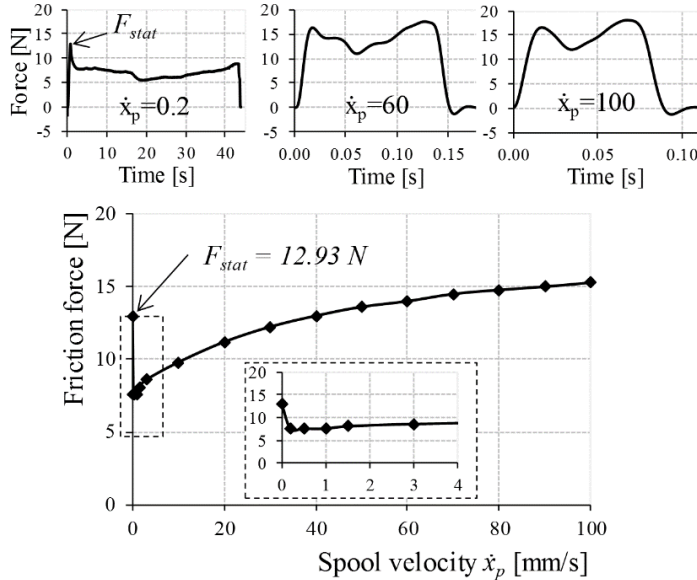
Figure 7: Static and dynamic friction force.

The comparison of pneumatic spools is based on three characteristic forces for each pneumatic spool which are presented in Figure 8. The results are shown for the positive (+x) spool stroke at velocity $\dot{x}_p = 30$ mm/s. Spool diameter, surface roughness and mass of the spools are also considered in the analysis by means of taking into account the correction factors [13].

	1	2	3	4	5	6	7	8	9	10	Al
Fstat	33.4	21.3	14.0	9.7	24.1	32.1	28.3	19.9	27.8	7.4	15.9
Fdyn,avg	22.2	18.7	12.4	8.4	17.9	25.7	26.2	15.8	20.8	6.8	12.2
Fdyn,min	20.6	17.3	11.1	6.5	15.1	22.5	22.7	12.8	18.3	5.3	9.8
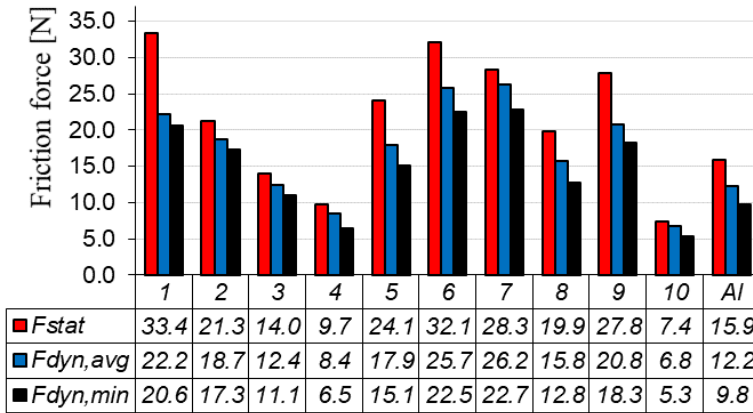
Figure 8: Friction force for different spools.

The highest static and dynamic friction forces at a given spool velocity are generated by the spool 1 followed by spools number 6, 7, 9 and 5. According to the measurement results of the surface roughness and spool mass it can be concluded that the type of material and the type of the surface texture have a major influence on the friction force. This may be confirmed with the spool number 6. It has a high friction force, nevertheless, it has the best surface roughness and the lowest mass. The hardness and the type of the surface texture could also be the reason for such a high friction forces in this cases. It is very interesting that spool 4 made of filament-wound composite has low friction forces although it has much higher surface roughness compared to the other spools. It is made of woven cotton fabrics with phenolic resins as the coupling agent. In this case, the self-lubricating conditions can be the reason for the low friction forces. Spools 2, 3 and 8 have very similar tribological characteristics as the aluminium spool.

The spool number 10 has the lowest friction force. It has similar surface roughness and spool mass compared to the others spools and therefore the reason for low friction forces could not be identified at this point. A detail FEM analysis, which will be performed in the future, can give the answer of micro holes influence on the friction behaviour in dry conditions under pressure.

Figure 9 presents the friction characteristic curves as a function of spool (piston) velocity for 10 spools made of different materials and compares them with the reference aluminium spool. The lowest friction forces are achieved using the laminated composite spool number 10 followed by spools number 4, 3 and Al. The laminated composite spool number 7 and spool number 6 made of engineering plastic have the worst characteristics. It can be seen that laminated composites have better tribological characteristics compared to the filament-wound composites. Laminated composites are much easier to machine and therefore the surface roughness is better and dimension tolerances can be achieved easier. According to the results, we can conclude that spools number 3, 4 and 10 have better friction behaviour compared to the Al spool.
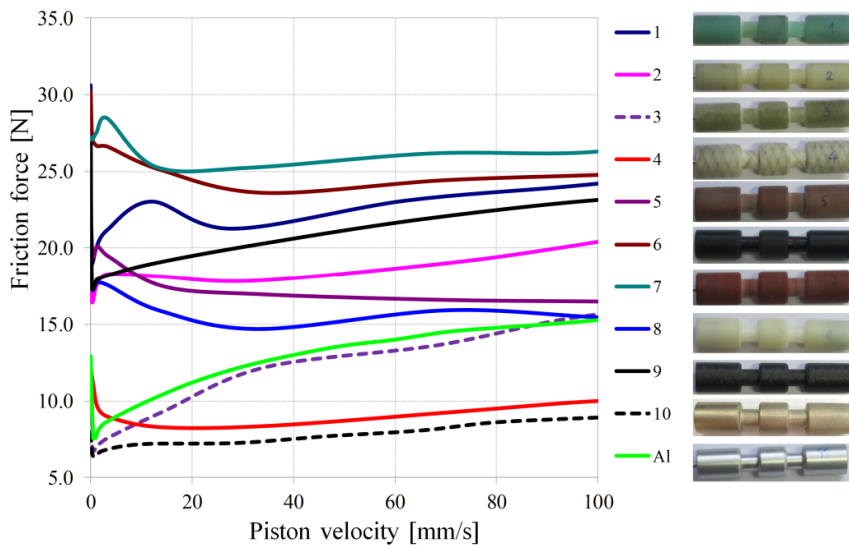
Figure 9: Friction force as a function of piston velocity.

6   Conclusion

In this study, we have done thorough experimental analyses of the tribological behaviour of new pneumatic spools made of different composite materials and engineering plastics. The main goal was to investigate the material influence on the friction force which appears in the contact areas between the spool and the seals. Especially the dynamic friction force is important for the use in switching control pneumatic valves used in servo pneumatic applications.

The results of the experimental testing show that the friction force can be reduced significantly if the proper material for the pneumatic spool is used. Spool material has a huge influence on manufacturing process and consequently on different dimension and surface roughness accuracy. Those initial spool parameters have major impact on the friction behaviour. Not only the size of the static and dynamic friction forces, but also the shape of the friction force curve varies a lot. Each spool made of a different material has its own unique shape of the friction force curve according to the non-homogenous surface structure of the single spool. The results of static friction forces show that the spool diameter has major impact. In general the spool with larger diameter corresponds to higher static friction force. In some cases the self-lubricated basic material helps to decrease not only static but especially the dynamic friction forces. On the basis of the experimental results we find that the best tribological characteristics related to the minimal friction force are achieved with the composite spool No. 10 manufactured with filament winding process. The main reason for low friction forces is the base material: polymer composite material based on complex nickel alloy. Spools No. 3, 4 and 10 have better friction characteristics compared to the aluminium spool while other composite spools have much higher static and dynamic friction forces.

References

[1]   Heraković, N., Bevk, T. (2010). Analysis of the Material and the Actuator Influence on the Characteristics of a Pneumatic Valve. *Materials and technology, 44,* pp. 37-40

[2]   Belforte, G., Mazza, L., and Visconte, C. (2014). Design methodology for air-lubricated seal. *Tribology International, 75*, doi.org/10.1016/j.triboint.2014.03.017, pp. 104-110

[3]   Belforte, G., Raparelli, T., Velardocchia, M. (1994). Study of the Behaviour of Lip Seals in Pneumatic Actuators. *Lubrication Engineering, 49*, pp. 775-780

[4]   Belforte, G., Conte, M., Manuello, A., Mazza, L. (2011). Performance and Behaviour of Seals for Pneumatic Spool Valves. *Tribology Transaction, 54*, pp. 237-246 doi: 10.1080/10402004.2010.538488

[5]   Schroeder, L. E., Singh, R. (1993). Experimental Study of Friction in Pneumatic Actuator at Constant Velocity. *Journal of Dynamical Systems Measurement and Control, 115(3)*, pp. 575-577. DOI: 10.1115/1.2899143

[6]   Belforte, G., Mattiazzo, G., Mauro, S. (2003). Measurement of Friction Force in Pneumatic Cylinders. *Tribotest journal, 09*, 10(1), 33-48. doi.org/10.1002/tt.3020100104

[7]   Belforte, G., Conte, M., Manuello, A., Mazza, L., Visconte, C. (2009). Experimental and Numerical Evaluation of Contact Pressure in Pneumatic Seals. *Tribology International, 42(1)*, pp. 169-175. doi.org/10.1016/j.triboint.2008.04.010

[8]   Verheyde, B., Vanhulsel, A., Rombousts, M., Meneve, J., Havermans, D., Wangenheim, M. (2009). Influence of Surface Treatment of Elastomers on Their Frictional Behaviour in Sliding Contact. *Wear, 266(3–4)*, pp. 468-475. doi.org/10.1016/j.wear.2008.04.040. doi.org/10.1016/j.wear.2008.04.040

[9]   Kligerman, Y., Etsion, I., Shinkarenko, A. (2005). Improving Tribological Performance of Spool Rings by Partial Surface Texturing. *Journal of Tribology, 127(3)*, pp. 632-638

[10]   Belforte, G., Manuello, A., Mazza, L. (2006). Optimization of the Cross Section of an Elastomeric Seal for Pneumatic Cylinders. *Journal of Tribology, 128*, pp. 406-413. doi: 10.1115/1.2162915

[11]   Dimeski D., Srebrenkoska V., Bogoeva-Gaceva G., Stefof, V. (2010). Research report - Development of new actuators, materials and technology for the production of advanced pneumatic and hydraulic valves. *Eureka project E4548 DE_AMATECH*

[12]   Belforte, G., Bertetto, M. A., Mazza, L. (2012). Test rig for friction force measurements in pneumatic components and seals. *Proceedings of the Institution of Mechanical Engineers, Part J: Journal of Engineering Tribology.* doi.org/10.1177/1350650112453522

[13]   Šimic, M., Heraković, N. (2016). Experimental Analysis of Tribological Behaviour of Advanced Composite Spools Used in Commercial Pneumatic Spool. *Tribology International, 97*, pp. 151-162. doi.org/10.1016/j.triboint.2016.01.012

University of Maribor Press

Influences on the Efficiency of a Water-Hydraulic Motor

FRANC MAJDIČ

Abstract Due to the relative motion between different mechanical parts, different contacts are formed. These contacts are very often lubricated with oil. Presently, environmental protection and ecological awareness are becoming increasingly important, which in turn has resulted in a shift to a low-carbon society. As a result, water, as an alternative to oil, has gained interest over the years. On the one hand, water is less environmentally damaging as a lubricant than oil, but on the other hand, water has very poor lubrication properties, as its viscosity is 100 times lower than the viscosity of oil. However, these limitations might be overcome with the appropriate surface engineering. Tribological tests were performed in oil and water for two different contacts: steel/steel and steel/DLC. The DLC was recognized as a very promising option, which ensures low friction and low wear. The DLC was deposited on a real hydraulic part in an orbital hydraulic motor and tested under real industrial conditions.

Keywords: • water-hydraulics • hydraulic motor • orbital • tribological tests • DLC coating •

CORRESPONDENCE ADDRESS: Franc Majdič, University of Ljubljana, Faculty of Mechanical Engineering, Ljubljana, Slovenia, e-mail: franc.majdic@fs.uni-lj.si.

1   Introduction

Fluid power is one of the ways that we can transfer power. Of course, the main part of fluid power is the fluid. Its main features are: power transfer, lubrication, cooling, removal of insoluble particles, corrosion resistance, sealing, foaming resistance, availability in large quantities, chemical and physical stability, etc. Different hydraulic fluids are in use. Mineral hydraulic oils are the most used hydraulic fluids. They are used in more than 85 % of cases. The second most used fluid group is the heavy, flammable hydraulic fluids and the third is bio-degradable fluids. This last group of hydraulic fluids includes ionic liquids, tap water and other alternatives [1], [2], [3].

One of most promising solutions to prevent harmful consequences for the environment is to use tap water as the hydraulic pressure medium. This solution is harmless to the environment, but it is very difficult to realize [4], [5], [6]. One reason being that only some relatively simple, water-hydraulic components exist on the market today. Despite many years of water-hydraulics research, there is still insufficient understanding of the mechanisms and performance and, consequently, the available component designs. Some of the reasons lie in many of the specifics that water has compared to oil in hydraulic systems, which already affect the research and development phase, and later – in the long term – the performance of the water-hydraulic system. Some of these are described below. For example, for any research on water hydraulics for real-scale components, home-made components and test rigs are required, because they do not exist on the market. However, this is associated with costs and technical problems. The much lower viscosity of water compared to oil causes a high rate of leakage when using clearances typical for oil, while reduced clearances result in excessive wear and high friction. Higher working temperatures, which are still common for oil hydraulics, i.e., around 70 or 80 °C, are hardly acceptable for water in hydraulic systems, because of the evaporation at local contact spots [7].

In water, micro-organisms develop with time. This causes several problems with chemical changes to the water and the growth of algae, which results in sediments. The tribological properties of conventional materials (typically stainless steel) in water are unfavourable, while comparable material selection is poor, and their properties are unknown. For example, a new class of high-potential diamond-like-carbon materials [8] to [18] that showed excellent properties in a variety of conditions that are in many ways comparable to those in water hydraulics have not been investigated in detail for this application yet. Furthermore, another class of materials that has already confirmed

excellent properties also suitable for water [19], [20], [21], i.e., ceramics, are probably too brittle for the required dynamic conditions in water hydraulics or are too expensive for precise manufacturing, but this has not been investigated either. Corrosion and cavitation are other well-known problems related to tribological performance and the lifetime of components. Therefore, research into the chemical and tribological properties that affect the life and performance, as well as the dynamic characteristics, of water hydraulics, are required for the successful development of new components, which is necessary for the wider use of water in power-control hydraulics. One of required water-hydraulic components is a high-torque hydraulic motor [22]. Such a motor works well with mineral hydraulic oil. The aim of this investigation is to find suitable material pairs for the sliding surfaces lubricated with water under high loads. Different tribological tests were carried out.

2   Orbital hydraulic motor

This study deals with the low-speed, but high-torque, orbital hydraulic motor (Figure 1), which normally operates under oil-lubricated conditions [8]. Such a hydraulic motor is a highly loaded mechanical component that converts hydraulic energy into the rotational motion of the shaft.

Figure 1: Investigated orbital hydraulic motor (Φ 174 mm × 250 mm).

The most important parts of a hydraulic motor, regarding the principle of operation, are: the inner rotor, the outer ring (Figure 2c), the housing (Figure 2d) and the valve plate (Figure 2b). A combination of an appropriate geometry of the mechanical parts, the holes in the valve plate and the pressure differences in the lobes ensures that the rotational speed of the shaft is up to 25 min^{-1} and that the torque is up to 1000 Nm.

a)   b)   c)   d)
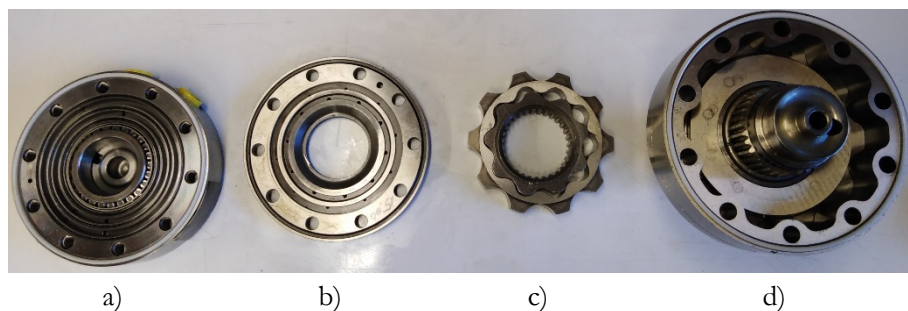
Figure 2: Parts of a disassembled orbital hydraulic motor.

3   Experimental study

Tribological tests were made using the ball-on-flat-disc testing geometry. A commercially available reciprocating sliding device (Cameron Plint TE77) was used. The specimen (ball and disc) is shown in Figure 3. We tested a variety of different specimens. Figure 3 shows two discs (left with a DLC coating and right without – the material is AISI 440). The diameter of ball was 25 mm and the diameter of the disc was 20 mm.

a)   b)   c)
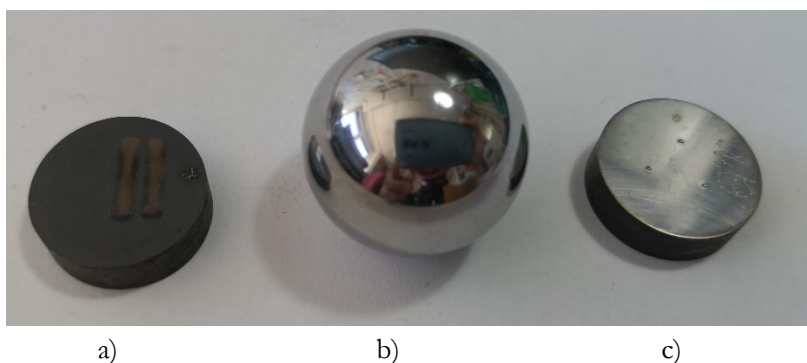
Figure 3: Specimens for tribological tests: a) disc with DLC, b) ball and c) disc AISI 440.

The conditions of the tribological tests:

Fluid: Mineral hydraulic oil / water
Material pairs: AISI440/AISI440 and AISI440/DLC coating
Hardness of sliding surface: 60 HRC
Roughness: 0.05 μm / 0.2 μm

4 Results

Figure 4 shows the experimental results for the coefficient of friction (COF) using two similar surfaces of stainless steel AISI 440 at two different roughnesses (0.05 μm and 0.2 μm), three different normal forces (14 N, 40 N and 112 N) lubricated with a) oil and b) water. The highest COF of AISI 440/AISI 440 lubricated with oil was 0.115 at a normal force of 14 N and a roughness of 0.2 μm. The lowest COF in the oil was 0.07 at a normal force of 112 N and a surface roughness of 0.05 μm. The highest COF during water lubrication was 0.46 at a normal force of 112 N and a roughness of 0.2 μm. This is four times higher in comparison to oil under the same conditions.
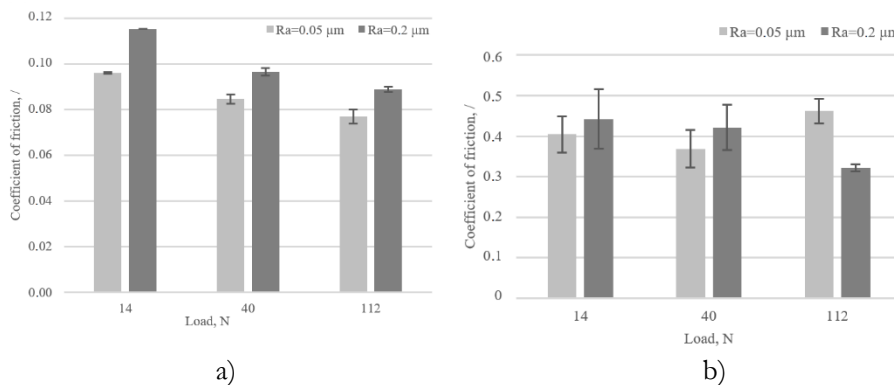
**Figure 4: Measured friction coefficient of stainless steel AISI440/AISI440
a) with oil, b) with water.**

Figure 5 shows the experimental results for the coefficient of friction (COF) for one surface (disc) with the DLC coating against the AISI 440 ball. The roughness of both surfaces was 0.05 μm. The test was conducted at three different normal forces (14 N, 40 N and 112 N) lubricated with a) oil and b) water. The highest COF of the DLC/AISI 440 lubricated with oil was 0.08 at a normal force of 112 N. The lowest COF in oil was

0.07 at a normal force of 14 N. The highest COF during water lubrication was 0.07 at a normal force of 14 N and the lowest COF in water was 0.06 at a normal force of 112 N. This is 15 % lower in comparison to oil under the same conditions.

a)

b)
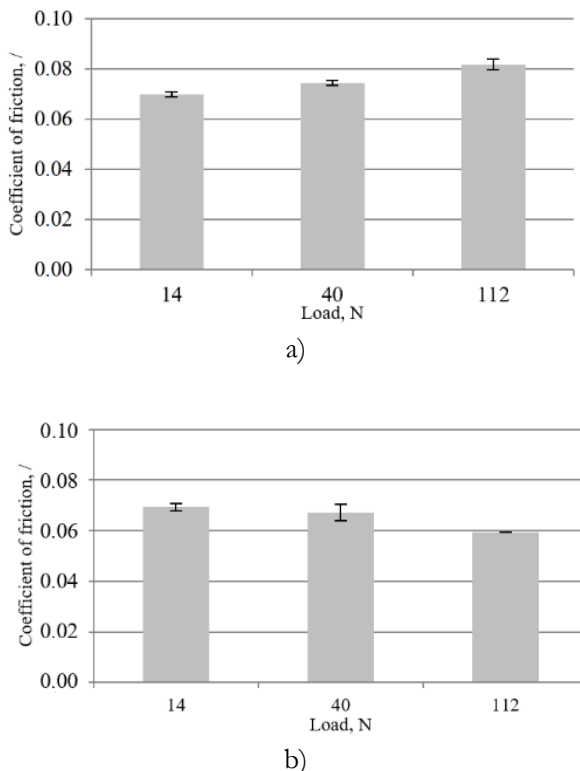
Figure 5: Measured friction coefficient of DLC against AISI 440 a) with oil, b) with water.

5   Conclusions

Basic tribological investigations with stainless-steel AISI 440 against the same material lubricated separately with oil and with water were undertaken. The coefficient of friction (COF) in the contact of the AISI 440 lubricated with oil was low, as expected, while the COF was four times higher in water under the same conditions. After the hard DLC coating was applied to the disc, it was found to greatly reduce the COF in water, even below the values of the COF in oil.

DLC coatings are very promising for water hydraulics, especially for a water hydraulic motor. After depositing the DLC coating on the floating ring of the hydraulic motor, it began to work.

References

[1]   Lovrec, D., Kambič, M. (2007). Hidravlične tekočine in njihova nega, 1.izdaja, Univerza v Mariboru, Fakulteta za strojništvo, Maribor
[2]   Kambič, M. (2015). Raziskava primernosti ionskih tekočin za uporabo v hidravličnih sistemih, doktorska disertacija, Univerza v Mariboru, Fakulteta za strojništvo, Maribor
[3]   Majdič, F. (2010). Voda kot hidravlična kapljevina v pogonsko-krmilni hidralviki, doktorska disertacija, Univerza v Ljubljani, Fakulteta za strojništvo, Ljubljana
[4]   Kalin, M., Vižintin, J. (2006). A comparison of the tribological behaviour of steel/steel, steel/DLC and DLC/DLC contact when lubricated with mineral and biodegradable oils, Wear 261(1), pp. 22-31
[5]   Adhvaryu, A., Erhan, S. Z., Perez J. M. (2004). Tribological studies of thermally and chemically modified vegetable oils for use as environmentally friendly lubricants, Wear 257 (3), pp. 359-367
[6]   Kalin, M., Vižintin, J. (2005). The tribological performance of DLC-coated gears lubricated with biodegradable oil in various pinion/gear material combinations, Wear 259, pp. 1270-1280
[7]   Kalin, M. (2004). Influence of flash temperatures on the tribological behaviour in low-speed sliding, a review, Mater. sci. eng., A Struct. mater. A374 (1/2), pp. 390-397
[8]   Donnet, C., Grill, A. (1997). Friction control of diamond-like carbon coatings, Surface and Coatings Technology 94-95, pp.456-462
[9]   Fontaine, J., Donnet, C., Grill, A., Mogne, T. L. (2001). Tribochemistry between hydrogen and diamond-like carbon films, Surface and Coatings Technology 146-147, pp. 286-291
[10]   Kalin, M., Vižintin, J., Barriga, J., Vercammen, J., Van Acker, K., Arnšek, A. (2004). The effect of doping elements and oil additives on the tribological performance of boundary-lubricated DLC/DLC contacts, Tribology Letters 17, pp. 679-688
[11]   Matthews, A., Leyland, A., Holmberg, K., Ronkainen, H. (1998): Design aspects for advanced tribological surface coatings, Surface and Coatings Technology 100-101, pp. 1-6
[12]   Kalin, M., Vižintin, J., Vercammen, K., Barriga, J., Arnšek A. (2006). The lubrication of DLC coatings with mineral and biodegradable oils having different polar and saturation characteristics, Surface and Coatings Technology 200, pp. 4515-4522
[13]   Neville, S. Matthews, A. (2007). A perspective on the optimisation of hard carbon and related coatings for engineering applications, Thin Solid Films 515, pp. 6619-6653
[14]   Andersson, J., Erck, R. A., Erdemir, A. (2003), Friction of diamond-like carbon films in different atmospheres, Wear 254, pp. 1070-1075

[15]   Kalin, M., Roman, E., Vižintin, J. (2007). The effect of temperature on the tribological mechanisms and reactivity of hydrogenated, amorphous diamond-like carbon coatings under oil-lubricated conditions, Thin Solid Films 515, pp. 3644-3652

[16]   Velkavrh, I., Kalin, M., Vižintin, J. (2008). The performance and mechanisms of DLC-coated surfaces in contact with steel in boundary-lubrication conditions – a review, Strojniški vestnik – Journal of Mechanical Engineering 54, pp. 189-206

[17]   Barriga, J., Kalin, M., Van Acker, K., Vercammen, K., Ortega, A., Leiaristi, L. (2006): Tribological performance of titanium doped and pure DLC coatings combined with a synthetic bio-lubricant, Wear 261(1), pp. 9-14

[18]   Kano, M. (2006). Super low friction of DLC applied to engine cam follower lubricated with ester-containing oil, Tribology International 39, pp. 1682-1685

[19]   Andersson, P. (1992). Water lubricated pin-on-disc tests with ceramics, Wear 154, pp. 37-47

[20]   Zhou, F., Adachi, K., Kato, K. (2006). Sliding friction and wear property of a-C and a-CNx coatings against SiC balls in water, Thin Solid Films 514(1), pp. 231-239

[21]   Novak, S., Kalin, M., Kosmac, T. (2012). Chemical aspects of wear of alumina ceramics, Wear 250 (1/12), pp. 318-321

[22]   Strmčnik, E., Kokot, G., Majdič, F. (2016). Vpliv velikosti izvrtin v ventilski plošči na volumetrični, mehansko-hidravlični in skupni izkoristek počasi vrtečega se hidravličnega motorja tipa gerotor, Ventil 22 (6/12), pp. 484-492

University of Maribor Press

Mean Time to Failure of a Hydraulic Valve

NEJC NOVAK, ANŽE ČELIK, MARKO ŽUST & FRANC MAJDIČ

Abstract Nowadays, great emphasis is put on the safety and reliability of machines and devices. One of the newer standards for the safety of machines and devices is SIST EN ISO 13849-1. An important topic in this standard is the determination of the mean time to failure of a component or an entire device. The objective of this study was to determine the mean time to dangerous failure (MTTFD) of a hydraulic brake valve. The valve is a key element in a braking system for heavy-duty machines. Since the valve is also a safety part of the control system, its potential failure would result in a hazardous situation for people. Therefore, it is necessary to prove analytically and experimentally the useful operating time of the brake valve. To do this, a sustainability test was carried out. After 1000 hours of testing, the test was stopped and the mean time to failure of the valve was calculated. None of the five valves failed during testing.

Keywords: • hydraulic brake valves • mean time to dangerous failure (MTTFD) • reliability • safety functions • pedals •

CORRESPONDENCE ADDRESS: Nejc Novak, University of Ljubljana, Faculty of Mechanical Engineering, Ljubljana, Slovenia, e-mail: nejc.novak077@gmail.com. Anže Čelik, Poclain Hydraulics d.o.o., Žiri, Slovenia, e-mail: anze.celik@poclain.com. Marko Žust, Poclain Hydraulics d.o.o., Žiri, Slovenia, e-mail: marko.zust@poclain.com. Franc Majdič, University of Ljubljana, Faculty of Mechanical Engineering, Ljubljana, Slovenia, e-mail: franc.majdic@fs.uni-lj.si.

1 Introduction

The hydraulic brake valve is a pressure-reducing valve and belongs to the group of control hydraulic components. The function of this valve is the proportional control of hydraulic cylinders that are used for the braking of working machinery. It is controlled by the foot through a pedal in the vehicle cabin. The brake valve is part of the braking system, which is considered as one of the most important systems in any type of vehicle. These systems must provide the function of braking and are therefore usually designed to operate in the event of the failure of one of the components. We say that in such a system several components that perform the same function are connected in parallel. In the case of a brake valve, it is important to perform the braking function, i.e., a safety function. If this function fails, people's safety is compromised. In order to increase the level of safety, we tried to determine the mean time to failure of the brake valve. One of the newer standards for the safety of machines and devices is SIST EN ISO 13849-1. It describes a method for determining the mean time to failure of the safety part of the control system and calculating the reliability of this part. To determine this time, it is necessary to determine the criteria or functional characteristics of the valve, for which we can claim that the valve failed. In order to determine the mean time to failure, we carried out a sustainability test on five brake valves. In addition, we needed to design a test station for this valve. The outlet working pressure (F1 and F2) was important for the valve; therefore, we monitored it throughout the test.

2 Summary of the standard SIST-ISO 13849-1

2.1 Determining the mean time to failure according to the standard SIST-ISO 13849-1

The standard SIST-ISO 13849-1 [1] is an example of a calculated and evaluated mean time to dangerous failure ($MTTF_D$) value for one component in a hydraulic system. A dangerous malfunction is defined as a failure in the standard that results in a loss of safety function.

Instead of using a fixed $MTTF_D$ value (e.g., 150 years) as listed in Table C.1 of Annex C [1], it can be calculated using the B_{10D} concept, which is used for pneumatic, mechanical and electromechanical components, and also for hydraulic components if the manufacturer can provide results. The average number of cycles until 10 % of the components fail dangerously (B10D) is determined by the manufacturer. The hazardous

failure mode of the component must be defined, e.g., sticking of the control piston in the end position of the valve. If all the components did not fail at the time of testing, then a more detailed analysis of the component's reliability is needed. This analysis takes into account that not all the components were defective. With B_{10D} and the average number of cycles per year (n_{op}), the $MTTF_D$ is defined by equation (1).

$$MTTF_D = \frac{B_{10D}}{0,1 \cdot n_{op}} \quad [years] \tag{1}$$

The ISO 13849-1 reliability methods assume that the defects are exponentially distributed over time: $F(t) = 1 - \exp(-\lambda dt)$. The constant level of hazardous failures (λ_D) can be calculated by knowing the probability of failure ($F(t)$) at a certain operating time (t). Thus, λ_D, for the time at which 10 % of the components fail (T_{10D}), is estimated by equation (2).

$$F(T_{10D}) = 1 - e^{-\lambda_D \cdot T_{10D}} = 10\ \%$$

$$\lambda_D = -\frac{\ln(0,9)}{T_{10D}} = \frac{0,10536}{T_{10D}} \approx \frac{0,1}{T_{10D}} \tag{2}$$

For an exponential distribution, equation (3) is assumed.

$$MTTF_D = \frac{1}{\lambda_D} \tag{3}$$

Using equation (1), the $MTTF_D$ value can be calculated. Because the calculation is performed using the B_{10D} concept, the average number of cycles until 10 % of the components fail dangerously is needed.

Reliability of the components in the testing without failures

The reliability of the components can be calculated by means of a cumulative binomial distribution, taking into account the number of samples (n), the number of samples that failed (f) and the probability (R_{TEST}) that each sample is defective. The confidence level (CL) tells us how confident we are about the test.

$$1 - CL = \sum_{i=0}^{f} \frac{n!}{i! \cdot (n-i)!} \cdot (1 - R_{TEST})^i \cdot R_{TEST}^{(n-i)} \tag{4}$$

For the probability of R_{TEST}, we can assume the exponential or Weibull distribution of the components' failure. In the exponential distribution, the previously described equation (2) would be taken into account, expressing the test time (t_{TEST}) and the time that we would like to demonstrate (t_{DEMO}), and merging with equation (4) to take into account that no component was defective f = 0.

$$t_{TEST} = t_{DEMO} \cdot \frac{1}{n_{samples}} \cdot \frac{\ln(1 - CL)}{\ln(R_{DEMO})} \tag{5}$$

Equation (5) gives the test time (t_{TEST}) to ensure the time of the component (t_{DEMO}), the reliability (R_{DEMO}), and the confidence level in the test (CL) for n samples. The above equation can be rearranged by listing only the reliability demonstration factor (RDF), which represents an extension or shortening of the test in real time and under normal circumstances. Thus, we obtain equation (6).

$$RDF = \frac{1}{n_{samples}} \cdot \frac{\ln(1 - CL)}{\ln(R_{DEMO})} \tag{6}$$

The demonstration factor is a coefficient that tells for how long the test time should be extended (RDF > 1) or shortened (RDF < 1) to demonstrate the real running time of the component. The value depends greatly on the number of samples to be tested. In the event that a large number of samples are being tested, it is possible to perform tests much more quickly to ensure that the reliability of the component is sufficiently high. In the case of the cumulative binomial distribution equation (4), the probability R_{TEST} can be a Weibull distribution and we obtain a slightly different equation. Nevertheless, due to the nature of the brake valves (several possible failure modes), the same equation will be obtained as in the exponential distribution, because the parameter that lists the shape of the function in the Weibull's distribution is equal to 1.

3 Hydraulic brake valve and test station

Hydraulic valves belong to a third group of hydraulic components that are primarily intended to control the hydraulic components of the hydraulic system [2]. Pressure-reducing valves, with their adjustable settings, determine the size of the outlet pressure, regardless of the size of the inlet pressure in the valve.

This section of the article presents more detailed pressure-reduction valves that control or brake hydraulic cylinders and are so-called brake valves. Hydraulic brake valves in combination with a pedal are designed to brake vehicles such as construction machinery, transport vehicles and agricultural and forestry machinery and, last but not least, special vehicles.

3.1 Purpose of use

The brake hydraulic valves control the pressure in the braking system. This pressure is proportional to the thrust on the pedal. This gives the driver the feeling of braking. The valves are designed for use in vehicles equipped with other hydraulic aggregates. This action eliminates the need for a separate hydraulic fluid system. There are single-circuit brake systems for valves, two-circuit valves and others [3] (Figure 1).
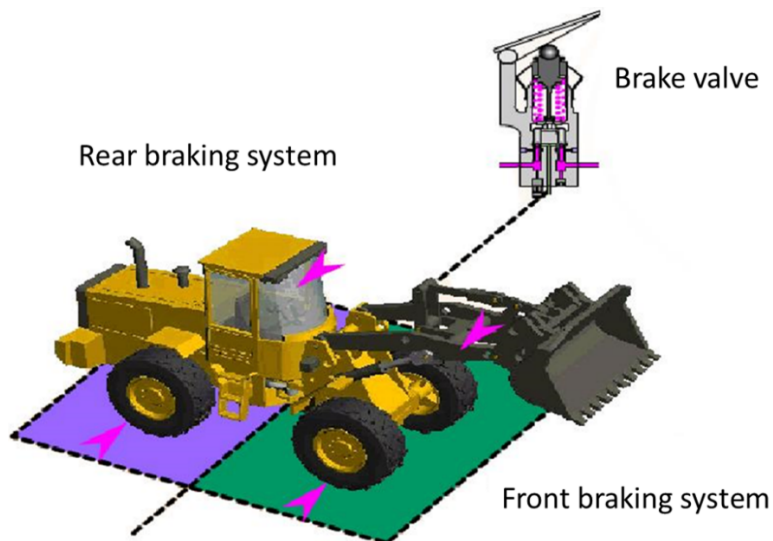
Figure 1: Schematic display of braking on the front and rear axles [3]**.**

The installation of the brake valve with the pedal can be horizontal or vertical. The valve itself and the entire assembly are not affected by the installation, but it must be installed correctly, taking into account the manufacturer's instructions. Figure 2 shows an example of the horizontal and vertical clamping of the valve. The layout depends on the requirements of the supplier or the designer of the entire device or vehicle in which the product is installed [4].
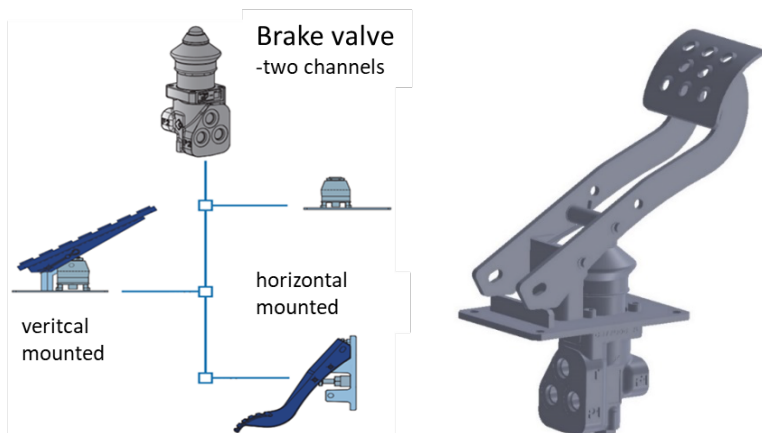
Figure 2: Vertical and horizontal mounting of the brake valve (on the left) and the tester (on the right) [4]**.**

3.2   Failure modes of the brake valve

The criteria that determine the loss of the safety function due to the failure of the valve must be made clear. The manufacturer Poclain Hydraulics and the Laboratory for Fluid Technology determined these criteria. The failure of the valve and thus the loss of the safety function are considered when the following permissible operating ranges of the valve are exceeded:

1) Maximum outlet pressure. The permissible deviation is 20 % of the maximum output pressure.
2) The maximum permissible difference between the working pressure on the valve (F1, F2) is 20 % of the maximum outlet pressure.
3) Maximum permissible external leakage.
4) Maximum allowed internal leakage.

Four failures of the valve are defined. These must be taken into account when calculating the reliability.

3.3 Test station

The measurements were made at the hydraulic test site for a sustainability test of the brake valves. Due to the need for a representative sample, five samples of brake valves were selected according to Errors and Practical Measurement [5]. The test station (Figure 3) was designed in the Laboratory for Fluid Technology at the Faculty of Mechanical Engineering. Due to the need for sustainable testing, the test station is automated.
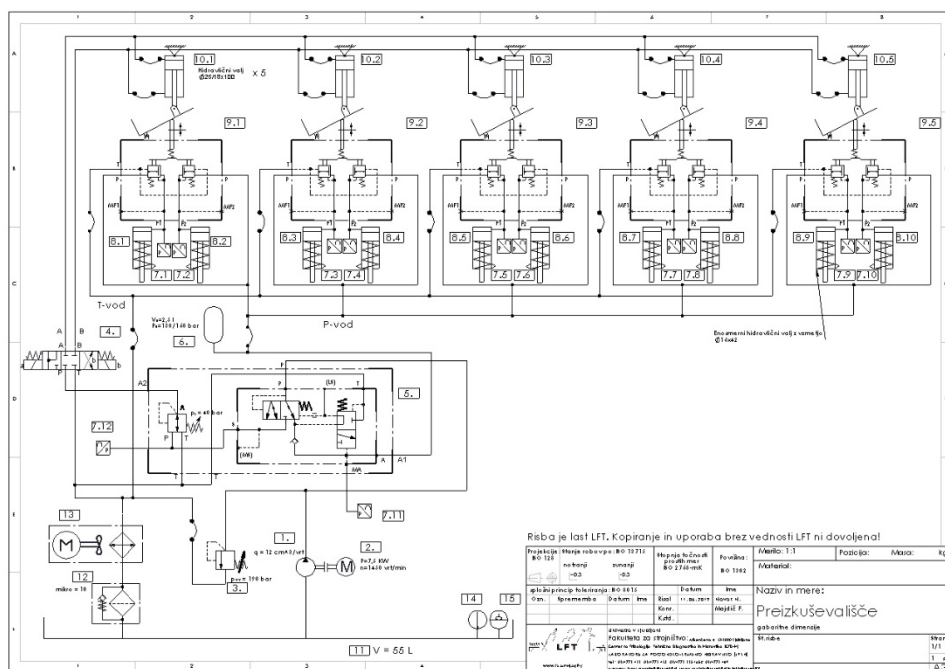
Figure 3: Hydraulic diagram of test station for brake valves.

Figure 4 shows the brake-valve test station. The tested brake valves with pedals are attached to the base plate. At the top there are point-mounted working hydraulic cylinders with ball joints. At the bottom, the bolts are also point-mounted with the ball joints on the welded semi-circular mounting, which is screwed to the pedal. In the background on the right, there is an aggregate of the hydraulic test station.
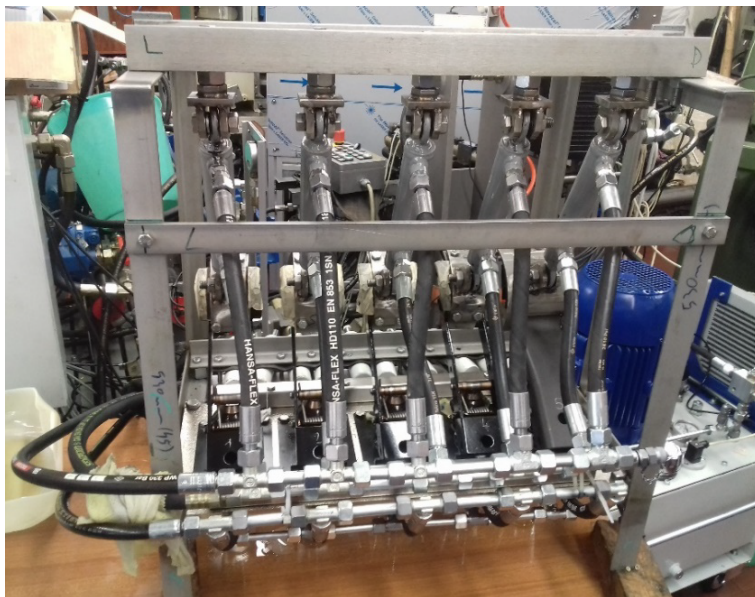
Figure 4: Test station for hydraulic brake valves.

Figure 5 shows an IR photograph of the test station taken with a FLIR thermo-camera. With it, the pressure losses can be detected.
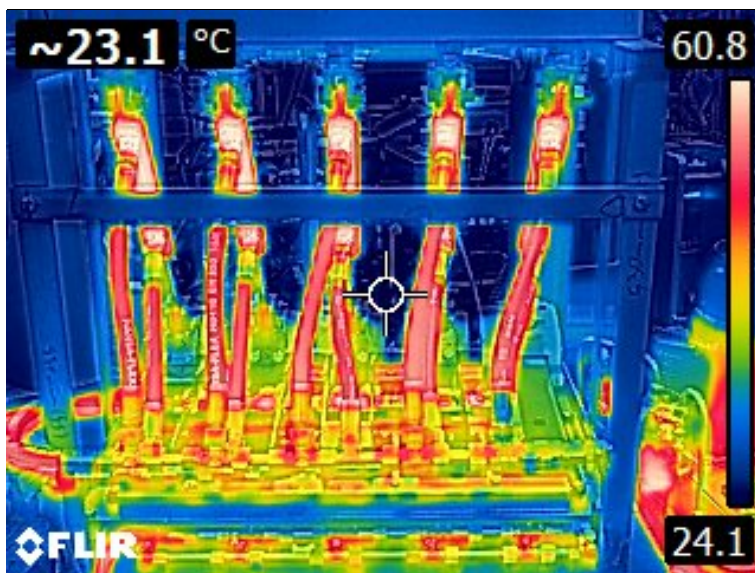
Figure 5: IR photograph of the test station.

4   Experimental research

The length of the entire working cycle was 2.6 seconds. The force with which the working hydraulic cylinder operated on the pedal, and illustrated the force of the leg, was 470 N. It was calculated according to the pressure-reduction valve set, which was set at 30 bar and indirectly, via a working hydraulic cylinder, determined the force on the foot. For a lower force, the pedal did not move to its final position in such a short time (Figure 6), but at the same time the foot and the entire assembly could not be overloaded, as plastic deformation of the pedal could occur, and consequently also the failure of the pedal and the valve. These types of results do not reflect realistic operating conditions. We measured and recorded the pressures of every 3 cycles per 1000 cycles. The sampling frequency of the operating cycle was 100 Hz (the data was captured every 10 milliseconds).

Figure 6 shows the conditions for a cycle length of 10 seconds at five different loads with a maximum of 470 N and five different pressure-reduction valve settings of 10 bar to 30 bar.
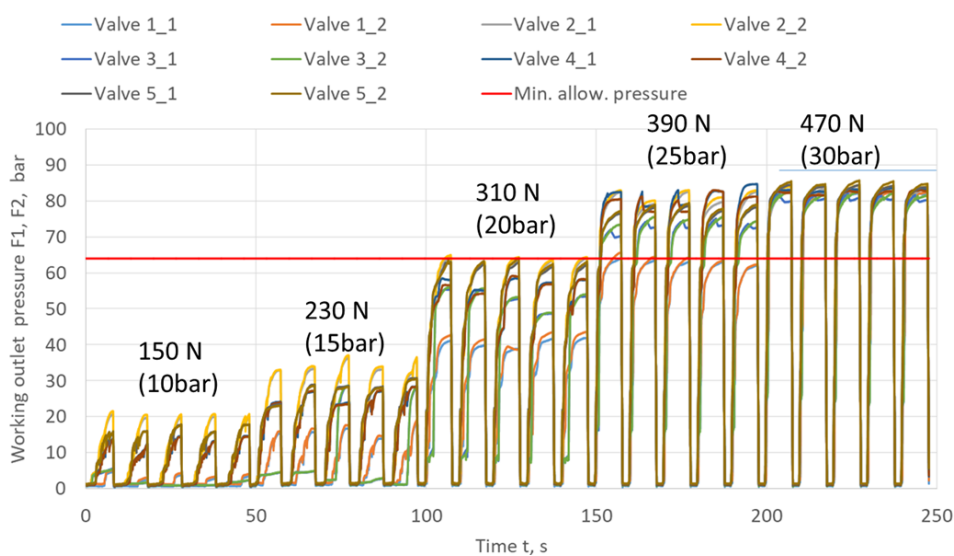
Figure 6: Optimization of the load on the pedal for a cycle length of 10 seconds.

Key pressure measurements were performed on the F1 and F2 working lines, for each valve separately. We then monitored the external and internal leakage of the brake valve. In the article by Chen Yunxia [6], a method for theoretically calculating the gap enlargement in the sliding type of valves is described. In this way it would be possible to calculate the wear of the sliding surfaces and theoretically determine the internal and external leakages. We also carried out measurements of cleanliness and monitored the mechanical wear on the external mechanical parts (pedals and the pushing part of the brake valve). The working pressures of the brake valves F1 and F2 were monitored by the pressure sensors (item 7.1 to 7.10) on the hydraulic diagram (Figure 3). We carried out an analysis of the measurements on a daily basis and determined the acceptability of the operation of the brake valves. We monitored the mechanical wear on the joints between the moving parts and the dynamic fatigue of the torsion springs, which ensured the return of the pedal to its initial position. We tested four steel pedals that were black-coloured and one grey-powder-coloured aluminium pedal.

5   Results

All the samples were subjected to 1003 hours of operation and 1,404,092 cycles. The length of the cycle was 2.6 seconds, with full load on the pedal.
B_test = 1,404,092 cycles

$$B_{test} = 1,404,092 \; cycles \tag{7}$$

5.1   Assumption and calculation of MTTF$_D$ value

The mean time to failure of the valve is very different from the assumed real load of the valve, and two MTTF$_D$ values are presented and calculated for two different assumptions. In practice, the realistic load depends on the end user, as does the useful life of the product.

5.1.1   Assumption 1

Assuming that the real load on the brake valves per day is equal to **10 full-load brakings per day**, then it follows from assumption 1 and equation (1), the demonstration factor of reliability (RDF), which is represented in equation (6) and the measured number of operating cycles Btest equation (7), that the MTTF$_D$ of these valves is at least:

$$MTTF_D = \frac{B_{test}}{0.1 \cdot n_{op}} \cdot \frac{1}{RDF} \tag{8}$$

According to equation (8), it was calculated that the MTTF$_D$ of the brake hydraulic valves is 880 years.

3.1.2   Assumption 2

Assuming that the actual load on the brake valves per day is equal to **100 full-load brakings per day**, then the MTTF$_D$ for the brake hydraulic valve is determined according to the same procedure. Now the MTTF$_D$ value is 88 years. The data is reasonable, since the useful time of the valve depends on the frequency of use.

5.2   Comparison of the outlet working pressures F1 and F2 on the tested valves

Pressure sensors detected the output operating pressures on the F1 and F2 working lines on all the valves at the same time. Figure 7 shows the pressure depending on the time for each valve, for three working cycles at the beginning of the sustainability test. In addition, the system pressure provided by the aggregate (charging pressure) and the pressure limit that the brake valves must achieve are shown in Figure 8.
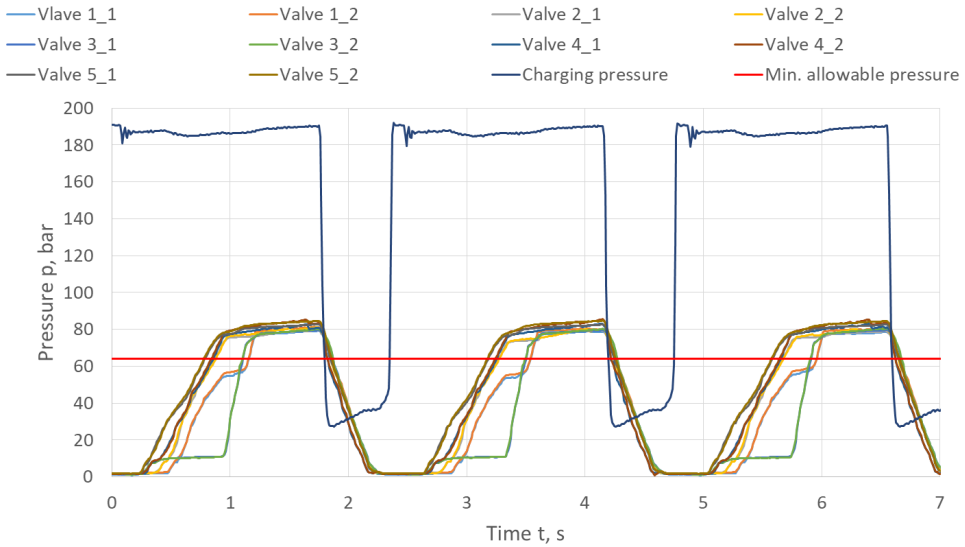
Figure 7: Graph shows the working pressure (F1, F2) depending on time of three cycles at the beginning of test.

Figure 8 shows the maximum pressures in each measured cycle, i.e., every three measurements per 1000 cycles. In the picture below, in a detailed view, it can be seen, that the number 3 valve worked most evenly throughout the entire sustainability test. For valve number 5, the maximum output pressure gradually decreased somewhere in the third quarter, and stabilized at the halfway point of the test, with an average pressure change of approximately 9 %.
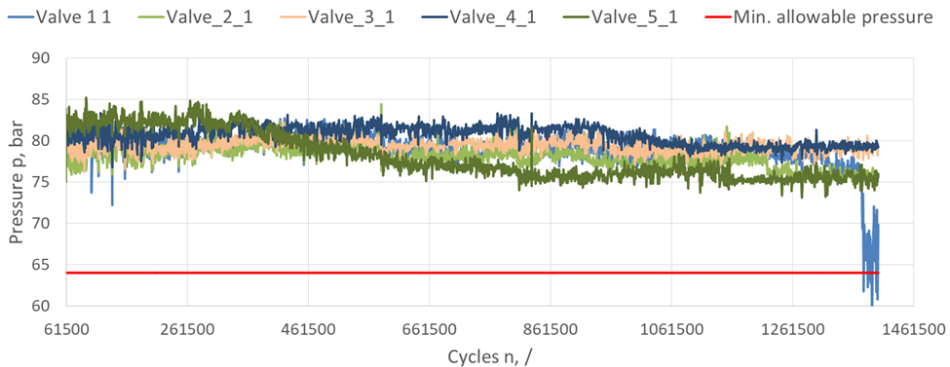
Figure 8: Highest measured pressures in each cycle for each valve.

Valve number 1 had the most similar operation run as valve number 3. In the end, valve number 1 began to achieve smaller pressures than the others, although the reason for this was unknown. It might be due to the friction between the mechanical parts in the construction. For example, the ball joints on the working hydraulic cylinder and the bolts on the construction had a larger friction at the end of the test than at the beginning of the test. This is not the result of the improper operation of the valve, but the construction and mounting of the pedal on the working hydraulic cylinder and the test station itself. At the end of the sustainability test, measurements were made for a longer cycle of 3.8 seconds. All the valves reached the maximum outlet pressure and thus performed their function.

6   Conclusion

1) We designed a test bench for a sustainability test of five brake valves and pedals.
2) We showed that all five valves performed 1003 hours of tests and carried out 1,404,096 cycles without failures. After the calculation according to the SIST-ISO 13849-1 standard, we proved that the minimum mean time to failure of the valve is 880 years, assuming 10 full-load braking per day. Because we carried out an accelerated test, we made calculations according to the operated cycles, but it was not possible to consider the aging of seals and other possible failures due to aging.
3) We measured the working pressure, which was not less than the smallest allowed. Internal leakage was negligible. On average, we maintained the cleanliness on 16/13/9.
4) All the valves still fulfil the conditions for performing their function and thus, performing the safety function.
5) We demonstrated real operating conditions on brake valves and pedals, with the implementation of an accelerated sustainability test. The overall contribution of the presented research is a conservative estimate of the mean time to failure of a brake-valve assembly with pedals that perform the braking function.

References

[1]   NF EN ISO 13849-1:2016. (2016). *Safety of machinery- Safety related parts of control systems-Part 1: General principles for design*

[2]   Pezdirnik, J., Majdič, F. (2012). *Pogonsko-krmilna hidravlika, Zapiski za predavanja – RRP del hidravlika*, Ljubljana

[3]   Klavžar, M. (2012). *Izboljšava karakteristik zavornega ventila, diplomsko delo*, Ljubljana

[4]   *VB brake valves*, V katalogu Poclain hydraulics, acces - https://www.poclain-hydraulics.com/_upload/ressources/media/pdf/A06604D.pdf

[5]   Austin, B. B. (1978). *Errors in Practical Measurement.* A Wiley-Intersicence publication, New York

[6]   Yunxia, C. (2015). *Coupling behaviour between adhesive and abrasive wear mechanism of aero-hydraulic spool valves*, Chinese Journal of Aeronautics 29, pp. 1119-1131

University of Maribor Press

An Endurance Test Scenario for Hydraulic Blocks in Respect of New Materials, Production Methods and Constructions

JÖRG EDLER, STEFAN HÖRHAN & VITO TIČ

Abstract The increasing of the efficiency, new functionalities and decreasing the costs are normally the motivation for new developments in the technique. This includes also the use of new materials or new production methods. This also applies to fluid power and especially the fluid power for mobile applications, where efficiency and a low weight have a high priority. In this work will be presented a test scenario for hydraulic block for mobile applications. In this test should be investigated different materials in respect to their fatigue strength. With new production methods, for instance selective laser melting, new possibilities in the construction are given. These new possibilities should also investigate in respect to the fatigue strength. Restrictions in the construction of parts which are produced with the method of selective laser melting are also described and part of the endurance test.

Keywords: • fluid power • additive manufacturing • Selective Laser Melting • construction • test scenario •

CORRESPONDENCE ADDRESS: Jörg Edler, Graz University of Technology, Institute of Production Engineering, Graz, Austria, e-mail: Joerg.edler@tugraz.at. Stefan Hörhan, Graz University of Technology, Institute of Production Engineering, Graz, Austria, e-mail: Joerg.edler@tugraz.at. Vito Tič, University of Maribor, Faculty of Mechanical Engineering, Maribor, Slovenia, vito.tic@um.si.

1   Introduction

Nowadays, 3D printing technologies are widely used in a lot of industries, in the medicine technology and in the field of research offering a range of advantages compared to conventional manufacturing techniques. By Wohlers [1], the benefits are shorter time to market, use of inexpensive materials, higher production rate, versatility, high part accuracy, ability to produce more functionality in the parts with unique design and intrinsic engineered features.

In the industry a lot of different 3d printing technologies are used. It can be said, that in the metal additive manufacturing three technologies are mostly used [2]:

- − the Selective Laser Melting (SLM),
- − the Laser Metal Depositing (LDM),
- − the Deposition Welding.

The Deposition Welding technology is a classical welding technology. The welding itself is done by a robot. The different to a classical welding job which is done by a robot is in that case, that the whole part is done by welding and not only the welding of different sections.

The LDM process is characterized that powder is used to create the additive manufactured part. The powder is applied accurately by a nozzle and a laser beam is welding the blowed powder on the part. One of the biggerst advantages of this technologie is that no support structures are neccessary, because the nozzle with the laser beam is always in the right angle to the surface of the part which is just in production [3], [4]. But there are also restrictions in the geometriy of this technologie. For instance when a laid tube is prduced. There is no possibility to align the laser when the cylinder surface of the laid tube should be closed by the laser process.

The last here described process is the SLM process. It is one of the most common additive manufacturing technologies in the industry.

J. Edler, S. Hörhan & V. Tič: An Endurance Test Scenario for Hydraulic Blocks in Respect of New Materials, Production Methods and Constructions

113

Consolidation of loose powder by local laser heating is becoming a promising manufacturing technique because of the easy control over both powder deposition and laser radiation. SLS/SLM technology makes it possible to create fully functional parts directly from metals, ceramics, plastics without using any intermediate binders or any additional processing steps after the laser sintering operation [5], [6].

In the fluid power technology the „new" manufacturing technology gives a lot of advantages [7]. Especially in mobile applications where the weight is an important factor the additive manufacturing technology gives new possibilities. Especially for prototypes or small lot sizes is the additive manufacturing technology one of the technologies of the hour. The advantages are [8], [9]:

Individual customer products:

- – Flexible production from quantity 1,
- – Short production time of a few weeks or days.

Energy efficiency:

- – Optimized oil flow,
- – Reduced pressure loss (excess pressure),
- – Less locking screws / leaks.

Weight and design optimization:

- – Grid structures,
- – Lower parts weights,
- – Flexible inside and outside geometry.

Functional integration:

- – New or optimized functionality,
- – Better control of mechanical properties,
- – Improved sustainability.

Hydraulic control blocks and housing of hydraulic valves are the most interesting things to produce with additive manufacturing techniques [10]. Especially mobile hydraulic control blocks are in the focus of this investigations. Here the freedom to create shot connections and to generate part of a low weight are the most interesting things. But depending on the additive production technology are also restrictions in the geometry of the parts. As before said one of the most common additive manufacturing processes is the Selective Laser Melting. Therefore, for this production technology the restrictions of the process to the possible geometries should be determined and the possible parameters should be determined to get the most freedom in the geometry of the hydraulic part.

2   The Selective Laser Melting process

2.1   Process

The Selective Laser Melting process is detailed described by Käfer [2] and Thomson [3]. Figure 1 shows the of a SLM Machine.
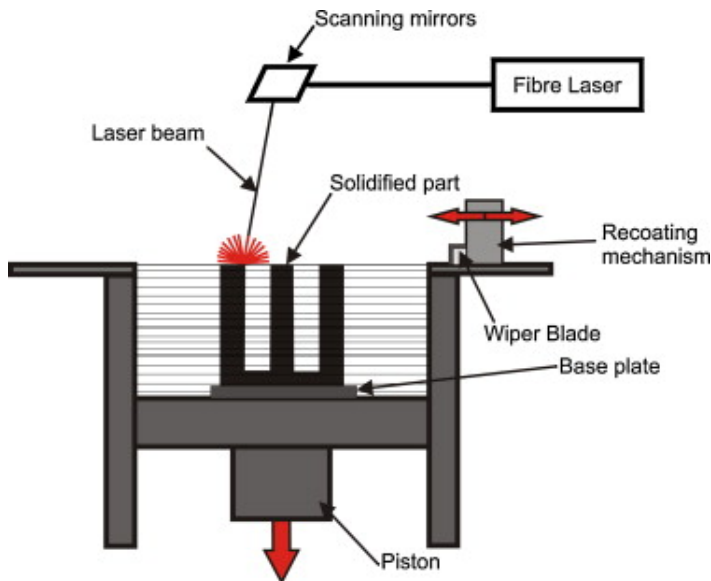
Figure 1: Principle of a Selective Laser Melting machine [11]**.**

J. Edler, S. Hörhan & V. Tič: An Endurance Test Scenario for Hydraulic Blocks in Respect of New Materials, Production Methods and Constructions

115

A base plate is movable placed in a box. On the top of this box is a recoating mechanism placed which apply a thin layer of powder in the box. After applying the thin layer of powder, the laser beam melts the powder on these places where the sliced part is at that time. After this process the movable base plate is lowered down about the thickness of one slice of the part and the process starts again. A big advantage of the SLM technology is that a lot of different materials can be used, for instance steel, aluminium alloys, nickel base alloys ore titanium alloys [11]. In the field of the fluid power the most interesting material is steel especially the alloy 1.4404.

2.2   Degrees of freedom and settings of the SLM process

When the Selective Laser Melting process is considered, the following parameters can be identified [12]:

- Laser beam power,
- Dwell time of the laser at one point (or the velocity of the laser beam on the surface of the powder),
- Thickness of one layer of the powder,
- The grain size of the powder,
- Dwell time between the individual layers.

There are many investigations on the field of the powder for instance XXX. In this case the influence of the powder on the geometry of the part should not be investigated. The investigation should include the process parameters of the Selective Laser Melting process which are the laser beam power, the dwell time of the laser beam at one point and the dwell time between the individual layers. The combination between laser beam power and dwell time at one point gives the heat input into the whole box which includes the melted part and the filled powder. The dwell time between the different layers gives the heat which is transferred from the box out of the machine [13].

A critical condition in the melting process is the circumstance when the laser beam melts direct into the powder. That means there is no structure under the powder layer which should be melted. In that case it can happen, that the laser beam break through the layer and melts uncontrolled in the powder bed. The result are structures and specially surfaces which cannot be used, they are named as so-called dross formation [14]. To prevent this situation, support structures are use during the Selective Laser

Melting process, which must be removed after the melting process [15]. This is associated with additional effort, especially inside of the part.

2.3 Geometric restrictions of the SLM process

As described is in certain situations the most restriction of the Selective Laser Melting process the need of support structure. Figure 2 shows different scenarios of the melting process where the laser beam break through the powder layer.
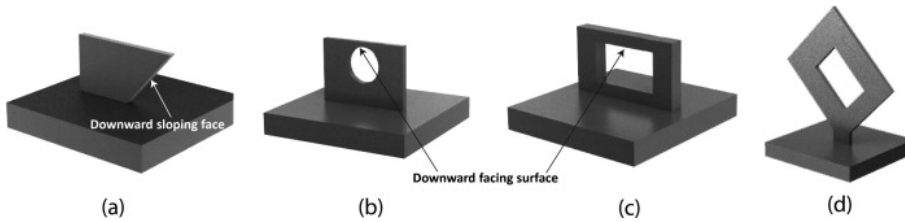
Figure 2: Example of overhanging structures [13]**.**

The missing structure under the powder layer is the reason to get bad results in the melting process. This can be prevented by support structures and the circumstance that there is a structure in the near of the beam. This can be enough when only on one side of the beam is a structure. It can be said, that there is a critical angle and when the surface of the part falls below this critical angle the melting results are not acceptable and support structures are needed. To determine this angle Pichler et.al. uses special parts which have the shape of a trumpet, see Figure 3. There can be seen how the surface quality of the part at decreasing angle of the surface to the base plate.

Figure 3: Test trumpet.

J. Edler, S. Hörhan & V. Tič: An Endurance Test Scenario for Hydraulic Blocks in Respect of New Materials, Production Methods and Constructions

117
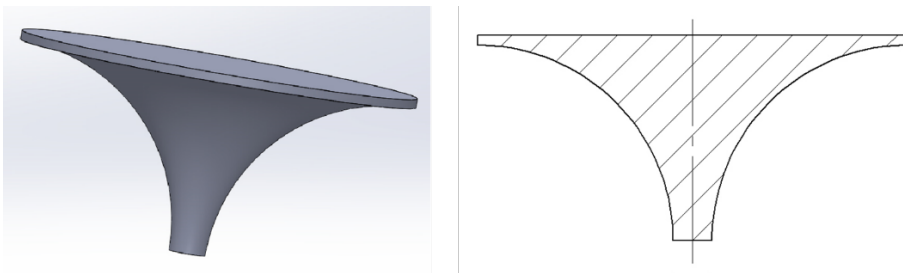
With the right process parameters of the Selective Laser Melting process this critical angle can be optimized.

3 Transfer to the fluid power

Figure 4 shows a simple transfer of a classical hydraulic construction to a optimized construction.
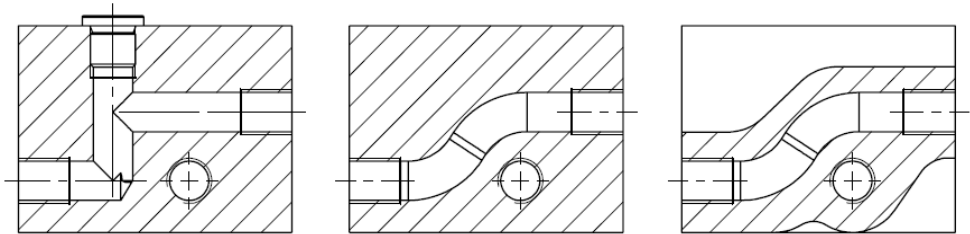
Figure 4: Optimized hydraulic part.

It can be seen, that the plug in the vertical drilling hole can be neglected. The cannel for the oil is optimized and the material around the cannel is also optimized. But when no support structures should be used the critical angle of the Selective Laser Melting process must be considerate. That means that the cannel cannot be designed arbitrarily flat and the shape of the cannel itself has also restrictions in the diameter. Is the diameter to big it is no longer possible to choose a circular shape, see Figure 5.
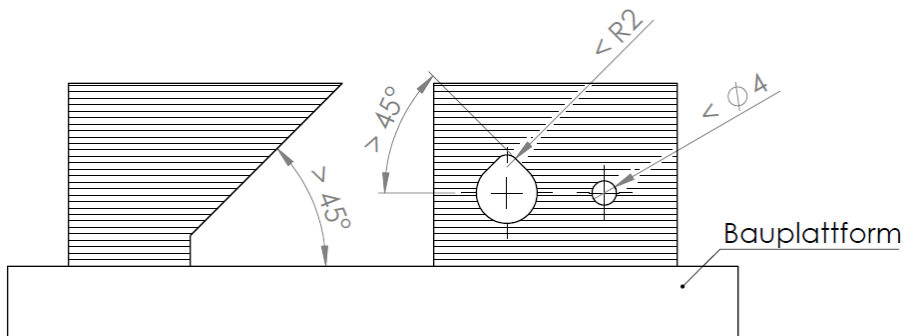
Figure 4: Geometric restrictions on a hydraulic part.

Based on this findings, different test parts and different test scenarios were developed to investigate the influence of the process parameters on the hydraulic conditions of hydraulic components und which degrees of freedom are possible in the geometry of these components.

4   Test components and test scenarios

4.1   Test scenarios

Two different test scenarios should be investigated. The influence of the process parameters on the leakage of the hydraulic component and the influence of the process parameters on the geometry of the hydraulic component.

The tests of the hydraulic components are:

- − static pressure test of the component,
- − dynamic endurance test of the component.

The static pressure test is to determine the burst pressure of the hydraulic component. This should show general the quality of the Selective Laser Melting process and should give a feeling to work with additive manufactured parts. The second part is the dynamic endurance test with at a pressure level of 350 bar. Preliminary tests have shown that a supposed part with no leakage at static pressure becomes leakage after a few load changes. The goals of the test are:

- − A min. static pressure of 450 bar of the hydraulic test parts,
- − A min. load change of 10e6 at 350 bar.

4.2   Hydraulic test components

To find the optimal process parameters of the Selective Laser Melting process simple "thimble" is used as test part, see Figure 5. This gives the advantage that the part is fast and cheap in the production and nevertheless all the test can be made with these simple parts. In one production job can put a lot of these small parts on the base blade and with some restrictions each part can be produced with other process parameters.

J. Edler, S. Hörhan & V. Tič: An Endurance Test Scenario for Hydraulic Blocks in Respect of New Materials, Production Methods and Constructions

119
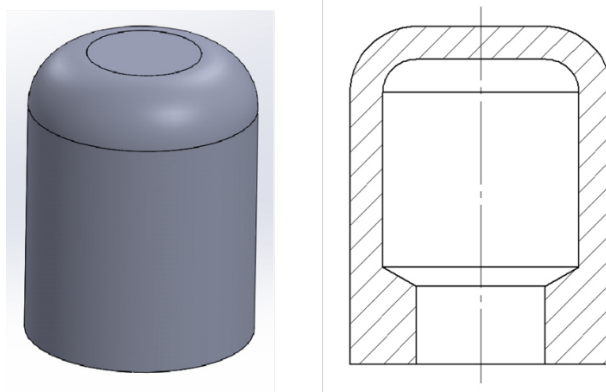
Figure 4: Geometric restrictions on a hydraulic part.

With this part both test the static and the dynamic test can be done. The whole in the bottom off the part a ¼ inch thread is made. There the hydraulic pressure supply for the test can be coupled on.

To test a combination of more than one property a simplified hydraulic block was designed, see Figure 5. This block represents a hydraulic block where cartridge valves are putted in and different channels are connected between the cartridge valves.
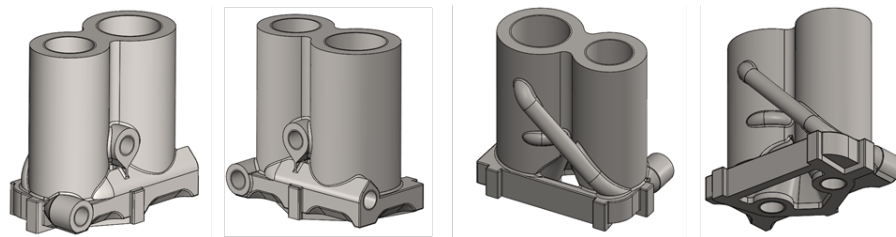
Figure 5: Hydraulic test block.

The part is also stress optimized to get a minimum of weight and a maximum of stiffness. The geometry optimized design is a challenge in the production of the surfaces because overhanging surfaces must be considered and the channels of the oil cannot be placed arbitrarily.

5   Conclusion

To investigate the possibilities of the additive manufacturing technologies in fluid power applications different production technologies were investigated. The in the industry most common production technology, the Selective Laser Melting Technology, gives a lot of new possibilities for the fluid power. The existing restrictions of this technology for hydraulic components were determined and test scenarios developed to optimize this technology.

These test gives information knowledge of the strength of the components, the endurance of these components and the possibility to build complex geometries.

This should result in hydraulic components which can be produced with a maximum of geometric freedom and a minimum of costs, when support structures can be omitted.

References

[1]   Wohlers, T. et al. (2005). Wohlers Report 2005. Rapid Prototyping, Tooling & Manufacturing State of the Industry, Annual Worldwide Progress Report

[2]   Käfer S., Seit, J. (2018). Methods of 3D Metal Printing, *SpotlightMetall*, [online] https://www.spotlightmetal.com/methods-of-3d-metal-printing-a-679124/

[3]   Thompson, S. M., Bian, L., Shamsaei, N., Yadollahi, A. (2015). An overview of Direct Laser Deposition for additive manufacturing; Part I: Transport phenomena, modeling and diagnostics. *Addit. Manuf*, 8, pp. 36–62

[4]   Pinkerton, A. J. (2015). Advances in the modeling of laser direct metal deposition. *J. Laser Appl.*, 27

[5]   Meiners, W., Wissenbach, K. Poprawe, R. (1997). Direct selective laser sintering of steel powder, *Proceedings of the LANE'97*, pp. 615-622

[6]   Over, C., Meiners, W., Wissenbach, K., Lindemann, M., Hammann, G. (2001). Selective laser melting: a new approach for the direct manufacturing of metal parts and tools, *Proceedings of the International Conferences on LANE*, pp. 391-398

[7]   Menger, D. (2018). 3D-Druck wird zum Standardverfahren für Hydraulikkomponenten, *fluid.de*, [online] https://www.fluid.de/hydraulik/id-3d-druck-wird-zum-standardverfahren-fuer-hydraulikkomponenten-318.html

[8]   Rexroth (2019). Additive Manufacturing – Eine Revolution in der Fertigung, [online] https://de.community.boschrexroth.com/t5/Rexroth-Blog/Additive-Manufacturing-Eine-Revolution-in-der-Fertigung/ba-p/6543

[9]   Tirelli, V. (2018). Bis zu 75 Prozent leichter dank additver Fertigung, *fluid.de*, [online] https://www.fluid.de/hydraulik/bis-zu-75-prozent-leichter-dank-additver-fertigung-110.html

J. Edler, S. Hörhan & V. Tič: An Endurance Test Scenario for Hydraulic Blocks in Respect of New Materials, Production Methods and Constructions

121

[10]   Schöpf, G. (2015). Hydraulische Steuer-Bloecke Additiv denken. *Additive Fertigung, DAs Fachmasgazin fuer RApid Prototyping,-Tooling, -Manufactur*, Vol 2, 2019, pp. 42-45

[11]   Louvis, E., Fox, P., Sutcliffe, C. J. (2011). Selective laser melting of aluminium components, *Journal of Materials Processing Technology*, Volume 211, Issue 2, pp. 275-284

[12]   Malý, M., Höller, C., Skalon, M., Meier, B., Koutný, D., Pichler, R., Paloušek, D. (2019). Effect of Process Parameters and High-Temperature Preheating on Residual Stress and Relative Density of Ti6Al4V Processed by Selective Laser Melting. Materials, 12(6), [930]

[13]   Pichler, R., Höller, C., Schwemberger, P. (2018). Economisation of Selective Laser Melting Processes via new Software Based Reductions of Support Structures and Enhanced Laser Strategies, *International Conference on Processing & Manufacturing of Advanced Materials 20,* Conference Paris

[14]   Calignano, F. (2014). Design optimization of supports for overhanging structures in aluminum and titanium alloys by selective laser melting, *Materials & Design,* Volume 64, pp. 203-213

[15]   Gan, M. X., Wong, C. H. (2016). Practical support structures for selective laser melting, *Journal of Materials Processing Technology,* Volume 238, pp. 474-484

University of Maribor Press

Data Acquisition and Management of Hydraulic Components Test Device

ALJAŽ ČAKŠ & VITO TIČ

Abstract When designing devices for testing of hydraulic fluids and hydraulic components there are a few things to consider: component selection, power consumption of the device, what kind of loading profile will be used and so on. Besides all these aspects it is also very important to decide which parameters will be observed during testing. This is tightly related to the selection of sensors and an appropriate control equipment for the acquisition of the signals from sensors. Besides reading sensor values, the controller is responsible for controlling the entire testing protocol including safety functions and actions in case of device malfunction. Another very important task of the controller is to log data. This article discusses this topic on a case of a custom designed device, intended for testing the effect of different types of hydraulic fluids on the main hydraulic components. The focus of the article is on signal acquisition, processing, interpretation and visualisation.

Keywords: • test device • hydraulic components • signal acquisition • data logging • visualisation •

CORRESPONDENCE ADDRESS: Aljaž Čakš, INEL d.o.o., Celje, Slovenia, e-mail: aljaz.caks@inel.si. Vito Tič, University of Maribor, Faculty of Mechanical Engineering, Maribor, Slovenia, vito.tic@um.si.

1   Introduction

There are a lot of different tests available for testing lubrication properties of hydraulic fluids. The main goal of all these tests is to achieve conditions as similar as possible to those that occur in real operation. They try to reproduce mechanical wear mechanisms on certain hydraulic components. After examining wear on the components used in the test, a statement can be made regarding the effectiveness of the tested hydraulic fluid. Tests which depend on analysing component wear are mainly divided in two major types: those based on pump wear and those based on valve wear [1].

Most established pump wear tests are designed on using a big pump from one of major manufacturers like Denison, Parker, Eaton-Vicker or Sundstrand pump. These tests are therefore generally named after the manufacturer of the pump being used. The main reason these pumps are used is the fact that their characteristics are generally well known. Most of these tests use a vane or a piston pump. After a test is finished or periodically during the test, the pump is analysed for wear. Criteria for wear is most often weight loss. The tests must follow strict testing protocols under defined conditions, in order to give relevant comparative results. Tests with big pumps are relatively very consumptive in means of energy, they use quite a lot of fluid and operate under relatively high pressure. There are also alternative testing methods for example the "MP-1 test" with a vane pump, which uses only 0,7 litres of fluid and operates at pressures lower than 100 bar. These are better in terms energy consumption, but the components used are far from real components [2].

Unfortunately, none of these tests give us information about the effect of hydraulic fluid on all the important components – pump, valve, cooler, gaskets and the material of pipes and connectors etc. It is also not possible to monitor energy consumption during different parts of cycles with them. That is why a combined custom testing rig for testing hydraulic fluids was designed to provide a more comprehensive insight into the wear of hydraulic components (Figure 1).
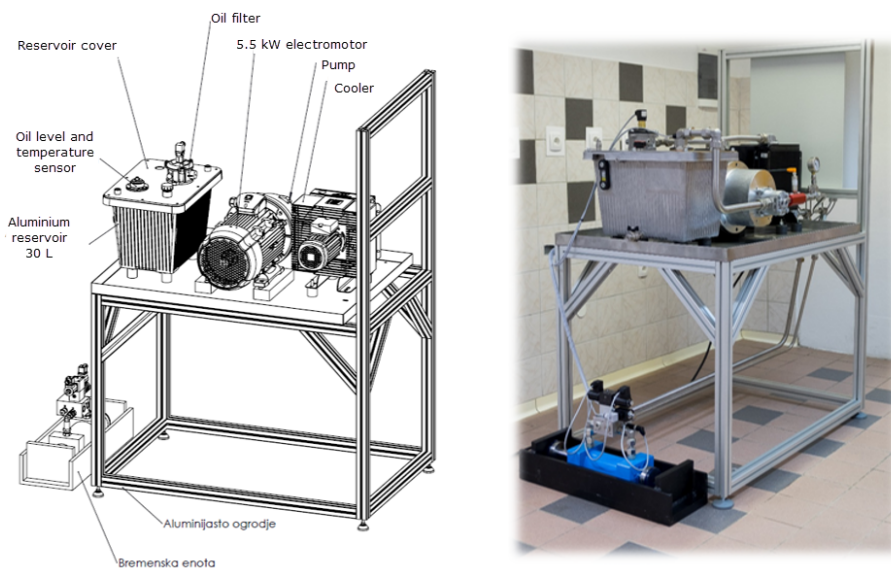
Figure 1: Testing rig.

The device is based on the use of a B&Cs BG20 gear pump. It uses a proportional valve which controls the movement of a two-sided hydraulic cylinder with resistance on each side. Schematic diagram of the device can be seen in Figure 2 [3]. The test is composed out of predefined number of load cycles. Each cycle consists of hydraulic fluid first moving the cylinder to one side until predefined pressure is exceeded and then to the other.

The device's main objective is to age and wear out hydraulic fluid and hydraulic components. By analysing components and hydraulic fluid after performing the test and by interpreting the measurements made during the test, we can find out about changes on the components that occurred during operation. Change of pump and valve pressures and pump flow can be noticed during testing which are consequences of component wear.
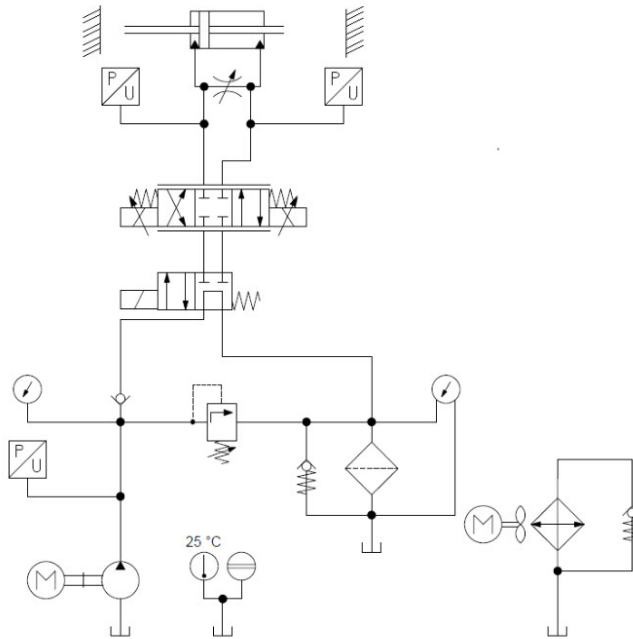
Figure 2: Schematic diagram of the testing rig [3]**.**

2   Components for control and data logging

The designed rig is intended for long autonomous continuous uninterrupted operation. for longer periods of time. It can run for a few months or for a predefined number of load cycles. Therefore, the components that are used must be high quality and very reliable. This applies to all the used parts, but especially the controller, its expansion modules and the sensors.

2.1   Components for controlling the device

For controlling the operation, we decided to use a Beckhoff embedded PC CX5140. Its 4 processor cores offer a lot of computing power for controlling machine operation, logging data, and providing user interface with visualisation. We expanded the controller with expansion modules listed and described in table 1. Because of modular design, controller and modules take up relatively little space in the electric cabinet - Figure 3.

Table 1: Used expansion modules

Module	Designation	Possible connections	Purpose
Digital input module	EL1008	8 24 V digital inputs	Gathering signals from buttons and sensors
Analog input module	EL3048	8 analog current inputs (0 – 20 mA)	Gathering signals from analog sensors
Digital output module	EL2008	8 24 V digital outputs	Controlling actuators and lights
Pulse width modulated output module	EL2535	2 PWM outputs	Controlling proportional valve
Power consumption module	EL3403	3 phase current and voltage	Measuring power consumption
Resistance measuring module	KL3208	8 analog inputs for resistance measurement measuring resistance	Measuring temperatures

Figure 3: Electric cabinet layout [4]**.**

2.2 Sensors

The parameters that we measure in our system are fluid level inside the tank, temperature, pressure and flow. A sensor for detecting filter jam is also used. Pressure sensors are located after the pump and on A and B ports of the proportional valve, while temperature sensors for measuring fluid temperature are located all over the system. There is also a sensor present for measuring ambient air temperature. Flow measuring turbine, pressure sensors and temperature sensor for measuring temperature of oil inside the reservoir have analog current outputs. Filter clogging detector and fluid level sensor have digital outputs, while all temperature sensors except for the one mentioned before, have analog resistance outputs. The choice of expansion modules for the controller is directly related to the types of sensors that we use. That, combined with the fact that sensors with analog current output are less vulnerable to noise is why all the analog sensors that we had chosen, have analog current instead of voltage outputs. Figure 4 shows all the parameters which we follow and a sample of measured values.

Field	Value
id_test	3
id_cycle	224870
datetime	23.11.2018 13:35:57
cycle_time	2808
press_P_avg	107,27
press_P_max	199,31
press_P_min	0,00
press_A_max	199,99
press_B_max	197,96
flow_avg	11,102
flow_load	9,658
flow_no_load	12,593
power_avg	3,1209
temp_oil	48,33
temp_pump	51,20
temp_pumpS	46,80
temp_pumpP	48,10
temp_valve	49,20
temp_valveP	48,60
temp_valveT	53,40
temp_cooler	50,10
temp_air	27,20
pumpON	True
fanON	False

Figure 4: Measured values.

3 Control program

The control program is made in TwinCAT 3. The program has a modular structure and is programmed using a combination of structured text and function block diagrams.

3.1 Control program design

The program controls the whole testing process. The hearth of the program is the main block which cyclically runs every millisecond as a task. This block controls the whole operation, takes care of initialising the test and organising the whole program by cyclically calling all other blocks throughout every program cycle. The blocks that are called from the main program do the following: control the proportional valve, handle errors, read measured values from sensors and measure flow through the pump as illustrated in figure 4. Main block and other simpler block are programmed using function block diagrams, while others are programmed in structured text. Some of the advantages of using the latter are the ease of writing complex mathematical formulas and the possibility of using more complex features like loops.
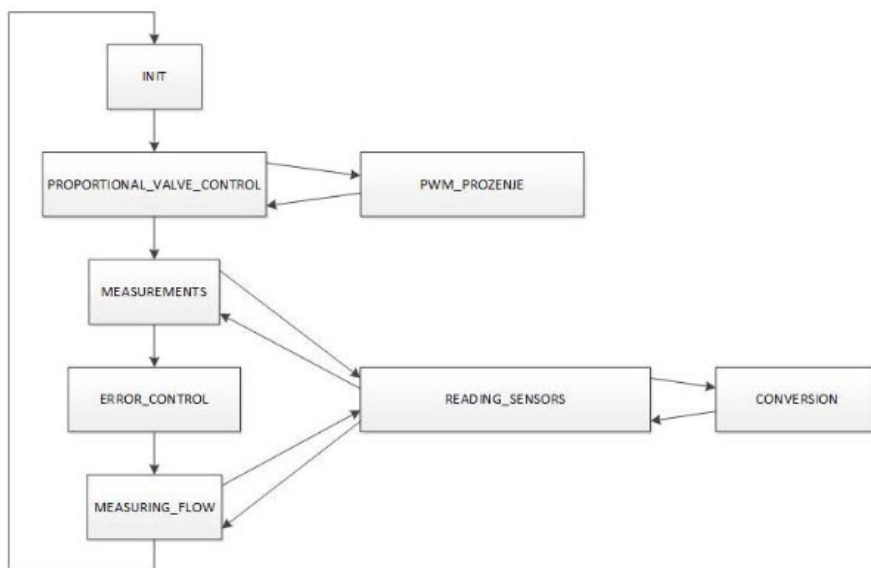
Figure 4: Main program block [4]**.**

3.2   Safety functions

A very important aspect to consider when designing a testing device which will run continuously for longer periods of time is handling abnormalities during operation. In order to assure safe and reliable operation, any anomalies found during testing need to be handled correctly. Operation is programmed in a way that when an error happens, the test is paused. The cause of error then needs to be eliminated before continuing with operation. Possible errors include low fluid level inside tank, lack of pump flow or pressure, cooling failure or abnormalities in current or voltage on any of the three phases. There is also an emergency stop button present on the machine which stops the operation. In case of an alarm, an email can be sent to a predefined address.

4.   Data logging

There are a lot of different aspects to consider when designing data logging applications. In our case the three most important were how and how often to read data, where and how to save it and how to visualise it.

4.1   Data acquisition

Controller reads values from temperature and pressure sensors as well as voltages and currents once per every program cycle. At the and of every test cycle, mean, maximum and minimum values are calculated from the values acquired during the cycle. Pump flow unlike other parameters changes more dynamically, that is why measuring it requires a different approach. It is not measured every test cycle like other parameters. Once every predefined number of cycles, normal test operation stops, and pump flow measurement procedure takes place. It is first measured without any load and then under full load. Before every flow measurement fluid must rest for a second. The entire measurement therefore takes around 4 seconds to finish. Flow measurement can provide us with information about pump wear.

4.2   Transferring and saving data

Measured data is saved to a table inside MySql database for further processing and analysis.

Writing data to the database requires active internet access, so in order to assure integrity of data, safety precautions need to be made in case machine cannot access the database. Machine therefore uses a local buffer in which data is saved if connection to database is unavailable. When connection to the database is active again, the data inside the buffer is transferred to the database. This way we can assure that no data gets lost. Buffer is big enough that machine can run uninterrupted for longer periods of time without database connection.

Data inside the database is protected from unauthorised access by username and password.

4.3   Data visualisation

A website was created for the purpose of visualising measured data. It reads data from the database and displays it in form of a graph (Figure 5). Graph can be displayed in real time, but it is also possible to view all data which has been saved in the database until the last reading.

User has an option to select which out of 21 possible parameters he is interested in. By select proper parameters to view we can make some interesting analysis. For example, by viewing changes of pressure on different ports of the proportional valve, we can determine the wear of proportional valve. By analysing how flow with and without load changes over time, or by following power consumption, we can determine pump wear.

Precise analysis is possible by use of zoom in function which allows the user to zoom selected parameters on the graph. This way we get a full insight in to the measured parameters, which can be viewed from a remote location from different devices including smart phones.
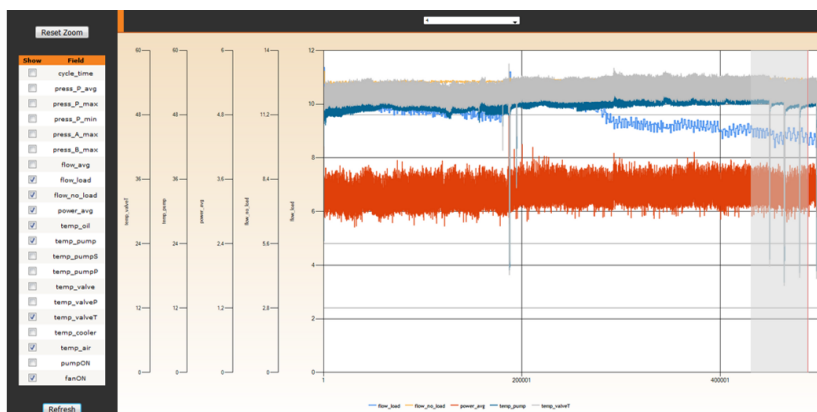
Figure 5: Web site with graph of selected parameters.

5. Conclusion

This article tries to explain the background of designing a testing rig with real time condition monitoring and data logging, the equipment used for such a complex machine and the control program for controlling the testing protocol. Because machine is intended for continuous operation, machine safety and test integrity also need to be taken care of. Another important aspect when designing a device like this, is how to manage such amounts of data and its safety. Web application gives us a precise insight into the test results and so allows us to interpret them and make useful conclusions. Upgrades which could be implemented in the future, among others include functionality of sending SMS messages when test is paused because of an alarm or finished and web camera with live picture of the test.

References

[1] Kambič, M., Lovrec, D. (2017). *Problems of testing new hydraulic fluids*. Fluid power conference 2017, Conference proceedings. 1st ed. Maribor: University of Maribor Press. 2017, pp. 281–293

[2] Lovrec, D., Tič, V. (2019). Vrste in značilnosti triboloških testov s hidravličnimi črpalkami. *Ventil 2/2019*, pp. 132–139

[3] Weichardt, J. (2018). *Kombinirana testna naprava za hidravlične tekočine: Magistrsko delo.* Maribor: Fakulteta za strojništvo

[4] Čakš, A. (2019). *Krmiljenje in nadzor naprave za vzdržljivostno testiranje hidravličnih komponent: Magistrsko delo.* Maribor: Fakulteta za strojništvo

University of Maribor Press

Seal Material Compatibility Test Procedure

ROLAND KALB & DARKO LOVREC

Abstract The compatibility of an elastomer with hydraulic fluid is a critical factor in system performance. Although considerable effort has been expended in the attempt to predict seal compatibility empirically, these efforts have not been successful to date. One reason is the inability to model the broad range of environmental conditions and chemical interactions encountered in an actual hydraulic system accurately. Another reason is the inability to define the term "compatibility" adequately. The paper deals with the problem of seal materials` compatibility testing-methods: The compatibility of commonly used hydraulic seals` materials in combination with mineral based oil. The emphasis is on testing three important changes in the properties of the seals: A change in hardness, and a change in volume – swelling or shrinkage of the seal material. The scope of testing, the parameters of the test and the procedure as prescribed by the Standard are presented and commented on shortly.

Keywords: • hydraulic seals • seal material • test method • fluid compatibility • test results •

CORRESPONDENCE ADDRESS: Roland Kalb, proionic GmbH, Parkring 18, Raaba-Grambach, Austria, e-mail: roland.kalb@proionic.at. University of Maribor, Faculty of Mechanical Engineering, Maribor, Slovenia, e-mail: darko.lovrec@um.si.

1   Introduction

A compatible elastomer is one that will function as an effective seal in an actual hydraulic system for an effective period of time. The property changes experienced by the elastomer exposed to the system's fluid and environment should not prematurely affect its ability to function as a seal.

The experimental approach principally addresses the chemical interaction between the elastomer and the fluid base stock only. This will identify elastomers which are obviously incompatible with the fluid base stock, but it does not address subtle chemical reactions due to the presence of additives, nor does it address the thermal effects that occur in actual systems. There are several of the experimental approaches to identifying large variations in seal material in-/compatibility with different hydraulic fluid types.

It is essential to select seal compounds that are compatible with the environment (hydraulic system) in which they are used. Even if the proper seal material is chosen based on system temperature and pressure, exposure to certain fluids can reduce seal performance drastically by altering a compound's typical physical properties.

A manufacturer of seals, as well those for use within hydraulic components, have tested thousands of fluids, and are testing many new, popular chemicals continuously to ensure seal material compatibility. Their findings, and the resulting guidance, are made available to users in order to avoid inappropriate selection of the sealant material for a particular type of hydraulic fluid and, thus, to avoid inconvenience [1] to [7].

2   Hydraulic seals – tasks, forms and materials

Generally, a seal is used between two surfaces to maintain a pressure drop from a higher fluid (liquid or gas) pressure area to a lower fluid pressure area, for a specific amount of time. A seal's effectiveness is measured in terms of leakage. Thus, a zero leak seal is one that, theoretically, allows no leakage across its interface or sealing contact surface. The earliest seals were nothing more than stuffing boxes packed with waxed string or cord, leather strips, pieces of rubber, cotton, wool, or even paper [8].

The first advance in sealing technology was the development of V-Rings (Chevron Rings) and U-Cups. These seals are reasonably effective, but require hardware modifications, which may be complex. Another disadvantage is that these seals are unidirectional, because they are pressure-activated. Thus, two seals are needed to seal in both directions. As pressure is increased, more V-seals must be added. Thus, three or more V-seals can be required to seal system pressures in excess of cca. 140 bar. U-Cups have a pressure limitation of cca. 100 bar.

The next advance in sealing technology was the O-ring (Figure 1). The O-ring was patented in the 19th century. The original application called for use of the 0-ring in a very long groove. The O-ring was intended to roll during the motion of the parts and, thus, act like a wiper and seal barrier. An elastomeric O-ring was developed around 1940. The sizes of the 0-rings were then standardised for universal use. The simple design allowed the O-ring to be used both as a static and dynamic seal. Because it was a compression seal, it was also a bidirectional seal, in that it was elastic and distorted with pressure, and acted as an effective barrier to prevent leakage.

Circular cross-section

Square cross-section

X-Type cross-section

Profile cross-section (s. c. Lip-seals)
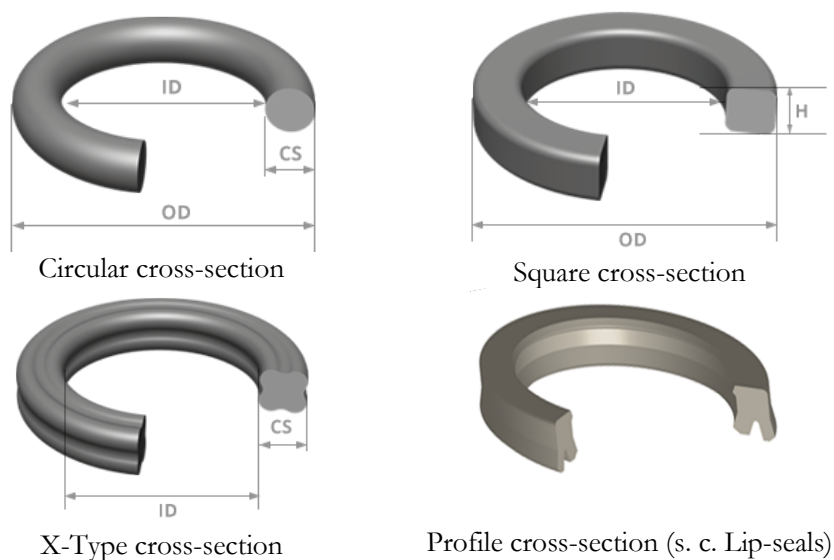
Figure 1: Different forms of ring seals.

During the Second World War, the O-ring became the seal of choice, because the war effort forced the simplification and standardisation of hydraulic components. During this time, many new applications were developed for O-rings, because of their simplicity and effectiveness in sealing.

In the area of fluid power technology, different profiled seals (so-called lip-seals) are implemented, in regard to application. Some examples of a very wide range and variety of different forms of piston-seals are shown in Figure 2.
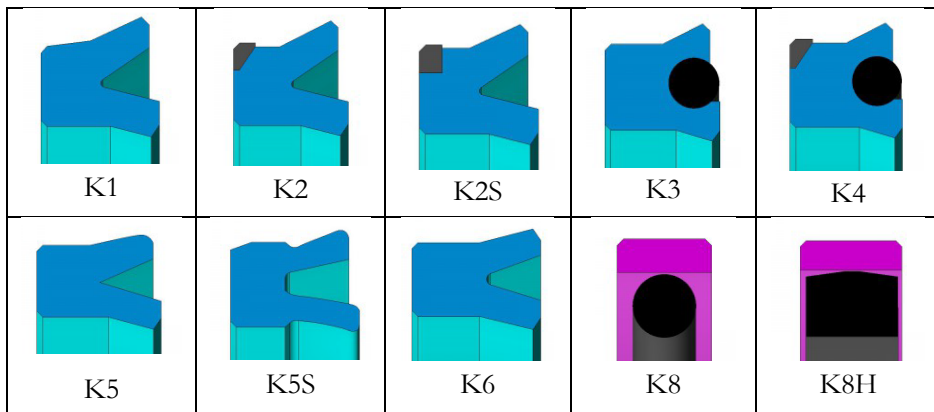
Figure 2: Some examples of different piston-seals cross-section forms (TESNILA Bogadi d.o.o.) [6].

In addition to the various seal-forms is a set of materials used for a very wide selection of seals – there are numerous elastomer seal materials. However, nitrile (NBR), fluorocarbon (FKM), ethylene propylene (EPR, EPDM), chloroprene (CR), and urethane (AU, EU) are the most commonly used materials for industrial applications. The designations for the various elastomers, such as NBR, EPDM, and so forth, were already developed in 1955, and they are still the subject of development.

These materials can be effective seals over the temperature range of -40 °C to 200 °C or more. For hydraulic drives operating under normal conditions, the temperature should not exceed 100 °C. Fluorocarbon elastomers can be used with petroleum fluids, diester lubricants, silicone fluids, halogenated hydrocarbons, and some acids. They cannot be used with phosphate esters, amines, ketones, hot water, steam, and brake fluids. However, etrafluoroethylenehexafluoropropylene elastomers are being used successfully with newer brake fluids. Fluorocarbon elastomers have relatively high cost,

and are normally used where high temperature and longer term compatibility requirements are essential.

As an example, Table 1 lists typical material codes that apply to the rubber energizer used with PTFE fluid power seals, as usually provided by seal manufacturers. Manufacturers have a full range of seal materials to suit various temperature, pressure and chemical compatibility requirements.

Table 1: Typical Application Ranges and Recommendations (Parker Hannifin Corp.) [3]

Material Description	Shore A Hardness	Temperature Range	Recommended Use	Not Recommend For Use
Nitrile (NBR)	70	-30°F to +250°F (-34°C to +121°C)	• Petroleum oils and fluids • Diesel fuel and fuel oils • Cold water • Silicone oil and grease • Mineral oil and grease • Vegetable oil • HFA, HFB and HFC fluids	• Aromatic hydrocarbons • Chlorinated hydrocarbons • Polar solvents (MEK, ketone, acetone) • Phosphate ester fluids • Strong acids • Automotive brake fluid
Low Temperature Nitrile (NBR)	75	-65°F to +225°F (-55°C to +107°C)		
Clean Grade Nitrile (NBR)	70	-30°F to +250°F (-34°C to +121°C)	• Potable water • Food service	
Hydrogenated Nitrile (HNBR)	70	-23°F to +300°F (-32°C to +149°C)	• Diesel fuel and fuel oils • Dilute acids and bases	
Fluorocarbon (FKM)	70	-15°F to +400°F (-26°C to +205°C)	• Petroleum oils and fluids • Cold water • Silicone greases and oils • Aliphatic hydrocarbons • Aromatic hydrocarbons • Fuels • Fuels with methanol content	• Glycol based brake fluids • Ammonia gas, amines, alkalis • Superheated steam • Low molecular organic acids
Silicone HT (VMQ)	70	-65°F to +450°F (-55°C to +232°C)	• Engine and transmission oil • Animal and vegetable oil and grease • Brake fluid • Fire-resistant hydraulic fluid • Ozone, aging and weather resistant	• Superheated steam • Acids and Alkalis • Aromatic mineral oil • Hydrocarbon-based fuels • Aromatic hydrocarbons
Silicone HT (VMQ) Food Grade				
Ethylene Propylene Rubber (EPDM)	70	-70°F to +250°F (-57°C to +121°C)	• Hot water • Glycol based brake fluids • Many organic and inorganic acids • Cleaning agents • Soda and potassium alkalis • Phosphate ester based fluids • Many polar solvents	• Petroleum oils and fluids • Mineral oil products
Ethylene Propylene Rubber (EPDM)	80	-70°F to +250°F (-57°C to +121°C)		

3   Standard seal compatibility test procedures

Seal compatibility test procedures that can be performed easily are described in detail in the Standards, e.g. ASTM D471, ASTM D4289, ASTM 1414, ASTM D2240 etc. A summary of procedures of testing individual properties is to be found in the relevant specialist literature, e.g. [8]. Laboratory equipment is required to perform the tests, whether for mechanical testing or for chemical tests (laboratory ovens). The obtained results will assist in evaluating optimal elastomers for specific applications.

The test fluid should be the actual system fluid, and the test temperature should be the maximum seal exposure temperature. Test samples should be analysed at 24, 70, 100, 250, 500, and 1000 h to assess the compatibility of the seal over the minimum service life of the fluid [8]. The test is concluded when the property changes exceed the established limits.

The test samples should approximate the cross-section of the actual seal used, so that the saturation effect is considered properly. The test samples should be either 2-021, -120, -214, or -320 O-rings per AS568, which is the specification that identifies the actual sizes of O-rings. These have an approximate inside diameter of 1 inch (according to the Standard, and represent the most popular cross-sections of seals used in industrial systems. The test specimens need to be moulded from the same compound as the actual seal.

The following tests should be performed on the O-rings (according to the literature and Standard) [8]:

    a) Hardness change,
    b) Volume swell,
    c) Shrinkage,
    d) Tensile strength change,
    e) Elongation change,
    f) Work function change.

In the context of the Standard, the procedure for the testing of an individual property is described more or less precisely. In each case, it is a combination of mechanical and thermal loading of the material under the prescribed test conditions, accurate measurement of changes in certain quantities (e.g. weighing, measurement of changes

in dimensions ...) and calculation of changes in a certain quantity. To make it easier to imagine the extent of the required tasks in the framework of individual property testing, only an example of testing the volume swell of the seal, as required by the Standard, will be given, as follows.

A quartz glass canning jar with a standard two-piece lid need to be used to prevent liquid and vapour from escaping. As a heating device, a forced-air oven should be used, wherein the temperature shall be maintained within $+/- 1$ °C. For determining the mass of a sample, a scientific advance level precision scale was used, with precision of 0,1 mg. The test specimen shall consist of an entire O-ring. The same specimen may be used for all tests, with hardness and volume determinations made prior to stress-strain tests.

Procedure:

1. Weigh each test specimen in air, $M1$, to the nearest 1 mg, and then weigh each specimen immersed in water, $M2$, at room temperature. It is important that all air bubbles clinging to the test specimen be removed before reading the weight in water. Blot the specimen dry on a lint-free paper towel.
2. Suspend the specimens in the glass jar by the use of corrosion-resistant wire. Separate the specimens by the use of glass beads or corrosion-resistant washers, or by bending small loops in the wire.
3. Suspend the specimen vertically so that cca. 1 inch, of test fluid is between the lower extremity of the specimen and the bottom of the apparatus. Add enough test fluid to cover the specimen to a depth of cca. 1 inch over the upper extremity of the specimen.
4. Place the test apparatus in the oven at the test temperature for the appropriate test time. At the end of the immersion period, remove the specimen from the apparatus. Cool the specimen to room temperature by immersing it in a fresh amount of the test fluid for 45 min.
5. At the end of the cooling period, remove the specimen from the fluid and blot dry. Weigh each test specimen in air, $M3$, and then weigh each specimen immersed in water, $M4$.

6. The change in volume is calculated as:

$$\Delta V = \frac{(M_3 - M_4) - (M_1 - M_2)}{(M_1 - M_2)} \; 100 \qquad [\%]$$

(1)

wherein:

$M1$ = the initial mass of the specimen in air [g]
$M2$ = the initial mass of the specimen in water [g]
$M3$ = the mass of the specimen in air after immersion [g]
$M4$ = the mass of the specimen in water after immersion [g]

Test results are presented as values in % and deviations from recommended values. When presented as a function of testing time, trends may be identified in changing a particular property. For a critical seal application, property changes limits should be monitored as detailed below. These limits have been given in Standards (ASTM, NPFA) as recommendations - compatibility programmes, and indicate good chemical compatibility. The compatibility test limits, as an example from the literature, are as follows [8]:

- – Hardness change: +/– 8 pts,
- – Volume swell: 0 to + 15 %,
- – Shrinkage after swell test: -4 %, maximum,
- – Tensile strength change: +/– 20 %,
- – Elongation change: +/– 20 %,
- – Work function change: +/– 12 %.

If all the changes are within these limits, the elastomer should be considered compatible. Once a seal material is found to be compatible, all seals for that system should be ordered by specific compound and not by ASTM D2000 Line Call Out or generic polymer designation. Selecting the initial seal carefully avoids problems later.

To illustrate the property changes that can be experienced in a compatibility test, a 2-120 NBR 0-ring set was submitted to the compatibility test programme. The O-rings were tested in a naphthenic fluid at 100°C. The average test results for the samples are shown in Table 2. An examination of the complete test results shows several interesting

points. The work function value exceeded 12 % after just 24 h, even though saturation did not occur until approximately 500 h, as indicated by the volume swell reaching the maximum. The lower the test temperature, the longer the time to saturation. This is why short-term tests at low temperatures are meaningless. Work function data also showed a reaction trend, with the value starting off as a significant negative change, getting positive gradually until the significant positive change at 1000 h.

Table 2: Compatibility Test Results; example for a 2-120 NBR O-Ring [8]

Test time [h]	Tensile change [%]	Elongation change [%]	Work function change [%]	Hardness change [pts]	Volume change [%]
0	0	0	0	0	0
24	+7,5	+2,9	−24,1	−1	+3,61
100	+4,3	−1,3	−12,4	−1	+4,16
250	−13,3	−17,0	−7,0	−1	+4,21
500	−63,9	−54,1	+0,5	−3	+4,70
1000	−73,0	−79,3	+126,0	+8	+2,78

This indicated that the chemical reaction, once begun, continued. If the work function was not monitored, the tensile and elongation data would not have indicated incompatibility until the 500-h test; thus, any short-term test would have indicated full compatibility. If only hardness change and volume change were monitored, there would have been no indication of incompatibility. This test sequence illustrates the problem of relying solely on volume-swell and hardness changes as compatibility indicators. Other recommendations linked to changes in the properties, change limits for determining compatibility of elastomer seals for industrial hydraulic fluid application… can be found in various literatures (e.g. [9] to [14]).

4. Implementation of material compatibility testing method

Testing the compatibility of seal materials consisted of several of the most commonly used materials. In the present case, we limited ourselves to testing the fusibility of sealant materials with conventional mineral hydraulic oil and water as an alternative hydraulic fluid. The testing was conducted in accordance with the aforementioned Standards and procedures.

In regard to seal materials, our focus was on the use of sealing materials which are used most commonly in hydraulics. For testing purposes we selected the following materials for the seals: NBR, FPM, POM, HPU FRANC, HPU USI, EPDM, MVQ, PTFE I, and two materials for the guide/wear bands: SCB, and PTFE. Of each material, five samples were manufactured, to ensure the reproducibility of the results.

The basic characteristics of the tested materials are summarised in Table 3. The listed number of tested material was used as the first number of a two-number test code system. The tested specimens were made from the materials listed in Table 3. They have ring-like form with a square cross-section with dimensions OD x ID x H: 25 x 20 x 5 mm, as shown in Figure 1. The tested seal form refers to the shape and dimensions specified in the Standard, but it is the sectional square shape (and not the circular one), which is closer to forms of dynamic seals used today within the field of Higher Operating Pressures. The Standard ASTM D1414 dates from 1956, and has since been updated twice, in 1999 and, most recently, in 2003.

Table 3: Basic characteristics of the tested materials

No.	Abbreviation	Type	Colour
1	FPM	Fluoro Elastomer	brown
2	POM	Poly Oxy Methylene	white
3	HPU Franc	Thermoplastic PU	green
4	NBR	Nitril Butadien Rubber	black
5	HPU USI	Thermoplastic PU	blue
6	EPDM	Etilen Propilen Rubber	black
7	MVQ	Metil Vinil Silicone	light gray-dirty white
8	PTFE I	Poli Tetra Fluor Etilen	white
9	SCB (wear tape)	Sila Ciklo Butadien	green
10	PTFE (wear tape)	Poli Tetra Fluor Etilen	black

Hydraulic mineral oil HLP-quality class (OLMA – Hydrolubric VG46) and demineralized water (suitable for use in the field of Water Hydraulics) were used as the tested hydraulic fluids.

5   Test results

Before testing and after each next stage of testing, the test subject must be weighed (in air and in water) and its dimensions measured. All three dimensions were measured in two positions, rotated by 90 degrees and in five repetitions - see Figure 3. An example of the result of seal-testing at 90 ^oC in duration of 70, 250 and 500 hours, are shown in Figure 4.

št.	I.D.	O.D.	I.D. (90 °)	O.D. (90 °)	T1	T2	T1 (90 °)	T2 (90 °)	W (0 °)	W (90 °)	
	mm	mm	mm	mm	mm	mm	mm	mm	mm	mm	
1	20,1120	30,1115	20,1215	30,1115	4,9715	5,0280	5,0060	4,9840	4,9495	4,9430	
2	20,2220	30,0330	20,2020	30,0280	4,8640	4,9470	4,9060	4,9200	4,9430	4,9630	
3	20,2190	30,0410	20,1950	30,0175	4,9140	4,9080	4,9285	4,8940	4,9435	4,9700	
4	20,1910	29,9750	20,2350	30,0240	4,8770	4,9070	4,8930	4,8960	4,9345	4,9200	
5	20,2145	30,0290	20,2200	30,0505	4,9195	4,8950	4,9125	4,9180	4,9075	4,9285	
povprečje	20,19	30,04	20,19	30,05	4,91	4,94	4,93	4,92	4,94	4,94	
razpon	0,11	0,14	0,11	0,09	0,11	0,13	0,11	0,09	0,04	0,05	

Figure 3: Example of geometry measurement results.

Material	Fluid	Change (70 h) [%]	Change (250 h) [%]	Change (500 h) [%]
		Usually for oil: Volume swell: 15 Shrinkage: -3 Hardness change: +/- 7	Usually for oil: Volume swell: 15 Shrinkage: -4 Hardness change: +/- 8	Usually for oil: Volume swell: 20 Shrinkage: -4 Hardness change: +/- 10
seal FPM	HLP VG46	Volume swell: 8 Shrinkage: 0 Hardness change: -2	Volume swell: 33 Shrinkage: -19 Hardness change: -2	Volume swell: 42 Shrinkage: -24 Hardness change: -3
	demi water		Volume swell: 0 Shrinkage: 0 Hardness change: -2	
seal POM	HLP VG46	Volume swell: 7 Shrinkage: 0 Hardness change: -2	Volume swell: 0 Shrinkage: 0 Hardness change: -2	Volume swell: 0 Shrinkage: 0 Hardness change: 0
	demi water		Volume swell: 0 Shrinkage: 0 Hardness change: -1	
seal HPU FRANC.	HLP VG46	Volume swell: 8 Shrinkage: -7 Hardness change: -1	Volume swell: 8 Shrinkage: -7 Hardness change: -1	/
	demi water		Volume swell: 0 Shrinkage: 0 Hardness change: -8	
seal NBR	HLP VG46	Volume swell: 14 Shrinkage: -4 Hardness change: 0	Volume swell: 14 Shrinkage: -8 Hardness change: 0	Volume swell: 14 Shrinkage: -8 Hardness change: 0
	demi water		Volume swell: 0 Shrinkage: 0 Hardness change: -4	
seal EPDM	HLP VG46	Volume swell: 24 Shrinkage: -33 Hardness change: -11	Volume swell: 29 Shrinkage: -45 Hardness change: -11	Volume swell: 35 Shrinkage: -48 Hardness change: -15
	demi water		Volume swell: 0 Shrinkage: 0 Hardness change: 0	
wear ring PTFE	HLP VG46	Volume swell: 0 Shrinkage: 0 Hardness change: -1	Volume swell: 0 Shrinkage: 0 Hardness change: -1	Volume swell: 0 Shrinkage: 0 Hardness change: -1
	demi water		Volume swell: 0 Shrinkage: 0 Hardness change: -2	

Figure 4: Example of geometry measurement results.

The results are shown in the form of deviations from specified limit values, which refer to the classic O-ring and conventional mineral hydraulic oil. Figure 4 shows only a small part of the otherwise very extensive Tables of results, which refers to some seal materials, and the two hydraulic fluids – a mineral based hydraulic oil and water.

6   Conclusion

Seal designers seek the ideal seal material to cover all possible operating conditions. The problem is particularly interesting, because new materials are emerging for sealss, new types of hydraulic fluids, or modified formulations of a known basic fluid (eg a new additive package).

The first step in this direction is certainly to test the compatibility of a particular sealant material with a particular fluid. This is very extensive and time-consuming. This paper presents the aforementioned issues faced by manufacturers of both seals and hydraulic fluids briefly. The procedure and scope of testing, as well the results of testing of conventional materials for seals used in combination with mineral hydraulic oil and water, are shown as an example.

References

[1]   Walker, J. (2017). Sealing Products and Services Ltd, Lion House, BP4400 0317/pdf, PIIL2766263, 48 pages
[2]   Whitlock, J. (2004). The Seal Man's O-Ring Handbook, EPM Inc., 229 pages
[3]   N.N. (2001). Parker O-Ring Handbook, Catalog ORD 5700A/US, 287 pages
[3]   N.N. (2014). Fluid Power Seal Design Guide, Catalog, EPS 5370, 28 pages
[4]   N.N. ERIKS, Sealing Elements – Technical Handbook O-rings, 265 pages
[5]   N.N. (2015). NewDealSeals BV, 330 pages
[6]   N.N. (2019). TESNILA Bogadi, Tehnični list materialov, https://www.bogadi.si/wp-content/uploads/2016/03/Tehnicni_list_materialov_A3.pdf, (23.7.2019)

[7]   Vidović, E. ˙(2014). Development of lubricating oils and their influence on the seals, goriva i maziva, ISSN 0350-350X, GOMABN 53, 3, pp. 220-235

[8]   Totten, G. E. (2000). Handbook of Hydraulic Fluid Technology, Marcel Decker Inc. ISBN: 0-8247-6022-0, 1296 pages

[9]   Seabury, M. (1995). Compatibility of Elastomer Seals and Industrial Hydraulic Fluids, in ASTM DO2 Meeting

[10]   Vander Laan, D. (1996). Compatibility of Elastomer Seals and Industrial Hydraulic Fluids, National Fluid Power Association Meeting

[11]   ASTM D 6546, Standard Test Methods for and Suggested Limits for Determining Compatibility of Elastomer Seals for Industrial Hydraulic Fluid Applications

[12]   ASTM D 4289, Standard Test Method for Elastomer Compatibility of Lubricating Greases and Fluids

[13]   Chemical compatibility study reveals shortfalls in standard methods, SystemSeals, October 2016, http://www.systemseals.com/new-chemical-compatibility-study-reveals-shortfalls-standard-testing-methods/ (26.6.2019)

[14]   Totten, G.E. (2003), Fuels and Lubrication handbook, 2nd edition, 370 pages

University of Maribor Press

Test Device and Automated Test Procedures for Measuring Valve Characteristics

VITO TIČ & DARKO LOVREC

Abstract Directional hydraulic valves are one of the basic and very important components of a hydraulic system as they control the direction and quantity of the flow of hydraulic fluid. In order to achieve successful closed loop control of the hydraulic system it is necessary to know the static and dynamic characteristics of the hydraulic valves, which depend on the operating conditions. Influence of operating conditions can be evaluated by using an appropriate test device, which must ensure comparability between measurements. The paper presents the development of fully automated test device for measuring static characteristics of directional hydraulic vales according to ISO 10770-1. The test device consists of hydraulic system equipped with modern sensors and is controlled by a soft PLC. The test procedure is fully automatic and the test results are displayed real-time.

Keywords: • hydraulic • valve characteristics • directional valves • test device • leakage •

_____

CORRESPONDENCE ADDRESS: Vito Tič, University of Maribor, Faculty of Mechanical Engineering, Maribor, Slovenia, e-mail: vito.tic@um.si. Darko Lovrec, University of Maribor, Faculty of Mechanical Engineering, Maribor, Slovenia, e-mail: darko.lovrec@um.si.

1   Introduction

Directional hydraulic control valves are hydraulic components for regulating the flow direction of the fluid and the flow velocity in the hydraulic system. Their use in the hydraulic system allows the actuator to move (cylinder, hydraulic motor ...). The most common design of directional valves uses control spool that moves from the starting position (usually the middle) to the left or right operating position, depending on the desired direction of movement of the actuator. The movement of the spool is controlled by either lever, coil, hydraulic force or a spring [1].

The properties and characteristics of directional hydraulic control valves have a strong influence on the behaviour of the entire hydraulic system. The performance of the valve is most influenced by its construction, but the characteristics also depend on the hydraulic fluid used, which changes the characteristics of the valve with different viscosity, compressibility and density.

With developed test device for measuring static characteristics of directional hydraulic valves it is possible to obtain information on the properties of a particular valve of a particular manufacturer in combination with a particular hydraulic fluid based on standardized procedures. At a later repetition measurement of the same valve, we can conclude on its wear and degradation of the characteristics.

If we want to compare the characteristics of the hydraulic equipment between different manufacturers and evaluate the variation of the characteristic over the useful life of the valve, the characteristics must be comparable. Comparability is achieved by standardized tests and a standardized presentation of results

2   ISO 10770 STATIC TESTS

ISO 10770 standard applies to electrically modulated hydraulic control valves and consists of three parts. The first part refers to the testing of four-port directional valves, the second part relates to the testing of three-port valves, and the third part to the pressure regulating valves [2].

The standard is divided into electrical tests, performance tests that are further divided into dynamic and static tests, and pressure impulse test. This paper focuses on the static performance tests of four-port directional valves. According to the standard these static tests exclude any dynamic effects. The standard also specifies the test conditions that are presented in Table 1.

Table 1: Required test conditions

Ambient temperature	20 ±5 °C
Filtration	According to ISO 4406
Hydraulic fluid	Mineral hdraulic oil (ISO 6743-4) or other hydraulic fluids according to the valve
Hydraulic fluid temperature	40 ±6 °C at valve inlet
Fluid viscosity grade	VG 32 (ISO 3448)
Pressure	±2,5 % according to specific test
Pressure on the return line	According to manufacturer's recommendations

source: ISO 10770-1 [2]

Further on, the paper will present development of fully automated test device for measuring static characteristics of directional hydraulic valves and results of three most important and common test for four-port directional valves.

2.1 Internal leakage versus input signal

The internal leakage test measures the internal leakage flow between the individual valve ports. During the test both control ports are closed and the tank port is opened. The pressure port is loaded with 100 bar or with valve's maximum pressure allowed.

Before performing the measurement, it is necessary to drive the valve several times over its entire control area. The flow of leakage on the tank port is then measured throughout the control area. The result is a graph of the leakage flow depending on the control signal as shown in Figure 1.
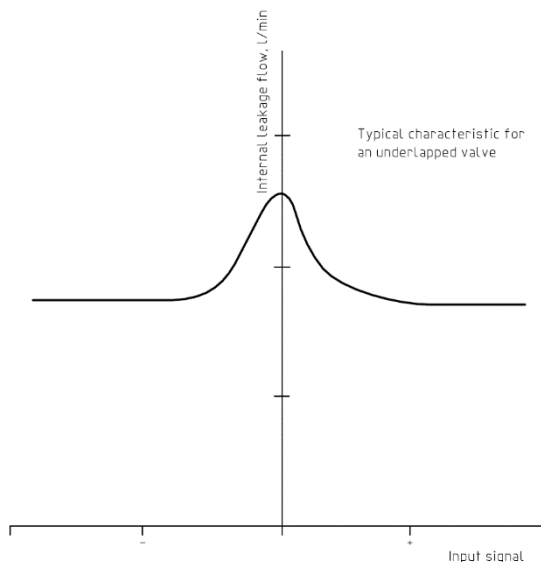
Figure 1: Internal leakage versus input signal [2]**.**

2.2   Output flow versus input signal at constant valve pressure drop

Figure 2 shows the static flow characteristics of the hydraulic fluid as a function of the control signal. This characteristic is defined at a constant pressure drop on the valve. Work ports are connected together via the flowmeter. The test is carried out at a pressure drop of 10 bar, of 70 bar or of one third of the maximum working pressure.

Before performing the measurement, it is necessary to drive the valve several times over its entire control area. During the test, the input control signal is adjusted from one limit (i.e. negative) to another limit (i.e. positive), while the flow value is recorded. The speed of the signal change must be slow enough so that the dynamic effects are not affected by the results. Between the test the pressure drop on the valve should be as constant as possible and should not deviate by more than 5 %.
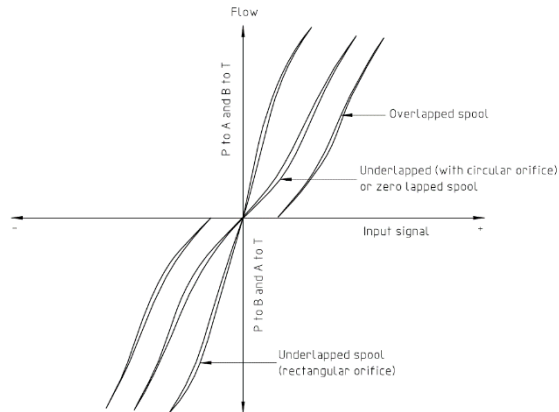
Figure 2: Output flow versus input signal at constant valve pressure drop [2]**.**

In the obtained results, the following characteristics of the valve can be identified: output flow at rated signal, flow gain, linearity, hysteresis, null zone characteristics (spool lap condition, symmetry, polarity and limiting power) [2].

2.3 Metering test

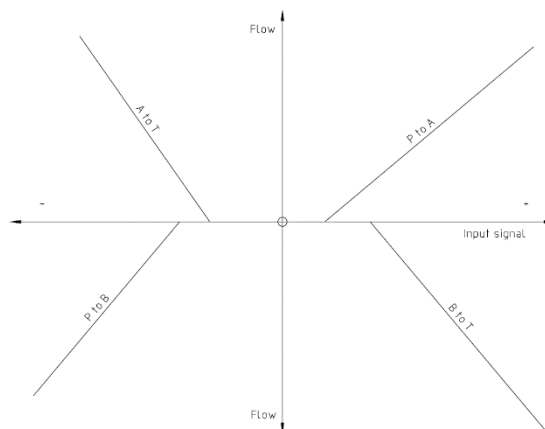The purpose of this test is to determine the characteristics of each land of the main spool as shown in Figure 3.

Figure 3: Metering test [2]**.**

The test is made of four different measurements of the flow between two control ports at constant pressure drop: the flow from port P to A, P to B, A to T and flow from port B to T [2].

3 Test device and automated test procedure

Based on the ISO 10770-1 test procedures (some described above) a test device was designed and built (Figure 4).

Figure 4: Developed test device.

The hydraulic system (Figure 5) is mounted on the frame made of aluminum profiles. It consists of pipes, shut-off valves and several sensors for pressure, flow and temperature. Hydraulic power is provided by a hydraulic power unit with variable axial piston pump powered by a three-phase asynchronous motor, controlled via frequency converter.

The use of variable axial piston pump powered by a three-phase asynchronous motor, controlled via frequency converter allows us to perform closed loop control (PID) of pump flow from 0 to 80 L/min to achieve desired constant pressure drop on the valve.
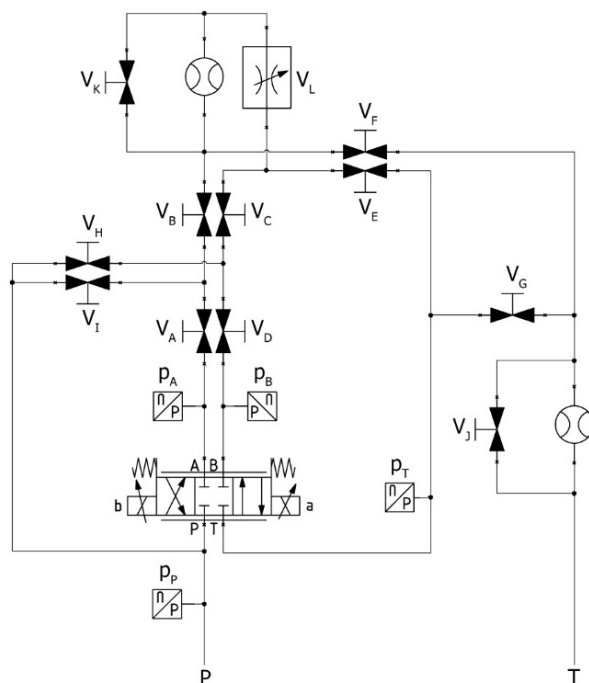
Figure 5: Hydraulic scheme of test device.

3.1 Automated control system

The PLC system is based on Beckhoff soft PLC with selected digital and analog input/output modules to control the system. Besides digital and analog modules, the system also incorporates counter modules to measure the flow by two gear type flow meters and a PWM current output module to control the coils of proportional directional valve. Using this special module (EL2535) allows us to have full control over pulse width modulation of closed loop current control together with PID parameters of PWM modulation and dither signal to the valve.

Figure 6 shows PWM current closed loop control of two valve coils using default settings (left), compared to optimized PID settings (right). It can be seen that optimized PID settings greatly improve response of the valve, since the set current (of approx.. 700 mA) is achieved a lot faster.
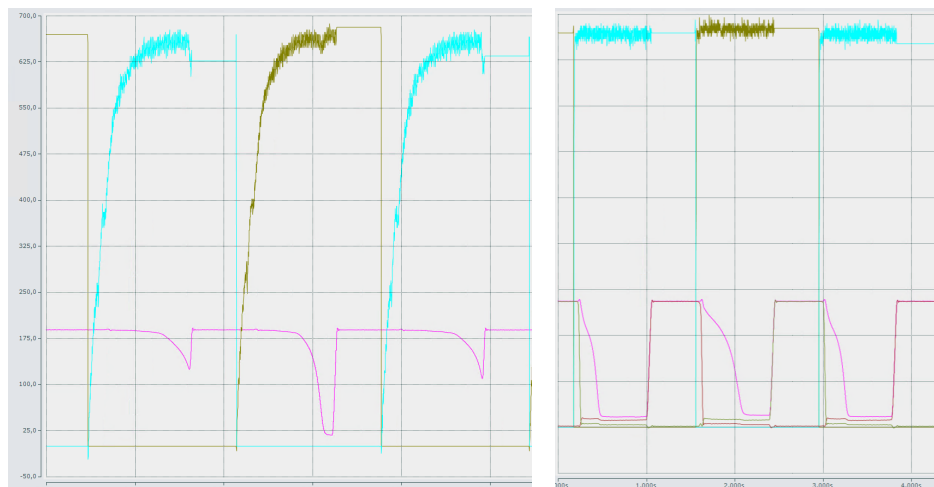
Figure 6: PWM closed loop control parameterization.

3.2 Control panel

The user interface (shown in Figure 7) is made in C# Windows Forms where it is possible to include libraries for the graphical display of signals directly from the PLC.

The HMI graphical interface serves to select the test we want to perform, set the appropriate parameters, capture data and monitor the measurement. The results are displayed in the form of a graph and a table, and can be exported to Microsoft Excel XLS file.

HMI application window contains a hydraulic diagram that is equipped with digital displays of pressure and temperature values and a marked pathway of the current pipeline, thus making it easier to visualize the path of the hydraulic fluid. Under the hydraulic diagram we have indicators of current pump parameters: the rotational speed can be set from 0 to 3000 rpm, the flow can be set from 0 to 100 %, and the pressure can be set from 0 to 315 bar. The user can also define the desired pressure drop on the valve and time/step interval of performing individual measurements. On the right side of the window the results of the test are displayed in real time in in the form of a graph and a table.
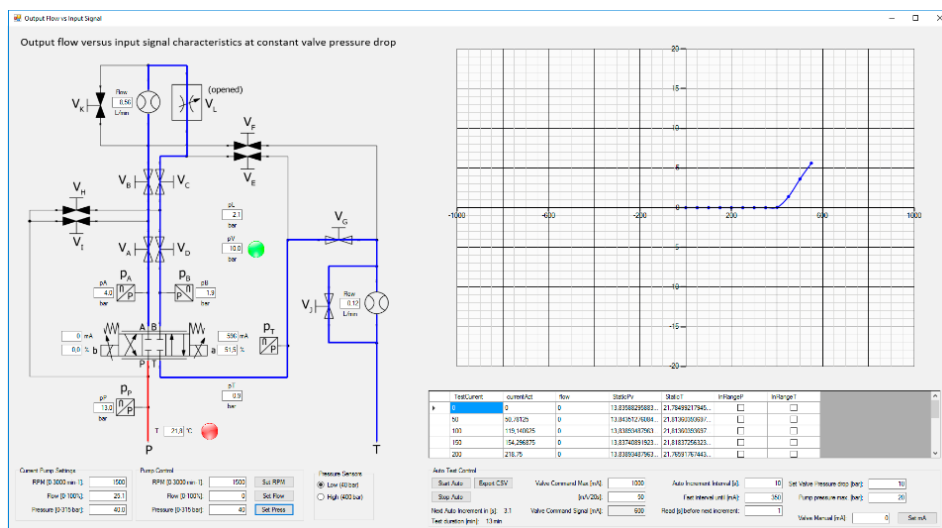
Figure 7: Control panel.

3.3   Test procedure

The test procedures are fully automated. For example, we will describe an automated test procedure for *Output flow vs Input signal test*.

Before starting the test, the user inputs maximal valve current (mA), interval increment (mA), interval (s) and valve pressure drop (bar). At the moment the automated test procedure is started, the current on the valve is set to 0 mA and the pump is set to minimal flow, thus the rpms are reduced to 800 rpms and the flow is set to 0 %.

While performing automated test procedure, each set time interval (30 s) the current on the valve is increased by interval current increment (25 mA). As the valve starts to open, the pump is automatically controlled to achieve the desired pressure drop on the valve (10 bar) by raising or lowering pump speed and flow. Adequate time increment allows the system to achieve steady state, while flow through the valve and pressure drop on the valve are constant. Just before the next increment, the recoding is started. The recording of the flow and pressure conditions takes 2 seconds, while a larger number of data points are recorded, which are then averaged to achieve most accurate results possible.

4   Results

Figure 8 shows the results of the internal leakage test.
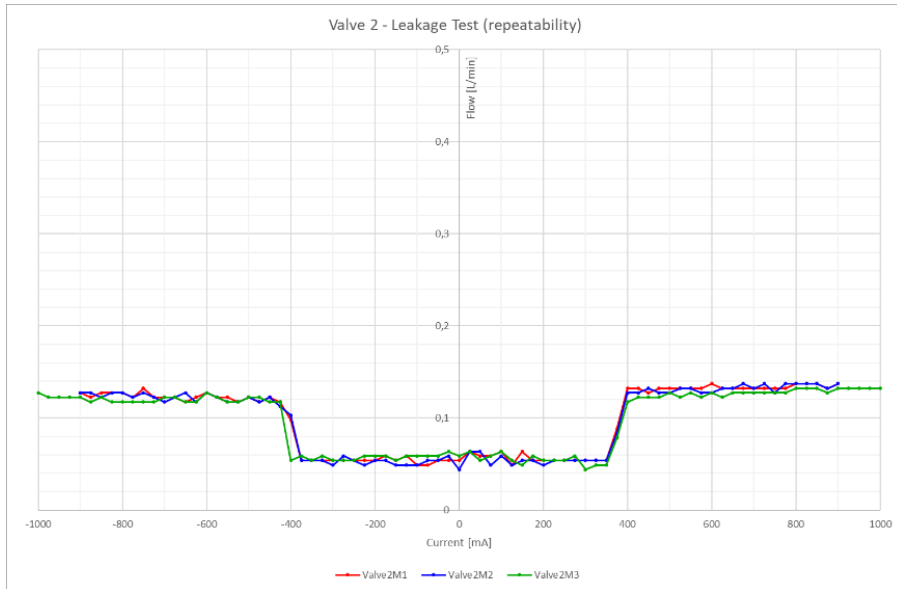

Figure 8: Results – Internal leakage test.

During the test both control ports are closed (A and B) and the tank port (T) is opened. The pressure port was loaded with 300 bar and valve's internal leakage was recorded. The measurement was started with maximum negative signal and increased to maximum positive signal with 25 mA steps. To evaluate the accuracy and repeatability of the test device, we have made three reiterations of each test (the results of each are shown as red, blue and green line).

The static flow characteristics of the hydraulic fluid as a function of the control signal is defined at a constant pressure difference on the valve. Since we were measuring a proportional directional control valve it was important to ensure a constant pressure drop of 10 bar. During the measurement, the signal changes from 0 to positive limit, then back to negative limit and back to 0. In this way also the hysteresis of the valve is recorded.
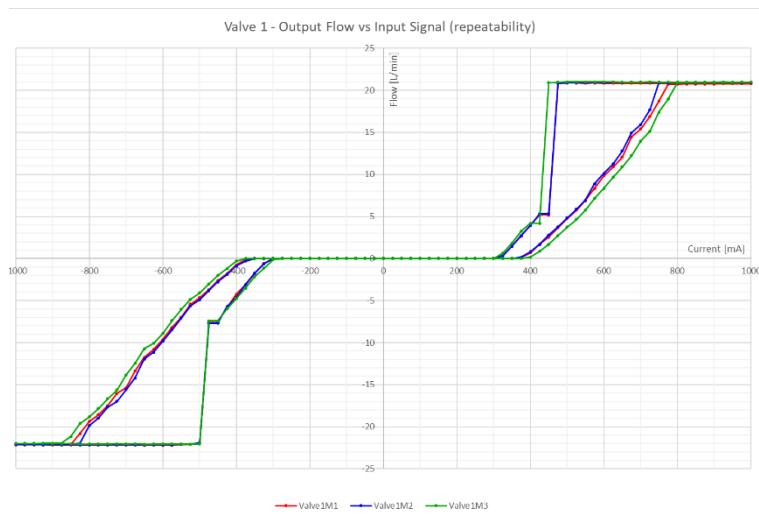
Figure 9: Results – Output flow vs Input signal.

The obtained results can be seen in Figure 9 and show three reiterations of the test. A large hysteresis on the valve and poor linearity when decreasing control signal in both directions can be noticed.
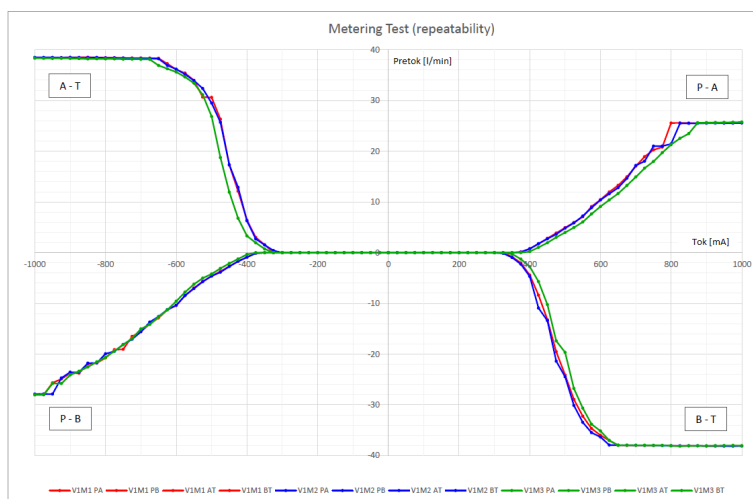

Figure 10: Results – Metering test.

Additionally, the metering test is used to determine the flow characteristics of four individual connections: P-A, P-B, A-T and B-T. The measurement was also done with 25 mA step increase of current signal. The results of (three reiterations) of the test are presented in Figure 10. Better flow conditions can be recognized in A-T and B-T flow connections compared to P-A and P-B flow connections which have more flow restriction.

5   Conclusion

A fully automated test device for measuring static characteristics of directional hydraulic valves was successfully developed and built. It allows us to perform all types of tests specified in ISO 10770-1 and determine the static characteristics of four-port directional hydraulic valves with desired accuracy and repeatability.

The test device allows us to compare properties and characteristics of different new valves or to evaluate the performance of a single valve before and after being exposed to long-term endurance test, evaluating its performance after the endurance test.

References

[1]   Lovrec, D. (2018). Uvod v hidravlično pogonsko-krmilno tehniko. Maribor : Univerzitetna založba Univerze : Fakulteta za strojništvo, 2018. https://doi.org/10.18690/ 978-961-286-191-9
[2]   ISO 10770-1 (2009). Hydraulic fluid power-Electrically modulated hydraulic control valves- Part 1: test methods for four-port directional flow-control valves

University of Maribor Press

Significance of Proportional Valve Steady-State Characteristics

DARKO LOVREC

Abstract Within controlled hydraulic fluid power systems, power is transmitted from a hydraulic power source to one or several actuators through electrically modulated hydraulic control valves. The control valves receive control signals in the form of an electrical signal, receive hydraulic power from a power source, and, then, control the direction and amount of hydraulic flow to the actuator, depending upon the electrical input signal – continuously operating valves. In terms of their structure and dynamics, there are several types of continuous-acting valves. These include proportional valves. In addition to different continuously acting valve types, there are a number of performance characteristics that must be known in order to apply electrically modulated hydraulic control valves successfully. This paper presents in more detail the importance of understanding the characteristics of these valves, their interpretation, and the, in some cases, need to know the actual characteristics of the valve used.

Keywords: • proportional hydraulic valves • valve characteristics • steady-state • interpretation and measuring • results •

CORRESPONDENCE ADDRESS: Darko Lovrec, University of Maribor, Faculty of Mechanical Engineering, Maribor, Slovenia, e-mail: darko.lovrec@um.si.

1   Introduction

Hydraulic valves are of different types and designed to perform different tasks: To determine the direction of fluid flow and, thus, the motion direction of the actuators, to determine the fluid rate and, thus, the motion speed, and for pressure and to regulate the pressure. Each task requires a certain type of valve. The simplest working of a directional valve is just opening/closing, for starting or stopping fluid flow through the system, but, any failures to these hydraulic valves will affect the accuracy and control of the entire hydraulic system.

Continuously acting valves can eliminate this disadvantage. In addition, several combined tasks can be performed simultaneously, eg, control the direction and speed of the actuator. These tasks can, in principle, be accomplished with two different types of continuously acting valves - with servo valves and with proportional valves – Figure 1.
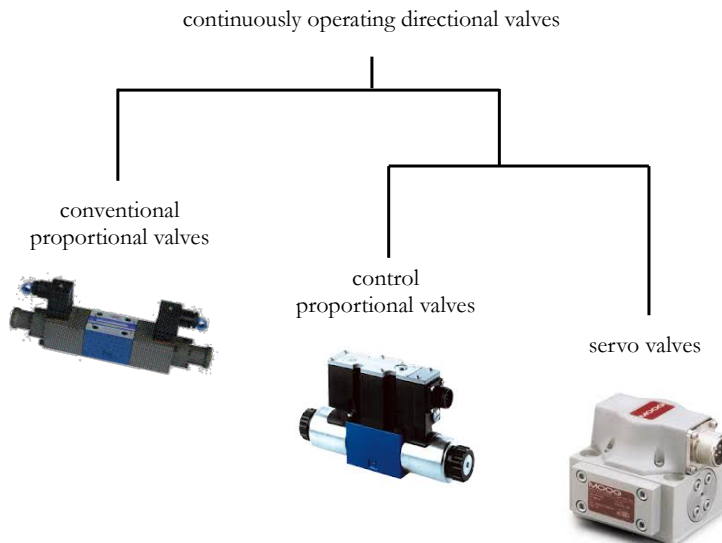

Figure 1: Basic types of continuously-acting valves.

Hydraulic servo valves are continuously acting, electrically modulated directional control valves that convert the electric input signal, varying from 0 to max. value to an accurate hydraulic output. Servo valves are high-performance devices that require an electrical input signal for controlling the flow. The low electrical signal input for the

servo valve can control powerful hydraulic actuators precisely. Normally, they are used for efficiency, repeatability, and for obtaining accurate outputs for high dinamical motion throughout the modern machinery and devices. The primary function of a servo valve usually includes monitoring, feedback, and correction of the control signal/output.

The proportional valves, which appeared later, were intended for use in rough industrial environments and for less demanding applications, especially in terms of dynamics. In contrast to the servo valves, which use a torque motor as an electromechanical transformer, using proportional directional valves, the proportional magnets - a variable solenoid to adjust a notched spool position in a cast housing for flow direction and throttling. With respect to the valve design and its dynamics, the proportional valves are further divided into two subtypes - the conventional proportional valves and the control proportional valves, which are used increasingly in broad areas of machinery.

High-response valves, regardless of whether they are servo valves or control proportional valves, basically provide the same function as directional valves, but at much higher speed and accuracy. Servo valves use a low power (torque) motor to balance hydraulic pilot pressures that control the main spool. This pilot structure is more sensitive to fluid contamination, but dynamics can be very high when used in closed loop applications. The servo also has a main spool that fits into a precise sleeve, which provides the throttling windows to optimise the mechanical/flow design. All three types may be considered, but the specific needs of the application determine which is the most appropriate.

These aforementioned design features, in regard to an electromechanical transformer, valve spool design, a type of spool overlap etc., are evident in the valve characteristics. Knowing the different valve characteristics is the starting point for selecting a suitable continuously acting valve-type for a particular application.

2   Steady-state characteristics of continuously acting valves

While for conventional solenoid valves in the datasheet we usually only find the Δp-Q characteristic and performance limit data, in the case of continuously acting valves there are other additional characteristics that we not only need to know, but also need to interpret correctly. These characteristics can be divided into static and dynamic valve characteristics. Valve flow vs. command value/signal in % or flow vs. stroke in %,

operating limits are static characteristics, step respond and Bode diagram related to valve dynamic are dynamic characteristics. In this paper, we will focus on the static characteristics and their importance.

Figure 2 shows an example of the flow-input signal characteristic of a conventional proportional valve and a controlled proportional valve, as usually provided by the manufacturers of these valves.
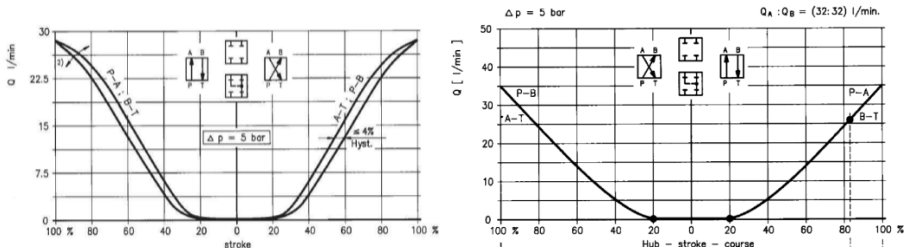

Figure 2: Typical flow-input signal characteristic of a conventional (left) and control proportional valve (right) [1].

Given characteristics for proportional valves are mainly principally, often also, simplified and unified, or even "idealised". Certain details, such as where the hysteresis is measured (in this case not shown on a graph), or the linearity given... are a matter of interpretation and decision by the manufacturer. However, they do not apply exactly to the valve used by the hydraulic control system specialist.

As an example of the characteristics interpreting, let's look at a valve's flow-signal characteristic – Figure 3.

A very important valve parameter is the *dead zone*. A valve with a substantial dead zone is rendered useless in applications that seek null as the ultimate operating condition, such as in positioning systems and some pressure-control systems. The valve *cracking point* is that instant where the valve just begins to open. That may seem a simple and clear statement, however, it is not. Because there is always leakage in spool valves, flow variations take place all through the overlap, or *dead zone* of the valve. The next important parameter is the *valve linearity,* the degree to which the metering curve agrees with a best fit straight line. For a proportional valve, *hysteresis* is the point of widest separation between the metering characteristic curve, with increasing input relative to

the characteristic with decreasing input, as measured along a horizontal line. This idea is presented in Figure 2 for a proportional valve with substantial overlap.
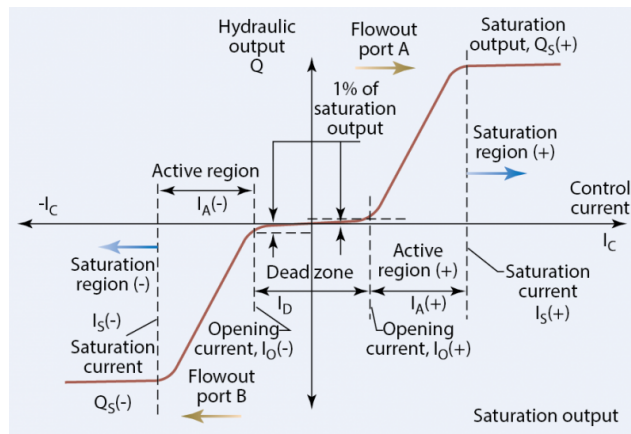

Figure 3:. More detailed given valve flow-signal characteristic [2]**.**

Threshold is an attempt to separate and measure the portion of valve hysteresis caused by friction from the portion caused by the magnetization properties of the torque motor's internal ferromagnetic parts. In that respect, the threshold represents the very minimum possible hysteresis when all the magnetic effects have been eliminated. Other parameters such as *valve flow gain* and *valve velocity gain* should be mentioned [2], [3], [4].

All very briefly mentioned parameters are important for the comparison of the characteristics of the different hydraulic continuously acting valves from different manufacturers, to check the characteristics of the same valve types of the same manufacturer, to compare the characteristics and evaluate the variation of the characteristic over the operational period of the valve, or to evaluate the wear impact… the characteristics of the valve under consideration must be known. This can only be achieved by measuring the characteristics according to the standardised measuring procedure, and a standardised presentation of results. For continuously acting hydraulic control valves the Standard ISO 10770 is valid [5].

3   ISO 10770-1 steady-state tests

The ISO 10770-1 Standard applies to modulate hydraulic control valves electrically and consists of three parts. The first part refers to the testing of 4-port directional valves, the second part relates to the testing of 3-port valves, and the third part to the pressure control valves [5].

The Standard is divided into electrical tests, performance tests that are further divided into dynamic and static tests, and pressure impulse tests. For the preselection of control valves, the static performance tests of 4-port directional valves are relevant. With this Standard, different static tests resp. characteristics are defined: Proof pressure tests, an internal leakage test, output flow versus input signal test, flows across lands versus input signal, output flow versus load pressure difference, output flow versus valve pressure drop, limiting output flow versus valve pressure drop, output flow versus fluid temperature, pressure difference versus fluid temperature etc. A typical steady-state test layout according the Standard ISO 10770-1 is depicted in Figure 4.
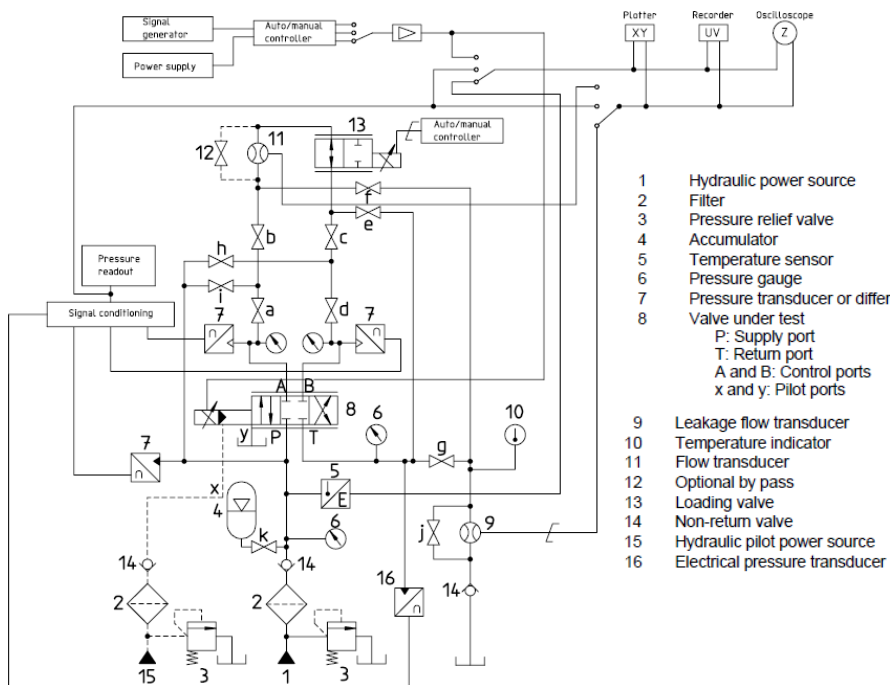

Figure 4: Layout for ISO 10770-1 steady-state tests as given in the Standard [5]

The set of steady-state tests is quite extensive. Proof pressure tests shall be performed prior to carrying out any other tests. In accordance with the Standard we focused on the following tests:

a) Internal leakage test:
b) Output flow versus input signal at constant valve pressure drop, to determine:
      1) Rated flow;
      2) Flow gain;
      3) Flow linearity;
      4) Flow hysteresis;
      5) Flow symmetry;
      6) Flow polarity;
      7) Spool lap condition;
      8) Threshold.
c) Flows across lands versus input signal,
d) Output flow versus load pressure difference,
e) Output flow versus valve pressure drop,
f) Limiting output flow versus valve pressure drop,
g) Output flow versus fluid temperature,
h) Pressure difference versus fluid temperature,
i) Pressure gain versus input signal,
j) Pressure null shift and
k) Fail-safe function test in accordance.

The Standard specifies the procedure for performing the test fairly accurately, as well as the conditions for conducting the individual tests.

To determine the actual characteristic of the proportional valve in question, to compare the characteristics of valves of the same size but different manufacturers, to compare the characteristics of the same type of valve of the same manufacturer (which serves as a starting point for the valve development valve manufacturer), for the pre-selection of identical valves of the same valve type for the purpose of comparative tribological research (in regard to using new fluid or material used – [6] to [11]), for monitoring the valve wear condition after certain operating periods... the most useful in terms of the data obtained are the flow- input signal test and the leakage test.

Some examples of the characteristics as shown in the Standard ISO 10770-1 are depicted in Figure 5.
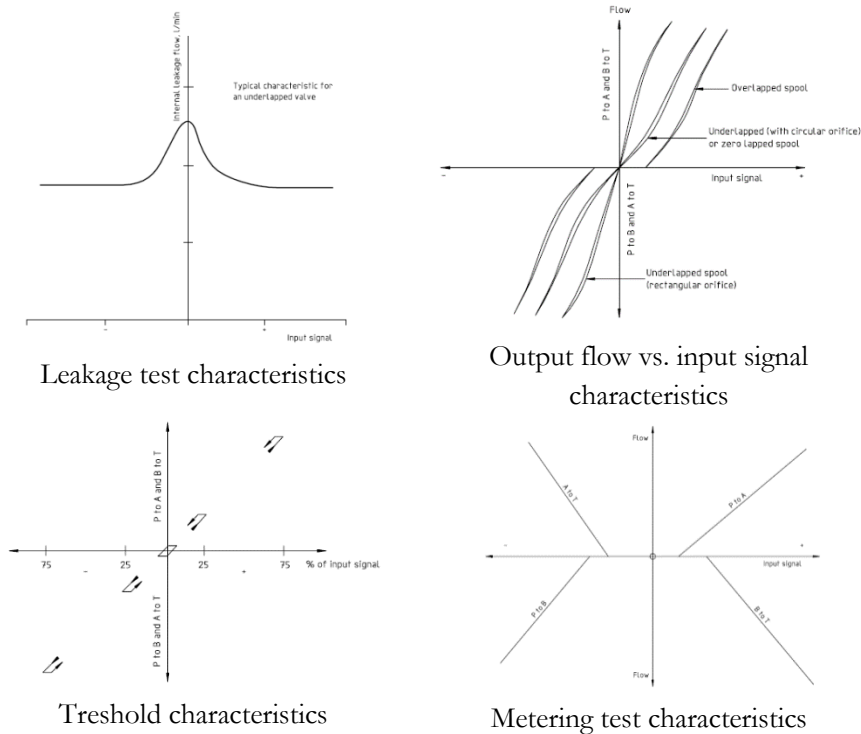

Leakage test characteristics

Output flow vs. input signal characteristics

Treshold characteristics

Metering test characteristics

Figure 5: Steady-state characteritics as shown in Standard ISO 10770-1.

4.   Steady test characteristic measuring device and test results

The characteristics shown in Figure 5 have only the principal course of the curve. In order to determine the actual course of these characteristics, it is necessary to build a measuring device. This contains, in addition to the hydraulic part of the device, designed in accordance with the Standard proposal, appropriate sensors and with the appropriate control and data acquisition system for the automated recording of the individual characteristic. The layout of the device for measuring of 4-way directional flow control valves and the appearance of the device equipped with sensors are shown in Figure 6.

With the device shown, the repeatability of the measurement procedure was performed first, and then the following most important characteristics were measured for three proportional valves of the same type: Leakage test, metering test, output flow vs. input signal test, null shift, dead-band/zone and hysteresis.
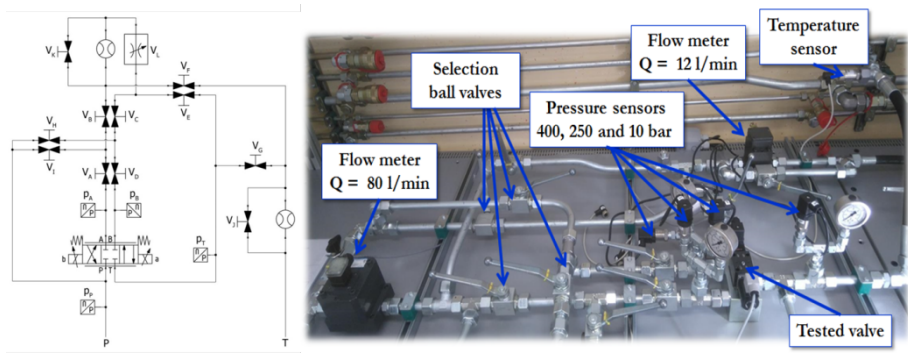

**Figure 6: Hydraulic scheme of measurement device layout (left) and
the actual appearance of the device with sensors (right).**

As an example of using a steady-state characteristics measuring device, let's look at its use for the purpose of pre-selection of proportional valves for further tribological research.

For this research purposes, it is of extraordinary importance that we use valves with exactly the same respectively identical characteristics. The importance of the preselection process of valves is shown on an example of a classical directional proportional valve type of usual market quality, without a control spool measuring system.

In the considered case, we used three identical valves of the same manufacturer, with the same label and code, and, thus, expected the same characteristics. The results of the preselection process are presented in the form of three different valve test-characteristics: A leakage test, metering test and output flow vs. input signal test. The results of the characteristics` measurements are shown in Figures 7, 8 and 9.

Based on a comparison of three different characteristics of the same type of valve, it is more than obvious that all valves are not identical, even though they are declared as the same type of valve.
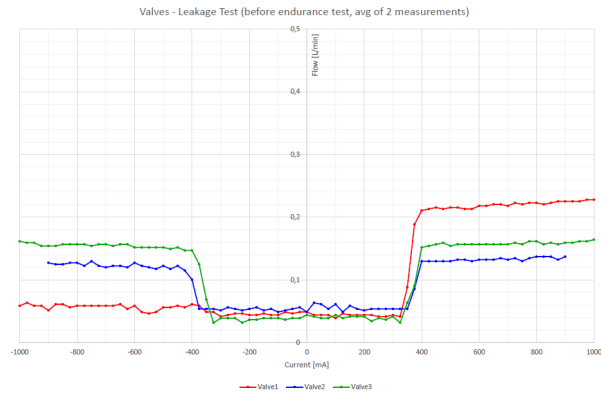
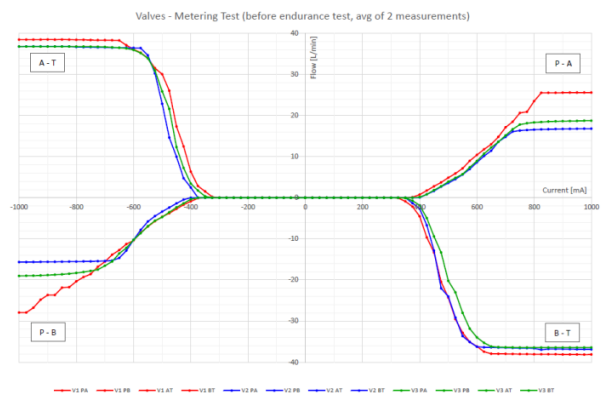**Figure 7: Comparison of an internal leakage test characteristic for three valves.**

Figure 8: Comparison of metering test characteristics for three valves.
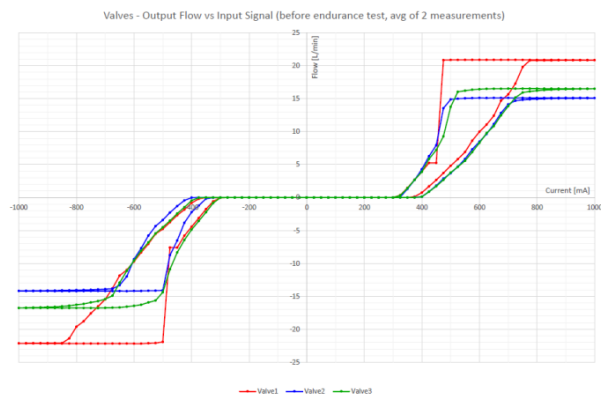

Figure 9: Comparison of output flow vs. input signal characteristics for three valves.

The differences between the characteristics of valves occur due to the valve manufacturer's fault, whether an incorrect/different built-in valve spool, or the error is due to the incorrect code listed on the valve plate.

Whatever is the cause of the mistake in these differences, this is reflected consequently as different valves with different properties. When conducting the tribological research, in this case, false conclusions would arise. If we know exactly the baseline situation, we will be able to give an appropriate assessment of the condition of the valve leakage range, degree of wear, wear and change in the geometry of the control edges.

5.   Conclusion

The paper highlights the background and the importance of understanding the characteristics of the continuously acting valves, in the considered case of proportional valves, their interpretation, and the usefulness of the individual characteristics.

When we come across characteristics and Standards, such as in the case of the static characteristics of proportional valves, we usually think that Standards are only necessary for valve manufacturers, as they must measure the characteristics and make them available to users in the data sheets. The starting point is really a certain Standard that should describe and define measuring procedures and interpretation of a characteristic very precisely. Although the Standards are, in part, very precise, on the other hand they leave a lot of open questions or undefined issues. These are left to the discretion of the manufacturers when specifying the characteristics and numerical values of a specific value or parameter.

When performing tribological tests with hydraulic pumps, the specific type of pump used is defined precisely. In the case of tribological tests with hydraulic valves, almost nothing or very little is specified. For example, in order to compare the impact of different hydraulic fluids on the wear of the same type of valve, it is necessary first of all to ensure the same starting points. Only in this case, can we rely on the credibility of results. In this case, the valve characteristics given in the manufacturer`s data sheet are not enough. They need to be measured by standardised procedures for each specific valve, since it is necessary to use identical valves for comparison purposes.

Except for the use of identical valves in all subsequent tests, we have also come up with other important information, for example: To know the actual leakage rate of the new valve and the leakage rate of the already worn-out valve, to determine the actual valve characteristic compared to those available in data sheets, to know all the characteristics of the same valve according the Standard.

The latter certainly includes knowledge of the actual characteristics of the built-in valve, as well as its actual condition, which allows monitoring the trend of valve wear and the impact of its efficiency.

References

[1]   Hanson, N. (2010). Hydraulic Proportional and Closed Loop System Design, Bosch Rexroth AG, pp. 86
[2]   Johnson, J. (2005). More About How to interpret Valve Specifications, Hydraulics & Pneumatics, 1-2005
[3]   Johnson, J. (2005). Pressure gain – an important valve characteristic, Hydraulics & Pneumatics, 2. 2005
[4]   SUN Hydraulics. (2010). Elektro-Proportional Terms and Definitions, Sun Hydraulics Corporation, pp. 12
[5]   ISO 10770-1. (2009). Hydraulic fluid power-Electrically modulated hydraulic control valves - Part 1: test methods for 4-port directional flow-control valves
[6]   Lawrence, M. (1989). Experimentelle und analytische Untersuchung der Verschmutzungs-empfindlichkeit hydraulischer Komponenten, Dissertation, RWTH Aachen, Germany
[7]   Lehner, S. (1996). Verschleißwechselwirkungen in hydraulischen Komponenten durch Feststoffverschmutzung des Druckmediums, Dissertation, RWTH, Aachen, Germany
[8]   Zhang, K., Yao, J., Jiang, T., Yin, X., Yu, X. (2013). Degradation Behavior Analysis of Electro-Hydraulic Servo Valve under Erosion Wear, 978-1-4673-5723-4/13/ ©2013 IEEE
[9]   Reinertz, O., Schlemmer, K., Schumacher, J., Murrenhoff, H. (2010). Development of an Accelerated Ageing Test for Hydraulic Spool and Poppet Valves, 7th International Fluid Power Conference, Aachen 2010, pp. 1-13
[10]   Weber, P., Schumacher, J., Murrenhoff, H. (2015). Wear Characterization of Hydraulic Spool Valves by Means of Short Time Ageing Tests O+P Journal 1/2015
[11]   Lovrec, D., Edler, J. (2019). Selection procedure of hydraulic valves for tribological research. Serbiatrib '19: Proceedings on Engineering Sciences, ISSN 2620-2832, vol. 1, no. 1-2019, Kragujevac, Serbia, pp. 646-651

University of Maribor Press

Control of Linear Servo Hydraulic High-cycle Fatigue Testing Device

ISHVARI FERNANDA ZUŇIGA TELLO, VITO TIČ & NENAD GUBELJAK

Abstract Many fatigue machines used for industrial or laboratory applications are limited to perform a single fatigue test and its components are commonly servo- hydraulic or pneumatic actuators of high capability, leading to high costs. In the present paper a fatigue machine which works up to 40 kN and it is used to investigate the fatigue behaviour for industrial materials is presented. This machine employs servo-axes mounted with a linear motion mechanism to develop fatigue tests from 0.1 to 20 Hz under tension. The control and programming of the machine is carried out by Beckhoff soft PLC and software, allowing an easy control.

Keywords: • servo hydraulic • fatigue testing device • control system • Beckhoff • soft PLC •

CORRESPONDENCE ADDRESS: Ishvari Fernanda Zuñiga Tello, Michoacan University of Saint Nicholas of Hidalgo, Faculty of Mechanical Engineering, Avenida Francisco J. Mugica, Ciudad Universitaria, Michoacan, Mexico, e-mail: isfernanda@hotmail.com. Vito Tič, University of Maribor, Faculty of Mechanical Engineering, Maribor, Slovenia, e-mail: vito.tic@um.si. Nenad Gubeljak, University of Maribor, Faculty of Mechanical Engineering, Maribor, Slovenia, e-mail: nenad.gubeljak@um.si.

1   Introduction

The introduction of new materials creates the necessity of understand them mechanical properties, one of the most important is the fatigue behaviour, the main interest in those tests is to warrant the safety of the component in service [1] to [3]. Evaluate fatigue endurance by experimental procedures becomes necessary arguing the fact that theoretical equations do not always fit the real fatigue behaviour [4].

Then, it results necessary to carry out mechanical fatigue tests in different modalities and on a wide variety of materials to investigate the principal causes of failure in engineering components subjected to uniaxial and multiaxial loading [5]. Fatigue test specimens are primarily described by the mode of loading these could be axial stress, plane bending, rotating beam, alternating torsion, combined stress testing machines, however, may be universal type machines that are capable of conducting all of the above modes of loading, depending on the fixturing used [6]. Several authors have designed and constructed their own machines for specific applications [7] to [11]. In regard fatigue machines, the market is saturated by expensive machines and the variety of fatigue machine also depend the regimen of frequencies used [11]. The systematic studies on fatigue have been carried out in the second half of the twenty century on aluminium alloys [12], [13]; whereas most recent developments are oriented to the fatigue machines controlled by a servo-actuator , or the use of a resonance system to induce failure by fatigue [14], [15]. This developed machine is oriented to perform fatigue tests under force-controlled mode. The description of the present fatigue machine includes the process to carry out fatigue tests in Aluminium alloy 7075-T6.

2   Materials and methods

The chemical composition (% in weight) and the principal mechanical properties are listed in Table 1 and Table 2, respectively. In order to obtain mechanical properties of AA7075-T6, tensile testing was conducted on universal testing machine Instron 1255 on 4 specimens (cold rolled Al7075-T6 sheet) of non-standard dimensions at room temperature.

Specimens used in fatigue test were machined from an AA7075-T6 plate, the design of the specimen were obtained upon specimens designed to ultrasonic fatigue tests, this is due to the requirement for the ultrasonic fatigue test are higher than for specimens in this regimen of fatigue.

Table 1: Chemical composition by weight of Aluminium alloy 7075-T6

Zn	Mg	Cu	Cr	Fe	Al
6.9 max.	2.7 max.	1.87 max.	0 of.2 max.	0.4 max.	Balance

Table 2: Principal mechanical properties Aluminium alloy 7075-T6

Density	Hardness	σ_y	σ_u	Poisson ratio	Elasticity Module
[kg/m³] 2800	[HV0.1] 155.12	[MPa] 453	[MPa] 538	0.33	[GPa] 70

2.1 Specimen´s geometry

Specimens used in fatigue tests, were designed upon the ultrasonic fatigue specimens, in order to adapt the specimens to the machine, Figure 5. The geometry of the fatigue specimens is designed with a reduced cross section that allows present the maximum stress amplitude in the middle section with the maximum stress intensity factor. Providing the specimen an effective clamping method is an important step of the procedure, that can allow the correct force distribution in the specimen, and the correct alignment in the axes of the machine avoiding with this other phenomena as can be torsion or flexion, wanted phenomena for the study.
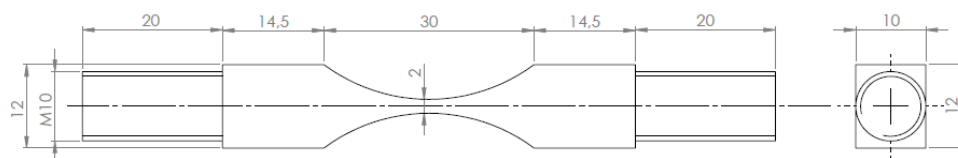

Figure 1: Fatigue specimen dimensions.

3   Design and description of the fatigue machine

Testing line was manufactured from high-quality materials and adapted to hydraulic cylinder and table that were previously manufactured. Original design of testing line made in SolidWorks is presented on Figure 2. Machine was adapted for experiments of dynamical tests with controlled force, where amplitude and frequency of the force are controlled. Testing line was dimensioned with respect to tensile forces. Machine can perform uniaxial static and dynamic tensile tests. If the machine would be tested on compression, the contact surfaces can be damaged or individual parts can be broken down. Maximum tensile force of the machine is 40 kN.
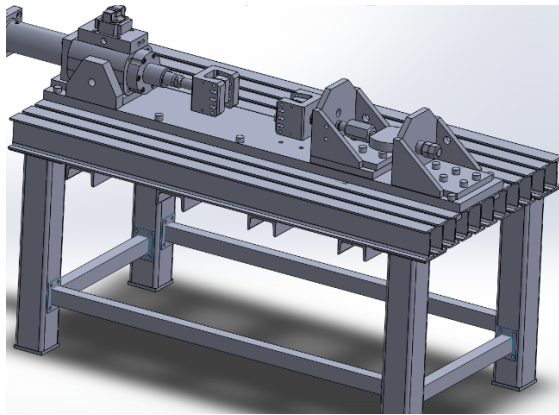

Figure 2: Original design of testing line in SolidWorks.

On the table is steel plate attached to I profiles on the table. On the steel plate is bolted the testing line. On one side of the testing line is hydraulic cylinder, with wedge grip (Figure3) attached to it. On the other side of the testing line is another wedge grip on one of the welded brackets. The distance between wedge grips can be adjusted by positioning of the hydraulic cylinder or by bolting welded brackets on another position of steel plate. System of the wedge grip is self-tightening.

Wedge grip has moving body and stationary jaws. The surface of jaw face that holds the specimen is ribbed. Holes through the wedge grip body and jaws were made for centring of the specimen with bolts, while preventing opening of the jaws and increasing stiffness. Opening of the jaws is also prevented by putting spring on the side of the jaws and inner part of wedge grip body, allowing the jaw width to increase when

dimensioning. Specimen is easy to set up for testing. When specimen is set in the wedge grip, while testing force increases, gripping force increases as well. Body and the jaws of the wedge grip is made of tool steel 115CrV3 (DIN). Body of the wedge grip is tempered on 850 ±20 MPa. Jaws of the wedge grip are quenched on 52 ±2 HRC.
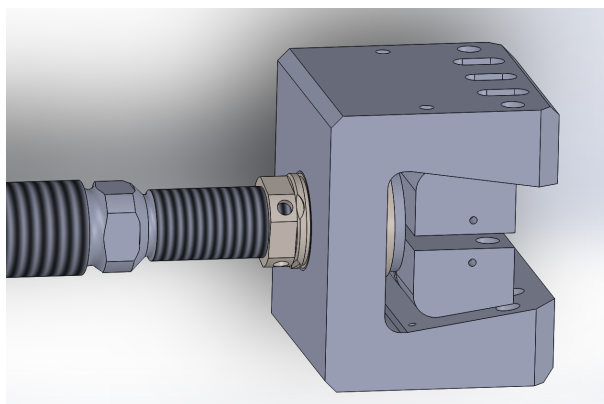

Figure 3: Wedge grip.

Force sensor is set on the opposite side of hydraulic cylinder, between two welded brackets, because the absolute displacement of the sensor is small between stiffening and the specimen. The system can be improved by using of sensor for measurement of deformation in order to obtain the tensile characteristics.

Figure 4: Lateral view of the fatigue test machine.

3.1   Hydraulic system

Hydraulic system is powered by Parker PAV 32 adjustable pump capable of delivering up to 45 L/min under 315 bar of pressure which controls 74,5/63 x 110 double rod hydraulic cylinder with the help of MOOG G761 servo valve.

3.2   Control system

Control system is based on Beckhoff CX5140 quad core soft PLC which runs the developed PLC program at 0.1 ms cycles. The CX5140 also runs the HMI application developed in Windows C# in parallel. The control runs on Windows 7 Embedded and it is used to setup the test and make the recordings during the test.

Figure 5: Control panel.

The control panel is presented in Figure 5 and allows the user to setup the main properties of the test, such as: test frequency (Hz), force (N), force amplitude (N) and number of cycles. User can also set the parameters of the PID closed loop controller and parameters of periodic auto recording.

3.3   First test

After manufacturing of the testing line, the system was tested up to 20 Hz as shown in Fig. 6, which presents systems response to PID closed loop force control at 20 Hz. The figure reveals that the actual force recorded is not ideal sinus since the lowest possible filter was used on the force input signal.
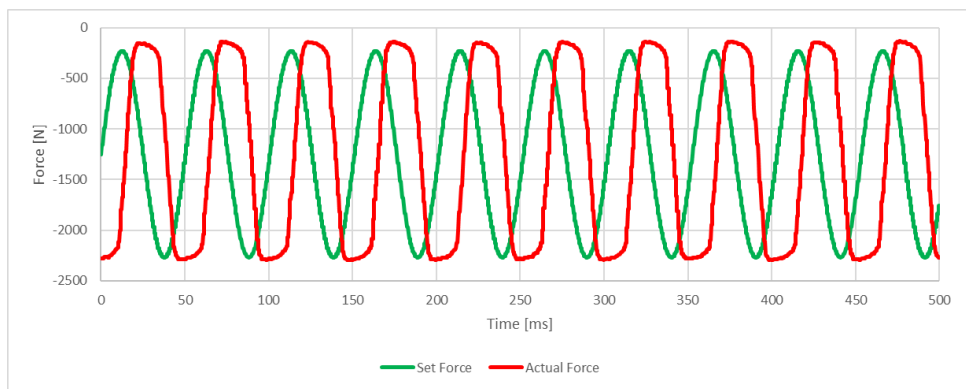

Figure 6: Machine performance at 20 Hz.

While testing the system, deformations were observed on welded bracket and on the horizontal steel plate on which the entire testing line was located. Numerical analysis of horizontal steel plate showed calculated maximum value of deformation more than 1 mm. In order to reduce the deformation and increase rigidity of the system, side plates (material S270) were set up. By placing the side plates, access to the sample is not prevented.

4   Results and discussion

Fatigue test were performed in load control, at a room temperature (20 °C). The maximum stress was 110 MPa (20 % of yield stress) and load ratio was R = 0.1, during the test the strain amplitude was recorded each 5000 cycle, the strain amplitude remained constant but the strain mean value decreases with increasing number of cycles. Figure 7 shows a shift of the mean strain between start, middle and end cycle, choosing from al the previous records data that we can get from the machine.
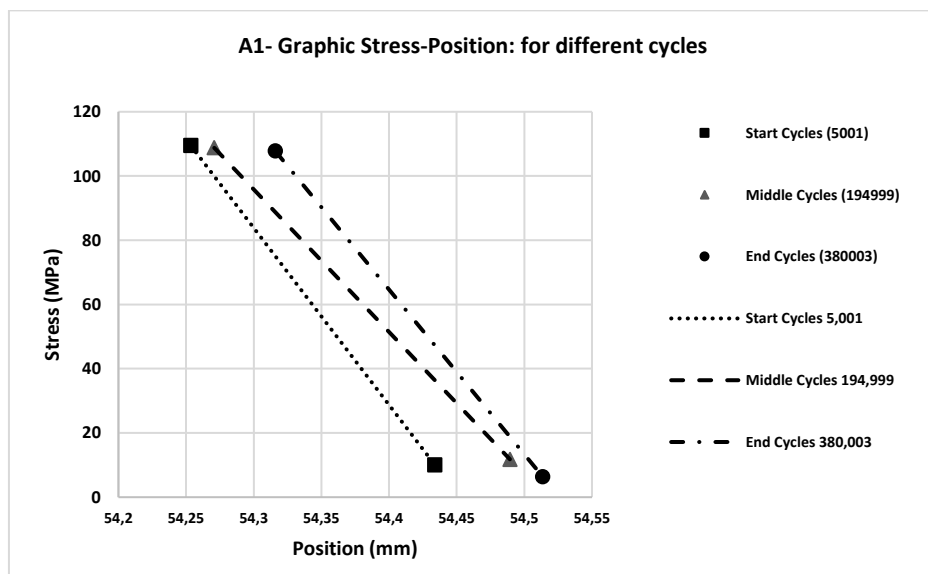

Figure 7: Characteristic stress-strain records during fatigue loading.

The degradation of the material, aluminium alloy 7075-T6, is not visible until the surface is analysed with microscope, optical microscope and SEM where used for this duty, it was observed degradation of the material during the test, evident up to 10^7 cycles, changing the roughness measurements and residual stresses values before and after the tests. Test were conducted under a frequency of 20 Hz, the machine was programed upon certain number of cycles, after those the machine automatically stopped if the material didn't fail.

5   Conclusion

The description of a fatigue machine is presented with successful experimental results on the AA 7075-T6.

The precision of the force applied with this fatigue machine is around ±2% of the theorical force values this do not represent a high variability in the results of the theoretical values and the real values during test, these results on the test, prove the capability of the machine to test small specimens under small forces, this means the control system prove that the machine is adequate to be adapted in a lot of type of specimens.

Adequate the holding system of the specimen result an easy procedure, this will depend the geometry of the base material, making this and advantage, because it is not required complex clamping systems.

Regarding the fatigue results of the tests in AA 7075-T6 it can be concluded that specimens with smooth surface can be tested over 10^7 cycles, where it start to appearing micro cracks and local plastification on the material, the investigation will not only be focus in to the control system but also in fatigue tests of different materials.

References

[1]   Pao, P. S., Gill, S. J., Feng, C. R. (2000). On fatigue crack initiation from corrosion pits in 7075-T7351 aluminum alloy, Scr. Mater., vol. 43, no. 5, pp. 391–396

[2]   Weißgraeber, P., Felger, J., Geipel, D., Becker, W. (2016). Cracks at elliptical holes: Stress intensity factor and Finite Fracture Mechanics solution, Eur. J. Mech. A/Solids, vol. 55, pp. 192–198

[3]   DuQuesnay, D. L., Underhill, P. R., Britt, H. J. (2003). Fatigue crack growth from corrosion damage in 7075-T6511 aluminium alloy under aircraft loading, Int. J. Fatigue, vol. 25, no. 5, pp. 371–377

[4]   Cui, W. (2002). A state-of-the-art review on fatigue life prediction methods for metal structures, J. Mar. Sci. Technol., vol. 7, no. 1, pp. 43–56

[5]   Doquet, V., De Greef, V. (2012). Dwell-fatigue of a titanium alloy at room temperature under uniaxial or biaxial tension, Int. J. Fatigue, vol. 38, no. 2012, pp. 118–129

[6]   Boyer, H. E. (1986). Atlas of Fatigue Curves: Fatigue testing

[7]   Marcelo, F., Bustos, P. (2012). Design and construction of a torsional fatigue testing machine operated by inertial loads, Dyna, year 79, No. 172, pp. 46–55

[8]   Petersen, D. Link, R. Fletcher, D., Beynon, J. (2000). Development of a Machine for Closely Controlled Rolling Contact Fatigue and Wear Testing, J. Test. Eval.

[9]   Feng, M., Li, M. (2010). Development of a Computerized Electrodynamic Resonant Fatigue Test Machine and Its Applications to Automotive Components, in SAE Technical Paper Series

[10]   Bathias, C. (2006). Piezoelectric fatigue testing machines and devices, Int. J. Fatigue, vol. 28, no. 11, pp. 1438–1445

[11]   Ambriz, J. L. A., Almaraz, G. M. D., Julio, C., Juarez, V., Gomez, E. C., Zuñiga, I. F. (2017). Design and construction of a torsion fatigue machine: torsion fatigue test on two industrial aluminum alloys, ISSN 1454-2358, vol. 79

[12]   Heinz, A., Haszler, A., Keidel, C., Moldenhauer, S., Benedictus, R., Miller, W. S. (2000) Recent development in aluminium alloys for aerospace applications, Mater. Sci. Eng. A, vol. 280, no. 1, pp. 102–107

[13]   Nwachukwu, O. P., Gridasov, A. V., Talskikh, K. Y., Grishin, A. V., Nikiforov, P. A., Sukhorada, A. E. (2017). Aluminum and its alloys in the very high cycle fatigue regime Aluminum and its alloys in the very high cycle fatigue regime, World Scientific News, WSN 81(2)(2017)121-13

[14]   Zuñiga, T. G. M., Ishvar,i F., Almaraz, D., Guzman Tapia, M., Avila Ambriz, J. L. (2017). Controlled Pre-Corrosion Attack and Ultrasonic Fatigue Endurance of Titanium Alloy Ti – 6Al – 4V, Lat. Am. J. Solids Struct., vol. 14, no. 3, pp. 512–527

[15]   Ouarabi, M., Mora, R. P., Bathias, C. (2016), Very high cycle fatigue strength and crack growth of thin steel sheets," vol. 36, pp. 112–118

University of Maribor Press

Position Controller for Direct Driven Electro-Hydraulic System

JURAJ BENIĆ & ŽELJKO ŠITUM

Abstract In the past few years, decentralized hydraulics gain advantage over classical hydraulics due to lower energy consumption, lower pressure losses in pipelines and easy automatization. In this paper, Direct Driven Electro-Hydraulic (DDEH) drive is made in parallel with a classical proportional hydraulic system. In DDEH control method the valve is replaced with reversible pumps/motors which are directly controlled with a servo motor. Such systems combine best properties of both hydraulic and electric drives. Proposed experimental setup is designed for easy switching between both systems which allows exact comparison of obtained experimental results. The nonlinear models of both systems have been derived using PID controller and simulated in Matlab program. Finally, the conclusion regarding precise position control and system dynamics is given in detail.

Keywords: • hydraulics • DDEH • control theory • system modeling • PID controller •

CORRESPONDENCE ADDRESS: Juraj Benić, University of Zagreb, Faculty of Mechanical Engineering and Naval Architecture, Zagreb, Croatia, e-mail: jbenic@fsb.hr. Željko Šitum, University of Zagreb, Faculty of Mechanical Engineering and Naval Architecture, Zagreb, Croatia, e-mail: zsitum@fsb.hr.

1   Introduction

In the last decade, energy efficiency become one of the most important research topics in hydraulics which lead to a compact electro-hydraulic system. Such systems are controlled by valve or pump and they can deliver powerful linear movement. Characteristics of these systems are their small-to-power ratio and ability to achieve very large forces and torques. The main drawback of valve-controlled hydraulic system is their low energy efficiency due to constant fluid throttling [1]. An alternative to valve-controlled systems are pump controlled systems which are directly driven by the servo motor [2], [3], [4], [5]. These systems have superior efficiency and compact structure then conventional systems. Additionally, speed control is directly done by the servo motor thus allowing us a wide range of regulated speeds, high accuracy and energy efficiency.

In the past few years, researches are focused in replacing a double rod cylinder, used in pump-controlled systems [6], [7], with a single rod cylinder where the inlet and outlet flow of the cylinder is unequal due to difference between cylinder's areas. The main problem of such system is related to the stability of the actuator velocity and the energy efficiency if the pump controller is only optimized for static operation. These problems are addressed in [8], [9].

A new concept of a single rod cylinder pump-controlled system called Direct Driven Hydraulic (DDH) drive is proposed in [10]. In the proposed system two reversible pumps/motors are utilized and mutually interconnected with a shaft and a servo motor via gear transmission. Through reversible pumps/motors units, servo motor directly controls inlet and outlet flow of an asymmetric cylinder. Detailed working principle is described in [10], [11]. A compact structure of a DDH setup was investigated in [11] where oil tank was replaced by the accumulator. The study showed that the proposed system can easily balance volume flow in asymmetrical cylinder. In [12], [13] a detailed thermal analysis of DDH was carried out and showed that DDH reached acceptable and safe temperature range within steady state operation point. All components of a DDH system were heated considerably and the temperature rise of the components presented an exponential trend. From energy efficiency point of view, the test carried out in [14] showed that energy efficiency considerably depends on piston motion and motor speed. Lifting efficiency varies from 48 % to 20 % while lowering efficiency varies from 32 % to 8 %. Energy efficiency of an excavator was investigated in [15]

where three DDH units replaced LS hydraulic system and simulations showed that overall energy efficient for a given cycle could reach 73.3 %.

In this paper, a PID control of direct driven electrohydraulic setup (DDEH) is being investigated and compared to a conventional hydraulic system. Comparison of both systems is done for the same working conditions thus allowing as to mutually compare obtained experimental results for both systems. In Section 2 a self-made experimental setup is introduced while in Section 3 and Section 4 a detailed mathematical model is derived and simulated. Conclusion and further work are given in Section 5.

2 Experimental setup

The partially build experimental setup is shown in Figure 1. The proposed setup consists of two independent subsystems as shown in Figure 2. The first subsystem is the classical electro hydraulic system controlled using proportional valve and designed for obtaining reference experimental results. The subsystem uses a 1.1 kW Končar AC motor and Hydronit gear pump with displacement of 3.7 cm³/rev for hydraulic power supply. Position control of a double acting hydraulic cylinder in a gravitational field is achieved with Argo-Hytos PRM2 proportional valve.
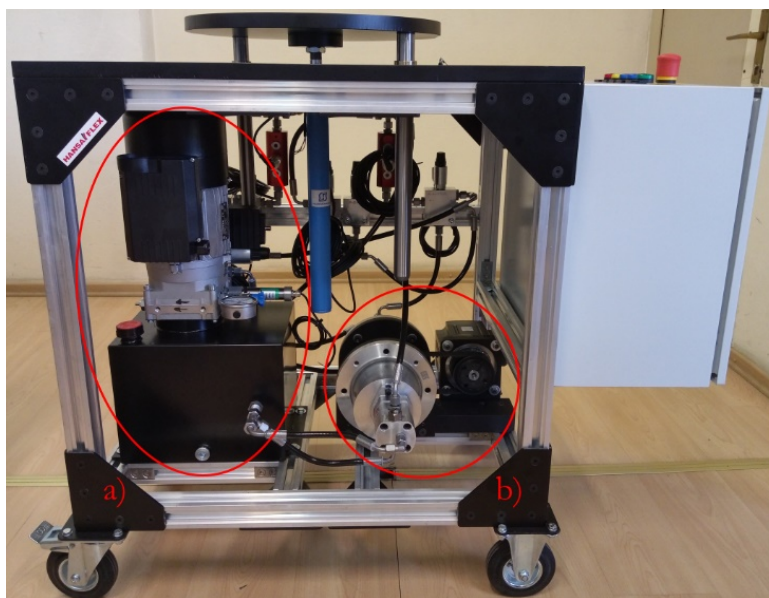

Figure 1: Experimental setup: a) classical hydraulic system, b) DDEH system.

The second subsystem is related to the proposed DDEH system. The DDEH system uses speed-controlled AC servo motor and belt transmission for propelling the hydraulic pumps connected to the cylinder's chambers. One hydraulic pump directly controls the amount of oil pumped into the system and at the same time second pump controls the amount of oil pumped from other side of double acting cylinder. Required operating system pressure is determined by the payload. Servo drive controls the fluid flow, position of the payload and direction of motion. Argo-Hytos gear pumps with displacement of 4.8 cm3/rev and 2.5 cm3/rev were used for reversible pump 1 and pump 2 respectably. The cylinder is chosen to match the pumps as described in [16].
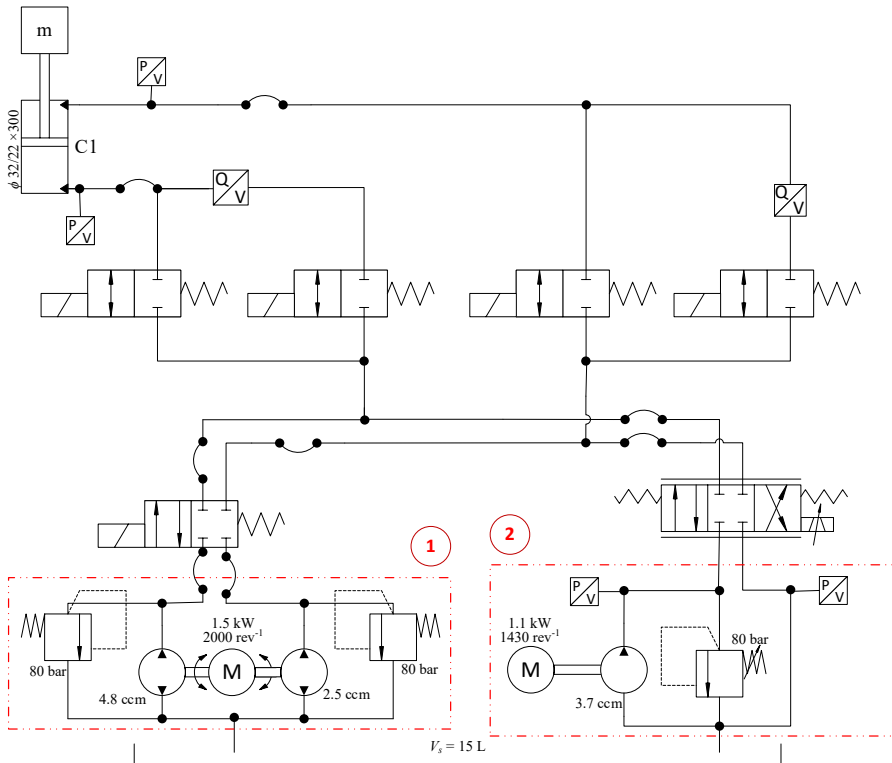

Figure 2: Schematic representation of experimental setup: 1) DDEH, 2) classical system.

The position of the cylinder is measured with Micro Epsilon analog wire sensor. The system pressure is measured with Hydac HAD 7446 pressure sensor and the flow is measured with Hydac EVS 3106 sensor. List of all used components is given in Table 1.

Table 2: Components of a DDEH system

Component		Model
Hydraulic part	Cylinder	Hidromehanika $\phi 32/22 \times 300$
	Valves (2/2 and 4/2)	ARGO-HYTOS SD2E-A2/L2I12M2-A
	Proportional valve	ARGO-HYTOS PRM2-063Z11/8-24EKBK1N2V-A 4/3
	A – side pump	ARGO-HYTOS GP1-4,8B-SAVB-SGBGB-N002
	B – side pump	ARGO-HYTOS GP1-2,5B-SAVB-SGBGB-N002
	Power pack pump	Hydronit gear pump 3.7 cm3/rev
Electric part	AC motor	Končar 5AZCD 90SB-4 B14 F115 1,1kW
	Servo motor	Mitsubishi electric servo motor HG-SN152JK
	Motor controller	Mitsubishi electric servo drive MR-JE-200A
	Control unit	Mitsubishi electric PLC FX5U-32MT/ESS
Sensors	Pressure sensors	HYDAC HDA 7446-A-100-000
	Flow sensors	HYDAC EVS 3106-A-0020-000
	Linear position sensor	MICRO-EPSILON WDS-500-P60-SR-U

The considered experimental electro-hydraulic system is made in the Laboratory for automation and robotics at the Faculty of Mechanical Engineering and Naval Architecture, University of Zagreb.

3   System modeling

3.1   Modeling of the hydraulic cylinder

The schematic representation of the asymmetric hydraulic cylinder and forces acting on it, is given in Figure 3. The goal is to model the actuator which lifts the load in the gravitational field.
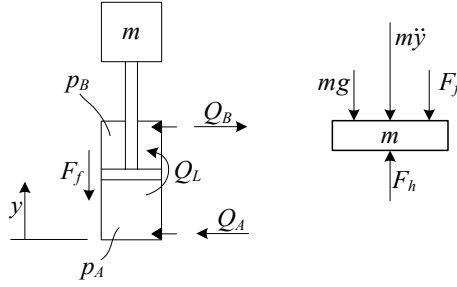
Figure 3: Schematic model of the hydraulic cylinder.

The force balance equation for the hydraulic cylinder can be written as follows:

$$m\ddot{y} = p_A A_A - p_B A_B - F_f - mg \tag{1}$$

Where m, y and g represent the mass, displacement and gravitational acceleration respectively, p_A and p_B are cylinder chamber pressures, A_A and A_B are piston head and rod-side areas while F_f represents friction force. For the friction force, the LuGre model [17] is utilized and it is given as:

$$F_f = \sigma_0 z + \sigma_1 \frac{dz}{dt} + \sigma_2 v \tag{2}$$

$$\frac{dz}{dt} = v - \frac{\sigma_o z}{g(v)} |v| \tag{3}$$

$$g(v) = F_c + (F_s - F_c) e^{-\left(\frac{v}{v_s}\right)^2} \tag{4}$$

where σ_0, σ_1 and z are average stiffness, dampening and deflection of bristles, σ_2 is viscous friction coefficient, v and v_s are relative and Stribeck velocity while F_c and F_s are Coulomb and static friction. Pressure dynamic of the cylinder chambers is given with equations:

$$\dot{p}_A = \frac{B}{V_{0,A} + A_A y} [Q_A - Q_L - A_A \dot{y}] \tag{5}$$

$$\dot{p}_B = \frac{B}{V_{0,B} + A_B(L-y)} [Q_B + Q_L + A_B \dot{y}] \tag{6}$$

where B is bulk modulus, Q_L is neglectable leakage flow between cylinder chambers, L is piston stroke while $V_{0,A}$ and $V_{0,B}$ are dead volumes.

3.2   Classical system modeling

Dynamics of the spool displacement x_v in relationship to the input voltage signal u can be expressed as second-order system in the following form:

$$\ddot{x}_v = -2\xi\omega_v\dot{x}_v - \omega_v^2 x_v + K_v\omega_v^2 u \tag{7}$$

where ω_v, ξ and K_v are natural frequency, damping and gain of the proportional valve. The flow through proportional valve orifices with assumed zero-overlap is given as:

$$Q_A = \begin{cases} C_d x_v w \sqrt{\dfrac{2}{\rho}}\sqrt{|p_S - p_A|}, & x_v \geq 0 \\ C_d x_v w \sqrt{\dfrac{2}{\rho}}\sqrt{|p_A - p_T|}, & x_v < 0 \end{cases} \tag{8}$$

$$Q_B = \begin{cases} -C_d x_v w \sqrt{\dfrac{2}{\rho}}\sqrt{|p_B - p_T|}, & x_v \geq 0 \\ -C_d x_v w \sqrt{\dfrac{2}{\rho}}\sqrt{|p_S - p_B|}, & x_v < 0 \end{cases} \tag{9}$$

where C_d, w and ρ are the discharge coefficient, the area gradient and the fluid mass density, respectively while p_s and p_T are supply and tank pressure respectively. For the position control of the hydraulic cylinder, a PID controller is utilized and it is given as:

$$u(t) = K_p\, e(t) + K_i \int e(t)dt + K_d\dot{e}(t) \tag{10}$$

where K_p, K_i, K_d represents proportional, integral and derivate gain and $e(t)$ represents the control error between the desired displacement trajectory and the measured cylinder displacement given as:

$$e(t) = y_r(t) - y(t) \tag{11}$$

The mathematical model of the classical electrohydraulic system with the proportional valve can be written in the standard state-space form as $\dot{\boldsymbol{x}} = \boldsymbol{f}\big(\boldsymbol{x}(t), \boldsymbol{u}(t)\big)$ where state variables $\boldsymbol{x} = [x_1 \ x_2 \ x_3 \ x_4 \ x_5 \ x_6 \ x_7 \ x_8]^T$ are chosen as: $x_1 = y$, $x_2 = \dot{y}$, $x_3 = z$, $x_4 = p_A$, $x_5 = p_B$, $x_6 = x_v$, $x_7 = \dot{x}_v$ and $x_8 = \int e(t)$, then the simplified representation of the actual system dynamics which includes the controller can be written in the state-space form as follows:

$$
\begin{aligned}
\dot{x}_1 &= x_2 \\
\dot{x}_2 &= x_4 \frac{A_A}{m} - x_5 \frac{A_B}{m} - \frac{1}{m} F_f - g \\
\dot{x}_3 &= x_2 - \frac{\sigma_0 x_3}{g(x_2)} |x_2| \\
\dot{x}_4 &= \frac{B}{V_{0,A} + A_A x_1} [Q_A - A_A x_2] \\
\dot{x}_5 &= \frac{B}{V_{0,B} + A_B (L - x_1)} [Q_B + A_B x_2] \\
\dot{x}_6 &= x_7 \\
\dot{x}_7 &= -2\xi \omega_v x_7 - \omega_v^2 x_6 + K_v \omega_v^2 u \\
\dot{x}_8 &= e
\end{aligned}
\tag{12}
$$

3.3   Modeling of DDEH system

For the DDEH drive, the simplified schematic representation is given in Figure 4. The flow and torque producing elements are two reversible pumps/motors mutually connected to the servo motor. Input to the system is rotational speed of the servo motor. The simplified nonlinear mathematical problem describing the DDEH drive interacting with its environment is derived below and dynamics of the servo motor is neglectable.
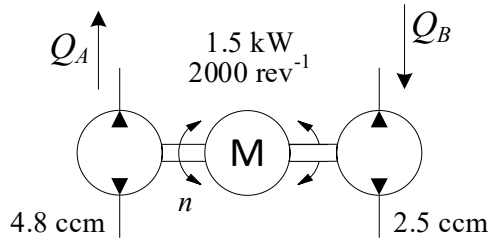

Figure 4: Schematic representation of DDEH drive.

The flow through the pumps is given as:

$$Q_A = nD_A \qquad (13)$$

$$Q_B = -nD_B \qquad (14)$$

where n is rotational speed of the servo motor, D_A and D_B are pump displacements and all leakages flow are neglectable. For the position control of the hydraulic cylinder, a PID controller is utilized and it is given with (10). The mathematical model of the DDEH system can be written in the standard state-space form as $\dot{x} = f(x(t), u(t))$ where state variables $x = [x_1 \ x_2 \ x_3 \ x_4 \ x_5 \ x_6]^T$ are chosen as: $x_1 = y$, $x_2 = \dot{y}$, $x_3 = z$, $x_4 = p_A$, $x_5 = p_B$ and $x_6 = \int e(t)$, then the simplified representation of the actual system dynamics which includes the controller can be written in the state-space form as follows:

$$
\begin{aligned}
\dot{x}_1 &= x_2 \\
\dot{x}_2 &= x_4 \frac{A_A}{m} - x_5 \frac{A_B}{m} - \frac{1}{m} F_f - g \\
\dot{x}_3 &= x_2 - \frac{\sigma_0 x_3}{g(x_2)} |x_2| \\
\dot{x}_4 &= \frac{B}{V_{0,A} + A_A x_1} [Q_A - A_A x_2] \\
\dot{x}_5 &= \frac{B}{V_{0,B} + A_B(L - x_1)} [Q_B + A_B x_2] \\
\dot{x}_6 &= e
\end{aligned}
\qquad (15)
$$

4 Simulation model and numerical results

The numerical simulations are carried out in Matlab program to verify the stability of the process for proposed controllers. The simulations were performed using the Matlab ODE solver. In these examples, the relative and absolute tolerance for the ODE routine was set to 10^{-6}. The developed controllers were tested for a sinusoidal and square wave reference signal. Parameters used for carrying out the numerical simulations are given in Table 2.

Table 3: Parameters values used in simulation

Par.	Value	Par.	Value	Par.	Value
B	1460 MPa	F_c	300 N	K_v	$0.12\cdot10^{-3}$ m/V
ρ	890.8 kg/m³	F_s	700 N	ω_v	100 rad/s
L	0.3 m	v_s	0.08 m/s	ξ	0.7
d_1	32 mm	p_s	100 bar	C_d	0.65
d_2	22 mm	σ_0	$3\cdot10^5$ N/m	w	7 mm
m	150 kg	σ_1	600 Ns/m	D_A	4.787 ccm
$V_{0,A}$	$27.5\cdot10^{-6}$ m³	σ_2	50000 Ns/m	D_B	2.514 ccm
$V_{0,B}$	$9\cdot10^{-6}$ m³	T	60 sec		

4.1   Simulation results

The numerical simulations for classical and DDEH systems were carried out for square and sine wave input signal. First, simulation results were obtained for square input signal and the results are shown in Figure 5 and Figure 6. From the obtained simulation results can be concluded that classical system has smaller steady state error in comparison to DDEH system. Dynamics of DDEH system is much slower than dynamics of classical system due to smaller flows through pumps, which is shown in Figure 6.
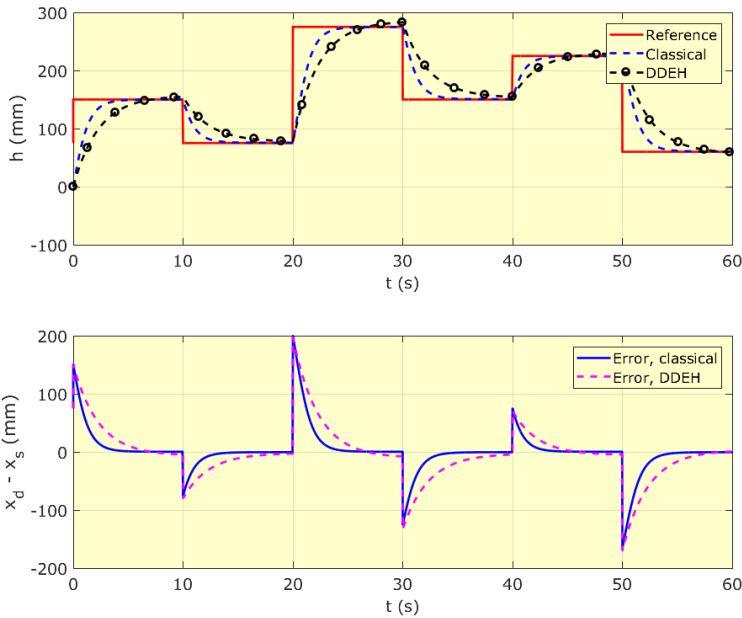
Figure 5: Position and tracking error for square wave input signal.

Second test case was done for sine wave input signal and simulation results are shown in Figure 7 and Figure 8. It is shown that for both systems phase shifting occurred, but for DDEH system phase shifting is more evident. Error in amplitude is higher for DDEH in comparison to classical system and also dynamics is slower, similar to the case for square wave input signal.
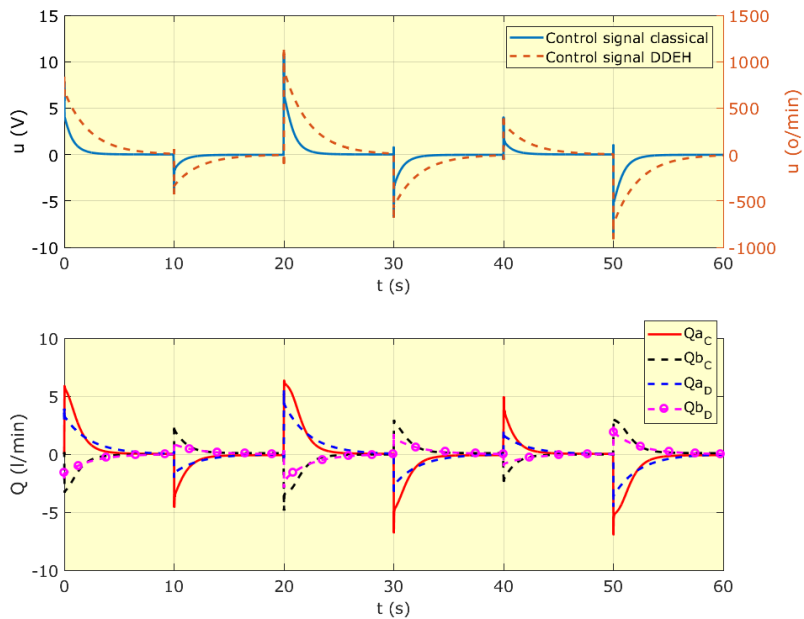

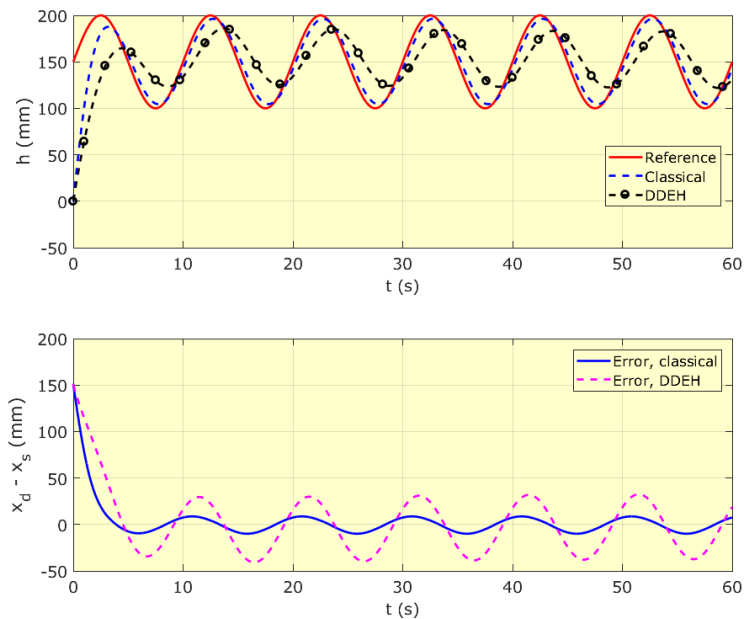**Figure 6: Control signal and flow for square wave input signal.**
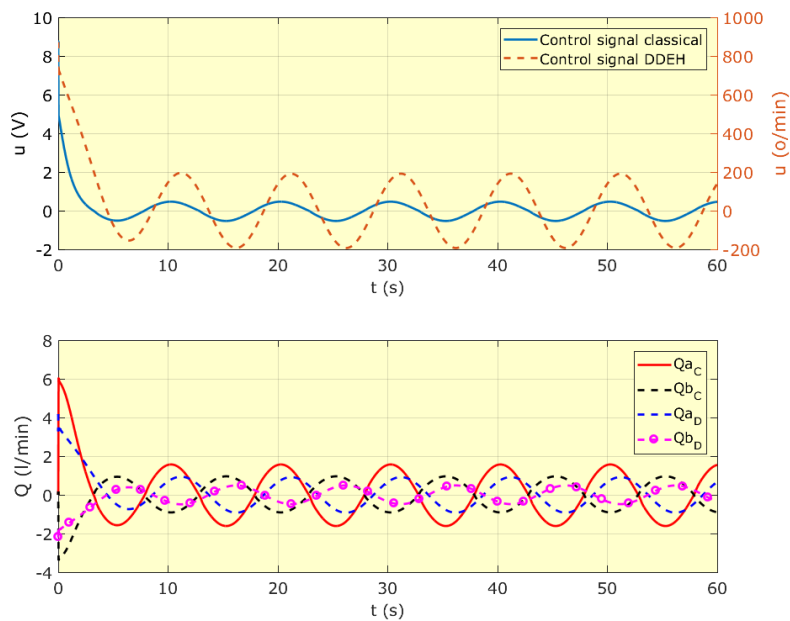
Figure 7: Position and tracking error for sine wave input signal.

Figure 8: Control signal and flow for sine wave input signal.

5 Conclusion

Simulation results have shown that PID controller for the DDEH system in comparison to classical system have larger tracking error and slower dynamics. For sine wave input signal significant phase shifting occurred. PID controller can only achieve satisfying results for slow square wave input signal where the settling time is a much higher. In future work, numerical simulations would be experimentally validated and nonlinear control algorithms such as fuzzy control or sliding mode control should be considered and implemented in order to achieve better results.

References

[1] Rydberg, K. E. (2015). Energy Efficient Hydraulics: System solutions for loss minimization, *Hydraulikdagar i Linköping 2015*

[2] Weber, J., Beck, B., Fischer, E., Ivantysyn, R., Kolks, G., Kunkis, M., Lohse, H., Lübbert, J., Michel, S., Schneider, M., Shabi, L., Sitte, A., Weber, J. (2016). Novel System Architectures by Individual Drives, *IFK Conference proceedings*

[3] Busquets, E., Ivantysynova, M. (2015). Priority-Based Supervisory Controller for a Displacement-Controlled Excavator With Pump Switching, *ASME/BATH 2015 Symposium on Fluid Power and Motion Control*

[4] Ohtsu, H., Ohtsu, K., Sato, H., Kanehiro, K. (2008). Designing advanced rudder roll stabilization system - Using High Power with Small Size Hydraulic System, *Proceedings of the JFPS International Symposium on Fluid Power,* vol. 2008, pp. 169-174

[5] Padovani, D., Ketelsen, S., Hagen, D., Schmidt, L. (2019). A Self-Contained Electro-Hydraulic Cylinder with Passive Load-Holding Capability," *Energies,* vol. 12, p. 292, 1

[6] Cologni, A. L., Mazzoleni, M., Previdi, F. (2016). Modeling and identification of an Electro-Hydraulic Actuator, *12th IEEE International Conference on Control and Automation (ICCA)*

[7] Baek, S. G., Ji, S., Koo, J. C. (2016). Experimental study of electro-hydraulic actuator with payload for precision motion control, *Microsystem Technologies,* vol. 24, pp. 1347-1357,

[8] Zheng, J. M., Zhao, S. D., Wei, S. D. (2009), Application of self-tuning fuzzy PID controller for a SRM direct drive volume control hydraulic press, *Control Engineering Practice,* vol. 17, pp. 1398-1404

[9] Minav, T., Laurila, L., Pyrhönen, J., Vtorov, D. V. (2001). Direct pump control effects on the energy efficiency in an electro-hydraulic lifting system, *International Review of Automatic Control (IREACO),* vol. 4, pp. 235-242

[10] Minav, T., Bonato, C., Sainio, P., Pietola, M. (2014). Direct Driven Hydraulic Drive, *Proceedings of the 9thInternational Fluid Power Conference*, Aachen

[11]   Minav, T., Sainio, P., Pietola, M. (2014). Direct-Driven Hydraulic Drive Without Conventional Oil Tank, *ASME/BATH 2014 Symposium on Fluid Power and Motion Control*

[12]   Minav, T., Papini, L., Pietola, M. (2016). A Thermal Analysis of Direct Driven Hydraulics. *Proceedings of the10th International Fluid Power Conference, Dresden, Germany*

[13]   Minav, T., Papini, L., Järf, A., Tammi, K., Pietola, M. (2016). Direct Driven Hydraulics: What can possibly go wrong? -A thermal analysis, *XXII International Conference on Electrical Machines (ICEM)*

[14]   Minav, T. A., Bonato, C., Sainio, P., Pietola, M. (2014). Efficiency of direct driven hydraulic drive for non-road mobile working machines," *International Conference on Electrical Machines (ICEM)*

[15]   Zhang, S., Minav, T., Pietola, M. (2017). Decentralized Hydraulics for Micro Excavator," in *Proceedings of 15th Scandinavian International Conference on Fluid Power, Fluid Power in the Digital Age, SICFP'17, June 7-9 2017 - Linköping, Sweden*

[16]   Minav, T. A., Heikkinen, J. E., Pietola, M. (2015). Electric-driven Zonal Hydraulics in Non-Road Mobile Machinery, *New Applications of Electric Drives*, IntechOpen, pp. 143-165.
[17]   Totten, G.E. (2003), Fuels and Lubrication handbook, 2nd edition, 370 pages

[16]   Wit, C. C., Olsson, H., Astrom, K. J., Lischinsky, P. (1995). A new model for control of systems with friction, *IEEE Transactions on Automatic Control,* vol. 40, pp. 419-425

University of Maribor Press

Comparison of different servo-hydraulic force control concept

LUKA JEREBIC, MITJA KASTREVC & VITO TIČ

Abstract The article describes the design, implementation and operation of linear electro-hydraulic unit for force measurement and control. Unit consists of hydraulic and electrical components. The three options for measuring force are presented, namely handmade sensor with strain gauges, load cell and force measurement with pressure difference in cylinder chambers. Measured force information enables implementation of closed loop force control, which is needed for the automation of a test station to determine the dynamic strength of the materials. For control a PLC Beckhoff CX5140 with additional I/O components is used.

Keywords: • hydraulic linear servo axis • force control • force measurement methods • control concepts • multi-core controller Beckhoff •

CORRESPONDENCE ADDRESS: Luka Jerebic, HAWE Hidravlika d.o.o., Ob Dragi 7, Štore, Slovenia, e-mail: l.jerebic@hawe.si. Mitja Kastrevc, University of Maribor, Faculty of Mechanical Engineering, Maribor, Slovenia, e-mail: mitja.kastrevc@um.si. Vito Tič, University of Maribor, Faculty of Mechanical Engineering, Maribor, Slovenia, e-mail: vito.tic@um.si.

1   Introduction

Testing of materials and components is necessary to improve design of new, renewed or repaired components. Spatially live time is tested to achieve best results. Popular method is to use standard equipment, which provides loads in one direction. For complex investigations, additional test facilities must be used. The goal of research is to build hydraulic servo axis suitable to use in multi-axis test facilities.

This article represents the continuing work by development of servo axis with suitable control unit [1]. Also, the possibilities of different measurement of force was tested [2]. By using universal hydraulic servo axis, the demand is on solved problems with control of position and force, therefore first step is to achieve stableness work of unit. Additionally, the development of suitable human interface is necessary. Multi-axis testing facilities need also independent control for each axis with different task demanded by test protocol. Therefore, development of suitable control is necessary [3], [4]. The used PLC enables with use of standard PID control approach also possibility to ad discrete version of control approach. This is necessary for further investigations, spatially for development of different reference functions, additional filters and nonlinear approaches for control algorithms.

2   Electrohydraulic servo system

Test rig was developed for experiments with testing of different mechanical parts. Rig consists of hydraulic system and control system with industrial computer for control and acquisition.

2.1   Hydraulic system
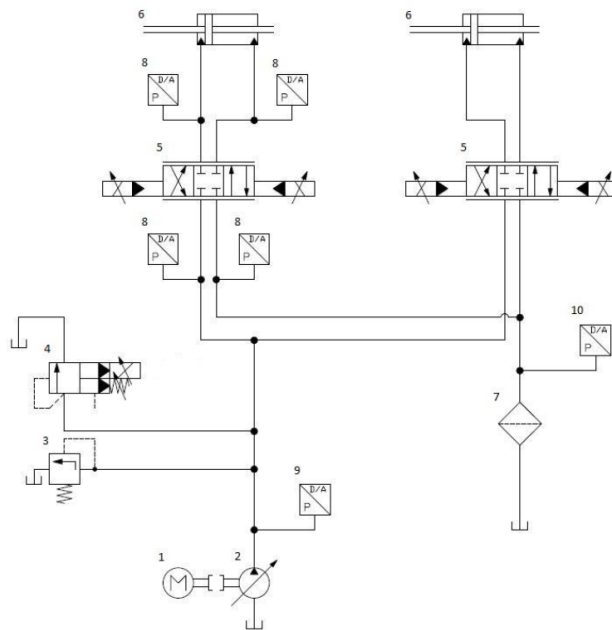
Hydraulic system is presented on Figure 1.

Figure 1: Hydraulic schema of test rig.

System consists of hydraulic pump driven by induction electromotor for supply of hydraulic fluid to two hydraulic cylinders. Hydraulic cylinder was designed for long term tests with integrated position sensor and is shown on Figure 2.
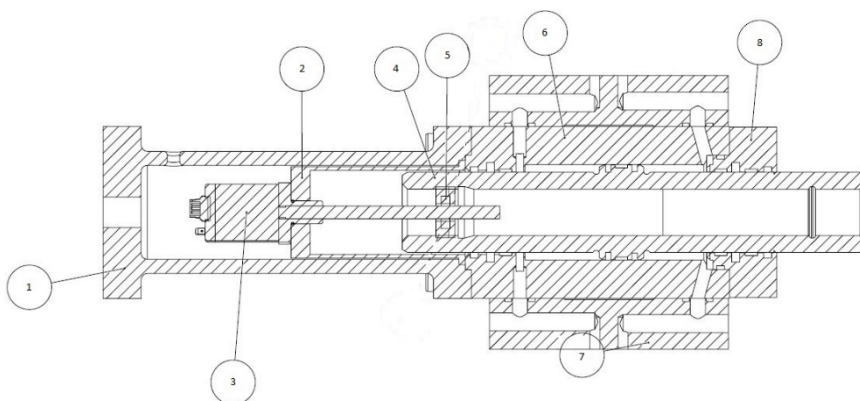

Figure 2: Hydraulic cylinder.

Test rig is also equipped with additional pressure sensors for observation of pressure in different points of system.

2.2   Control part of test system

For control of two hydraulic servo axis, industrial control system based on industrial PLC controller vas used. Figure 3 shows PLC controller in electrical cabinet.
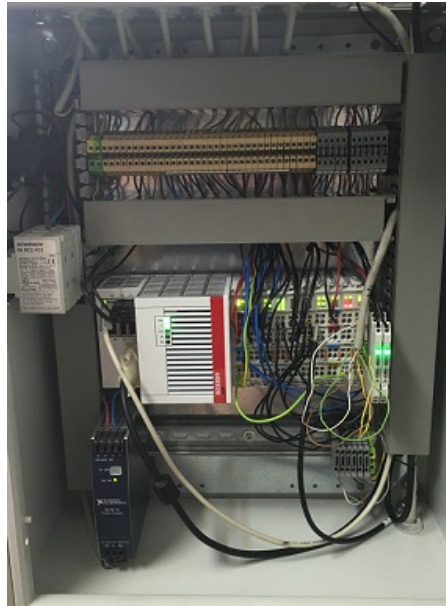
Figure 3: PLC for control and data acquisition.

Beckhoff CX5140 industrial PLC was used for control and data acquisition. For performing control additional modules to control digital and analogue signals are added to base unit. Additional to standard modules for PLC, additional electronic control for servo valves was used. Different methods of force control were tested; a Wheatstone bridge module was added (Beckhoff module EL3356).

2.3   Force measurement

To perform adequate force control, a force measurement must be implemented. We tested three different approaches.

The most common approach is use of standard force transducer provided from measurement equipment manufacturer. We used Force transducer U10M/25kN from manufacturer HBM.

When tests for long term loads is applied, there are problems with installation space of standard measurement transducers. Therefore, two concepts of transducers were made to test applicability of this.

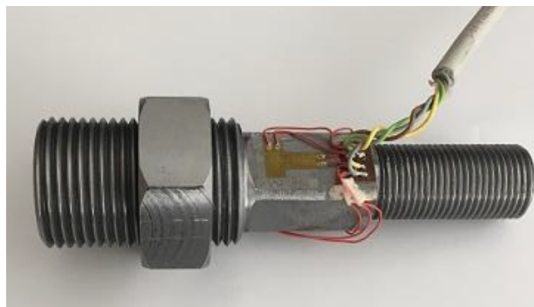Test transducer A is suitable for tension and compression measurement of force load and is shown on Figure 4.

Figure 4: Transducer type A.

Test transducer B is construct for measurements of compression force load and is shown on Figure 5.

Figure 5: Transducer type B.

For construction of transducers, standard strain gauge with resistance of 120 Ω was used. Both transducers use full bridge connection. The body of transducer is prepared for nominal load (40 kN), which gives a deformation of approximately 1000 μstrain. Producer advises, that higher value of internal resistance is used for building force transducers (for example 350 Ω or 1000 Ω) and deformation by nominal load of 1000 μstrain. Using lover resistance strain gauges enables better noise reduction ratio, which is recommended for industrial environment. For Wheatstone bridge the full bridge connection was used. We also want to prove possibility of using low cost transducers in such environment.

Another possibility to achieve a data for force is by measuring pressure drop between two chambers of cylinder.

3   Experimental results

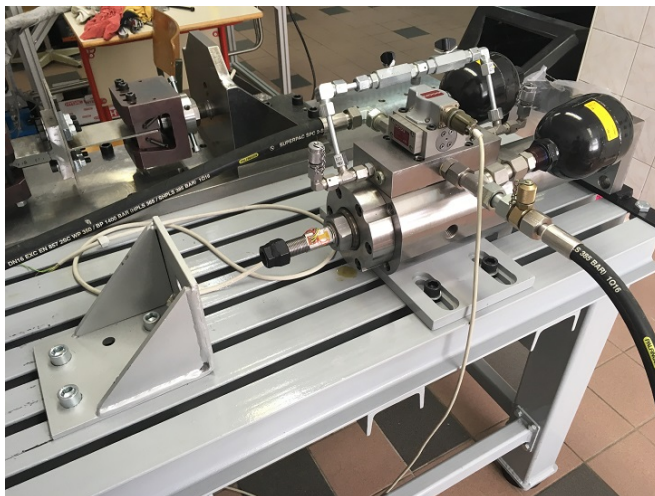For testing purpose one servo cylinder was used in configuration shown on Figure 6 and Figure 7.

Figure 6: Testing system 1.

Figure 7: Testing system 2 with experimental specimen.

First test was using triangular reference value to see the difference between standard measurement transducer, test transducer and measurement of force with pressure difference, as shown on Figure 8.
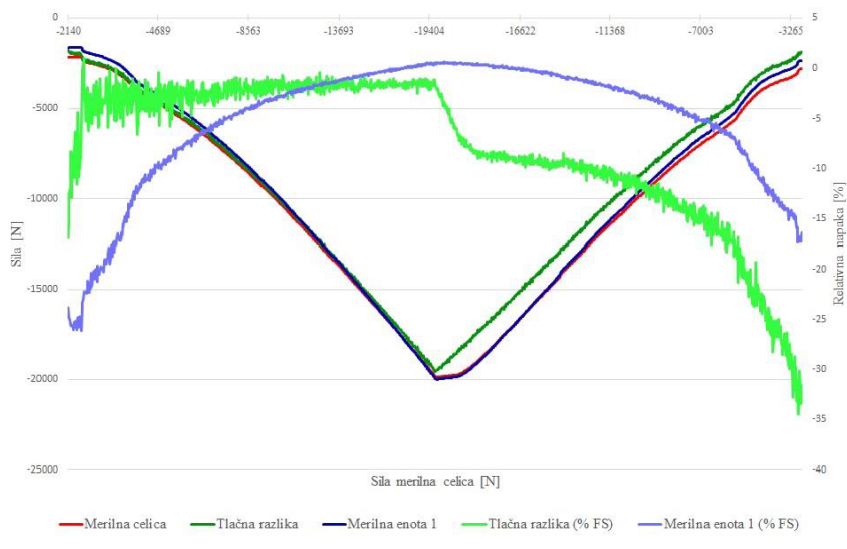

Figure 8: Comparison of measured results.

Then the closed loop force control with use of PID control concept was applied. For reference the sinusoidal form was used, result is shown on Figure 9.
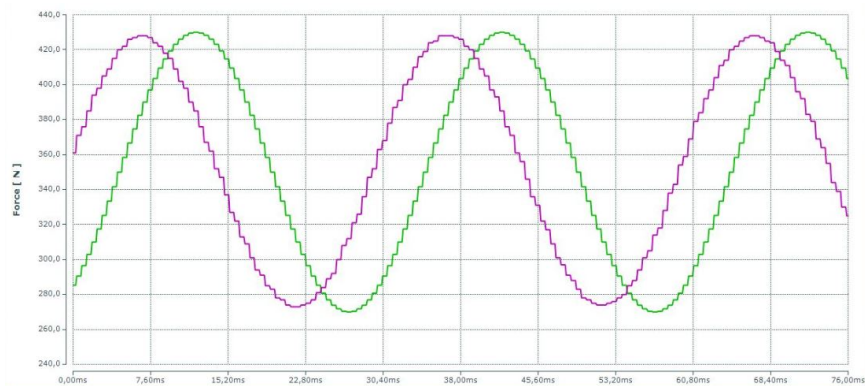
Figure 9: Time diagram of Force control with sinusoidal reference.

For tests mostly sinusoidal reference of force is applied. Figure 10 shows the reference signal and the measured force versus time by using frequency of 10 Hz.
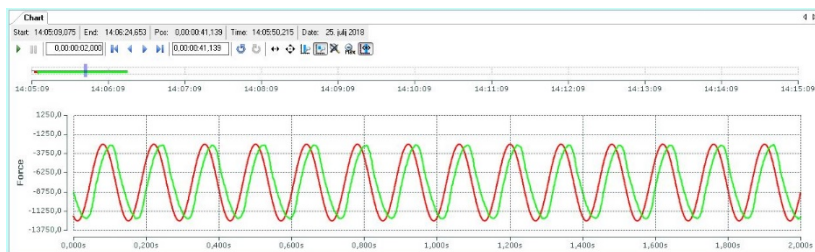

Figure 10: Time diagram of force control with sinusoidal reference f = 10Hz.

4   Conclusions

Representing results show that by long term test on designed experimental rigs, transducer with applied strain gauge can bring satisfying results.

Construction of testing equipment was made mostly with standard elements. For control purposes, industrial multicore controller was used. The usage of equipment suitable for industrial environment enables scope of use for developed test rig.

The tests also give the answer to usage of self-produced transducers. The concept of tensile - compression and compression transducers enables designing custom environments for different types of tests. Using of standard bridge modules gives opportunity to build complex testing devices. Good results by achieved accuracy expands field of application also for control purposes. Simplification of used components for design also lowers costs for build the test environments.

References

[1]   Štefane, M., Lovrec, D. (2015). Modern control system for servo hydraulic linear drive, International Conference Fluid Power, Sept.14.-15., Maribor, Slovenia, University of Maribor Press, pp. 85-94

[2]   Jerebic, L. (2018). Closed loop force control on linear hydraulic servo axis, master thesis, University of Maribor, Faculty of Mechanical Engineering

[3]   Detiček, E., Kastrevc, M. (2017). Nonlinear position control of electrohydraulic servo systems, International Conference Fluid Power, Sept.14.-15., Maribor, Slovenia, University of Maribor Press, pp. 73-84

[4]   Nakkarat, P., Kuntanapreeda, S. (2009). Observer-based backstepping force control of an electrohydraulic actuator, *Control Engineering Practice*, vol. 17, no. 8, pp. 895-902, DOI:10.1016/j.conengprac.2009.02.011

[5]   Hoffman, K. (1998). An Introduction to Measurement using Strain Gages, published by Hottinger Baldwin Messtechnik GmbH, Darmstadt, Germany

[6]   N.N. (2008). HBM publication, The Route to Measurement Transducers- A Guide to the Use of the HBM K Series Foil Strain Gages and Accessories

University of Maribor Press

Nonlinear Mathematical Modelling of Electrohydraulic Servo Systems

MITJA KASTREVC & EDVARD DETIČEK

Abstract Highly nonlinear nature of electrohydraulic servo system is well known. Main reasons for nonlinear and non-differentiable mathematical description of systems dynamics are the fluid compressibility, leakage flows, friction forces and nonlinear fluid flow through servo valve orifices. Accurate nonlinear mathematical models based on physical analysis are necessary for construction of computer simulation models. These models are used for detailed analysis of nonlinear dynamic behaviour and for development of different control strategies. Article presents a nonlinear mathematical model for electrohydraulic servo rotational system and using of diferent aproach to simulate dynamical behaviour of such system.

Keywords: • electrohydraulic servo system • nonlinear model • computer simulation • dynamic simulation • analysis •

1   Introduction

Conventional hydraulic systems have been widely used as power units because they can generate very large power compared with their size. Combining these actuators with electro hydraulic servo-valves and sensors as well as appropriate control electronics, we get electrohydraulic servo systems.

Detecting, transmitting and processing the signal by use of electric and electronic components, driving the load with hydraulic transmission in the electro-hydraulic servo control system. So, it can make full use of electrical system for its convenience and aptitude, make full use of hydraulic system for its rapid response speed, big load stiffness and accurate positioning characteristics to make the whole system more adaptable.

Electro-Hydraulic Actuators (EHA) are highly non-linear systems with uncertain dynamics in which the mathematical representation of the system cannot sufficiently represent the practical circumstances [1], [2]. The electro-hydraulic actuator can use either proportional valve or servo valve [3]. It converts electrical signal to hydraulic power [4], [5], as well as conversion to the pneumatic power [6].

An electrohydraulic servo system is composed of the following components: a pump that feeds the system with hydraulic fluid from a tank, an accumulator located on the discharge side of the pump that acts as a supporting source of energy, a relief valve to limit maximum operating pressure. The main components of the system are axial-piston hydraulic motor and a servovalve. The servovalve directs the oil flow through the appropriate position of its spool according to electric input signal, and consequently, determines the direction of the motion and speed of the hydraulic actuator. Besides control computer and power electronics, an important elements of such control systems are also low noise velocity sensor and pressure sensors [7].

For engineering analysis, it is always preferable to develop explicit equations that include symbols, but this is not always practical. In cases where the equations are too costly to develop, numerical methods can be used. The general process of analysing systems of differential equations involves first putting the equations into standard form, and then integrating these with one of a number of techniques. State variable equations are the most common standard equation form. In this form all of the equations are reduced to first-order differential equations. These first order equations are then easily integrated to provide a solution for the system of equations. Repetitive calculations can be used to

develop an approximate solution to a set of differential equations. Starting from given initial conditions, the equation is solved with small time steps. Smaller time steps result in a higher level of accuracy, while larger time steps give a faster solution. First-order integration provides reasonable solutions to differential equations. That accuracy can be improved by using higher order derivatives to compensate for function curvature. The Runge-Kutta technique uses first-order differential equations (such as state equations) to estimate the higher order derivatives, thus providing higher accuracy without requiring other than first-order differential equations.

For computer simulation, different software is available from professional like Matlab Simulink to different free software. In this article two very similar programs are used for dynamical simulations, namely Matlab Simulink and SCILAB Xcos. Simulink is a graphical environment for dynamic system modelling, simulation and analysis interactively [8], [9]. Using Simulink or Xcos environment, can build complex system simulation model, using the mask function to simplify the model, using script files to initial the module variables, which provides great convenience for PID parameters setting and change the variable value of the various modules.

2   Analysis and mathematical modelling of electrohydraulic system

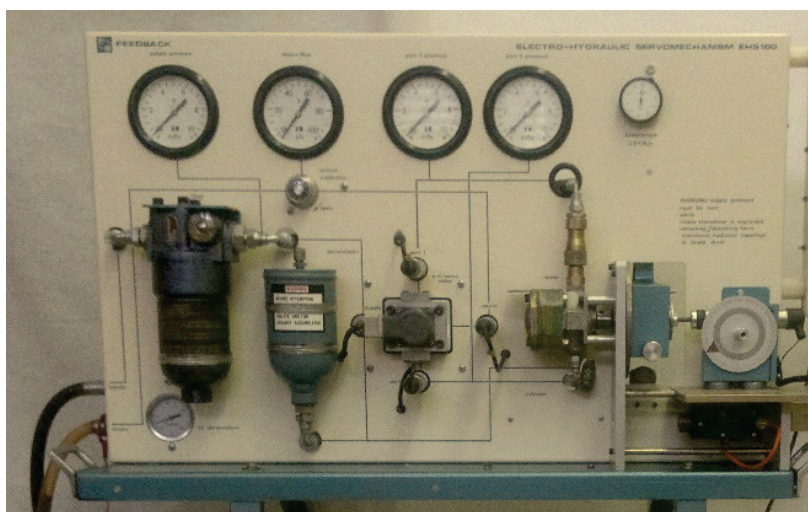Layout of the experimental rotary electrohydraulic servo system is shown in Figure 1.

Figure 1: Experimental rotary electrohydraulic servo system EHS 160.

Two stages servo valve consists of three main parts: the electrical torque motor, the hydraulic amplifier and the valve spool assembly. The dynamics of the valve spool with no noticeable decline in accuracy in a wide range of frequencies can be described through the first order transfer function between the valve opening area (A_{sv}) and control input (u):

$$\tau_{sv} \cdot \dot{A}_{sv} + A_{sv} = K_{sv} \cdot u \tag{1}$$

where K_{sv} is the servo valve gain and τ_{sv} is the servovalve time constant. The constant mentioned can be determined for the manufacturer's catalogue or by certain tests. Due to the fact that the input of the valve is an electric current, but the interface card output is in the form of an electric voltage it is in common to use a current to voltage converter. The constant of this converter is considered in the servo valve gain coefficient [8], [9]. For an ideal critical centre, servo valve with a matched and symmetric orifice the input/output flow rate from the servo valve through the orifices (assuming negligible leakage) can be expressed in the following form:

$$Q_L = C_d A_{sv} \sqrt{\frac{P_s - p_L sign(A_{sv})}{\rho}} \tag{2}$$

Where $p_L = p_{C1} - p_{C2}$ is a load pressure or pressure difference between both chambers, $P_S = p_{C1} + p_{C2}$ is the supply pressure and Q_L is the load flow. Assuming no external leakage, Q_L can be considered as the average flow in each path $Q_L = \dfrac{Q_{C1} + Q_{C2}}{2}$. Where Q_{C1} and Q_{C2} are flow rates to and from the servo valve.

C_d and ρ in equation (2) indicate the flow discharge coefficient and fluid density, respectively. The *sign* function stands for the change in the direction of fluid flow through the servo valve. Employing the compressibility equation for the fluid flow in the actuator dynamics along with the oil leakage will result in the following expression:

$$\frac{V_0}{2\beta} \dot{p}_L = C_d A_{sv} \sqrt{\frac{P_s - p_L sign(A_{sv})}{\rho}} - D_m \dot{\Theta} - C_L p_L \tag{3}$$

Where β and V_0 are, respectively, the fluid bulk modulus and the oil under compression in one chamber of the actuator. D_m and C_L represent the actuator volumetric displacement and total leakage coefficient, respectively. By applying Newton's second low for rotary motion of a hydraulic actuator and neglecting the Coulomb's frictional torque:

Where D_m is the volumetric displacement of hydromotor. B is the viscous damping coefficient, J_T is the total inertia of the motor and load referred to the motor shaft and T_L is the load torque, while $\dot{\Theta}, \ddot{\Theta}$ are angular velocity and acceleration. By combining Equations (1) to (3) we get:

$$\ddot{\Theta} = \frac{D_m}{J_t} \cdot p_L - \frac{B}{J_t} \cdot \dot{\Theta} - \frac{T_L}{J_t}$$

$$\dot{p}_L = \left(\frac{2\beta \cdot C_d}{V_0 \sqrt{\rho}} \sqrt{P_S - p_L} \right) A_{sv} - \frac{2\beta}{V_0} D_m \cdot \dot{\Theta} - \frac{2\beta}{V_0} C_L \cdot p_L \qquad (4)$$

$$\dot{A}_{sv} = -\frac{1}{\tau_{sv}} A_{sv} + \frac{K_{sv}}{\tau_{sv}} \cdot u$$

By choose $x_1 = \dot{\Theta}$, $x_2 = p_L$ and $x_3 = A_{SV}$ as a state variables we can finally the system described with third order nonlinear state space model:

$$\dot{x}_1 = -a_1 x_1 + a_2 x_2 - a_3$$

$$\dot{x}_2 = -a_4 x_1 - a_5 x_2 + a_6 \left(\sqrt{P_S - p_L} \right) x_3 \qquad (5)$$

$$\dot{x}_3 = -a_7 x_3 + a_8 u$$

Where the constants in equation (5) represents: $a_1 = \dfrac{B}{J_t}$, $a_2 = \dfrac{D_m}{J_t}$, $a_3 = \dfrac{T_L}{J_t}$,

$a_4 = \dfrac{2\beta}{V_0} D_m$, $a_5 = \dfrac{2\beta}{V_0} C_L$, $a_6 = \dfrac{2\beta \cdot C_d}{V_0 \sqrt{\rho}}$, $a_7 = \dfrac{1}{\tau_{sv}}$ and $a_8 = \dfrac{K_{sv}}{\tau_{sv}}$.

3   Simulation model

By using programs like Simulink and Xcos the approach is very similar. Advantage of using such software is that the description of the mathematical model is made by using graphically introduction with standard (prepared in forward) blocks. Most of such software have prepared libraries, such as Sinks (output module group), Source (input module group), Linear (Linear link -module group), Nonlinear (non-linear links module group), Math (mathematical operation module group), Continuous and Connections modules group and so on. Each module contains many sub-module.

Models are supported with constants (due the simulation) which can be used as exact numbers or symbol constants. Therefore, the script files are used. This enables user to change some constants due the process of investigation. For the simulation script file is used to transfer parameters, which are not input or output parameter but refers to the use of variable in script files to passes parameters. Because the variables that script files created are variables of program working space, when a program run to the end, the variables store in the working space. The other programs or simulation model can directly call these variables, in order to achieve the purpose of transmitting parameters.

Because of complex structure, user is able to combine some features from different parts of software package, for example some calculations described in script file.

A complex simulation model, in order to be versatile and portable, each module parameter often set in parameter name rather than specific value. Assign or initialize these variables before simulation. Figure 2 the Simulink model represented with two control loops. Each use PI controller block and nonlinear described process model (described in section 2) for velocity control. The first system is manual tuned. For second system, tuning of controller parameter is used with prepared producer tuning operation.
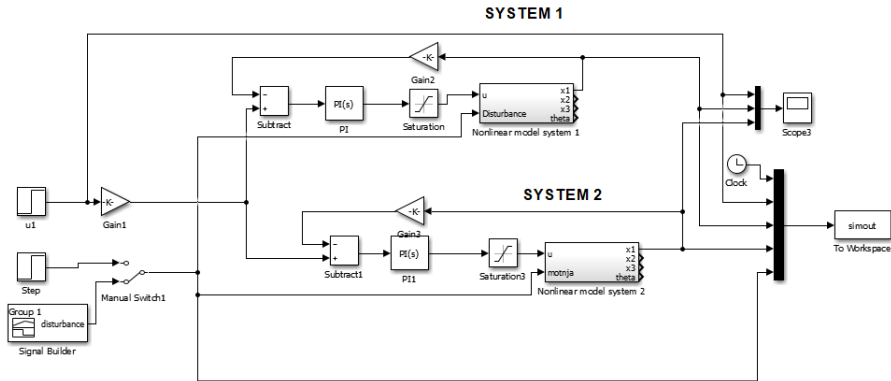
Figure 2: Matlab –Simulink simulation scheme.

Figure 3 shows the inside of the subsystem - nonlinear model. The Matlab script is used for initialize the start constants and parameters needed for simulation. For represents the results of simulation, the Matlab graphic representation is used, customized by usage of Matlab graphics commands and script file.
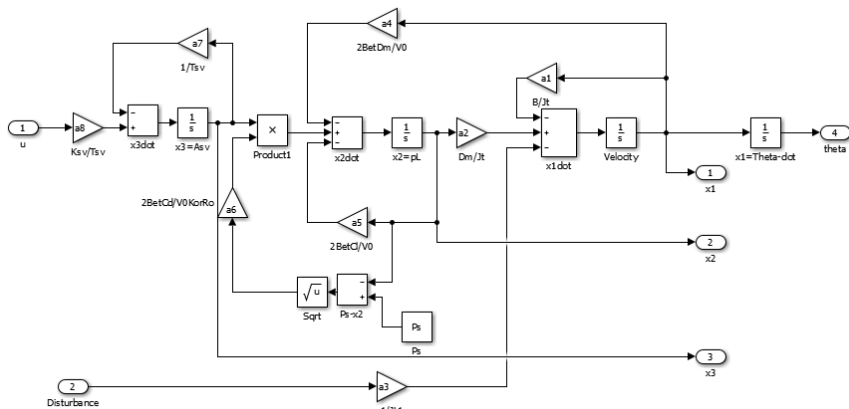

**Figure 3: Matlab –Simulink subsystem –nonlinear model.**

Similar procedure is used by use of the SCILAB and Xcos. The figures 4 represents the Xcos simulation scheme with similar to that used with Matlab-Simulink (shown on Figure2). Likewise, in Figure 5 representation of subsystem called superblock for nonlinear system, is shown.

Figure 4: SCILAB-Xcos simulation scheme.

Figure 5: SCILAB-Xcos subsystem (Superblock) –nonlinear model.

4   Results

For velocity control systems, two cases where investigated. First, the traction control, where the step response is use as a reference. In second part, the disturbance is applied on working system with switch on and of load. Both cases where investigated with two PI closed loop configuration, where the first system has manually obtained parameters for PI controller, where in second case the parameters are obtained by provided tuning tool in Matlab-Simulink. The parameters for simulation in SCILAB are identical to those in Matlab-Simulik for comparison purposes

The results of simulation is presenting in the same figures, where the notation *a* is used for Matlab –Simulink and *b* for SCILAB-Xcos results.

Table 1: Main parameters of the EHS system

$J_t = 3,4 \cdot 10^{-3} \; \left[\text{kgm}^2 \right]$	$V_0 = 2,7121 \cdot 10^{-5} \; \left[\text{m}^3 \right]$	$B = 1,1 \cdot 10^{-6} \; \left[\dfrac{\text{Nms}}{\text{rad}} \right]$
$K_{sv} = 5,527 \cdot 10^{-7} \; \left[\dfrac{\text{m}^2}{\text{V}} \right]$	$D_m = 0,72 \cdot 10^{-6} \; \left[\dfrac{\text{m}^3}{\text{rad}} \right]$	$C_L = 9,25 \cdot 10^{-12} \; \left[\dfrac{\text{m}^5}{\text{Ns}} \right]$
$\beta = 0,35 \cdot 10^9 \; \left[\text{Pa} \right]$	$\tau_{sv} = 0,0023 \; \left[\text{s} \right]$	$C_d = 0,63$
$T_L = 0,7 \; \left[\text{Nm} \right]$		

Figure 6 shows the complete simulation with step response and disturbance switched "on" and "of".
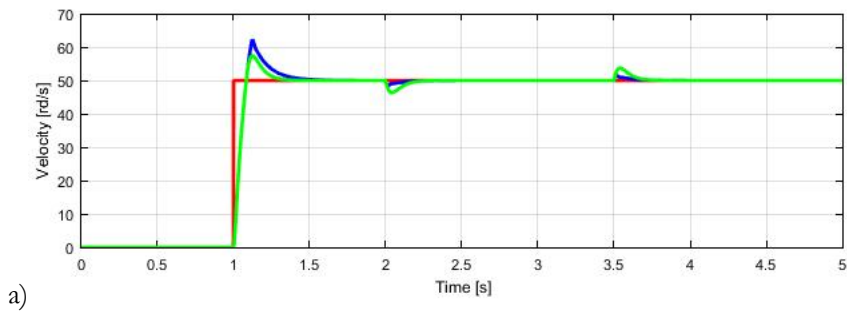
a)

b)

Figure 6: Results of complete simulation process.

5   Conclusions

In this paper, a development of nonlinear model for velocity controlled electrohydraulic servo system is presented. Comprehensive investigation was carried out on the mathematical modelling and computer simulation of dynamic behaviour of whole system, based on real experimental setup.

Two different software was used for simulation of dynamical behaviour of proposed nonlinear system. The results of simulation give detailed information about behaviour of the system. Information provided thru this simulation is important for choose best control and for search for optimal parameters of it. Mostly this can be done with a different software, which is available on market. Two software Matlab and SCILAB were selected because of similarity in used mathematical solvers and principle of operation.

Matlab is already very popular commercial program which give customer best possibility spatially by combination of different libraries and modules for achieve results comparable with experiments. Due to this complexity computer with higher preferences is necessary, also user must be aware that development of product sometimes give additional adaptation of already tested research. Therefore, a good technical support is necessary. Because this is a commercial product, the support is provided for all payed parts of product.

In the odder way a similar product SCILAB is available under GNU General Public License. That means that is free for use with some legal limitation which comes with the license. Interesting is that the user interface for both products is very similar what enable user to work easily with both products. That is important spatially for researcher, teachers and students. Because of this licence normally the technical support is poor, documentation is mostly available in electronically form (helps, forums…).

Generally, both software's satisfy for investigation, which was presented in this article. Authors have noticed that error diagnostic by SCILAB is not so supportive as by Matlab, what is very important for newcomers by solving complex task. It is preferable to learn the usage systematically with supplier tasks (on web there are some very useful training tutorials and hints for other users).

References

[1] Detiček, E., Kastrevc, M. (2016). Design of Lyapunov Based Nonlinear Position Control of Electrohydraulic Servo Systems // Journal of Mechanical Engineering, pp. 163-170 DOI:10.5545/sv-jme.2015.2921

[2] Merritt, H.E. (1967). *Hydraulic Control Systems*. Wiley, NewYork

[3] Kastrevc, M., Detiček, E. (2017). The nonlinear mathematical model of electrohydraulic position servo system, International Conference Fluid Power, Sept.14.-15. 2017, Maribor, Slovenia, University of Maribor Press, pp. 163-173. https://doi.org/978-961-286-086-8.17

[4] Pahič, R., Tič, V., Lovrec, D. (2017). Test stand for determining the performance characteristics of hydraulic directional control valves. *Conference proceedings*. 1st ed. Maribor: University of Maribor Press. 2017, pp. 271-280

[5] Zulfatman, R. A., Rahmat, M. F. (2009). Modeling and controller design of electro-hydraulic actuator. Proceeding of the 2nd International Conference on Control, Instrumentation and Mechatronic Engineering, June 9-9, UTM Publisher, Malacca, Melaka, Malaysia, pp. 225-231

[6] Lovrec, D., Tašner, T., Tič, V. (2017). Dynamic behaviour of different hydraulic drive concepts - comparison and limits. *International journal of simulation modelling*, ISSN 1726-4529, Sep. 2017, vol. 16, iss. 3, pp. 448-457

[7] Šitum, Ž. (2013) Control of a Pneumatic Drive Using Electronic Preasure Valves, Transaction of the institute of Measurement and Control 35, no. 8

[8] Detiček, E., Gubeljak, N., Kastrevc, M. (2017). Design of Lyapunov based nonlinear velocity control of electrohydraulic velocity servo systems. *Tehnički vjesnik: znanstveno-stručni časopis tehničkih fakulteta Sveučilišta u Osijeku*, ISSN 1330-3651, 2017, vol. 24, no. 3, pp. 745-751, DOI: 10.17559/TV-20160930073953

[9] Lopez, C. P. (2014), MATLAB Control System Engineering, Apress Academic, Springer –Verlag, London, Berlin, Heidelberg

[10] Bang, B., Draxler, J., James, G. (1990). Dynamic Hydraulic System Simulation-An Integrated Approach, SAE Technical Paper 902003,

University of Maribor Press

Nonlinear Velocity Control of Electrohydraulic Servo Systems

EDVARD DETIČEK & MITJA KASTREVC

Abstract This paper studies the nonlinear closed loop control of an electrohydraulic velocity servo system with use of Lyapunov theory of nonlinear systems using integrator backstepping. Two different nonlinear design procedures are employed feedback linearization and backstepping. It is shown that both these techniques can be successfully used to stabilize any chosen operating point of the system. All derived results are validated by computer simulation of the nonlinear mathematical model of the system. Because of highly nonlinear nature of electrohydraulic servo system, the conventional control strategies mostly cannot reach desired control objectives. Nonlinear mathematical model of the system contains many nonlinear terms, which influence also the dynamic errors of the control system. Modern control strategy should be able to cope with these nonlinearities. The research studies represented in the paper shows big potential of Lyapunov based nonlinear controller design procedures, to obtain desired control objectives.

Keywords: • electrohydraulic servo system • nonlinear control • Lyapunov theory • integrators backstepping • computer simulation•

CORRESPONDENCE ADDRESS: Edvard Detiček, University of Maribor, Faculty of Mechanical Engineering, Maribor, Slovenia, e-mail: edvard.deticek@um.si. Mitja Kastrevc, University of Maribor, Faculty of Mechanical Engineering, Maribor, Slovenia, e-mail: mitja.kastrevc@um.si.

1   Introduction

Electrohydraulic servo systems are encountered in a wide range of modern industrial applications because of their ability to handle large inertia and torque loads and, at the same time, achieve fast responses and high degree of both accuracy and performance. Typical applications include processing of plastics, industrial robots, aircrafts, flight simulators, lunch vehicles, flight simulators, floating cranes [1], testing systems [2] and numerous of military applications. Depending on desired control objectives, an electrohydraulic servo system can be classified as either a position, velocity or a force-torque system.

This paper investigates velocity closed loop control system of hydraulically driven process of iron centrifugal die casting in industry. The research is conducted in laboratory environment and by computer simulations.

An electrohydraulic servo system is basically composed of the following components: a pump that feeds the system with hydraulic fluid from a tank, an accumulator located on the discharge side of the pump that acts as a supporting source of energy, a relief valve to limit maximum operation pressure. The main components of the system are axial-piston hydraulic motor and a servovalve. The servovalve directed the oil flow through the appropriate position of its spool according to electric input signal, and consequently, determines the direction of the motion and speed of the hydraulic actuator. Besides control computer and power electronics are important elements of such control systems also low noise velocity and pressure sensors.

For successful closed loop velocity control, development of suitable controller, which could reflect such characteristics, is very significant, although the dynamics of electro hydraulic servo system is highly nonlinear [3] and [4].

The presence of flow nonlinearities and internal friction make the selection of appropriate closed loop controllers, based on classical linear control theory difficult. Therefore, a nonlinear design procedure is employed here. A stabilizing controller has been designed using the technique of feedback linearization. Even though this controller successfully achieves the desired objectives, another controller is designed using the backstepping approach, which avoids unnecessary cancellations that can have a detrimental effect in the presence of parametric uncertainties or unmoulded dynamics.

The appropriate simulation of nonlinear mathematical model of the system validates the performance of designed controller.

The fundamental concept of backstepping method is introduced by Krstic et.al. in their book [5]. The approach focusing on the stabilization problem in stochastic nonlinear systems is developed in the extension of this book. The backstepping control method is also presented in [6], [7], [8], [9] and [10] where this technique is explained in detail for regulating and tracking problem.

Feedback linearization employs changes of coordinates and feedback control to transform a given nonlinear system into an equivalent linear system. A major advantage of feedback linearization approach is related to the cancellations that are introduced in design process. Namely some kinds of nonlinearities can have positive effect on system stability. Their cancellation can lead to instability in the presence of modelling uncertainties. On the other hand, backstepping represents a recursive design scheme that can be used for systems in strict feedback form with nonlinearities no constrained by linear bounds. At every step of backstepping a new Control Lyapunov Function (CLF) is constructed by augmentation of CLF from previous step by a term which penalizes the error between »virtual control« and its desired value, so called stabilizing function. A major advantage of backstepping is the construction of a Lyapunov function whose derivative can be made negative definite by a variety of control laws rather by a specific control law. Additionally, as a design tool, backstepping is less restrictive than feedback linearization and its previously mentioned design flexibility can put »beneficial nonlinearities« to good in use.

2 Simplified model of the system

For the purpose of design of a closed loop controller the complete mathematical model of the system, which consists of the hydraulic motor dynamics, including the load and SV dynamics, can be simplified according to manufacturer's data of real system components [11]. Usually a simplification can be obtained when the dynamic of the servo valve with control electronics is much higher than the dynamic of the hydraulic motor and load.

For hydraulic system with $D_m = 0.72 \; 10^{-6}$ [m³/rad], $V_t = 2.7143 \; 10^{-5}$ [m³] and $J_t = 3.4 \; 10^{-3}$ [kgm²] the minimum natural frequency is:

$$\omega_{H\min} = \sqrt{\frac{4\beta \cdot D_m^2}{J_t \cdot V_t}} = 88,68 \left[\frac{\text{rad}}{\text{s}}\right] \quad \Rightarrow \quad 14,11 \; [\text{Hz}] \tag{1}$$

Natural frequency of servovalve can be read out, from the manufacturer's data sheet. In our experimental electrohydraulic system we have additional limitation of fluid flow so we use only 10 % of signal, what means that natural frequency of servovalve is high (acc. more than 150 Hz).

Because of very high natural frequency of servo valve with comparison to hydraulic system ($\omega_{Hsv} \gg \omega_{Hmin}$), considering also dynamic effect of manifold which decreases hydraulic natural frequency, the dynamic of servovalve can be neglected.

For calculation we use a first order transfer function between the valve opening area (A_s) and control input (u):

$$\tau_{sv} \cdot \dot{A}_{sv} + A_{sv} = K_{sv} \cdot u \tag{2}$$

where K_{sv} the servo valve is gain and τ_{sv} is the servovalve time constant. Therefore, the simplified system equations have the following form:

$$\ddot{\Theta} = \frac{D_m}{J_t} \cdot p_L - \frac{B}{J_t} \cdot \dot{\Theta} - \frac{T_L}{J_t}$$

$$\dot{p}_L = \left(\frac{2\beta \cdot C_d}{V_0 \sqrt{\rho}} \sqrt{P_S - p_L}\right) A_{sv} - \frac{2\beta}{V_0} D_m \cdot \dot{\Theta} - \frac{2\beta}{V_0} C_L \cdot p_L \tag{3}$$

$$\dot{A}_{sv} = -\frac{1}{\tau_{sv}} A_{sv} + \frac{K_{sv}}{\tau_{sv}} \cdot u$$

3   Controller design

For a special class of nonlinear dynamical systems, the backstepping control has emerged us successful control strategy. Some of nonlinear systems can be observed as a system constructed from subsystems. The number of subsystems depends of dynamic model order. Because of this recursive structure, the designer can start the design process at the known-stable system and design "back out", new controllers that progressively stabilize each outer subsystem. The process is finished when the final external control is reached.

The mathematical description of nonlinear system in new set of coordinates allows us to use the backstepping approach to force it to behave like a linear one.

By choosing state variables $x_1 = \dot{\Theta}$, $x_2 = p_L$ and $x_3 = A_{SV}$ the system described in equation (3) become:

$$
\begin{aligned}
\dot{x}_1 &= -a_1 x_1 + a_2 x_2 - a_3 \\
\dot{x}_2 &= -a_4 x_1 - a_5 x_2 + a_6 \left(\sqrt{P_S - p_L} \right) x_3 \\
\dot{x}_3 &= -a_7 x_3 + a_8 u
\end{aligned}
\tag{4}
$$

Where constants a_1-a_8 are defined as:

$$
\begin{aligned}
a_1 &= \frac{B}{J_t}, \; a_2 = \frac{D_m}{J_t}, & a_3 &= \frac{T_L}{J_t}, & a_4 &= \frac{2\beta}{V_0} D_m, \\
a_5 &= \frac{2\beta}{V_0} C_L, & a_6 &= \frac{2\beta \cdot C_d}{V_0 \sqrt{\rho}}, & a_7 &= \frac{1}{\tau_{sv}}, & a_8 &= \frac{K_{sv}}{\tau_{sv}}
\end{aligned}
\tag{5}
$$

A symbolic representation of the applied rotary electrohydraulic servo system is suggested in Figure 1.
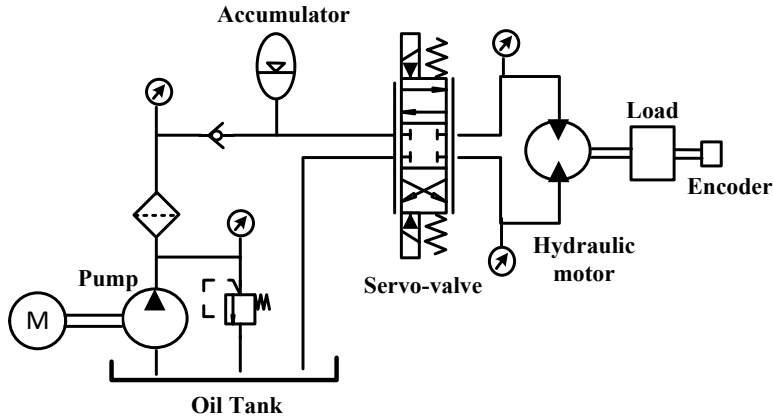
Figure 1: Shema of Electrohydraulic velocity servo system.

The problem of designing a controller, which provides asymptotic stability of the operating point of interest. Assuming that the full state information is available, the underlying technique for solving this problem is backstepping. Backstepping control is a technique for designing stabilizing controls for special class of nonlinear dynamic systems. These systems are built from subsystems that radiate out form an irreducible subsystem that can be stabilized using some other method. Because of this recursive structure, the designer can start the design process at known stable system and »back out« new controllers that progressively stabilize each outer subsystem. The process terminates when the final external control is reached.

The detailed derivations of finding backstepping control input are covered in next 4 steps:

First, we define negative errors for system (4):

$$
\begin{aligned}
e_1 &= x_1 - r &&\Rightarrow\quad x_1 = e_1 + r \\
e_2 &= x_2 - \alpha_1 &&\Rightarrow\quad x_2 = e_2 + \alpha_1 \\
e_3 &= x_3 - \alpha_2 &&\Rightarrow\quad x_3 = e_3 + \alpha_2
\end{aligned}
\tag{6}
$$

Step 1a

First negative error and its derivative is:

$$e_1 = x_1 - r \qquad \Rightarrow \qquad x_1 = z_1 + r$$
$$\dot{e}_1 = \dot{x}_1 - \dot{r}$$

(7)

Step 1b

Define first candidate of control Lyapunov function (CLF1):

$$V_1 = \frac{1}{2} e_1^2$$

(8)

Here we introduce first negative control error $e_1 = x_1 - r$. The derivative of Lyapunov function is:

$$\dot{V}_1 = e_1 \dot{e}_1 = z_1 (\dot{x}_1 - \dot{r})$$

(9)

Inserting the first equation of system (5) and second term in equation (6) we get:

$$\dot{V}_1 = e_1 \dot{e}_1 = e_1 \left(-a_1 x_1 + a_2 \overbrace{(e_2 + \alpha_1)}^{x_2} - a_3 - \dot{r} \right) =$$
$$= e_1 \left(-a_1 x_1 + a_2 e_2 + a_2 \alpha_1 - a_3 - \dot{r} \right)$$

(10)

Step 1c
First virtual control is defined as:

$$\alpha_1 = \frac{1}{a_2} \left(a_1 x_1 + a_3 + \dot{r} - C_1 e_1 \right)$$

(11)

With selection of virtual control, we achieve the following form of augmented Lyapunov function:

$$\dot{V}_1 = a_2 e_1 e_2 - C_1 e_1^2 \tag{12}$$

Partial differentiations of α_1 with respect to the terms $x_1, r\ \dot{r}$ are performed below:

$$\frac{\partial \alpha_1}{\partial x_1} = \frac{\partial \frac{1}{a_2}\left[(a_1 - C_1)x_1 + C_1 r + \dot{r} + a_3\right]}{\partial x_1} = \frac{1}{a_2}(a_1 - C_1)$$

$$\frac{\partial \alpha_1}{\partial r} = \frac{\partial \frac{1}{a_2}\left[(a_1 - C_1)x_1 + C_1 r + \dot{r} + a_3\right]}{\partial r} = \frac{k_1}{a_2} \tag{13}$$

$$\frac{\partial \alpha_1}{\partial \dot{r}} = \frac{\partial \frac{1}{a_2}\left[(a_1 - C_1)x_1 + C_1 r + \dot{r} + a_3\right]}{\partial \dot{r}} = \frac{1}{a_2}$$

$$\dot{\alpha}_1 = \frac{\partial(\alpha_1)}{\partial x_1}\dot{x}_1 + \frac{\partial(\alpha_1)}{\partial r}\dot{r} + \frac{\partial(\alpha_1)}{\partial \dot{r}}\ddot{r} = \frac{1}{a_2}(a_1 - C_1)\dot{x}_1 + \frac{k_1}{a_2}\dot{r} + \frac{1}{a_2}\cdot\ddot{r} \tag{14}$$

Now we define virtual control for the second equation of (4).

Step 2a

Second error term and its derivative are:

$$e_2 = x_2 - \alpha_1$$
$$\dot{e}_2 = \dot{x}_2 - \dot{\alpha}_1 \tag{15}$$

Inserting second equation of system (4) and above derivative, we become following term:

$$\dot{e}_2 = \dot{x}_2 - \dot{\alpha}_1 = \underbrace{\left(-a_4 x_1 - a_5 x_2 + \left(a_6 \sqrt{P_s - x_2}\right)x_3\right)}_{\dot{x}_2} - \dot{\alpha}_1 \tag{16}$$

Step 2b

Selection of second virtual control. With the augmentation of first Lyapunov function, we define the second Lyapunov function:

$$V_2 = V_1 + \frac{1}{2} e_2^2 \tag{17}$$

With differentiation of second Lyapunov function V_2 is:

$$
\begin{aligned}
\dot{V}_2 &= \dot{V}_1 + e_2 \dot{e}_2 = -C_1 e_1^2 + \left(a_6 \sqrt{P_s - x_2} \right) e_2 e_3 + \\
&+ e_2 \left[a_2 e_1 - a_4 x_1 - a_5 x_2 + \left(a_6 \sqrt{P_s - x_2} \right) \alpha_2 - \dot{\alpha}_1 \right]
\end{aligned}
\tag{18}
$$

Step 2c
As a second virtual control select in above equation and define:

$$\alpha_2 = \frac{1}{a_6 \sqrt{P_s - x_2}} \left[-a_2 e_1 + a_4 x_1 + a_5 x_2 + \dot{\alpha}_1 - C_2 e_2 \right] \tag{19}$$

With selection of second virtual control, we achieve the following form of augmented Lyapunov function:

$$\dot{V}_2 = -C_1 e_1^2 - C_2 e_2^2 + \left(a_6 \sqrt{P_s - x_2} \right) e_2 e_3 \tag{20}$$

In next step we will need the partial derivative of α_2 with respect the variables $x_1, x_2,$ $r, \dot{r}, \ddot{r}$, so introduce the first equation of system (4):

$$\alpha_2 = \frac{1}{a_6 \sqrt{P_s - x_2}} \left[-a_2 e_1 + a_4 x_1 + a_5 x_2 + \dot{\alpha}_1 - C_2 e_2 \right] \tag{21}$$

We get:

$$\alpha_2 = \frac{1}{a_6\sqrt{P_s - x_2}}\left\{\left[-a_2 + a_4 + \frac{(a_1 - C_1)}{a_2}(C_2 - a_1)\right]x_1 + (a_5 + a_1 - C_1 - C_2)x_2 + \right.$$

$$\left. + \left(a_2 + \frac{C_1 C_2}{a_2}\right)r + \left(\frac{C_1 + C_2}{a_2}\right)\dot{r} + + \frac{1}{a_2}\cdot\ddot{r} + \frac{a_3}{a_2}(C_2 - a_1 + C_1)\right\} \tag{22}$$

In final step, we define the third control, which is no more virtual. Namely, we introduce here real control variable u. Define the third error term:

$$\begin{aligned} e_3 &= x_3 - \alpha_2 \\ \dot{e}_3 &= \dot{x}_3 - \dot{\alpha}_2 \end{aligned} \tag{23}$$

and introduce the third equation of system (4):

$$V_3 = V_2 + \frac{1}{2}e_3^2 \tag{23}$$

Put into equation of derivative of second augmented Lyapunov function:

$$\dot{V}_3 = -C_1 e_1^2 - C_2 e_2^2 + \left(a_6\sqrt{P_s - x_2}\right)e_2 e_3 + e_3\left[\overbrace{(-a_7 x_3 + a_8 u)}^{\dot{x}_3} - \dot{\alpha}_2\right] =$$

$$= -C_1 e_1^2 - C_2 e_2^2 + e_3\left[\left(a_6\sqrt{P_s - x_2}\right)e_2 - a_7 x_3 + a_8 u - \dot{\alpha}_2\right] \tag{24}$$

Now we select real control law u in such a way that the $\dot{V}_3$ get the form – equation (25):

$$\dot{V}_3 = -C_1 e_1^2 - C_2 e_2^2 - C_3 e_3^2 \tag{25}$$

Finally, we get a controller equation:

$$u = \frac{1}{a_8}\left[-\left(a_6\sqrt{P_s - x_2}\right)e_2 + a_7 x_3 + \dot{\alpha}_2 - C_3 e_3\right] \tag{26}$$

4   Results

In order to verify the effectiveness of the proposed backstepping control algorithm, simulation experiments have been done on the electrohydraulic servo system. Main parameters of the system are given in table1. Computer simulation scheme i.e. Simulink model represents Figure 2.
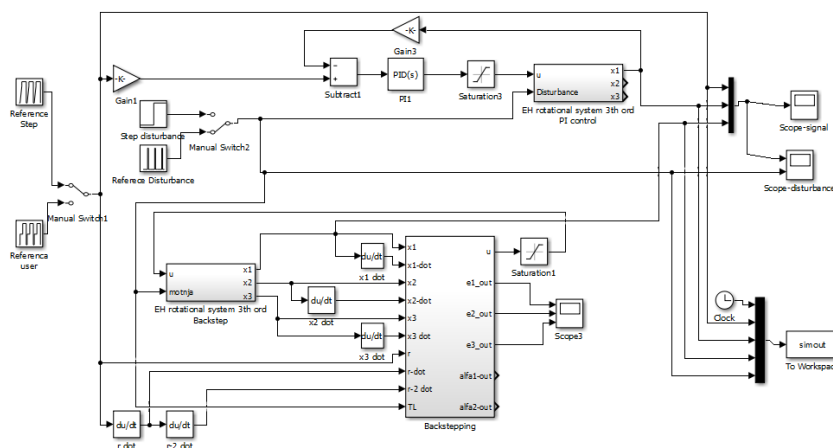
Figure 2: Computer simulation scheme in Matlab-Simulink.
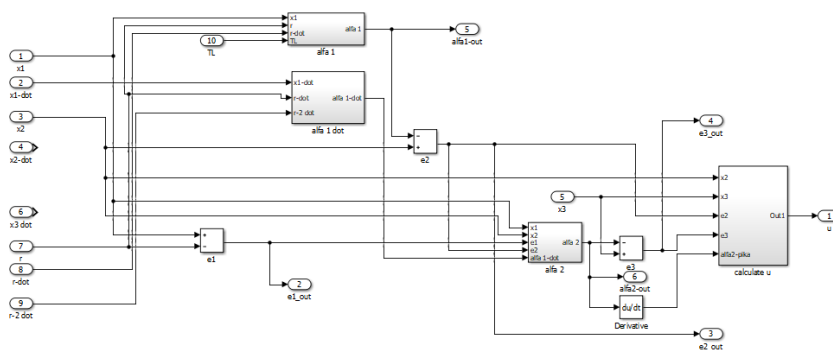
Figure 3: Detail of backstepping block in scheme on Figure 2.

Table 1: Main parameters of the EHS system

$J_t = 3,4 \cdot 10^{-3} \left[\text{kgm}^2 \right]$	$V_0 = 2,7121 \cdot 10^{-5} \left[\text{m}^3 \right]$	$B = 1,1 \cdot 10^{-6} \left[\dfrac{\text{Nms}}{\text{rad}} \right]$
$K_{sv} = 5,527 \cdot 10^{-7} \left[\dfrac{\text{m}^2}{\text{V}} \right]$	$D_m = 0,72 \cdot 10^{-6} \left[\dfrac{\text{m}^3}{\text{rad}} \right]$	$C_L = 9,25 \cdot 10^{-12} \left[\dfrac{\text{m}^5}{\text{Ns}} \right]$
$\beta = 0,35 \cdot 10^{9} \left[\text{Pa} \right]$	$\tau_{sv} = 0,0023 \left[\text{s} \right]$	$C_d = 0,63$
$T_L = 0,7 \left[\text{Nm} \right]$		

For presentation of dynamical behaviour, the step reference us used. Commonly the systems in practice are mostly exposed to change of load; therefore, PI controller was optimized for such load case.
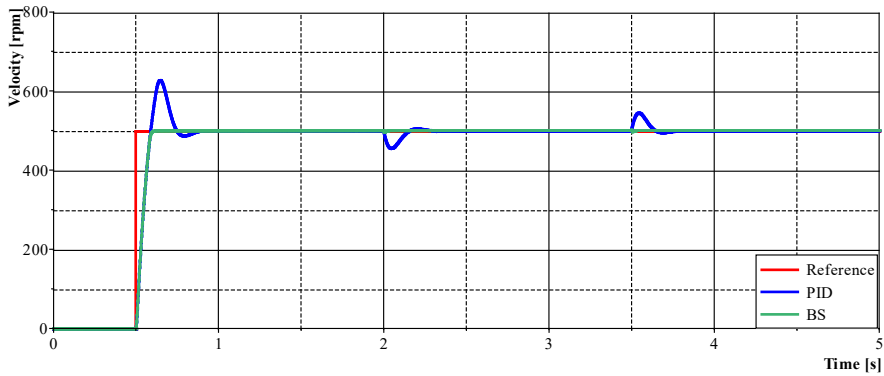
Figure 4: Simulation results of the system step response.

In Figure 4 the comparison of systems dynamic response between PI-controller and backstepping controller on step reference (0 - 500 rpm) is shown. First we can see the similar response in first part by step response, where PI controller have overshoot and backstepping controller (BS controller) have none (see Figure 5).
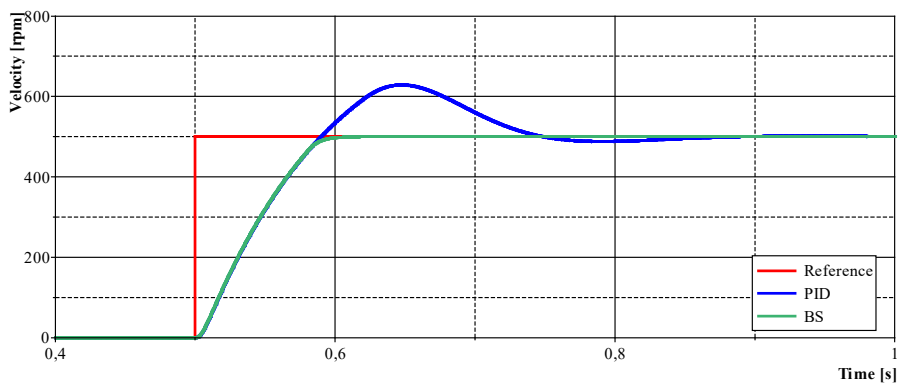
Figure 5: Dynamic response on Step reference.

In Figure 6 the comparison of systems dynamic response by step implementation of load change is shown.
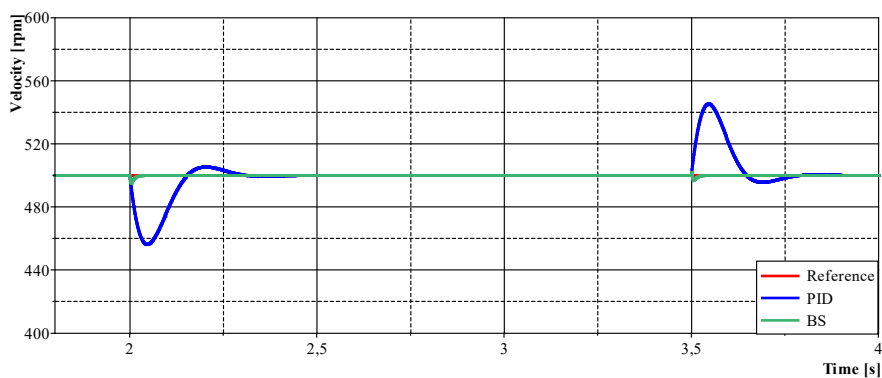

Figure 6: Dynamic response by implementation of disturbance.

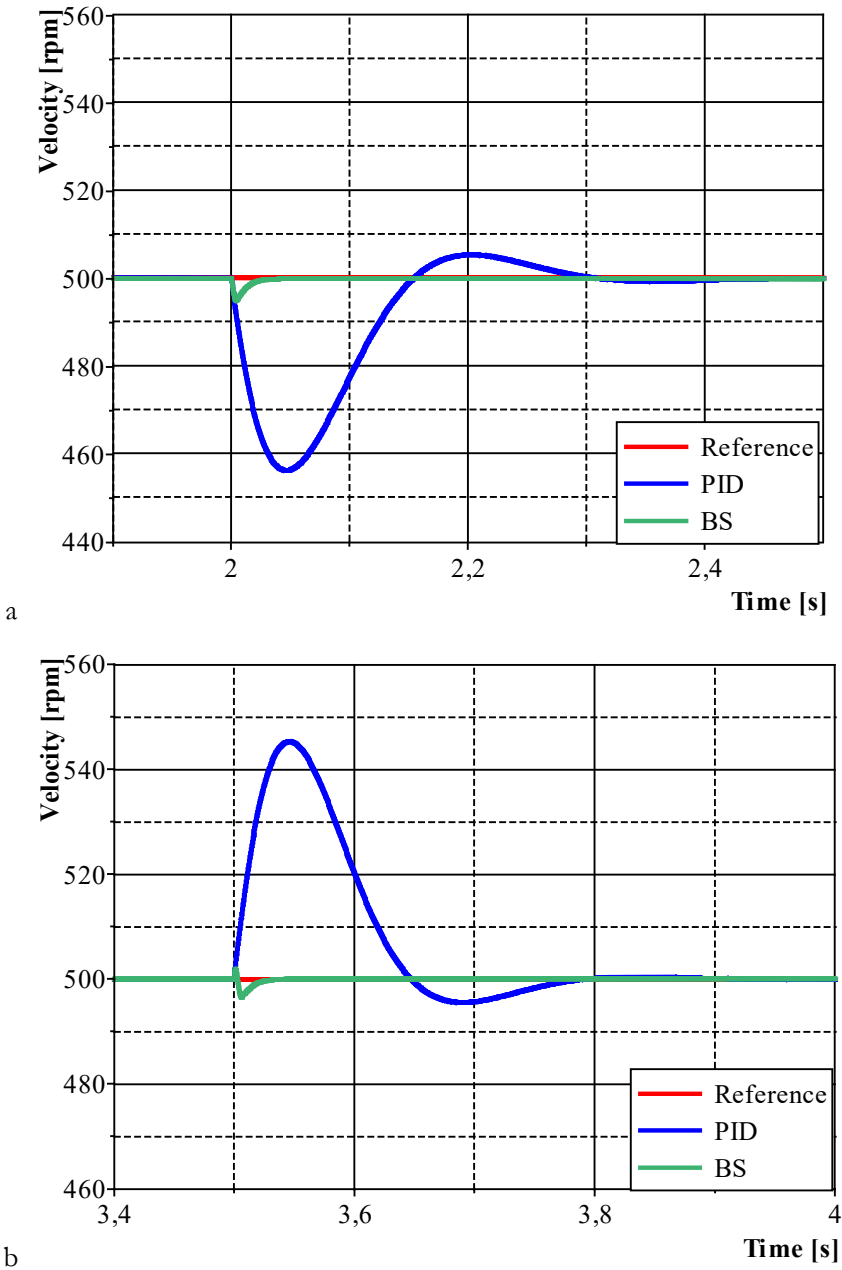Figure 7 shows details by switching disturbance shown on Figure 6.

a

b

Figure 7: Detail dynamic response by implementation of disturbance;
a - switching on, b - switching off.

5   Conclusions

In this paper, a controller design procedure is presented in order to control velocity of the electro-hydraulic servo system. Comprehensive investigation was carried out on the mathematical modelling and computer simulation of dynamic behaviour of whole system, based on real laboratory experimental data.

The nonlinear control of a velocity servo system consisting of an electrohydraulic servo valve and an axial piston hydraulic motor, which has third relative degree and is minimum phase, was investigated. These facts allow the design of a stabilizing control law based on feedback linearization. Due to potentially harmful influence of cancellations in the presence of unmodeled dynamics and parametric uncertainties the controller has been designed using the backstepping design procedure. Studies have shown that Lyapunov based approaches are the best strategies for the systems with complex dynamics. This is because the Lyapunov function is based on the system dynamics itself, thus, offering more flexibility in building the control signals. Firstly, backstepping relaxes the matching conditions, which means that the perturbation signals or the uncertainties in the system model are not restricted to show in the state equations that contains the input signal of the system. Secondly, backstepping avoids the cancellations of useful nonlinearities and takes the advantage of the useful ones to increase the system stability and reduce the amplitude of the control signal in order to avoid saturation.

All derived results are validated by computer simulation of the nonlinear mathematical model of the system. Additionally, the functionality of different mathematical software for dynamical analysis were investigated. Investigations were conducted as a preliminary research of closed loop control of hydraulically driven process of iron centrifugal die casting in industry.

References

[1]   Sun, Y., Li, W., Dong, D., Mei, X., Qiang, H. (2015). Dynamics analysis and active control of a floating crane, Technical Gazette 22,6, pp. 1383-1391. DOI:10.17559/TV-20151026154842

[2]   Veg, E., Veg, A., Sinkovic, G., Andrejevic, R., Gubeljak, N. (2015). Design of coupled slider crank mechanism for orbiting motion, International Journal of Simulation Modelling, vol. 14, no. 2, pp. 189-200, DOI:10.2507/IJSIMM14(2)1.283

[3]   Merrit, H. E. (1967). Hydraulic Control Systems. John Whiley and Sons, Inc. New York

[4]   Lovrec, D., Tič, V., Tašner, T. (2015). Simulation-aided determination of an efficiency field as a basis for maximum efficiency controller design, International Journal of Simulation Modelling, vol. 14, no. 4, pp. 669-682, DOI:10.2507/IJSIMM10(3)3.184

[5]   Kristic, M., Kanellakopouls, I., Kokotovic, P. V. (1995). *Nonlinear and Adaptive Control Design*, John Wiley and Sons Hoboken

[6]   Khalil, H. (2002). Non-Linear Systems, 3rd ed. Upper Saddle River, Prentice-Hall

[7]   Lee, S. J., Tsao, T. C. (2002). Nonlinear Backstepping Control of an Electrohydraulic Material Testing System, Proceedings of the American Control Conference, vol 6. pp. 4852-4830, DOI:10.1109/ACC.2002.1025422

[8]   Kaddissi, J., Kenne, P., Saad, M. (2007). Identification and Real-Time Control of an Electrohydraulic Servo System Based on Nonlinear Backstepping, IEEE/ASME Trasactions on Mechatronics, Vol. 12, February, DOI:10.1109/TMECH.2006.886190

[9]   Detiček, E., Kastrevc, M. (2016). Design of Lyapunov Based Nonlinear Position Control of Electrohydraulic Servo Systems, Journal of Mechanical Engineering, pp.163-170 DOI:10.5545/sv-jme.2015.2921

[10]   Detiček, E., Gubeljak, N., Kastrevc, M. (2017). Design of Lyapunov based nonlinear velocity control of electrohydraulic velocity servo systems, *Tehnički vjesnik : znanstveno-stručni časopis tehničkih fakulteta Sveučilišta u Osijeku*, ISSN 1330-3651, 2017, vol. 24, no. 3, pp. 745-751, DOI: 10.17559/TV-20160930073953

[11]   Jelali, M., Kroll, A. (2003). *Hydraulic Servo-systems:modelling, identification and control*, Springer –Verlag, London, Berlin, Heidelberg

University of Maribor Press

Hydraulic Power Drives for Shredders

ALEŠ NOVAK & ANŽE ŽAKELJ

Abstract Intensive heavy-duty continuous operation is typical of shredders, which cut through tough materials such as tires, plastic, wood and metal. The materials vary in size and hardness, requiring constant shaft speed and torque adaptation. Shredders are one of the most heavy-duty applications in the waste treatment segment and require reliable and efficient power units to generate the power and rugged motors to convert it into torque. The duty cycles are very demanding and machines in large waste treatment plants work 24/7 shredding up to 1 million tons of waste per year. Poclain Hydraulics has developed the complete system solution for such machines consisting of high torque low speed radial piston motors, dedicated valves and power units named Hydraulic Power Drive (HPD).

Keywords: • shredder • hydraulic drive • closed-loop • heavy-duty • recycling • waste •

CORRESPONDENCE ADDRESS: Aleš Novak, Poclain Hydraulics d.o.o., Žiri, Slovenia, e-mail: ales.novak@poclain.com. Anže Žakelj, Poclain Hydraulics d.o.o., Žiri, Slovenia, e-mail: anze.zakelj@poclain.com.

1   Introduction

Waste treatment and recycling are one of the hot topics these days when we generate more and more waste. After more ecological way of life to decrease waste, there are several approaches and solutions how to treat generated waste. Typically, the waste is pressed (e.g. presses, automatic balers) or shredded before further treatment.

Power units from Poclain Hydraulics used in recycling industry were mainly dedicated to presses (e.g. automatic balers). Recently we have extended the range of power units to offer hydraulic drives also for shredders. During the project to propose the best system solution we got new knowledge and know-how on another technological approach in waste recycling – heavy-duty rotating tools.

All sorts of waste are fed into the horizontal shears of a shredder: wood, furniture, electronics, household appliances, used asphalt, tires and other plastic material etc. [1]. Shredders are working at low speed and high torque that is typical application for hydraulic radial piston motors in direct drive. Other possibilities are electric motor driven shredders with gear-box for recycling of less demanding materials or hydraulic high speed motors (axial piston motors) with gear-box. Heavy-duty shredders (shredding also tires, plastic foil etc.) are typically hydraulic driven to be able to withstand the frequent shocks and changes in the rotation direction. Shredders are designed as single or dual shafts.

Figure 1: Dual shaft shredder.

The goal of the project was to meet the severe requirements of the machine and to build the standard offer of power units for shredders of different sizes.

2 Hydraulic system solution

Poclain Hydraulics has developed the complete system solution for shredders consisting of:

– One or two high torque low speed radial piston motors (HTLSM).
– Cross-over relief and anti-cavitation valves (CORAC).
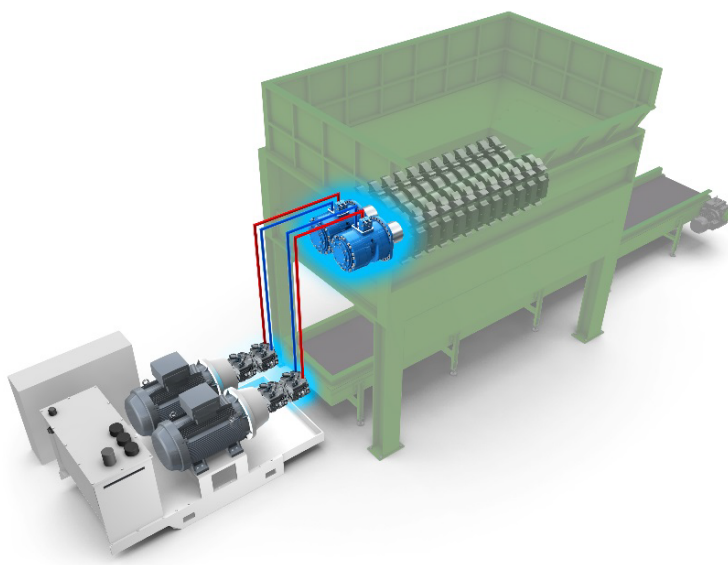– Power unit Hydraulic Power Drive (HPD).

Figure 2: Hydraulic system solution.

2.1 Hydraulic HTLS motors

High torque low speed radial piston motors enable direct drive without the need for less efficient gearbox. There are several advantages of the HTLS motors – see Figure 3:

– Cam-lobe technology: heavy duty (450 bar), precise movement, constant speed,

- Modularity,
- Direct drive (high efficiency, compactness),
- High power density,
- Flat ports for valve block mounting (relief and anti-cavitation valves),
- Hollow shaft option shortens the time required to replace the shredder shaft that are very often renewed.
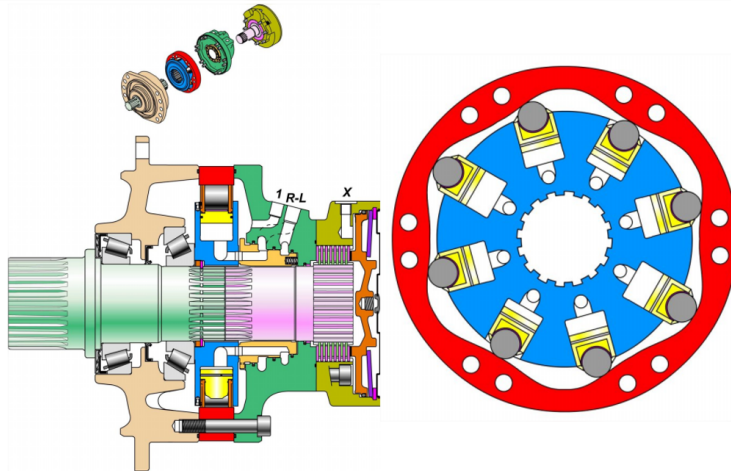
Figure 3: Modularity, cam-lobe technology.

The developed industrial motor range - see Figure 4, fulfilling the need of industrial applications (shredders, paper industry, tunnel boring machines, plastic injection machines, marine winches etc.). The range exists with several shaft possibilities (splined shaft, female splined shaft, shrink disk) and mounting kits (torque arms, shrink discs).

	MHP20/27	MS50	MS83 HF	MS125 HF	MI250
Displacement Range	1420 to 3530 cc [86 to 214 cu.in]	4010 to 6010 cc [245 to 367 cu.in]	6680 to 10,020 cc [408 to 611 cu.in]	10,000 to 15,000 cc [610 to 915 cu.in]	17,500 to 30000 cc [1067 to 1268 cu.in]
Max Speed	Up to 505 rpm	Up to 150 rpm	Up to 200 rpm	Up to 130 rpm	Up to 100 rpm
Max Torque	Up to 28,000 N.m [20,700 lbf.ft]	Up to 43,000 N.m [31,700 lbf.ft]	Up to 71,800 N.m [53,000 lbf.ft]	Up to 77,000 N.m [56,800 lbf.ft]	Up to 167,000 N.m [123,200 lbf.ft]
Max Power (Continuous)	Up to 280 kW [375 HP]	Up to 140 kW [188 HP]	Up to 200 kW [268 HP]	Up to 240 kW [322 HP]	Up to 500 kW [671 HP]

Figure 4: HTLS motors for industrial applications.

2.2 Power transmission valves

Pressure peaks, shown on Figure 5, are part of the shredding working cycle and without relief and anti-cavitation valves the hydraulic motors and pumps would be destroyed in a short time. Functionally are separated cross-over relief valve block, anti-cavitation block or both functions combined in a single block – CORAC; see figure 6. The valve blocks are designed to be flanged on the motor as separate functions or combined functions in a single block.
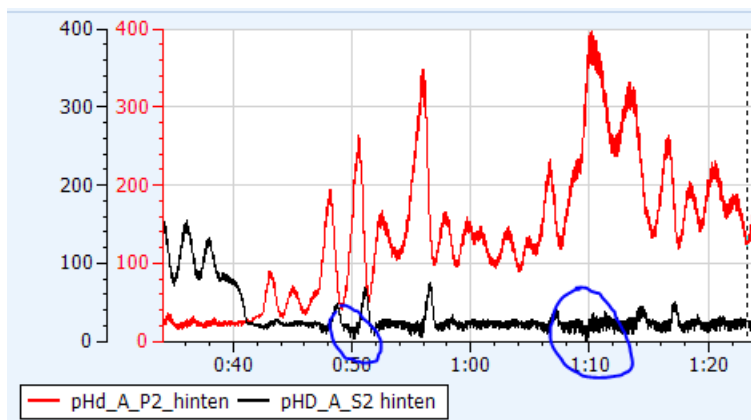
Figure 5: Pressure peaks showing loss of charge pressure.

Typical situation and the worst case of the shredder operation that is showing the need for anti-cavitation valves are the high-pressure peaks. During these pressure peaks in the high-pressure line the pressure in the low-pressure line (charge pressure) is lost almost or nearly to zero bar. During this situation, the motors are cavitating unless anti-cavitation valves are used.
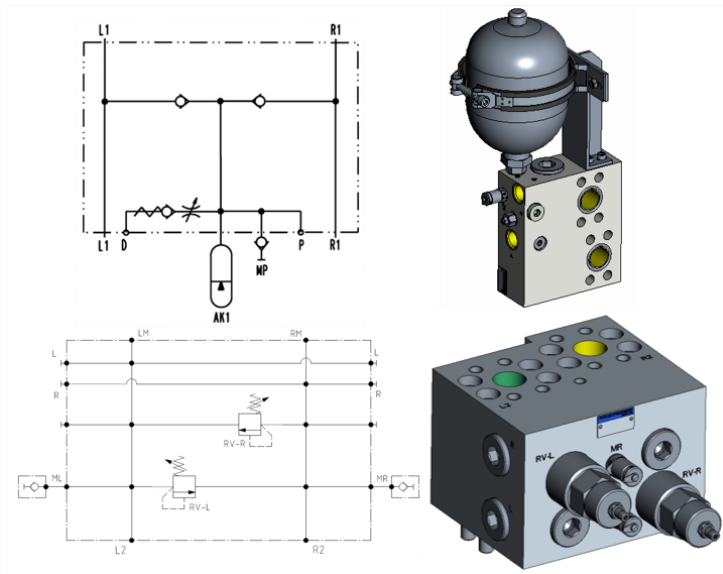

Figure 6: CORAC valves.

The relief valves are direct acting relief cartridges with quick response time of 2 ms operating at high flow to be able to react quickly when the object gets jammed in the machine.

2.3 Hydraulic power unit

The machine slows down, stops and/or reverses the direction of the rotation very quickly; the obvious system design was in closed-loop circuit taking in to consideration maximum efficiency and optimal components sizing. The power units consist of:

- High-pressure axial piston closed-loop pumps up to 280 ccm per rev. The big size shredders requests tandem pumps per one shredder shaft.
- Gear pumps for charge flow, anti-cavitation and auxiliary functions.

- Cross-Over Relief and Anti-Cavitation valves (CORAC) to protect the motor from over pressure and cavitation. Valve blocks are either mounted on the power unit or flanged on the hydraulic motor.
- AC electric motors up to 250 kW per pump or shaft.
- Hydraulic accumulators for anti-cavitation and fast pumps' command response time.
- Heat exchanger (air or water cooler).
- Reservoir with frame.
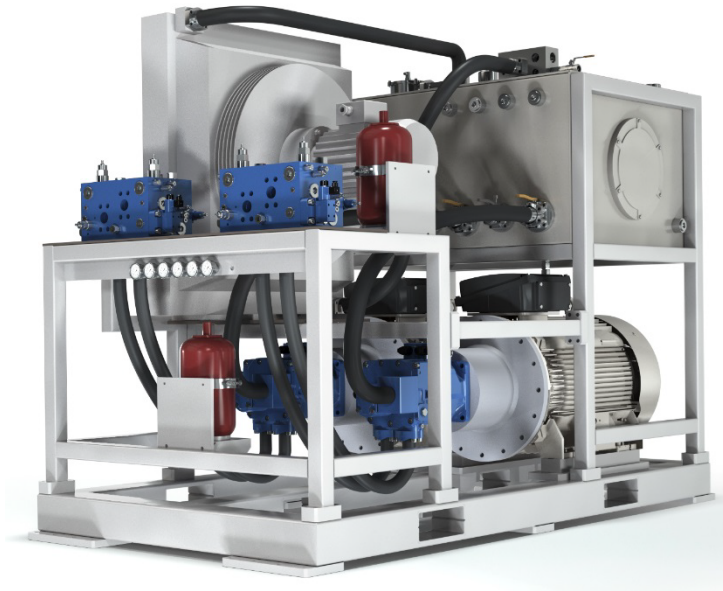- Electric wiring cabinet.
- Diagnostic components prepared for power limitation and condition monitoring.

Figure 7: HPD – Hydraulic Power Drive for dual shaft shredder.

Poclain Hydraulics has developed a range of standard hydraulic power drives (HPD) for different shredder sizes, for single and dual shaft drives:

- up to 250 kW per shaft drive and
- up to 560 ccm/rev per shaft drive.

Beside the severe technical characteristics, another design challenge was to develop the range of standard drive units. The standard offer currently consists of 16 power drives for single and dual shredders that helps customers decide together with the radial motor the best choice to fit their machine.

2.3.1   Pumps and valves solution

In terms of the best technical solution, system standardization and cost effective solution we decided to integrate some valve functions on pump. Beside the main pump, the unit integrates also exchange valve; pressure relief valve; intermediate block for condition monitoring; anti-cavitation valves; filter; pumps for charge flow, anti-cavitation and auxiliaries; accumulators for anti-cavitation and fast pump command – Figure 8.
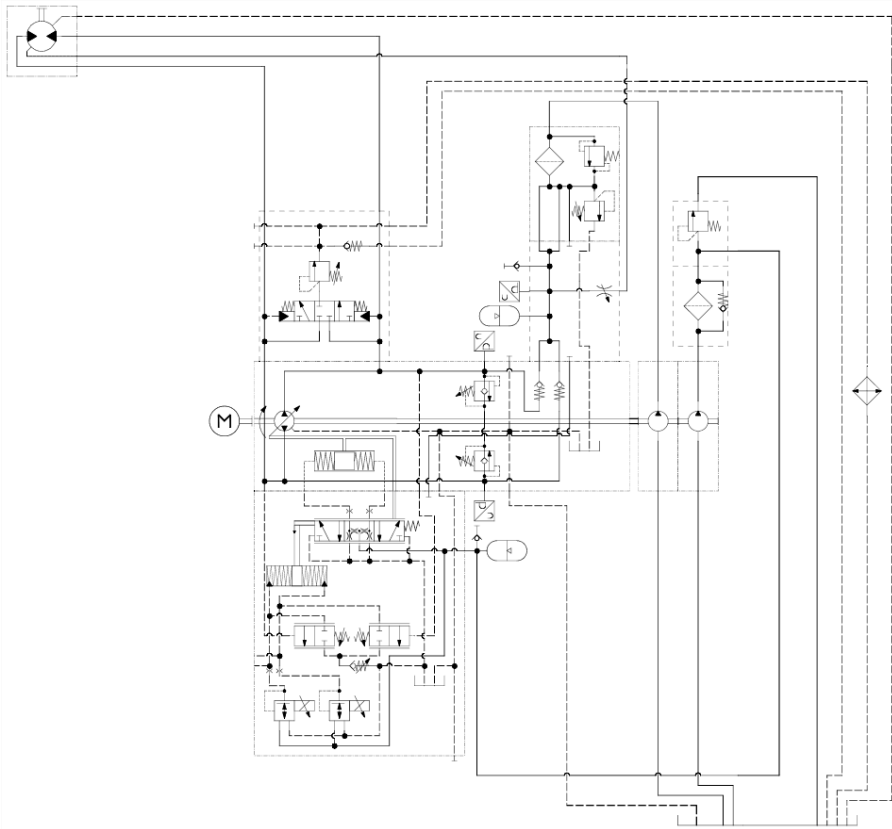
Figure 8: Hydraulic schematic of the single shaft drive.
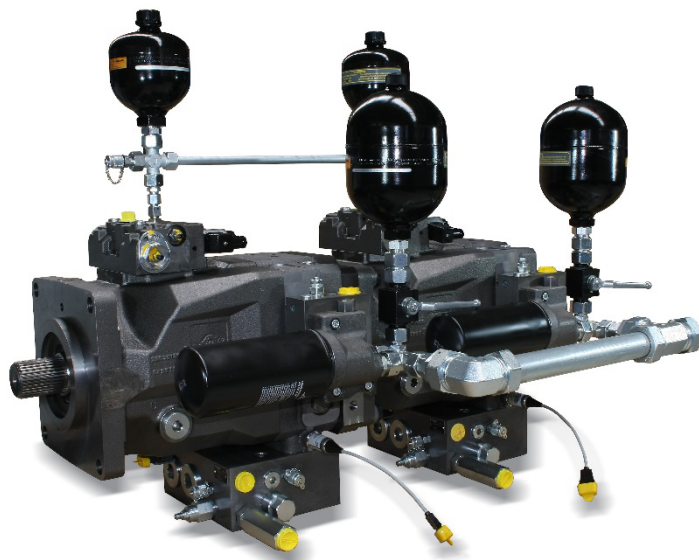
Figure 7: Tandem pump equipped with valves.

3 Condition monitoring and predictive maintenance

We are monitoring on several running shredders the main parameters (several pressure values, temperature, speed etc.) for predictive maintenance and on-line monitoring of the processes and equipment. Industrial machines are very sensitive to brake-downs causing production line stop and huge costs that both could be avoided in case of predictive maintenance.

Condition monitoring is the major component of the predictive maintenance. In case of hydraulic system solution for shredders the main components are hydraulic motors and pump and the main factor of its lifetime are pressure peaks. We are already monitoring several shredders on the market, building the algorithm to help customers plan the maintenance service to extend the lifetime of the machine and to avoid eventual breakdowns.

4   Conclusions

HPD standard range of power units for shredders was developed based on long-term experiences and know-how from using Poclain Hydraulics' HTLS motors on shredder drives. In terms of heavy-duty cycles, constant changes in the direction of rotation and in terms of reliability, roughness, cost-effectiveness and optimal sizing of components a closed-loop hydraulic circuit was the best choice. The main component of the power unit, as are pumps and valves, were chosen to meet high-pressure values and fast response time. The design of the power units has been proven during the first commissioning. We expect the future development of the system to be continued and oriented in to condition monitoring and developing algorithm for preventive maintenance planning.

References

[1]   POCLAIN MAG #13 – April 2019

University of Maribor Press

Adaptive hydrostatic drive for airport passengers stair

VINCENT KNAB & MARKO ŠTEGER

Abstract Poclain Hydraulics and Tips have been working together on a new version of airport passenger stairs that uses complete hydrostatic drive for its movement around the airport. Its main advantages are high torque and high accuracy at extremely low speeds, which are the qualities needed when steering a vehicle in the proximity of multi-million euros worth aircrafts. Hydrostatic technology on this vehicle offers smooth operation without any need of shifting during acceleration from stand still to its full speed. Direct wheel drive hydraulic motors eliminate the need of additional mechanical transmission which increases efficiency and saves space on the vehicle.

Keywords: • hydraulic drive • passenger stairs • low speed precision • radial motor • valve •

CORRESPONDENCE ADDRESS: Vincent Knab, Poclain Hydraulics France S. A. S., Verberie, France, e-mail: vincent.knab@poclain.com. Marko Šteger, Poclain Hydraulics d.o.o., Žiri, Slovenia, e-mail: marko.steger@poclain.com.

1   Introduction

Airports throughout the world use a variety of machines for their daily operations of servicing airlines, passengers and cargo. Most of the ground support machines operate in busy environments which obliges them to move carefully and also slowly, especially when it comes to manoeuvring in direct proximity of the aircrafts. While moving carefully and slowly, some of the ground support vehicles also need to move under heavy loads. An example of such machine would be airport passenger stairs which has to move its mass of around 10 tons directly towards the aircraft and coming to halt right next to it.

A type of powertrain which includes both low speed drive precision and high torque for heavy load movements is direct hydraulic drive. To move around, Tips' passenger stairs use Poclain Hydraulics' smart hydraulic system, consisting of a pump, control valves and two in-wheel hydraulic motors. All hydraulic components are monitored and managed by the electronic unit, which processes signals recorded by on-board system condition sensors, giving information to the IC engine in order to achieve maximized efficiency at any given moment.

Figure 1: TIPS 2458Cd passenger stairs.
Source: https://www.tips.si/si/runway2458cd.html

2 Hydraulics drive system

2.1 General technical architecture

Passenger stairs' power source is a diesel engine, powering Poclain Hydraulics P90 heavy duty pump, supplying hydraulic flow in the system which is fully operational at pressure as high as 450 bar. Hydraulic flow supplies two MS05 radial motors which are mounted directly on the rear shaft. The positioning of the motors presents a huge improvement in comparison to competition's in-direct motor installation products, where additional gear box is needed for reducing the final speed on the wheels. On the way from the pump to the motors, there are two additional valves that assure smooth and safe drive. They are called FD-H2 flow divider and VE60 high performance exchange valve.

2.2 Hydraulics P90 pump

The main source of hydraulic power on the vehicle is the Poclain PH P90 pump. Displacement is controlled by the system's electronic control unit, which sends PWM (Pulse Width Modulation) signals to the two main control solenoid valves that pilot the servo cylinder of the pump. The exact position of the pump swashplate is tracked by a Hall effect feedback potentiometer of which inputs are constantly processed by the ECU to reach a very high pump displacement control accuracy. Maximum hydraulic limit of 450 bar enables the P90 pump to be included in different heavy duty applications, such as airport passenger stairs.
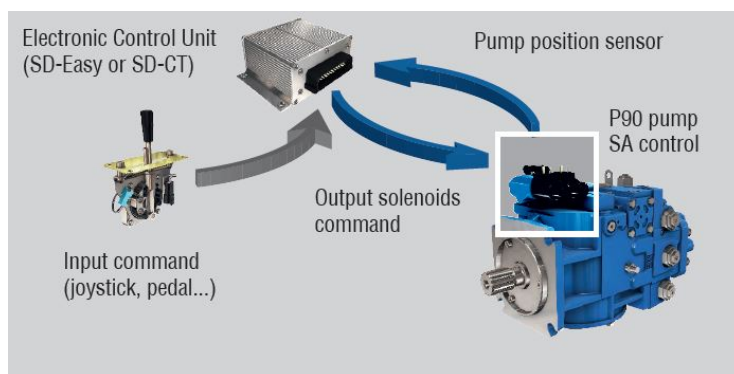
Figure 2: P90 pump control schematics.
Source: https://www.poclain-hydraulics.com/_upload/ressources/media/pdf/pump-range.pdf

2.3   Hydraulics MS motor

The modular design of the MS range of motors lets you create a motor that matches performance requirements while easily integrating into your design constraints. This flexibility will reduce your development costs and speed up the market entry of new machines. Radial piston cam design enables high efficiency at any speed and operating pressure while minimizing downtime due extreme durability.

The passenger stairs machine uses two MS-05 motors for its drive, enabling drive under heavy loads with high precision at low speeds. Besides moving the machine, the motors also provide two additional functions: service brake and parking brake. Service brake is controlled hydraulically with drum mounted directly on the motor, while the negative parking brake requires inducing pressure for motors to start moving, which provides a fail-safe feature while the vehicle is not in use.
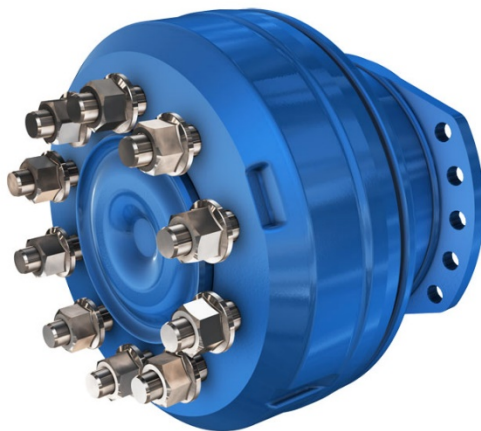
Figure 3: MS motor with drum brake.
Source: https://www.poclain-hydraulics.com/en/products/motors/ms/ms-mse05

2.4   Hydraulics FD-H2 flow divider

Uneven loading and diverse driving surface can cause motors on the same axle to rotate at different speed at the same. The consequence of this effect is slipping of drive wheels. Poclain Hydraulics' system uses FD-H2 flow divider valve to cope with the described phenomenon. In case of one wheel spinning faster than the other, electronically

operated valve limits and equilibrates the flow to provide required wheel adherence. The FD-H2 is a high performance valve, capable of operating at pressure as high as 500 bar.
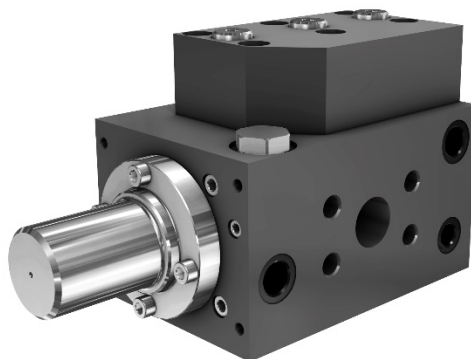

Figure 4: FD-H2 flow divider.
Source: https://www.poclain-hydraulics.com/en/products/valves/flow-divider/fd-h2-2

2.5   Hydraulics VE60 exhange valve

Compact exchange valves bleed hot oil from the low pressure side of a hydrostatic transmission circuit to be cooled, filtered or used as a source of oil for flushing pump and motor cases. VE60 high performance exchange valve is used on the drive system of the Tips 2458Cd passengers stairs vehicle. Exchange valve insures safety of operations and top performances in harsh climate conditions, even when the machine is constantly in use.

Figure 5: VE60.
Source: https://www.poclain-hydraulics.com/en/products/valves/exchange-valves/ve60hp
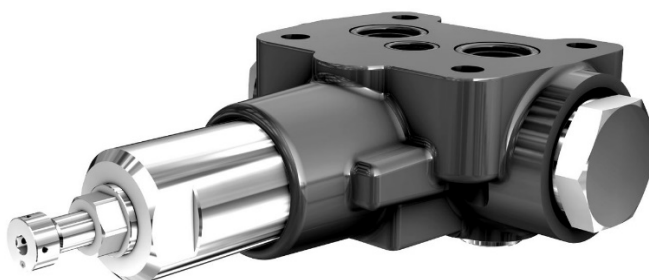
3   Conclusion

Cooperation between Poclain Hydraulics and Tips resulted in several successful projects in recent years. The 2458 Cd passenger stairs vehicle is the first Tips' product which uses only Poclain components in the hydraulic drive architecture. One of its most important features is a combination of smart sensors which send signals to the on-board computer in case of direct proximity of the aircraft. The computer limits the speed of hydraulic motors, so the vehicle can travel at the top speed of 0.22 m/s in this mode. The combination of hydraulic drive and the use of high tech sensors contributes to the possibility of driving the vehicle with high precision at low speeds and assuring high safety standards when closing the distance to the aircraft.

References

[1]   Poclain Hydraulics – MS motor range catalogue (2019)
[2]   Poclain Hydraulics – Valve range catalogue (2019)

University of Maribor Press

AddiDrive Technology - Hydraulic Drive System for Optimum Mobility of Trucks in Harsh Environment

PAOLA IPSA

Abstract Since 2005, Poclain Hydraulics has helped more than 25,000 Heavy Commercial Vehicles conquer the last off-road mile. The hydraulic hybrid transmission, AddiDrive, transfers torque to a non-mechanically powered axle only when needed. The system, including in-wheel hydraulic motors, closed loop heavy-duty pump, valve, electronic control, tank, cooler and filter, drives at speeds up to 30 kph. AddiDrive delivers torque to the front wheels while augmenting the efficiency and safety of trucks used in construction, forestry & municipal applications. A more economical and environmentally friendly solution, AddiDrive helps users maximize uptime and payload.

Keywords: • AddiDrive • hydraulic hybrid transmission • torque transfer • improved Total Cost of Ownership • heavy commercial vehicles •

CORRESPONDENCE ADDRESS: Paola Ipsa, Poclain Hydraulics Industrie, Verberie, France, e-mail: paola.ipsa@poclain.com.

1   Introduction

Poclain Hydraulics, as a part of the Poclain Group, is a global leader in hydrostatic transmissions based on radial pistons and cam-lobe motors technology. The independent and family owned Group has more than 2000 employees worldwide. Poclain's solutions have been employed for decades for agriculture, construction, forestry, industrial and trucking activities.

For off-road mobile applications such as agriculture or construction equipment, Poclain Hydraulics hydrostatic transmission generally consists in the main transmission of the machine. For on-road applications such as Heavy Commercial Vehicles (Class 6-8) or Light Commercial vehicles (Class 1-2), Poclain has developed various AddiDrive on-demand additional mobility solutions.

This paper will focus on AddiDrive closed loop system for Heavy Commercial Vehicles.

2   Vocational truck market needs

Today the most popular trucks on the market are those used for on-road application such as long haul. Those trucks are optimized when driving on the road, although, not for the rough terrains, as they are not supposed to go off-road. On the other hand, the mechanical AWD trucks are perfect off-road, however, with a limited on-road performance. Having only these two alternatives can represent a big problem for vocational application users who spend the 95 % of their time on-road and 5 % off road. Either they are based on standard, long haul, truck and they can get stuck in off-road conditions, or, if based on mechanical AWD transmission, their performance are very limited on-road.

Truck driver's and fleet manager's main concern is maximizing the productivity and safety. In this regard, maximizing payload and minimizing downtime, along with maximizing tires' lifetime, minimizing fuel consumption and extending material's lifetime are the most valuable levers. Thus, having such needs implies finding the right compromise between several criteria.

3   AddiDrive concept

3.1   Mechanical AWD truck

A common solution to avoid any risk in terms of mobility is to acquire a mechanical AWD truck which will cope to any kind of difficult situation with or without load. However, mechanical AWD is associated with constraints, such as reduced turning radius which limit dramatically the truck's manoeuvrability. Furthermore, as the ride height is higher, it brings constraints when driving on-road (e.g. when it comes to height restrictions for bridges and tunnels). Moreover, mechanical AWD is reducing the payload and increasing the fuel consumption, which is not suitable when driving from 90 to 95 % of time on the road. Mechanical AWD is a solution for high mobility needs and low distance driving.

3.2   AddiDrive

Poclain Hydraulics has developed a compromise solution, trying to combine the best of both worlds by giving to a standard truck more capability in off-road condition without changing significantly its on-road performance. In fact AddiDrive guarantees great mobility in difficult driving conditions such as mud, snow, slope or sand, improving truck's manoeuvrability by keeping standard truck's turning radius and improving the grip in low adherence conditions.

The system has a minimal impact on payload (-400 kg vs. a standard truck, while the mechanical AWD truck impacts payload by -1000 kg to -1200 kg) and fuel consumption (1,5 to 2 % in addition to standard truck, while mechanical AWD impacts the fuel consumption by 10-15 % vs. a standard truck) [1]. On the other hand, avoiding the slippage, AddiDrive increases the tires' lifetime [1]. Additionally, keeping the same cabin height as standard truck, AddiDrive improves driver's comfort compared to mechanical AWD truck.
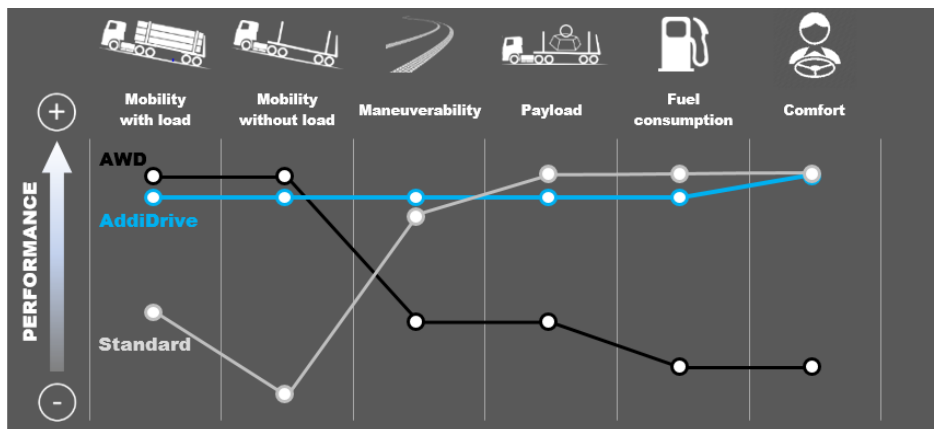
Figure 1: AddiDrive strategical positioning.

Besides the affirmed advantages to end users, AddiDrive has a positive impact on the environment. When having AddiDrive, there is no need of paving the acces to the working site for standard trucks, the tires lifetime is extended, while the fuel consumption is reduced. Finally, AddiDrive helps reducing the risk of cash out, usually spent for towing the standard truck when getting stuck.

Given the benefits of AddiDrive on the total cost of ownership and the environment, since 2005 the system has been installed in Europe and the USA on more than 25,000 Heavy Duty trucks dedicated to construction, earthmoving, forestry, utility, heavy haulage and other activities. The solution is adopted[1] by MAN, Daimler, Renault Trucks, Terberg (for Volvo) and Iveco in Europe and by Terra Drive System in North America.

3.3   System architecture and working mode

AddiDrive is a complementary hydraulic hybrid transmission that increases the mobility of a vehicle by transferring the torque on a non-mechanically powered axle.

The system includes two hydraulic radial piston motors, integrated directly in the spindle of a steering or straight axle, axial variable piston heavy duty pump, mounted at the engine PTO, the valve block, electronic control, tank, cooler and filter (Figure 2).

---

[1] In closed loop version. Open loop versions available in Europe with SAF Holland and Paul Nutzfahrzeuge (for DAF).
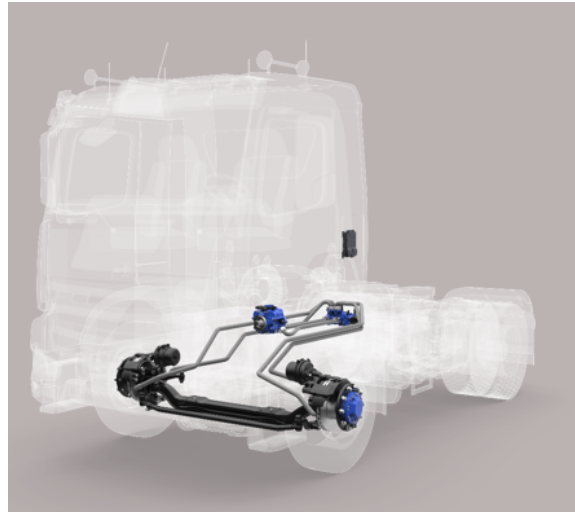
Figure 2: Representation of AddiDrive integration.

When the system is activated, the pump, powered by the internal combustion engine PTO, generates and provides the flow to the valve block. The valve block, which ensures the safety and manages motors' activation, splits the flow between two motors, which, finally, provide traction. The system is piloted by the electronic control, which manages the communication and additional functions. To ensure cooling of the running system, a constant flow of oil is exchanged out of the closed circuit and cool down before returning to the oil tank.

Contrary to a mechanical axle, AddiDrive delivers the torque only on-demand. The driver, manoeuvring the switch on the dashboard, activates the system making it ready to engage and disengage. The engagement and disengagement can be done on-the-fly, even while the vehicle is moving.

Two modes are provided: The Traction mode where torque can be transferred to the hydraulic powered axle and Freewheeling mode where the two hydraulic motors are disengaged.
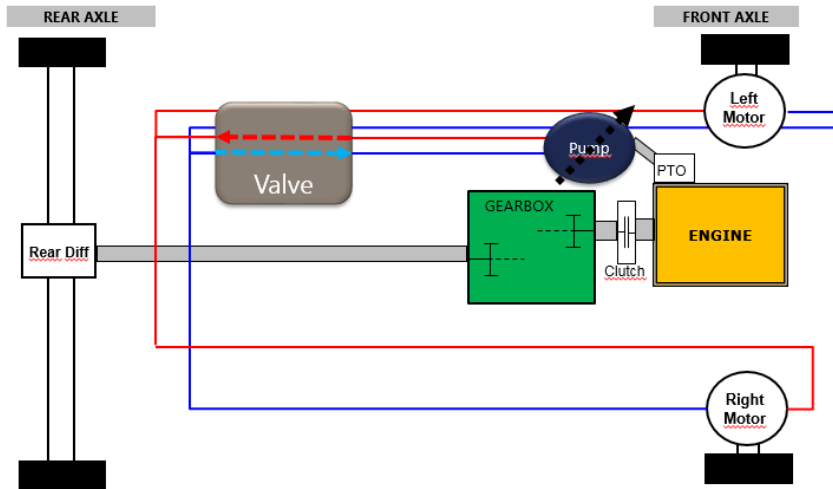
Figure 3: AddiDrive closed loop system architecture.

When in Traction mode, the system can drive the truck up to the speed of 30 kph, after what AddiDrive automatically disengages. Depending on the resistance created by the machine, max torque of the motors can be provided from 0 kph until the system reaches maximum allowed power of 82 kW, maximum system pressure is up to 450 bar. Moreover, maximum tractive effort generated by 1L hydraulic motors at 450 bar is optimized with truck load and low condition adherence typically encountered in difficult situation (adherence coefficient around 0,3). While the Traction mode is active, the pump stroke is controlled to ensure the synchronization between the front and rear wheels (see Figure 3).
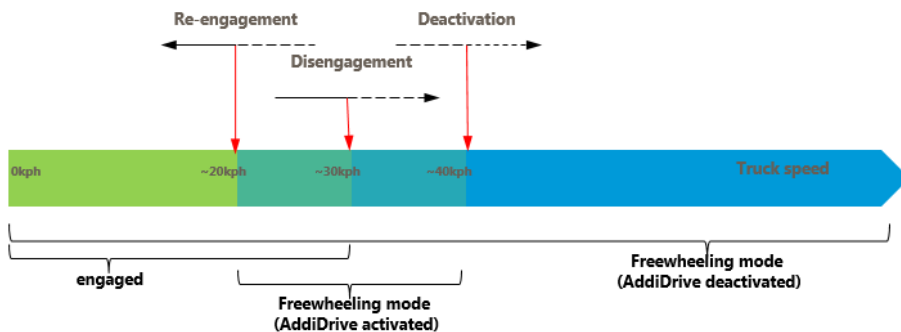
Figure 4: AddiDrive engagement strategy.

When the system is disengaged, the pump remains in neutral position, while the charge pump is de-rated through the valve block. Consequently, the two motors are in Freewheeling mode, thus the system drag losses are minimum. If the speed drops under 20 kph, the system will re-engage automatically, while after 40 kph, it is automatically deactivated.

3.3.1 Additional functions

Besides the standard Traction and Freewheeling mode, AddiDrive performs the Creep and Boost functions.

Creep mode is tailored for activities which require a high precision on a constant slow speed. Once the Creep mode is activated, the pump displacement is proportional to the driver command and to the engine speed, while the vehicle is driven exclusively by the system at constant slow speed. The function is running up to 18 kph and can climb the maximum slope of 13 %[2]. The driver can set up the speed with cruise control, throttle pedal or joystick. When the targeted speed is reached, it will be regulated by the system, whatever the engine speed. Indeed, if ICE rpm increases to pilot the auxiliaries, the pump swash plate is adjusted to keep constant the vehicle speed.

When in Boost mode, the system brings the highest pressure as soon as the gas pedal is applied on a stationary vehicle, delivering the highest torque to take off the truck. This function is appreciated after tipping (when the rear truck or trailer's wheels are typically covered with the discharged material) and when starting the vehicle on the slope or irregular and rough terrains.

3.3.1 System management

During steering and braking phases, thanks to the Bypass function, the system has no influence on vehicle's behaviour. The software prevents unexpected torque during gear shifting and braking. Furthermore, to avoid any unexpected movement while the vehicle is driving at very low speed or stationery, the software keeps the system disengaged as long as the throttle pedal is at less than 5 %.

---

[2] Depending on truck cinematic and loads.

Warm-up Standstill function controls the temperature while the vehicle is stationary, increasing it up to the level needed by the pump for piloting. On the other side, Warm-up Driving function increases and/or maintains the oil temperature to prepare for a potential system activation while the vehicle is driving in Freewheeling mode.

Furthermore, the software makes sure the system will avoid over power, over pressure and over torque situations. While, in case of use of pump rear PTO to operate auxiliary system on the truck, following driver request, the torque can be reduced to protect the engine PTO.

4   Conclusion

When introduced on Heavy Commercial Vehicles in Europe and in the USA, AddiDrive has revolutionized the truck world:

— improving dramatically their traction and manoeuvrability, thus vocational truck drivers never get stuck,
— improving at the same time their productivity, profitability and safety, as the fleet's uptime is maximized, while fuel and tires expenses are optimized – which reduces truck's environmental impact.

Finally, AddiDrive has raised hydraulic transmission's innovation bar widening the technology to commercial vehicles.

References

[1]   Poclain Hydraulics internal database

University of Maribor Press

Flow Optimization of a Hydraulic Fast Change Coupling System for Mobile Excavators

JÖRG EDLER, MARCO HAAS & FRIEDRICH WAGNER

Abstract To increase the flexibility of modern hydraulic working machines, the end of the booms of hydraulic excavators will be equipped with different devices, for example with different excavating buckets or with hydraulic hammers. The change of these devices can be done manual by hand or automatically by a Fast Change System. But it has to be pointed out, that the change with a Fast Change System must also be done by the worker, but it can be done with the booms of the excavator and only the mechanical lock is done automatically. The tasks of the Fast Change System are the save mechanical locking of the devices and the passage of hydraulic lines. That means, that hydraulic couplings must be integrated in the Fast Change System. Which can be coupled under pressure, which are working without leakage and have a high live time. This article shows the flow optimization of a hydraulic coupling system for hydraulic Fast Change Systems with the goal to minimize the pressure losses in the coupling system and to increase the efficiency of the system excavator, Fast Change System and working device.

Keywords: • simulation • excavator • hydraulic Coupling • flow optimization • Fast Change Systems •

CORRESPONDENCE ADDRESS: Jörg Edler, Graz University of Technology, Institute of Production Engineering, Graz, Austria, e-mail: Joerg.edler@tugraz.at. Marco Haas, Graz University of Technology, Institute of Production Engineering, Graz, Austria, e-mail: Marco.haas@student.tugraz.at. Friedrich Wagner, Winkelbauer GmbH, Anger, Austria, e-mail: f.wagner@winkelbauer.com.

# 1		Introduction

Modern excavators are normally equipped with a Fast-Changing Coupling System. This gives more flexibility in the use of the excavator, because the worker can change the working tool at the end of the boom of the excavator very fast and it is normally not necessary to leave the carbine of the excavator. There existing al lot of different buckets which can be changed but is can also be used other tools, for instance hydraulic hammers, which needs a hydraulic power supply. Also, are systems available which supply the tool with electrical and with hydraulic power [1].
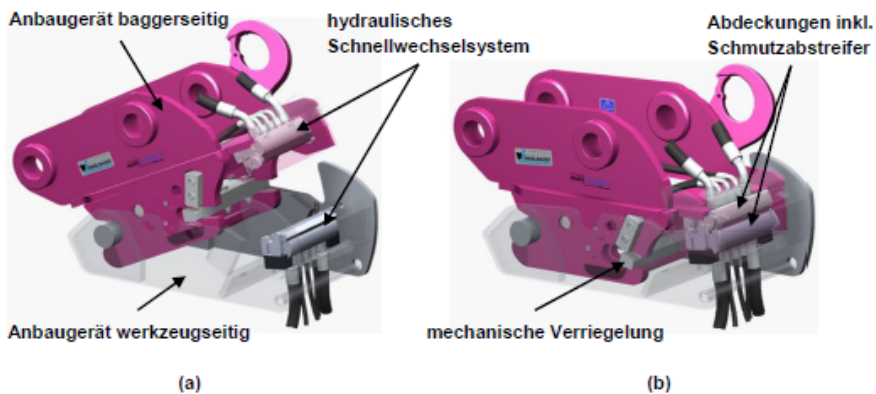
Figure 1: Fast-Changing Coupling System [5]**.**

To generate this hydraulic power supply hydraulic couplings are needed in the Fast-Changing Coupling System. There are many regulations for the safety operating of these Fast-Changing Coupling System [2], but also the hydraulic power supply must work reliable and efficient. There are different ways to equip an excavator with a Fast-Changing Coupling System. One possibility is to use a Fast-Changing Coupling System of the manufacturer of the excavator for instance of Liebherr [3] or Volvo [4]. The other possibility is to use a Fast-Changing Coupling System of a third party like the company Winkelbauer GmbH [5]. The requirements mentioned above are shared by all systems.

A Fast-Changing Coupling System is shown in Figure 1. It consists of a part which is mounted on the excavator and a part which is mounted on the working tool. All these systems consist of the mechanical part of the steel construction, the hydraulic lock and the hydraulic coupling system [5].

2   Simulation of the existing Hydraulic Coupling

2.1   Geometry and Mesh

In a first step the existing hydraulic coupling will be build up in a cad 3D drawing. In Figure 2 is a 2D view shown. It can be seen, that in the hydraulic coupling system are some springs implemented. These springs are necessary for the function of the hydraulic coupling system, but for the simulation they will be neglected. This give the advantage, that the symmetry can be used. A further advantage is that the mesh is easier to generate, because the complicated geometries of the springs are not in the model.
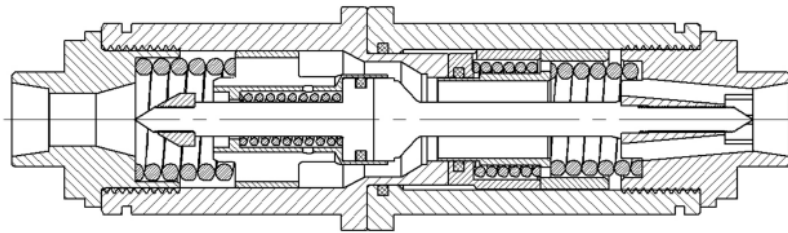
Figure 2: Existing hydraulic coupling.

In the next step the negative volume or the hydraulic coupling will be generated. This volume represents the fluid in the hydraulic coupling system and this volume will be used in the flow simulation. To get better results the mesh should be generated with a finer mesh wide in the critically regions of the model. Therefore, the geometry of the fluid will be split into separate volumes as in Figure 3 can be seen.
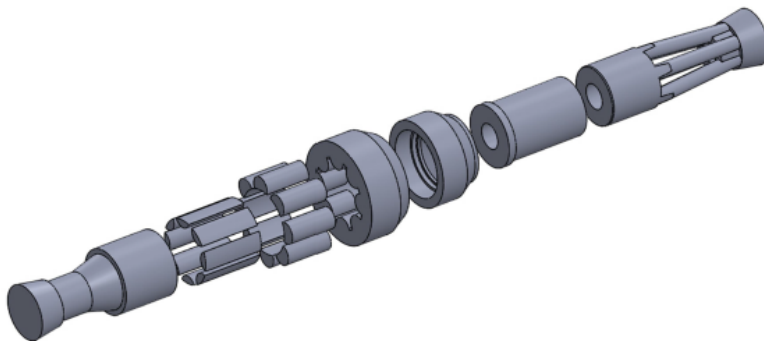
Figure 3: Separated volumes of the fluid.

The final setup of the model is shown in Figure 4. There can be seen only a quarter is considered. Also, the final mesh is shown in Figure 4. This final mesh is the result of a mesh study, which is described by Finck [6] and Fritsch [7]. The mesh has been refined until the simulations result didn't change anymore, that means the result of the simulation is independent of the mesh size.
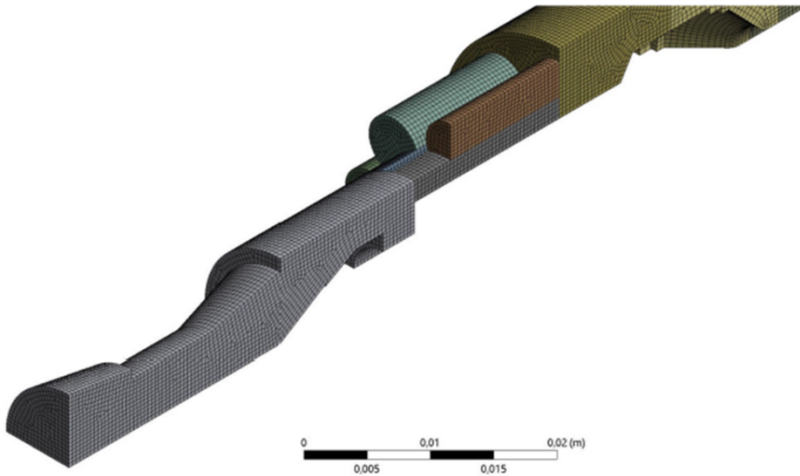

Figure 4: Final simulation model.

2.2   Setup and Boundary Conditions

In modern excavators are a lot of different mineral oils used which depends on the environment conditions where the excavator is working, on environmental regulations and on the company, which is building the excavators. In this case it cannot be said which oil is used in the hydraulic coupling and so it will be used a standard oil model of a mineral oil HLP46, see Table 1.

In the simulation will be used three boundary conditions. The inlet boundary condition defines the flow through the hydraulic coupling, which is given as the nominal flow from the manufacturer. In our case the nominal flow is 250 l/min. A further point is, the flow through the hydraulic coupling system can be in both sides, that means the simulation must also be done in both flow directions. The outlet boundary condition is a pressure condition and is set up to 270 bar. This pressure is not so important, because only the pressure drop in the hydraulic coupling is interesting.

Table 1: Specifications HLP46

	Value	Unit
kinematic viscosity	16	$\dfrac{mm^2}{s}$
density	852	$\dfrac{kg}{m^3}$
dynamic viscosity	0,01363	$\dfrac{kg}{m\ s}$
specific heat capacity	1885	$\dfrac{J}{kg\ K}$
molar mass	530	$\dfrac{kg}{kmol}$
coefficient of thermal expansion	0,0007	$\dfrac{1}{K}$

The last boundary condition is a symmetry condition to consider the symmetry of the model. In Figure 5 are the boundary conditions on the model shown. The simulation is done stationary and no turbulence model was used, see Edler [8] and Mörwald [9].
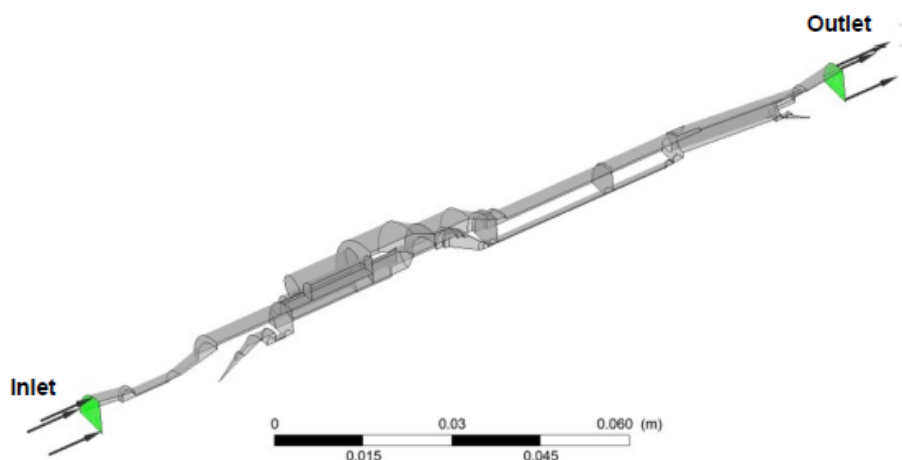
Figure 5: Boundary conditions.

2.3   Results of the simulation of the existing hydraulic coupling

Figure 6 shows the pressure distribution in the hydraulic coupling. The whole pressure drop over the hydraulic coupling is 32 bar. It can be seen that the pressure drop is not constant over the whole hydraulic coupling.
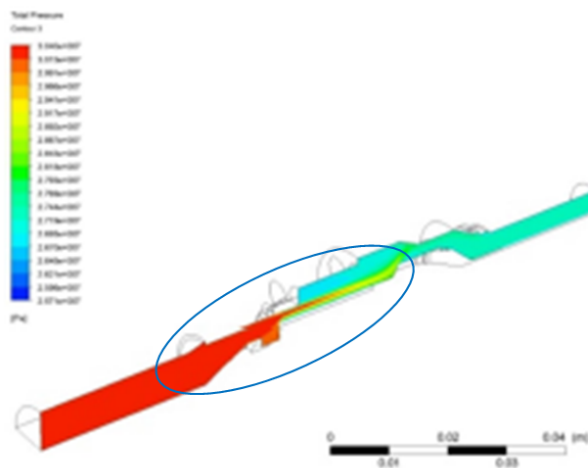
Figure 6: Pressure distribution in the hydraulic coupling.

There is a bottleneck between some holes and a spring which generates a big pressure drop. This bottleneck can also be seen in Figure 6. In the velocity distribution over the hydraulic coupling can this bottleneck also be seen, Figure 7. Another region with a higher-pressure drop is an inlet area of the hydraulic coupling. Here are also holes which decrease the cross section of the hydraulic coupling. This area should also be improved.
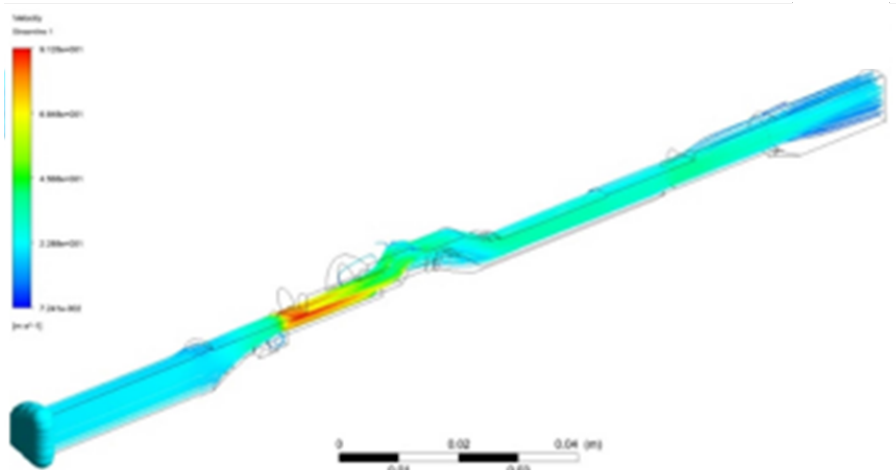
Figure 7: Velocity distribution in the hydraulic coupling.

Figure 8 shows the areas which are identified for the redesign to decrease the pressure drop. The redesign is done in two steps. The first one is the area with the highest pressure drop and the second one is the area if the nut in one part of the hydraulic coupling system.
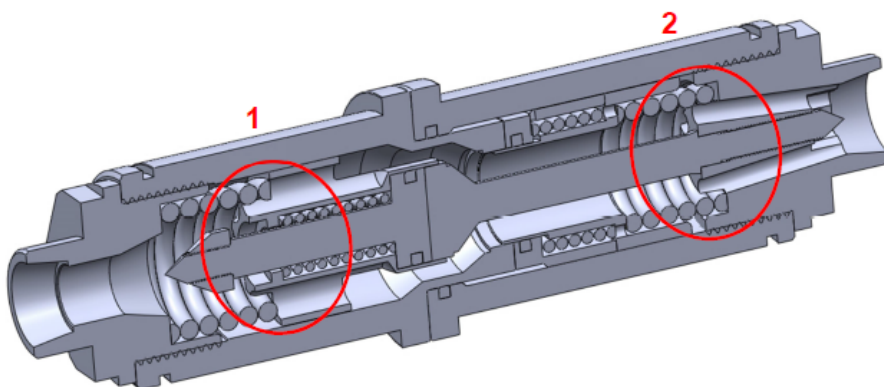

Figure 8: Areas for the optimization.

3 Redesign and Simulation of the Hydraulic Fast Coupling System

Figure 9 shows the different steps of the optimisation. Based on the existing system was in the first step the area of the highest pressure drop optimized (area 1 in Figure 8). One point of the optimization was that the redesign must be compatible with the old design. Figure 9b shows that the bottleneck between the holes in the coupling and the spring which is necessary to close one part of the coupling is neglected. This optimization hast the most potential to decrease the pressure drop in the hydraulic coupling.
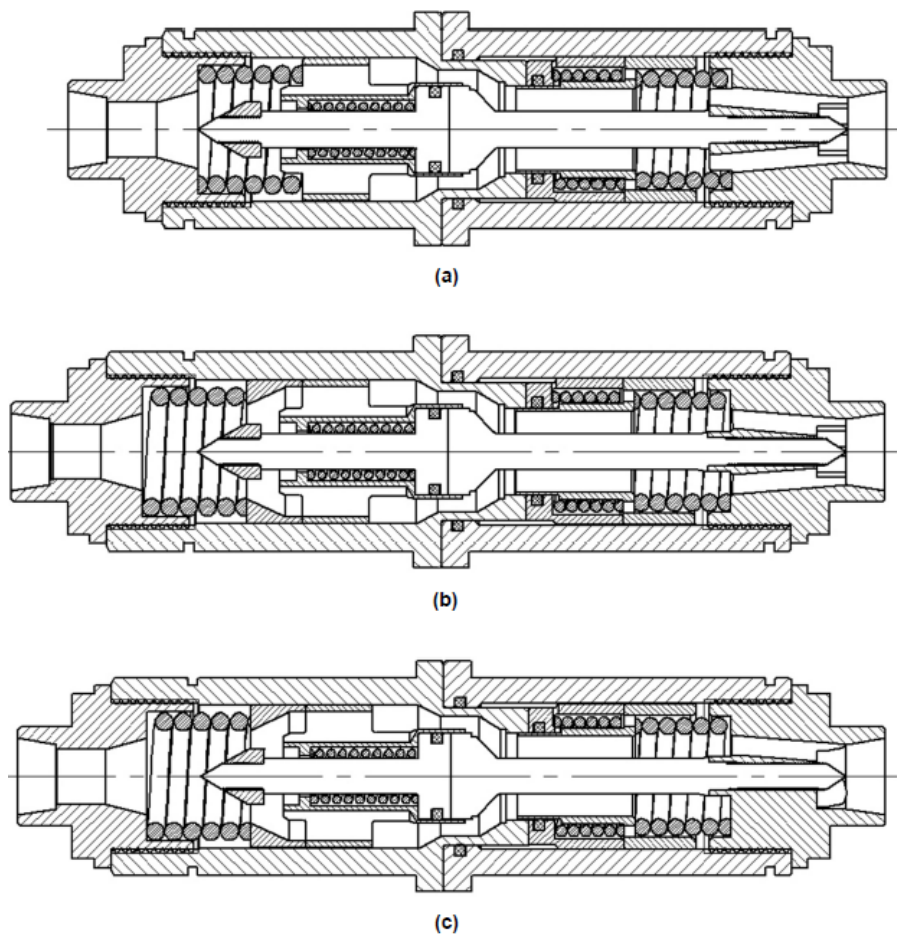
Figure 9: Optimized hydraulic coupling, a) original, b) step one area 1 and
c) step two area 2.

Figure 9c shows the second and final optimized version of the hydraulic coupling system. The holes in the nut on one side, see detail A in Figure 9c, will be redesigned. Figure 10 shows the different steps of this redesign. The last version gives the biggest cross section for the flow, but is not so easy to manufacturing.
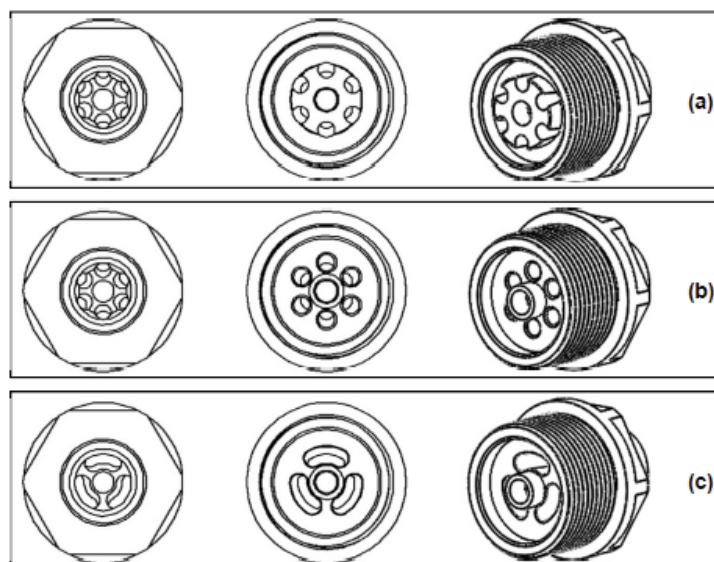

Figure 10: Optimized nut, a) original, b) step one and c) final version

The redesign consists of some iteration steps between redesign and simulation. At the end of this steps the pressure drop can be lowered up to 5,67 bar. That means that the pressure drop could be decreased about 81,25 %. In a view that two hydraulic coupling systems are necessary on a Hydraulic Fast Change Coupling System then the efficiency is extremely increased with the redesign of the hydraulic couplings. Table 2 shows the results of the different iterations steps of the redesign.

Table 2: Results

	pressure drop in bar	max. velocity in m/s	optimization in %
original version	32	92,7	
step one	6,7	41,3	76,3
step two	5,67	40,5	81,25

4   Conclusion

With the redesign of the hydraulic couplings it is possible to decrease significant the pressure drop of the hydraulic couplings. With the new design is the pressure drop in the hydraulic coupling von be decreased from 32 bar up to 5,67 bar. This is a massive advantage in the efficiency. At a nominal flow of 250 l/min and the use of two hydraulic couplings the power losses are decreased from 27 kW up to 5 kW. Second the requirement that the new design must be compatible with the original design can also be met. This is very important, because there are al lot of existing hydraulic coupling in the field and it make no sense to exchange all these couplings.

References

[1]   Schwab, C. (2014). Beitrag zu einer universellen Baggerschnittstelle zur Übertragung elektrischer und hydraulischer Leistung sowie elektronischer Signale für komplexe Anbaugeräte, in Frank Gauterin (Hrsg.), *Karlsruher Schriftenreihe Fahrzeugsystemtechnik*, Band 27, Karlsruhe: Verlag: Scientific Publishing

[2]   Winkler, P. (2019). Technische Sicherheitseinrichtungen an hydraulischen Schnellwechseleinrichtungen. *BauPortal*, 3, pp. 40-41

[3]   Liebherr (2019). Hydraulische Schnellwechsler, [online] https://www.liebherr.com/de/aut/produkte/anbauwerkzeug/schnellwechsler/hydraulischer-schnellwechsler/hydraulische-schnellwechsler.html.

[4]   Volvo (2019). Construction Equipment, [online] https://www.volvoce.com/oesterreich/de-at/attachments/wheel-loader-attachments/attachment-brackets/volvo-attachment-bracket-vabl

[5]   Winkelbauer GmbH (2019). Schnellwechsler für Bagger, [online] https://www.winkelbauer.com/baumaschinen-ausruestung/schnellwechsler-fuer-bagger/

[6]   Fink, S. (2015). CFD-Untersuchung einer Kaplan-Rohrturbine in OpenFOAM, Diplomarbeit im Fach Energietechnik und Energiewirtschaft an der Fachhochschule Vorarlberg

[7]   Fritsch, A. (2018). An Analysis of Potential of Solar Tower Power PlantsUsing Liquid Metals as Heat Transfer Fluid, Dissertation an nischenHochschule Aacheder Fakultät für Maschinenwesen der Rheinisch-Westfälischen Technischen Hochschule Aachen

[8]   Edler, J. (2011). Estimation of the hydraulic conditions in piezo-pilot-valves. *Fluidna Tehnika 2011*, pp. 103-112, Maribor

[9]   Mörwald, G., Edler, J., Tic, V. (2015). Calculation of Control Edges with Simulation. *Fluidna Tehnika 2015*, pp. 249-254, Maribor

University of Maribor Press

Comparison of the Quality of Synchronous Motion of Radial Gates for Different Configurations of Electric-eydraulic Drives

DRAGAN NAUPARAC, NEMANJA VIŠNJIĆ & NELA CERO

Abstract This paper considers the problem of selection of the optimal configuration of an electric-hydraulic drive with two hydraulic cylinders for lifting and lowering of a radial gate. Beside the general theoretical approach to confirm the right design choice, adaptation criteria relative to the change of expected external conditions as well as the experimental verification of the quality of performance of the selected electric-hydraulic configuration and the control structure of said electric-hydaraulic configuration are proposed.

Keywords: • radial gates • hydraulic drive • hydraulic cylinder • synchronous motion • ptimal design criteria •

_____

CORRESPONDENCE ADDRESS: Dragan Nauparac, PPT Inženjering, Belgrade, Serbia, e-mail: dragan.nauparac@ppt-inzenjering.rs. Nemanja Višnjić, PPT Inženjering, Belgrade, Serbia, nemanja.visnjic@ppt-inzenjering.rs. Nela Cero, PPT Inženjering, Belgrade, Serbia, nela.cero@ppt-inzenjering.rs

1   Introduction

The main issue with the motion of radial gates, Figure 1, which are most often used at the spillway of dams of hydroenergy objects, is to provide the synchronous motion of gate endpoints within allowed error tolerance to avoid the tilting of a gate, which would in turn prevent the guiding mechanism of a gate to function properly causing the gate to get stuck. The guiding of radial gates is provided by the parallelism of lateral concrete walls which are in contact with sealing rubber (sliding friction) or with guiding wheels (rolling friction) - Figure 2.

Figure 1: Radial gate.

Synchronous motion can be provided by passive and active synchronization. Passive synchronization is provided by equalizing pressures in hydraulic cylinders at both ends of a gate relying on the property of the gate (sufficient stiffness) to obtain the self-synchronization. Passive synchronization does not envisage generating any external control signals to guarantee synchronous motion.

Active synchronization includes the stroke measurement of each hydraulic cylinder, creation of control signal proportional to the current position difference between the left-hand side and the right-hand side hydraulic cylinder which accelerates or decelerates the motion of the hydraulic cylinder piston rods by activating certain hydraulic valves. Radial gates can be manufactured with various stiffness which directly determines the choice of synchronous motion control, i. e. passive or active synchronization.

D. Nauparac, N. Višnjić & N. Cero: Comparison of the Quality of Synchronous Motion of Radial Gates for Different Configurations of Electric-eydraulic Drives

269

Figure 2: Guiding and sealing details of a radial gate.

To provide the synchronous motion of small and relatively light radial gates with width up to 12 m, i. e. the gates with low water pressure, the configurations of electric-hydraulic drives with active synchronization must be selected, because the small wieght of the gate is obtained at the expense of reduced stiffness of the gate construction.

This paper does not consider the alternatives of volumetric control of a hydraulic drive (the change of the pump oil flow and/or pump/motor regime), but only the throttle control of oil flow for lifting and lowering. It should also be pointed out that with lighter gates, the hydraulic cylinder dimensions are such that full oil circulation from the piston rod cylinder chamber to the reservoir happens during the gate lowering. For this reason, the alternatives with direct oil flow from piston rod cylinder chamber to piston cylinder chamber will not be taken into consideration.

The real load of the hydraulic cylinders is inertial, approximately 50 % of the gate weight per cylinder. Also, the load from the external friction of the sealing rubber or the rolling wheels should be taken into account. The friction force should be up to 20 % of the gate weight and distributed in such a way that the diference due to friction load between the left-hand and the right-hand side of the gate is not greater than 50 % [5].

2   Selection of the design solution

In order to compare the two hydraulic configurations, it is necessary to consider the design approach that defined the two different configurations. When an electric-hydraulic drive is designed, a criterion which determines the optimal design solution must be defined. It is the most important part of the design activity.

There are four criteria to follow when we define the structure of the electric-hydraulic drive (i. e. the hydraulic functional schematic):

1. Structure and parameters,
2. Adaptation to external conditions,
3. Minimal number of elements,
4. Modular principle.

After an optimal configuration of the electric-hydraulic drive is defined, a couple of criteria regarding the adequate control of the drive are taken into consideration, such as:

1. Response time
2. Stability
3. Accuracy.

Regarding the electric-hydraulic drives for synchronous motion, the criterion for selection of the optimal structure is response time of the drive because, if higher, it, in any case, provides the better quality of the synchronous motion, i.e. the smaller error. Other criteria are second in importance and will influence the final structure only when and if they do not contradict the time response criterion.

Figure 3 and Figure 4 show the hydraulic functional schematics which are the subject of the design analysis and comparison.

It is clear that both hydraulic functional schematics comply with the modularity principle. Structurally, the two configurations are different. The configuration shown in Figure 3 provides synchronization by oil bleed-off. The faster hydraulic cylinder decelerates during lifting and the slower hydraulic cylinder accelerates during gate lowering. Configuration shown in Figure 4 (Module 1) doesn't have the option to bleed off hydraulic oil directly, but through the pressure relief valve during gate lifting. During gate lowering, there is no bleed-off at all, but hydraulic oil remains in the hydraulic cylinder and its motion decelerates. This is the key difference between these two configurations.
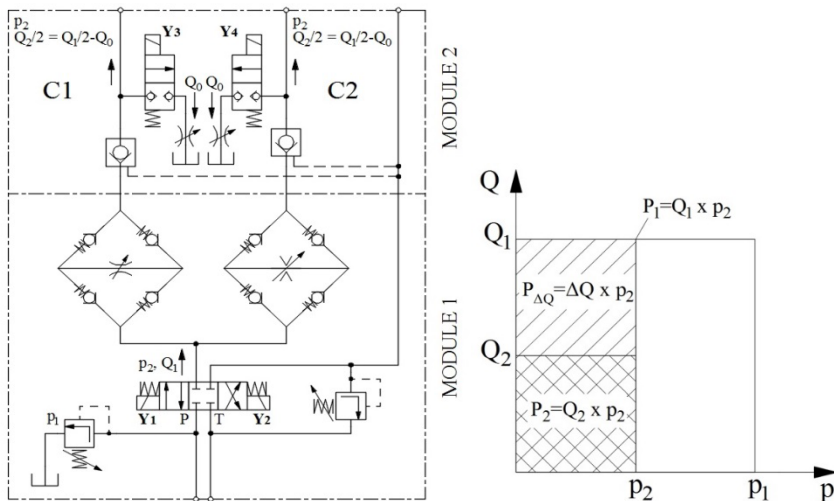
D. Nauparac, N. Višnjić & N. Cero: *Comparison of the Quality of Synchronous Motion of Radial Gates for Different Configurations of Electric-eydraulic Drives*

271

Figure 3: Hydraulic functional schematic of a configuration with bleed-off valves (left) and its energy efficiency diagram (right).

When compared by the number of elements, the solution shown in Figure 4 (without module 2) is more favourable.

When compared by the number of parameters, both configurations have 4 variable parameters each (alternative in Figure 3 – regulation of two flow regulators in Graetz bridge rectifier and two distributor valves for bleed-off synchronization and alternative in Figure 4 – regulation of two flow regulators for each of the two distributor valves in Graetz bridge rectifier – module 1). If the intensity of the control signal for synchronization exceeds 50 % of its maximum value, then another module (module 2) can be added to the configuration shown in Figure 4 for additional regulation of oil flow by means of a 4/3 distributor valve and a pair of flow regulators.

Since both configurations have synchronization based on on-off distributor valves, they have approximately similar time responses.
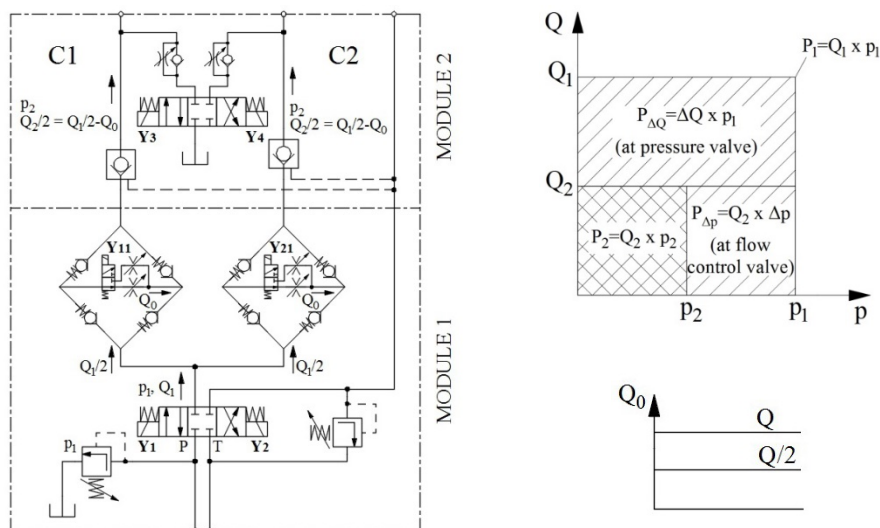
Figure 4: Hydraulic functional schematic of a configuration with direct throttling and its energy efficiency diagram.

Altenative shown in Figure 4 always decelerates the faster cylinder which affects the total time of radial gate manipulation. It is usually not important, but at flow-through hydroelectric power plants, where the radial gate should compensate the failure of the turbine in a short period of time (couple of minutes) it could be quite significant. In such cases the advantage is with the alternative shown in Figure 3 with bleed off valves.

Anyway, the final selection among the alternatives shown in Figure 3 and Figure 4, depends on the configuration of mechanical guiding and the possibility to compensate the error in verticality when building the concrete walls. Alternative shown in Figure 4 has greater flexibility because it provides two different oil flow values amplitude-wise (50 % and 100 % of the flow value), and not just regarding the different time intervals when the flow correction control signal is active, as is the case with alternative in Figure 3. If the error trend is constant (one side of the gate is always slower), then the more favourable soulution is given in Figure 4, specifically the upgraded version (module 1 + module 2), because the position difference of two sides of the gate can more easily be regulated by independently adjusting the flow throttles that control the flows through the 4/3 distributor valve.
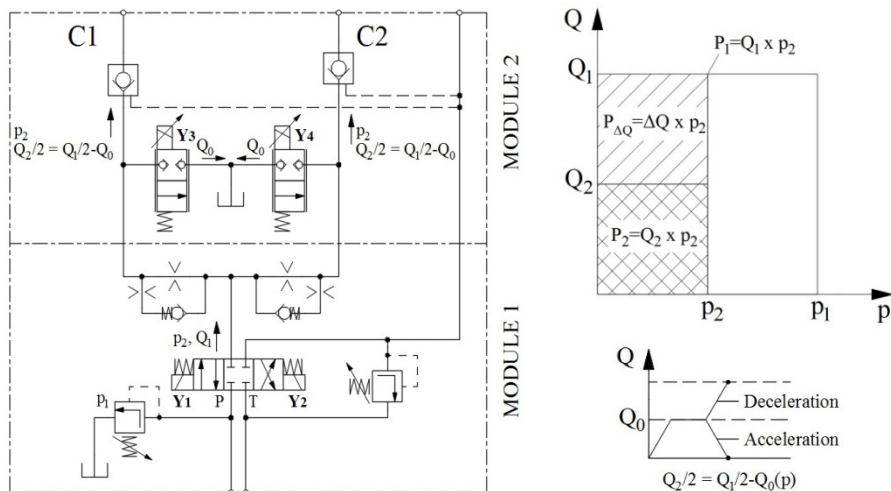
D. Nauparac, N. Višnjić & N. Cero: Comparison of the Quality of Synchronous Motion of Radial Gates
for Different Configurations of Electric-eydraulic Drives

273

Figure 5: Hydraulic functional schematics of a configuration with proportional valves and its energy efficiency diagram.

If the criterion of minimal number of hydraulic components is taken into consideration, than the alternative given in the hydraulic functional schematic in Fig.5 is proposed, because it provides either acceleration or deceleration when gate motion is about to begin or end (stop) with the same proportional control valves used to synchronize the cylinder motion [6], [8].

3 Control component of an electric-hydraulic drive for synchronous motion of radial gates

The quality of synchronous motion which is provided by an electric-hydraulic drive for lifting and lowering of radial gates is estimated using the following criteria:

1. Total error integral of synchronous motion above the defined error threshold.
2. Maximum error of synchronous motion during lifting and lowering manipulations.
3. Maximum control intensity for error correction of synchronous motion.

The criterion of total error integral above the defined threshold is based on comparison of the actual total error integral of the actual control configuration with the maximum error that would theoretically occur if there was no control at all and no constraints on the gate to stop its tilting. According to this criterion, the control configuration is better if its total error integral relative to the maximum total error integral is smaller.
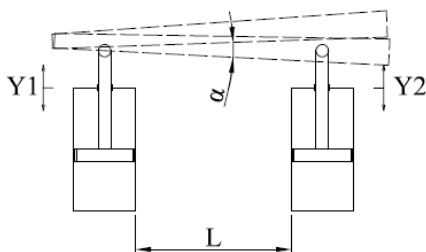

Figure 6: Error integral and tilting angle.

$$\Delta s = v_1 t - v_2 t \text{ - total error integral,} \tag{1}$$

$$t = \frac{S}{v} \text{ - total gate motion time,} \tag{2}$$

$$tg\alpha = \frac{\Delta s}{L} = \frac{\Delta v \cdot t}{L} = \frac{\Delta v \cdot S}{L \cdot v} = \frac{\Delta v}{v}\frac{S}{L} \text{ - gate tilting angle,} \tag{3}$$

wherein:

S - maximum cylinder stroke (m),

L - gate width (m).

For known geometric characteristics of the gate and known relative velocity difference, it is possible to calculate the tangent of angle α and the maximum error integral (Figure 6) – equation (4):

$$\Delta s = L tg\alpha \text{ . [2]} \tag{4}$$

The criterion of maximum control intensity for error correction of synchronous motion enables us to complete the control structure of an electric-hydraulic drive for radial gate manipulation. If the control intensity does not exceed 50 % of its maximum value during radial gate lifting and lowering, it means that the selected drive is robust enough to withstand external disturbances, with minimum risk to fail to correct the error and

D. *Nauparac, N. Višnjić & N. Cero: Comparison of the Quality of Synchronous Motion of Radial Gates for Different Configurations of Electric-eydraulic Drives*

275

to cause the gate to stop unexpectedly. If control signal intensity exceeds 50 %, then the issue of structural adaptation opens up, i. e. introduction of another control component to provide synchronous motion. In this way, the quality of the selected design solution is improved.

4   Experimental results

Figures 7, 9 and 10 show experimental results of load distribution during radial gates lifting and lowering for different electric-hydraulic configurations. Figure 8 shows the experimental result of error of synchronization.
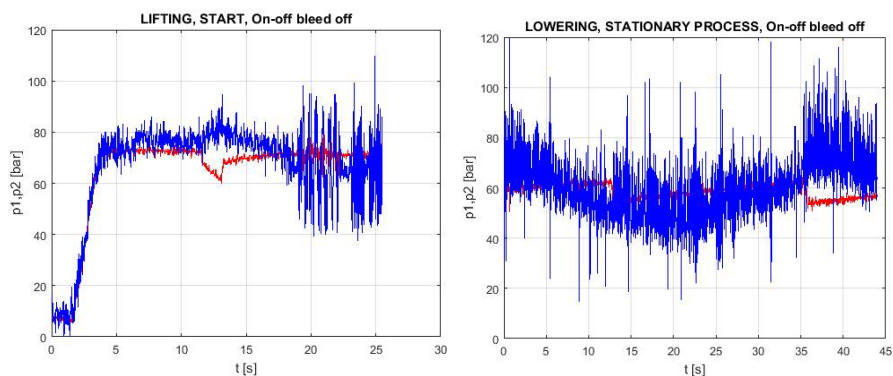
Figure 7: Gate lifting and lowering, small HPP „Crveni breg", Serbia.

Figure 7 shows the start of the transient regime of lifting and the stationary process of lowering of a radial gate at the small HPP Crveni breg", the Nišava river, Serbia. The configuration of the hydraulic drive is equivavelent to the configuration with distributor valves with bleed off shown in Figure 3. The stiffness of the gate steel construction is unsufficient to absorb the changing load and for that reason one of the cylinders is subjected to low pressure oscillations (from 2 to 4 bar), while the peaks in pressure oscillations in the other are 10 times higher [7].
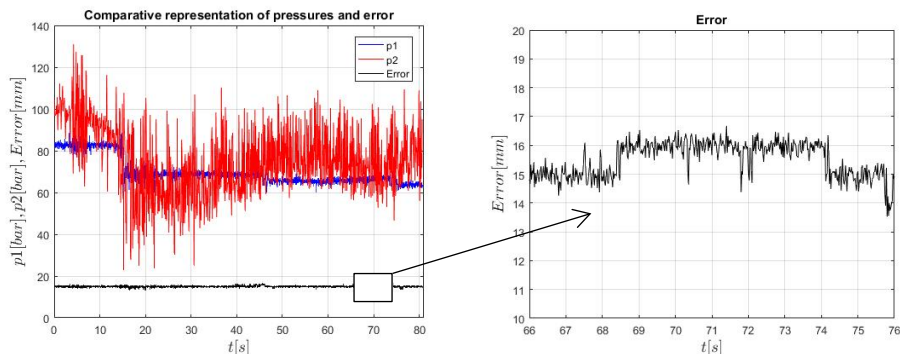
Figure 8: Load distribution and synchronization error, small HPP „Crveni breg", Serbia.

Figure8 shows error of synchronization during stationary process of lowering of the radial gate at the small HPP Crveni breg". The error threshold is 15 mm and the hydraulic drive with the control unit allows the error to rise no more than 2 mm above the threshold before it reduces the error to its design values [7].
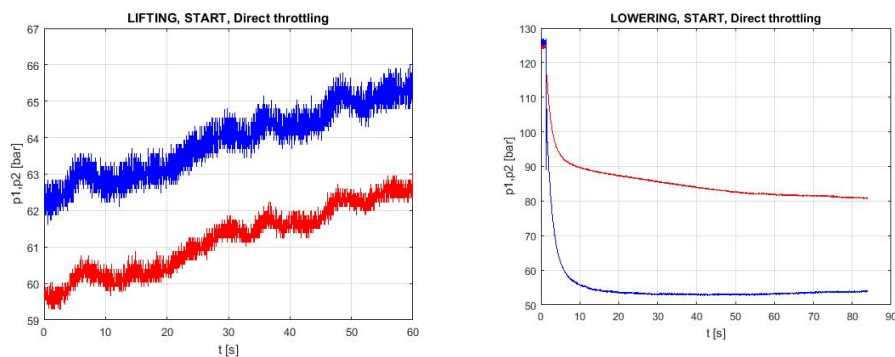

Figure 9: Gate lifting and lowering, sluice „Opovo", Serbia.

Figure 8 shows the start of the motion of the radial gate at the sluice „Opovo", the Tamiš river, Serbia. Both lifting and lowering transient regimes at the beginning of gate motion are depicted. The configuration of the hydraulic drive is equivavelent to the configuration with direct throttling shown in Figure 4. The lowering diagram shows that, because of the high stiffness of the steel construction of the gate, the accuracy of synchronization is high, the error is maintained below the threshold, but the distribution of load is uneven so that the difference in pressure values in hydrauli cylinders is up to 30 % [4].

D. *Nauparac, N. Višnjić & N. Cero: Comparison of the Quality of Synchronous Motion of Radial Gates for Different Configurations of Electric-eydraulic Drives*

277
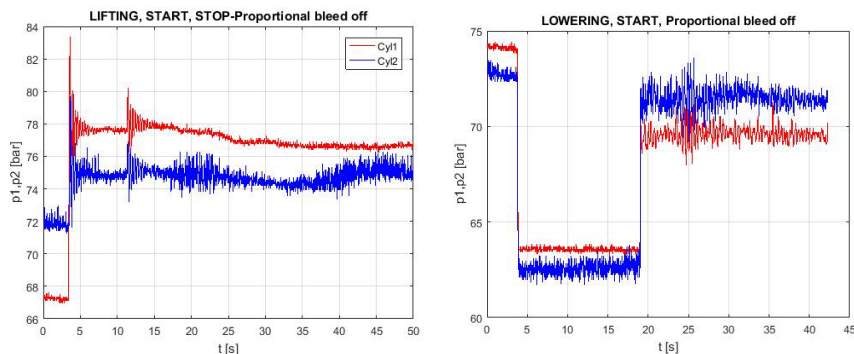
**Figure 10: Gate lifting and lowering, complex of hydro-objects „Gorodets",
Russian Federation.**

Figure 10 left shows the start of the motion of the gate at the complex of hydro-objects (navigation locks) „Gorodets", the Volga river, Russian Federation. Both lifting and lowering transient regimes at the beginning of gate motion are depicted. The configuration of the hydraulic drive is equivavelent to the configuration with proportional distributor valves with bleed off shown in Figure 5. The lifting diagram shows pressure peaks which correspond to the moment when hydraulic drive overcomes the static friction of the gate and its guiding mechanism. The lowering diagram shows pressure drop at the start of motion. Both diagrams show a satisfactory distribution of load of the steel construction and sufficient level of stiffness [3].

During final commissioning works of a radial gate with its electric-hydraulic drive, it is necessary to determine the real stiffness of the gate since the value of synchronous motion error depends on it and on the motion resistance force. The gate stiffness is determined by calculation or most precisely by experiment using (5), in the direction of piston rod motion, with unitary pressure change:

$$K_z = \frac{\Delta p}{z} \quad \left[\text{Pa/mm}\right] \tag{5}$$

And the permissible gate tilt [1] as:

$$\Delta s = \frac{F_{max}^{lift} - F_{max}^{hold}}{A \dfrac{\Delta p}{z}} \quad \left[\text{mm}\right] \tag{6}$$

The above explained calculation of stiffness should be a part of the off-line identification parameter procedure.

5   Conclusion

Taking into consideration the specific disturbance effects which are not easily forseen and determined in the course of design process for electric-hydraulic drives for radial gates, the above mentioned design principles give the solution of the problem in the first iteration of commissioning, error trend identification and the possibility to add another control module. Based on experimental results of the load distribution (by pressure measurements) with or without tracking the changes of the synchronous motion velocity, it is possible to compare similar configurations of electric-hydraulic drives for radial gates with different stiffness. The influence of steel construction stiffness is most obvious during radial gate lowering when the error of synchronous motion is within permissible limits, but a very unfavourable load distribution occurs caused by drastic difference between pressure values in piston rod chambers of left-hand and right-hand side cylinder. That is the situation when one of the cylinders carries almost the entire weight of the radial gate.

Beside the hydraulic configuration of the drive, special attention should be payed to the control algorithm structure that is applicable for the actual hydraulic configuration. Final estimation of the design solution is obtained with software comparison of the maximum theoretical error integral and the actual one.

References

[1]   Vujić, D. (1980). *Problematika sinhronizacije rada hidrauličkih pogona zatvarača na hidrotehničkim postrojenjima sa posebnim osvrtom na vibracionu stabilnost,* magistarski rad, Mašinski fakultet u Kragujevcu

[2]   Casey, B., Tumarkin, M. (2006). *How To Synchronize Hydraulic Cylinders*, Hydraulic Supermarket

[3]   *Гидропривод для маневрированя рабочими воротами верхних голов шлюзов №13-16 Городецкого РГСиС*, проект ООО «Техтрансстрой», г. Самара, 2011

[4]   *Projekat elektrohidrauličke instalacije za pogon segmentnih zatvarača, Ustava Opovo*, projekat PPT-Inženjering, Beograd, SRB, 2012

[5]   Rae, S. (2014). *Drive & Control Systems for Gates in Civil Engineering Application*, Bosch-Rexroth

D. Nauparac, N. Višnjić & N. Cero: Comparison of the Quality of Synchronous Motion of Radial Gates for Different Configurations of Electric-eydraulic Drives

279

[6]   Vasiliu, N., Vasiliu, D., Calinoiu, C., Dragoi, C. (2018). *Energy Saving System For Heavy Duty Electrohydraulic Servomechanisms – Theory and Experiment*, U.P.B. Sci. Bull, Series C, Vol.80, Iss. 3

[7]   *Projekat elektrohidrauličke instalacije za pogon segmentnih zatvarača*, MHE "Crveni breg", projekat PPT-Inženjering, Beograd, 2019

[8]   Авторский коллектив, *Гидромеханические системы стационарных и мобильных технологических машин*, Бакалавриат, г. Москва, 2019

University of Maribor Press

Mechatronic Systems with Pneumatic Drive

ŽELJKO ŠITUM, JURAJ BENIĆ, ŠIME GRBIĆ, FILIP VLAHOVIĆ, DINO JELENIĆ & TOMISLAV KOSOR

Abstract This paper presents four mechatronic systems with pneumatic drive which have been designed as test models in the field of pneumatic power systems and in automatic control educational process for the mechanical engineering students. The paper first presents a prototype of an autonomous vehicle which uses compressed air and pneumatic muscle actuators for its drive. Then the paper presents the design and construction of a pneumatic manipulator with two-degrees-of-freedom actuated by pneumatic cylinders that performs the task of transferring work items. The article then describes the design, construction and angular position control of the rudder blade on a wooden boat model. The experimental setup shows the way the ship's steering system works, but with the use of a pneumatic drive instead of hydraulic drives that are used in realistic watercraft. The final section of the article describes the design and construction of a rotary device driven by two pneumatic cylinders.

Keywords: • mechatronics • pneumatics • robotics • autonomous vehicle • automatic control •

CORRESPONDENCE ADDRESS: Željko Šitum, University of Zagreb, Faculty of Mechanical Engineering and Naval Architecture, Zagreb, Croatia, e-mail: zeljko.situm@fsb.hr. Juraj Benić, University of Zagreb, Faculty of Mechanical Engineering and Naval Architecture, Zagreb, Croatia, e-mail: jbenic@fsb.hr. Šime Grbić, University of Zagreb, Faculty of Mechanical Engineering and Naval Architecture, Zagreb, Croatia, e-mail: sg204046@stud.fsb.hr. Filip Vlahović, University of Zagreb, Faculty of Mechanical Engineering and Naval Architecture, Zagreb, Croatia, e-mail: fv197955@stud.fsb.hr. Dino Jelenić, University of Zagreb, Faculty of Mechanical Engineering and Naval Architecture, Zagreb, Croatia, e-mail: dj205085@stud.fsb.hr. Tomislav Kosor, University of Zagreb, Faculty of Mechanical Engineering and Naval Architecture, Zagreb, Croatia, e-mail: tk189327@stud.fsb.hr.

1   Introduction

Modern technical systems are most often highly complex and interdisciplinary in nature involving synergistic integration of many branches of engineering. Designing advanced technical systems requires combined action and cooperation which then results in increased effectiveness and productivity. Mechatronic engineering is *an exciting new* multidisciplinary branch of the engineering field which combines mechanical, electrical and computer engineering, but also includes a combination of robotics, electronics, sensorics, telecommunications, systems and control engineering [1].

In mechatronic engineering applications, actuators play an important role for generating movement in a mechanism or system. Generally speaking, mechatronic systems may have three main types of actuators: electric, hydraulic, or pneumatic drives. Electrical motors are by far the most widely used actuators within mechatronic systems, because they are reliable and accurate and they are relatively easy to control, so they dominate in all segments of application. In mobile systems DC motors are preferred due to the technology of today's batteries, while AC motors are preferred in stationary applications since it is very easy to use electric power from the electric grid. Owing to the fact that hydraulic drives provide high force multiplication they are used to manipulate heavy loads.

This paper presents several self-made experimental systems actuated by pneumatic drives, which have been designed and manufactured as test models within the fields of electro-pneumatic systems, mechatronics, autonomous systems and feedback control education. Pneumatic drives are used in applications that require relatively high power-to-weight ratio, high speed action capabilities and clean operation, combined with lower price of overall system. In many applications, they can be a cheaper alternative to electric and hydraulic systems, especially for light loads [2]. Unfortunately, position and force control of pneumatic actuators are difficult due to nonlinear effects in pneumatic systems caused by the phenomena associated with air compressibility, friction effects, variations of load and process parameters in time etc. Thus, increased attention is being paid to development of pneumatic equipment, as well as to improvement of control strategies. Realization of controlled pneumatic drives today is a symbiosis of mechanical systems with other technologies such as microelectronics, sensorics, and sophisticated controls to achieve high qualities in modern industrial applications [3].

The introduction of the electronic control signal has made possible to apply modern control techniques to pneumatic powered drives. This way the range of potential applications of pneumatic systems is extended to the field of flexible manipulation tasks and robotics [4]. One of the research directions in pneumatics relates to the area of pneumatic artificial muscle actuators (PAMs) using biological principles for system design and control as an attempt to replicate natural human movement. Pneumatic muscles are suitable for use in bionic systems, i.e. biologically inspired designs of technical systems, where the applications of biological methods and processes found in nature are used to improve engineering systems and modern technological products [5]. Scientific and technical works have shown that overall system performance can improve when some biological principles are incorporated within the designing of engineering solutions. Some new applications are also identified, particularly in the areas of bio-robotics, human-friendly orthopaedic aid devices for the rehabilitations of polio patients as well as within industrial applications for the actuation of new devices and manipulators ([6] to [9]). Their properties such as compactness, high strength, high power-to-weight ratio, inherent safety and simplicity are worthy features in advanced manipulating systems.

2   Autonomous vehicle driven by pneumatic muscles

Autonomous robot vehicles with alternative drives, advanced motion control capabilities, driverless technology and moving in an unstructured environment with obstacles are one of the most demanding tasks of modern engineering. From the environmental point of view, autonomous vehicles can have an advantage in terms of reducing greenhouse gas emissions and increasing energy efficiency, so autonomous vehicles usually have a hybrid or full electric drive. Pneumatic artificial muscles as soft, lightweight and compliant actuators could have a great potential as a drive for new types of mobile systems and they allow some new features of the controlled system.

The prototype of an autonomous vehicle powered by pneumatic artificial muscles is shown in Figure 1. The autonomous vehicle has a crankshaft mechanism that converts linear motion of the pneumatic muscles (they can exert a pulling force) into rotational motion of the driving wheels on the vehicle. The crankshaft is used to drive the vehicle and takes over the total pulling force of the pneumatic muscles. Three pneumatic muscles are used and each segment of the crankshaft is rotated in relation to the previous segment by 120° to get a full circle after activating all three muscles. The crankshaft mechanism is mounted in four bearings, because there is an unbalanced

bending load on certain shaft rotation segments. The crankshaft is made of stainless steel using the turning and milling process [10].
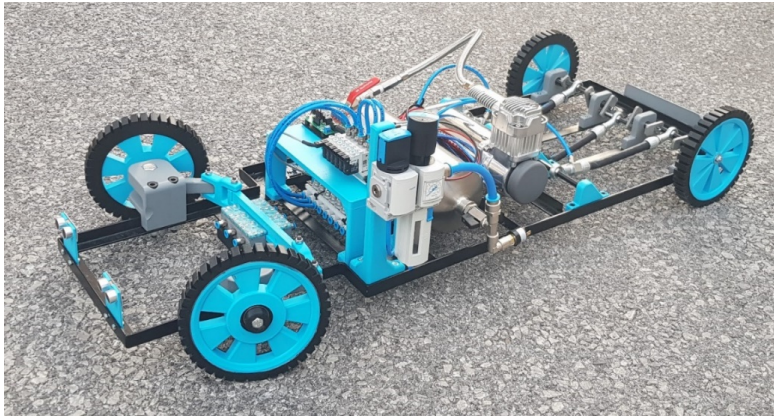

Figure 1: Autonomous vehicle driven by pneumatic muscles.

In the chassis construction process the main criterion was to design a strong chassis on which all components can be connected using screws. Another criterion was the simplicity of the construction. The L-profile 20x20x2 mm was chosen as the main structural element. The parts under the influence of the dynamic stress are further strengthened. The chassis dimensions are 1100x360 mm and the whole chassis was made in welding technology. For the realization of this autonomous system it was necessary to design vehicle mechanics, especially the drive shaft and the system for steering the vehicle. The steering mechanism of the vehicle is achieved by using a pneumatic linear stepper motor controlled by a microcontroller. For the vehicle steering, rack and pinion geometry is chosen which allows the difference in rotating the inner and outer wheel. The features of the pneumatic linear stepper motor can be found in [11].
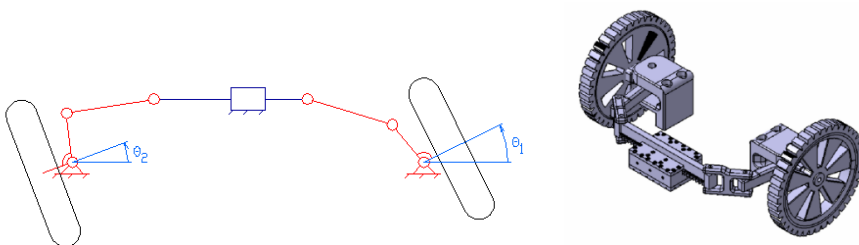
Figure 2: Vehicle steering mechanism.

The actuator has a lightweight, completely metal-free and fully customizable design. The pneumatic linear stepper motor consists of a toothed rack and 3 pistons with teeth. Since the cylinders have a phase shift, the individual cylinder activation causes the toothed rack to move. Each cylinder in one activation moves the toothed rack by 1/3 steps. The size of the steps depends on geometry and dimensions of the teeth. The operation of this actuator is quite simple and relatively accurate positioning can be obtained.
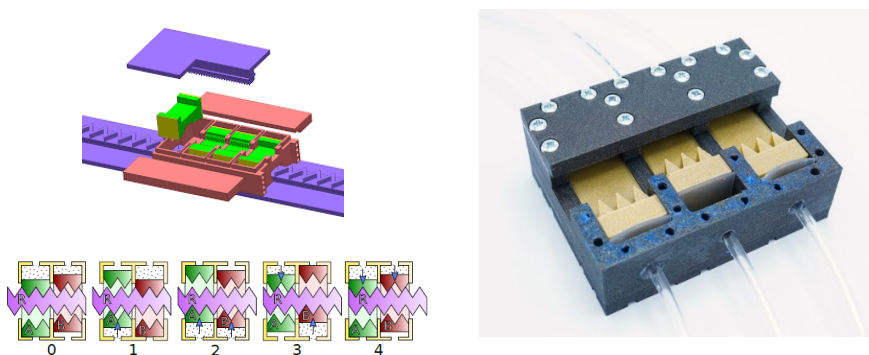
Figure 3: Pneumatic stepper motor [11].

There are two power sources on the vehicle. The first source is used to start the compressor and allows 12 V and up to 300 A maximum current. The other source provides power for the valve block and uses a Turnigy 6S rechargeable battery with a capacity of 3000 mAh, rated voltage 22.2 V. The control system is implemented using the Arduino microcontroller. The vehicle control and rules for autonomous driving are programmed in the Arduino CAE code using several program libraries. The Arduino microcontroller monitors the obstacles using ultrasonic sensors and controls the air flow into the drive system via MOSFET transistors. This module has LED diodes that serve as a power indicator for the control system. An air compressor produces compressed air that is stored in a tank. The air then passes into the pneumatic muscles using electromagnetic valves controlled by the microcontroller. The compressor, as the largest consumer, uses the power suplly that is controlled by using the pressure switch, regardless of the control system. The pressure switch starts the compressor when the pressure in the tank drops below 5 bar. This vehicle has many advantages such as increased safety and lower adverse environmental impact because the vehicle's drive is achieved by using compressed air.

Further work on system upgrade will be focused on enabling the vehicle to overcome obstacles and drive without human control. The vehicle will have the ability for desired trajectory tracking and when detecting an obstacle by using sensors, the control program will start the algorithm for stopping or avoiding the obstacle.

Table 1: Vehicle specifications

Vehicle specifications	Components
Actuators	Festo DMSP-10-150N pneumatic muscles
Vehicle steering	Linear pneumatic stepper motor T-84
Valve block	Festo VTUG-10-SH2-S1T-Q6
Air preparation units	Festo MSB4-1/4:C3:J1-WP
Air reservoir	Festo CRZVS-2
Compressor	AirLift 400C Viair Dual Chrome Compressors
Power supply	12V 8000mAh Li-Po battery
Control unit	Arduino MEGA 2560
Valves control	N-channel MOSFET transistor RFP30N06LE

3   Electro-pneumatic manipulator

The majority of modern industrial robots and manipulators are successfully applied for repetitive and relatively simple manufacturing tasks that require organized work space and little interaction between robot and its environment. Robotic manipulators with pneumatic drive are used mostly for pick and place operations such as loading machines, placing components on assembly lines, taking parts from conveyor belts, lifting or carrying payload to a predetermined position, etc. [12]. Such drive units are fast, accurate and very cost effective. Therefore, pneumatic drives are traditionally used in manipulation tasks to quickly move loads between two positions using simple on-off valves.

A prototype of an electro-pneumatic manipulator, with two-degrees-of-freedom is shown in Figure 4. The manipulator simulates continuous delivery and transfer of workpieces in some production process. Automation of the process is achieved by adding an inductive sensor to the manipulator working space.
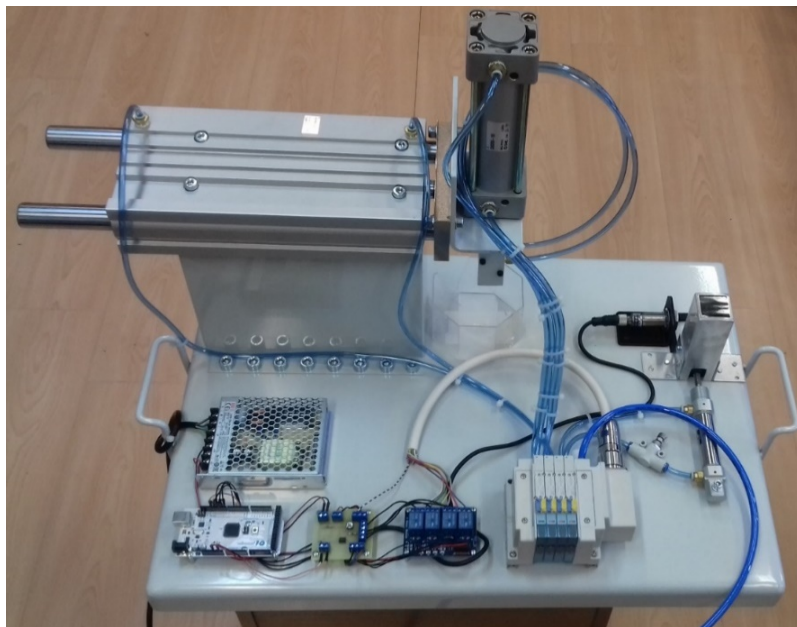
Figure 4: Robotic manipulator actuated by pneumatic cylindrical drives.

The inductive sensor is used to detect the presence of metal object and to send signals to a microcontroller, which controls the pneumatic manipulator. In order to reduce the cost of construction, the parts are mainly made of metal sheet and then laminated, but also some parts are made using 3D printer. The manipulator was designed and manufactured in the Laboratory for automation and robotics to enable students to gain practical knowledge in the field of mechatronics, electro-pneumatics, robotics, industrial engineering, automated manufacturing systems, etc. Pneumatic cylinders are used as the main actuating system for the manipulator arm and they are controlled by a solenoid valve manifold (SMC, type SS5Y3–10–2259OHV). The valve block has one input and four outputs which provides air flow to the actuators, which can be independently controlled by a 24 V voltage signal that activates the particular solenoid One compact guide cylinder (SMC, type MGPM50 – 250) and one standard double acting cylinder (SMC, type C95SB50 – 100) are used to achieve the translational movement of the manipulator. A pneumatic gripper was realized by using a small pneumatic cylinder (SMC, type CDQSKB16–10DM). The gripper was attached at the end of mechanical structure of the manipulator arm which is used as the end effector to grasp objects. Permanent work items delivery to the manipulator was achieved using a pneumatic cylinder (SMC, type C85N20-40-XB6 ISO) with a cylinder stroke of 40 mm.

This manipulator acts as a pick and place robot, capable of picking objects from one location and drop them at another location. For detecting the presence of a workpiece and sending the signal to the control unit, an inductive sensor (Winston, type LM18-3005PN) was used. An Arduino Mega2560 micro-controller was used as a control unit. The microcontroller contains all the necessary parts to be able to operate independently of additional external control units. Because of the high reliability, low cost and small dimensions they are often used in low-cost control applications. The microcontroller is programmed using the Arduino software tool based on the C++ programming language. The air flow is provided through an air supply unit and directional control valves, which are controlled by a relay module, supplying each cylinder connected to the valve block with compressed air.

4   Rudder blade control on a wooden boat model

Angular position control of a wooden boat rudder blade was a project with the aim of enabling students to explain the way in which the ship's control is carried out. The project consists of designing, manufacturing and controlling the experimental model where a pneumatic drive is used instead of a hydraulic drive that is commonly used in real systems due to much larger forces in real ships. The model consists of a wooden back, a pneumatic cylinder, two electro-pneumatic valves, a relay module, a microcontroller, two angular encoders, a voltage stabilizer and a voltage inverter. The wooden part of the boat stern was made of a 15 mm thick panel that was used to make boat ribs, Figure 5. The pneumatic cylinder (SMC, type C95SDB160-100) with a cylinder stroke of 100 mm was chosen for the movement of the rudder blade mechanism. Through two electro-pneumatic on/off valves (Festo, type VUVS-LK20-M32C) air is supplied to the cylinder chamber. The valves are controlled by a digital voltage signal of 24 V. An Arduino Uno microcontroller was used as a control unit. Since such a module can give its digital outputs a 5 V amplitude signal, and to activate the valve it is necessary to have a 24 V signal, a relay module converter for Arduino microcontroller has been added. The voltage converter (MDR-60-24) was selected for supplying the valve, and the Arduino module was powered by a 12V voltage stabilizer. Two rotary encoders with 600 digital pulses per shaft revolution were used to measure the angle of the steering wheel and the angle of the rudder blade.

Figure 5: Construction process of the boat stern.

The user rotates the steering wheel and sets the desired angle of the boat's rudder. This angle is read by a rotary sensor and the measured signal is sent to the processor. At the same time, the second rotary sensor reads the achieved rudder blade angle and sends the measured signal of the current position in the processor. The processor calculates the angle error and decides which output pin will be set to 5 V and thus activate the relay module. When the relay module is activated, a 24 V voltage signal is sent to the connected electro-pneumatic valve. The valve opens and releases compressed air into the appropriate cylinder chamber. Consequently, the cylinder rotates the rudder blade through the lever mechanism.

On that way, the rotating rudder blade mechanism automatically tracks the desired angular position that the user achieves on the boat steering wheel. Special attention was given to the precise control of the rotating mechanism achieved by using the PID controller. The controller acts on a control error calculated from the measured signal of the current position of the rudder blade and decides which electro-pneumatic valve should be opened to achieve the cylinder motion in the right direction. This system is very suitable for demonstration of the principle of real ships control.

Figure 6: Boat rudder blade control.

5 Rotary device driven by pneumatic cylinders

Pneumatic cylinders are mechanical devices that use the power of compressed air to produce a force and because they do not contaminate the environment is the preferred type of actuator where a clean process is required. Compressed air machines can have many potential advantages over other types of drives due to their simplicity in design, durability and compact size of pneumatic systems, low cost, easy maintenance, readily available, cheap energy source, etc. This project-oriented work shows details of the design, fabrication and testing of a pneumatically powered slider-crank mechanism for the purpose of classroom demonstration and experimentation. The model consists of two pneumatic cylinders, two bistable pneumatic valves, four mechanically activated valves and a crankshaft mechanism mounted in four bearings, Figure 7.

Two pneumatic cylinders (Festo, type DSNU-16-40-P) with a cylinder stroke of 40mm were used to drive the crankshaft mechanism. Two bistable 5/2 valves (Festo, type VUWS-L20-B52-G18) release compressed air to the cylinders. Bistable valves are pneumatically activated by four mono-stable roller lever valve (Festo, type R/O-3-PK-3) which are mechanically activated and they are switched to the open position using cam mechanism on the rotating shaft.

Figure 8. shows a rotary device that is designed for educational purposes to demonstrate the functioning of different valve types and to demonstrate the working principle of a slider-crank mechanism that converts straight-line motion into rotary motion. The teaching model was successfully manufactured and operated as originally planned and the continuation of the work will be aimed at achieving the crankshaft speed control.

Figure 7: Manufacturing process of slider-crank mechanism.
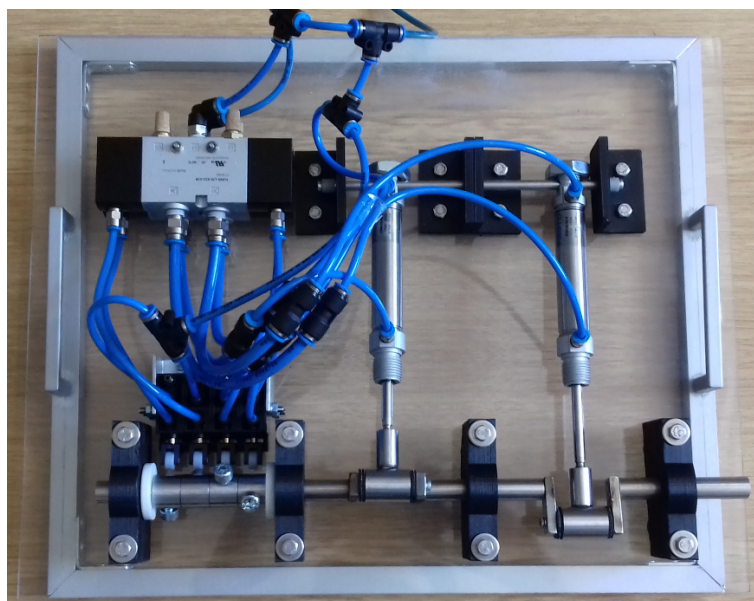
Figure 8: Rotary device driven by pneumatic cylinders.

6   Conclusion

This paper has presented several experimental systems powered by pneumatic actuators. These systems have been designed in the Laboratory for automation and robotics at the Faculty of Mechanical Engineering and Naval Architecture, University of Zagreb as test models within the field of mechatronic systems, pneumatic drives and automatic control education of mechanical engineering students. The complete educational experience involving theoretical and practical applications of different control techniques is recognized by educators in universities and control laboratories around the world.

The article was first introduced the design and practical realization of a prototype of an autonomous vehicle which uses compressed air and pneumatic muscle actuators for its drive. This project is largely based on experiences from past activities in our Laboratory, which has resulted in several successfully implemented experimental systems in the field of mechatronic systems actuated by pneumatic actuators [13], [14]. Then the paper has described the design and construction of a robotic manipulator with two degrees of freedom actuated by pneumatic cylinders that allows the actions of transferring the work items. Then the article has presented the design, construction and angular position control of the rudder blade on a wooden boat model. Finally, the article describes the design and construction of a slider-crank mechanism actuated by pneumatic cylinders.

By using these pneumatic-based experimental models that have an intuitive and attractive operating principle, students have the opportunity to learn about mechanical systems construction and control of practical systems built from real industrial components.

References

[1]   Bishop, *R. H. (2007).* Mechatronic Systems, Sensors, and Actuators: Fundamentals and Modeling. *Taylor & Francis Inc.*
[2]   Sandoval, D., Latino, F. (1997). Servopneumatic Systems Stress Simplicity Economy for Motion Solutions. *Control Engineering Online*, Magazine Articles.
[3]   Murrenhoff, H. (1997). Fluid Power Tomorrow – Part 1, *Ventil 3*, *3-4*, pp. 117-122.

[4] Bobrow, J. E., McDonell, B. W. (1998). Modeling, Identification and Control of a Pneumatically Actuated, Force Controllable Robot. *IEEE Transactions on Robotics and Automation*, *14*, *5*, pp. 732-742

[5] Caldwell, D.G., Tsagarakis, N., Medrano-Cerda, G.A. (2000). Bio-mimetic actuators: polymeric pseudo muscular actuators and pneumatic muscle actuators for biological emulation. *Mechatronics*, *10*, pp. 499-530

[6] Andrikopoulos, G., Nikolakopoulos, G., Manesis, S. (2011). A Survey on applications of Pneumatic Artificial Muscles. *19th Mediterranean Conference on Control & Automation (MED)*, Corfu, pp. 1439-1446. doi: 10.1109/MED.2011.5982983

[7] Daerden, F., Lefeber, D. (2002). Pneumatic artificial muscles: actuators for robotics and automation. *European Journal of Mechanical and Environmental Engineering*, *47*, pp. 10-21.

[8] Rus, D., Tolley, M. T. (2015). Design, fabrication and control of soft robots. *Nature*, *521*, *7553*, pp. 467-475

[9] Martens, M., Boblan, I. (2017). Modeling the static force of a Festo pneumatic muscle actuator: A new approach and a comparison to existing models. *Actuators*, *6*, *33*. doi:10.3390/act6040033

[10] Grbić, Š. (2019). Design and control of a compressed air powered vehicle, B.Sc. Thesis, Faculty of Mechanical Engineering and Naval Architecture, University of Zagreb

[11] Groenhuis, V., Stramigioli, S. (2018). Rapid Prototyping High-Performance MR Safe Pneumatic Stepper Motors. *IEEE/ASME Transactions on Mechatronics, 23, 4, pp. 1843-1853.* https://doi.org/10.1109/TMECH.2018.2840682

[12] Hesse, S. (2000). Modular Pick-and Place Devices. In: *Blue Digest on Automation* (Festo AG & Co.) Handling Pneumatics, Esslingen, Germany

[13] Šitum, Ž., Trslić, P., Trivić, D., Štahan, V., Brezak, H., Sremić, D. (2015). Pneumatic muscle actuators within robotic and mechatronic systems. *Proceedings of International Fluid Power Conference 2015*, Maribor, Slovenija, pp. 175-188.

[14] Šitum, Ž. (2017). Fluid power drives in robotic systems. Invited Lecture. *International Conference Fluid Power 2017*, Maribor, Slovenija, pp. 11-23.

University of Maribor Press

Comparison of Mobile Machine Oil Diagnostics Results by Standard and OTC - Kittiwake Correlation Method

MITAR JOCANOVIĆ, VELIBOR KARANOVIĆ, MARKO OROŠNJAK, NEBOJŠA NIKOLIĆ & DRAGAN SELINIĆ

Abstract To attain quick results on the state of oil filling, and to downsize the research cost, several different construction devices for "quick" inspection of the oil characteristics, from the so-called first level of examination, have been developed. Within the framework of this work, the results of reliability testing of the OTC - KITTIWAKE device have been presented, by conducting parallel testing of the same samples and with the standardized methods. During numerous testing processes, a satisfactory degree of the reliability of the OTC device has been achieved.

Keywords: • maintenance • oil test • diagnostic of the lubricating oil • lubrication• correlation method •

CORRESPONDENCE ADDRESS: Mitar Jocanović, University of Novi Sad, Faculty of Technical Sciences, Novi Sad, Serbia, e-mail: mitarj@uns.ac.rs. Velibor Karanović, University of Novi Sad, Faculty of Technical Sciences, Novi Sad, Serbia, e-mail: velja_82@uns.ac.rs. Marko Orošnjak, University of Novi Sad, Faculty of Technical Sciences, Novi Sad, Serbia, e-mail: orosnjak@uns.ac.rs. Nebojša Nikolić, University of Novi Sad, Faculty of Technical Sciences, Novi Sad, Serbia, e-mail: nebnik@uns.ac.rs. Dragan Selinić, Olma lubricants d.o.o, Novi Beograd, Serbia, e-mail: dselinic@olma.si.

1   Introduction

Diagnostic of the states of industrial and motor oils are becoming a more and more important segment of the maintenance process for the newly constructed machines and motors. It is true that the oil analysis is, at first glance, an expensive process, and that therefore only the users of expensive and highly productive machines, decide on the systematic approach, as do the organized systems with a high degree of insight on the effects of lubrication process regarding the proper work of machines and/or motors with internal combustion. The state of oil process diagnostic can be approached on several criteria, but always with the same starting assumption, that for a machine or a motor with internal combustion, oil with appropriate exploitation characteristics has been chosen.

The end purpose is the same:

a)   to lubricate a machine or a motor with oil of required and unchangeable characteristics for as long as possible,
b)   use oil in the course of its whole potential capacity,
c)   realize oil change in a time that is correlated with the useful exploitation cycle,
d)   always keep the costs of oil examination economically affordable and technically justifiable.

Industrial (hydraulic, circular, reductive, turbine and other) and motor oils represent different chemical systems. Machines and motors are two different worlds; during the exploitation, they are loaded in entirely different ways. Mechanism of the characteristic changes is also different, and so the approach to the diagnostic of the industrial and motor oils is different.

Out of the mentioned groups of industrial oils, the next stand out:

–   transformer oils, which are used mainly because of their dielectric characteristics, and
–   emulsions for cooling and lubricating within the process of metal refinement with rubbing of the metallic chips, which are exposed to the process of the biological degradation because of the flourishing of the microbiological systems (aerobic and anaerobic bacteria, fungus), moreover, due to their particularities, they are not the object of this analysis.

M. Jocanović, v. Karanović, M. Orošnjak, N. Nikloić & D. Selinić: Comparison of Mobile Machine Oil Diagnostics Results by Standard and OTC - Kittiwake Correlation Method

297

2   Degradation mechanisms of industrial and motor oils

The general conception of oil degradation comprises the processes of chemical and mechanical oil degradation. With industrial and motor oils, these are mostly two different mechanisms.

2.1   Degradation mechanism of industrial oil

The process of chemical degradation of industrial oils is defined in the most significant number of cases with the change of the acidity degree. Oils are by their universal nature acidic. The degree of acidity is defined by an acidic or neutralizing number, which is used to define the amount (mg) of basic calcium-hydroxide (KOH) which must be added to one gram of the oil sample until the complete neutralization of all the present acids in the oil.

The conception of oil acidity comprises the total acidity (TAN – total acid number), which consists of three segments:

- the acidity of the base oil – the natural characteristic which is low due to the conducted process of refinement, and it is between 0,01 and 0,05 mgKOH/g;
- additive acidity – additives which are used to correct the starting characteristics of the essential oil or define new ones, are acidic materials. The degree of acidity depends on the chemistry of the additives, which means that the package of additives of the same configuration, intended for the same type of oil can have a different degree of acidity. Characteristic examples are the packages of additives for hydraulic oils whose degree of acidity for the same type of oil can be between 0,4 to 1,0 mgKOH/g.
- Acids created during the use of oil – they are the products of the chemical degradation, created as a result of the chemical bond of oil molecules with oxygen.

The allowed degree of the oil acidity defines the lifetime of oil usage (from the viewpoint of the chemical degradation process), because parallel with the rising of the oil acidity rises its aggressive reaction with metal surfaces, and its viscosity and density grow too. Parallel with the process of chemical degradation, the ability of the oil to complete the function of lubricating (enduring high pressures and stopping the abrasion) is falling.

Mechanical degradation of industrial oils is the result of contamination with hard particles, water, and air [1] to [3]. Most of the time, the hard particles infiltrate the oil from the outside, but they can result from the abrasion processes of the lubricated elements. The index of hard particles in oil defines the degree of cleanliness of the oil, and it is also defined in relation with the size of the gap inside the tribological construction, the character of the tribological construction and the value of the oil work pressure. Hard particles in oil lead to the process of abrasive wearing of the surfaces which are in contact. The degree of oil cleanliness is defined about the size and number of the hard particles in the sample of oil, according to ISO 4406/17, NAS 1638, SAE AS4059F (latest revised) and some other standards [4]. The first three standards are most frequently used.

Water infiltrates the oil from the environment – for example, condensation in the free space of the reservoir or breach through the sealing system. Water in oil increases the: viscosity, climbing, corrosion, and decreases the lubricating ability of the oil. Unto a certain amount and a certain point in time, it can be said that there is free water in oil, but it later builds stable emulsions with oil in which specific molecules of oil have chemically bound water. Air can exist in oil in an un-solute state (if it is in shape of air bubbles) or solute state (inside the oil molecules). It changes from one state to another during the pressure change and then it comes to the climbing of and to the mechanism of the so-called aeration surface abrasion.

2.2   Degradation mechanism of motor oil

The process of chemical degradation of oil is entirely different from the processes described with industrial oils. Motor oils have qualities of base materials, and they receive that characteristic in a disperses manner – by detergent additives. The degree of required baseness of the motor oil is defined according to the contents of sulphur in the fuel because oil conducts the role of neutralization of sulphuric acid which is created in the process of fuel combustion in the motor. While the degree of the oil baseness decreases parallel with the process of acid neutralization, the interval of motor oil utilization is defined concerning the remaining base potential. The baseness of the motor oil (TBN) is defined as the same as the neutralization number in mg KOH/g.

Contamination of motor oil is most often internal and is a result of washing the surfaces of the combusted products.

M. Jocanović, v. Karanović, M. Orošnjak, N. Nikloić & D. Selinić: Comparison of Mobile Machine Oil Diagnostics Results by Standard and OTC - Kittiwake Correlation Method

299

3 Procedures for examining the industrial and motor oils

Two or three levels of oil examination are defined to economically rationalize the procedures of examining the states of industrial oils (hydraulic, circular, reductive, turbine, and other).

3.1 Procedures for examining the industrial oil

The first level of the examination are the following characteristics: viscosity, neutralization number, water content (not in all oil systems) and the degree of oil contamination (not in all oil systems).

The second level of the examination is all the characteristics from the first level of examination + viscosity index (only with oils with VI over 100), flash point, corrosion, de-emulsion characteristic, anti-foaming characteristic.

In the third level of the examination are all the characteristics from the second level of examination + submission extreme pressures (EP) and abrasion prevention (AW), the content of additives and contaminants (based on origin and material).

The volume of the examined merits and the level of examination (first, second, third) depend on the demand of the installation to be lubricated, type of oil, and the size of oil charge. Examining of oil in the first level is conducted via practices that are defined by methods regulated by various standards (ISO, ASTM, DIN, IP, and others) or by non-standardized practices – simulation of standard methods or completely new practices.

Examination of oil in the second level is conducted via practices that are defined by standard regulated methods, and in the third level examination is conducted via standard and new methods which are not defined by standards [1] to [3].

3.2 Procedures of examining the motor oil

Examination of motor oils is conducted mostly in two levels. In the first level of examination the value of viscosity is measured, out of the total base number TBN, and contents of un-solute materials, and in the second level, and in the second level the

sulphate ash, burner, fuel content (if the focus of burner is decreased), and viscosity index.

Especially noteworthy is the first level examination, which is most often realized, due to its low cost.

3.3   Alternative methods for oil state diagnostic

By the development of the measuring equipment, but also due to the real need to quickly attain the actual representation of the state of oil, and keep the costs of examination as low as possible, several alternative methods for oil state diagnostic have been developed, mostly on the first level of examination. The next methods are listed here: measuring the dielectric characteristics, method of oil stain, and method of examination via the chemical-electrical procedure using the KITTIWAKE device. Devices for the diagnostic of the state of oil based on the change of dielectric characteristics have been developed by a large number of manufacturers, and they add up to value comparison and the character change of the dielectric characteristics of the new oil and the oil currently exploited. These devices have been widely applied in the continuous process of motor oil diagnostics on the heavy load vehicles used for transporting materials to distant localities.

Results shown provide direction for further activities, and they cannot be used in problematic areas. The method of oil stain was developed in the USA and it is defined by the ASTM standard. It is the character assessment based on the spilling of a drop of oil over the filter paper. Based on the appearance of the oil stain, a conclusion is provided regarding the possible process of degradation or contamination of the oil. This method has not found a broader field of application.

A very close degree of approaching to the results of testing with the standard methods has the electronic-chemical procedure on the Oil Test Center (OTC)- KITTIWAKE device, whose results were the object of the author's research.

In the last couple of years, the analysis of oil with the spectrometric method is the one most frequently used. There are a few different procedures, but each one registers the contents: additives, metals (iron, copper, zinc...), elastomer, admixtures from the environment (sand, silicon...) and other. Based on the attained results of testing and the known conception of the additive packages the state of oil, from the outlook of the

M. Jocanović, v. Karanović, M. Orošnjak, N. Nikloić & D. Selinić: Comparison of Mobile Machine Oil Diagnostics Results by Standard and OTC - Kittiwake Correlation Method

301

additive content, can be identified and eventual processes of wearing surfaces in contact. Moreover, if the material of the parts of the tribological construction is known, the component whose surface is exposed to the process of wearing can be exposed. The lack of method is the high price of the device, but disregarding that, this is the method that will be used more and more often in the future and which will significantly contribute to the advancement of the diagnostic procedure of the state of oil.

4   Correlation of the examination results

The authors of this work have been examining the essential characteristics of the oil with the OTC - KITTIWAKE device in the last ten years. The examination has been conducted on 1100 samples of used hydraulic, and motor oils, and based on the attained results, the state of the examined oil charge has been identified.

Identification of the state in the first level:

- of hydraulic oils has been conducted based on the examination of viscosity, total neutralization number (TAN), water content, and degree of oil purity (examination conducted on a different device), and
- of motor oils based on the examination of viscosity, TBN, the total content of un-solute materials and water content.

The OTC – KITTIWAKE is a mobile computerized device (figure 1) whose basic model was developed for the need of dislocated units of NATO pact – ships, tank units, mechanized units and other. Later, the basic configuration has been remodeled for the need of the civil sector.

Figure 1: The appearance of the KITTIWAKE device [5]**.**

Device manufacturer, in his professional publications, cites the good correlation of the devices examination results with the results of standard examination methods, which the authors of this work have confirmed through examination. In the following text is a short review of the examination procedures with the OTC – KITTIWAKE device and a correlation with the results of examination with standard methods, and of the most critical merits in the first level of examination: viscosity, the neutralization number and the total base number (TBN).

4.1   Viscosity

A partial appearance of the autonomous viscosity measuring device is shown in Figure 2.

The procedure of viscosity measuring corresponds to the procedure of measuring using the viscosimeter with a ball (Höppler). The oil is poured into the examination tube, the ball is put in, and then the entire mass is heated to the examination temperature (40 or 50 °C).

M. Jocanović, v. Karanović, M. Orošnjak, N. Nikloić & D. Selinić: Comparison of Mobile Machine Oil Diagnostics Results by Standard and OTC - Kittiwake Correlation Method

303

Figure 2: The appearance of the viscosity measuring device [5]**.**

The temperature is shown on display, which is an integral part of the device. When the oil mass is heated, the device turns and lays to the opposite, a slope side. Inside the tube, the ball falls through the oil, and the sensors measure the fall time. In the integrated computer, the measured time is calculated into viscosity, and its value is shown on display.

Co-ordinate measuring of viscosity with the standardized method and the KITTIWAKE method has been conducted on about the fifth hundred samples. Satisfactory comparative results have been produced with deviations of about 5%, and this is illustrated with the results from motor oil sample examinations taken from the motor of mobile machines in the course of its complete exploitation lifetime of 500 hours (Table 1).

Table 1: Comparative viscosity results of engine oils [6], [7]

Sample's Age	Standard Method	Standard Method	Deviation
Zero hours	114,0 mm²/s	114,0 mm²/s	- 1,4 %
250 hours	116,5 mm²/s	107,9 mm²/s	- 7,14 %
330 hours	121,1 mm²/s	125,4 mm²/s	+ 3,55 %
420 hours	133,1 mm²/s	131,4 mm²/s	- 1,27 %
500 hours	136,2 mm²/s	142,3 mm²/s	+ 4,47 %
		Average	± 3,57 %

4.2   Neutralization number

The base part of the device is the same for the measuring of the neutralization number (TAN), total base number (TBN), water content, and un-solute materials. The different parts are the construction of the measuring cell, chemicals that are added to the sample, and the measuring procedure.

Figure 3: The appearance of the KITTIWAKE device – measuring of neutralization number [5].

Figure 3 shows the appearance of the base part of the device with a built-in computer and a display and a measuring cell as a separate element for measuring the values of the neutralization number.

The procedure of measuring the neutralization number is next: into unique test tube for the TAN examination, 10 ml of a specific red-coloured reagent (A) is poured, and with the other colourless reagent, vibration (neutralization) of the first reagent is performed until a green liquid appears. The test tube is inserted into the TAN examination cell, and the display shows the value which should be under the order of 80.

When the reagent is vibrated long enough, it is then calibrated to the value of zero, and then the test tube is opened, and 1 ml of examination oil is added. Reagent turns red if the oil is acidic, and then, the procedure of vibrating with the reagent B is once again applied in order to neutralize the acidity and restore the liquid to its original colour – green. Before the vibrating, reagent B is picked with a specialized pipette in the amount of 1 ml. After the vibrating, instead, adding specific amounts of reagent and when the liquid turns green again to the level under 80, measurement and calculation of the TAN

M. Jocanović, v. Karanović, M. Orošnjak, N. Nikloić & D. Selinić: Comparison of Mobile Machine Oil Diagnostics Results by Standard and OTC - Kittiwake Correlation Method

305

value of the oil which is being examined, is conducted. The added value of the reagent B is measured on the pipette and typed into the computer, which completes the calculation and shows the results on display.

Co-ordinate measuring of the neutralization with the standard, and the KITTIWAKE method has been conducted on about sixth hundred samples. The results of testing on the KITTIWAKE device are excellent because minimal deviations between ±0,05 and 0,1 accrued – depending on the actual value of the neutralization number, which oscillated between 0,05 to 1,1 mg KOH/g with the examined samples.

4.3   Total base number TBN

It should be mentioned that this examination method is comparative, which means that the value of the new and old oil is compared. For examination purposes, it is necessary to pour 10 ml of a specific reagent into a particular TBN examination cell, and add into it 20 ml of new oil when determining the benchmark value of the new oil, and the same amount of the used oil conducting a research and determination of the TBN value of the used oil. The cell with mixed oil and reagent is shaken about 2 minutes and placed on the TBN value reading spot, where it remains until the figure on display stabilizes – Figure 4.

Figure 4: Measuring the total base number [5]**.**

When the value stabilizes, the referent values can be read. After reading the referent value for the new, once more repeated procedure for the used oil, the figures from the display are inputted into the computer, and it calculates the TBN value of the used oil.

Co-ordinate measuring of the total number with the standard method, and the KITTIWAKE method has been conducted on over fifth hundred samples. In a chart that follows, the results of the parallel examination of samples of the mobile machine motor oil (in the course of its complete exploitation lifetime of 500 hours), are shown.

Table 2: Comparative TBN results of engine oils [6] **to** [9]

Sample's Age	Value of the TBN (mg KOH/g)		Deviation
	Standard Method	Kittiwake Method	
Zero hour	9,71	9,6	- 5,5
250 hours	8,13	8,5	+ 4,5
330 hours	7,65	7,9	+ 5,3
420 hours	6,26	7,0	+ 11,8
500 hours	5,76	5,8	+ 0,7
		Average	±5,56

Attained results with a deviation of ±5,56 can be considered satisfying.

5   Conclusions

1. Examining the oil is becoming a more and more important segment of the common maintenance process of motors with internal combustion.
2. Since the costs of examination with standard methods are high, and the time from taking samples to receiving results long, examination with the devices whose measuring procedures are not standardized is more and more frequent.
3. Devices for fast measuring of oil characteristics are usually electronical, and they function based on change: dielectric characteristics of oil, the character of infrared or laser beam movement.
4. One of the several devices for the fast examination of essential characteristics of oil is a computerized KITTIWAKE device which functions based on measuring the time of movement, dielectric characteristics, or infrared movement.

M. Jocanović, v. Karanović, M. Orošnjak, N. Nikloić & D. Selinić: Comparison of Mobile Machine Oil Diagnostics Results by Standard and OTC - Kittiwake Correlation Method

307

5. With the KITTIWAKE device, essential characteristics are measured on the first level: viscosity, TAN, TBN, water content, and content of un-solute materials.

6. While working with the KITTIWAKE device, the examination of the reliability of attained results has been conducted, by comparing the attained results with the results of testing the same samples using standardized methods.

7. Since the deviations are minimal (viscosity: ± 3,57 %; TAN: 0,05 to 0,1 and TBN: ±5,56) it can be concluded that the KITTIWAKE device possesses a high degree of reliability and that it can be used for oil examination on the first level of examination

References

[1] Savić, V., Jocanović, M. (2004). Oil characteristics and diagnostics. Novi Sad: IKOS Novi Sad

[2] Jocanović, M., Karanović, V., Orošnjak, M. (2019). Tribologija i podmazivanje, 1st ed. Novi Sad: Faculty of Technical Sciences Novi Sad

[3] Jocanović, M., Karanović, V., Knežević, D., Orošnjak, M. (2015). Model for monitoring of the physical and chemical characteristics of the oil filling in hydraulic systems', in 12th International Conference on Accomplishments in Electrical and Mechanical Engineering - DEMI, pp. 1-6

[4] PARKER, Guide to Contamination Standards ISO Cleanliness Code. [Online]. Available: https://www.parker.com/Literature/EMHFF/ConMon/Guide to Contamination Standards.pdf. [Accessed: 15-Mar-2019]

[5] Parker Kittiwake. (2015). [Online]. Available: http://www.kittiwake.com/total-acid-number-drop-test. [Accessed: 10-May-2019]

[6] Wakiru, J. M., Pintelon, L., Karanović, V. V., Jocanović, M. T., Orošnjak, M. D. (2018). Analysis of lubrication oil towards maintenance grouping for multiple equipment using fuzzy cluster analysis', IOP Conf. Ser. Mater. Sci. Eng., vol. 393, no. 1

[7] Karanović, V. V, Jocanović, M. T., Wakiru, J. M., Orošnjak, M. D. (2018). Benefits of lubricant oil analysis for maintenance decision support: a case study', in IOP Conference Series: Materials Science and Engineering, 2018, vol. 393, no. 1, pp. 1-8

[8] NTC NIS-Naftagas d.o.o. Laboratory Department, Spoljno starčevačka 199, 26000 Pančevo, Serbia

[9] Laboratory of FAM-Kruševac, Mike Stojanovića 15, 37000 Kruševac, Serbia

University of Maribor Press

Eliminating Oil Mist from the Air

NIKOLA PETROVIĆ

Abstract While the gas, steam and hydro turbines and generators are in the operation, oil mist is being created in the air. Oil mist emission can bring serious consequences both for human and the machines, like health risks by inhalation, lack of work safety, lube oil loss in the system, fire hazard etc. This work represents the installation of oil mist separators for six vertical Kaplan turbines on Djerdap.

Keywords: • hydro plant • separators • oil mist • air • emission •

CORRESPONDENCE ADDRESS: Nikola Petrović, Hydac Hydraulic Gmbh-representative Niš, Serbia, e-mail: nikola.petrovic@hydac.rs.

1   Introduction

While the gas, steam and hydro turbines and generators are in the operation, oil mist is being created in the air. Oil mist emission can bring serious consequences both for human and the machines, like health risks by inhalation, lack of work safety, lube oil loss in the system, fire hazard etc.

Oil droplets are only the size 0.15 μm to 1.0 μm and they can escape through the seals of the bearings. To prevent that oil droplets, escape from the turbine bearings or the tank, it is necessary to filter the air from that area with oil mist separators.

Oil mist separators are important component of lubricating oil systems in turbines.

In Serbia, the first hydro power plant who had good experience with this kind of device was Serbian HPP Djerdap 1. The separator called STENO has been successfully connected to carrying bearing of the generator. It is interesting that the name of the device was inspired by nature. There are small black beetles that live in the desert and use their wings to separate water droplets from the desert air.

The Iron Gate I Hydroelectric Power Station is the largest dam on the Danube River and one of the largest hydro power plants in Europe. It is located on the Iron Gate gorge, between Romania and Serbia. It has 12 vertical Kaplan turbines (6 Serbian / 6 Romanian), with water throughput of approximately 750 m³/s per turbine, and overall electrical output approximately 2300 MW (Serbia + Romania). Serbian side of the power station produces approximately 5.65 TWh annually.

In December 2016 the manufacturer of STENO got the inquiry to install oil mist separators for six vertical Kaplan turbines on Djerdap. However, the flow rate of STENO was undefined, so it was agreed to use a STENO 300-S which has a maximum flow rate of 350 Nm³/h in standard configuration. To assure a volume flow of 450 m³/h, STENO has been equipped with a frequency converter. The engineers also agreed to support during the commissioning of STENO at the first turbine A1 and do measurements of the flow rate [1].

2 Installation of STENO at turbine A1

STENO has been connected only to the generator carrying bearing. One extraction connection is installed at the bearing. Another one is placed below the bearing. The location where STENO is installed can be seen in Figure 1.
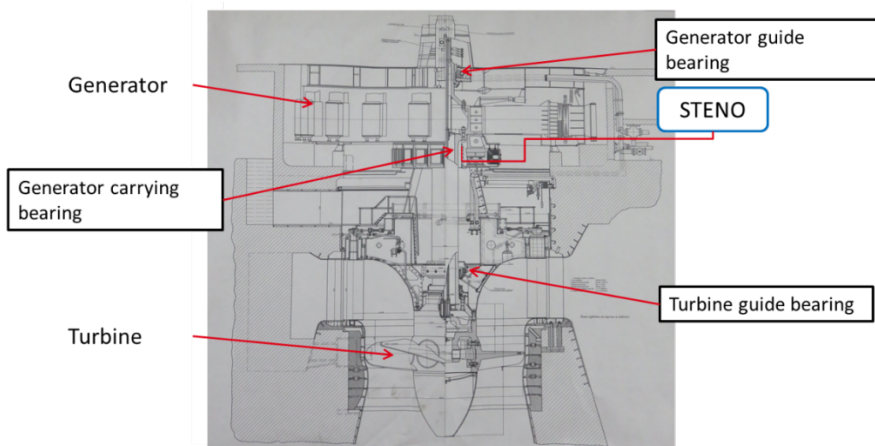
Figure 1: Drawing Turbine A1.
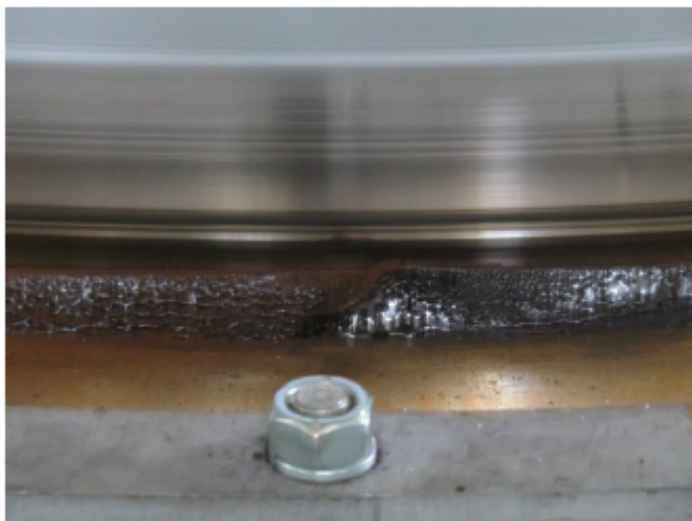
Figure 2: Seal of generator carrying bearing.

Since the maximum allowed vacuum pressure of seal (Figure 2) at the generator carrying bearing is 150 Pa (1, 5 mbar) a flow through the seal should be avoided. Dirt ingress is expected. To avoid this effect piping has been installed that a continuous flow through the bearing is reached. Therefore, two circuit ring pipes have been installed (Figure 3).
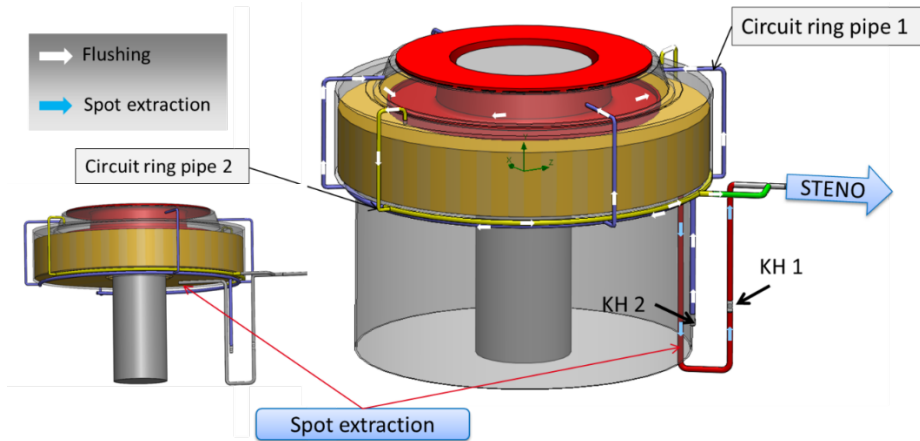
Figure 3: Piping connection to STENO.

Circuit ring pipe 2 (DN 80) is connected to the extraction pipe of STENO and at two points (DN 50) at the horizontal top surface of the bearing (Figure 4). Between the connection at the bearing and the maximum oil level is a distance of 150 mm. A view through the sight glass at the bearing showed that due to rotating effects the oil level at the border of the bearing is higher. Circuit ring pipe 1 is connected to the upper side of the bearing with four connections (DN 50).

The other end of circuit ring pipe 1 is connected to the environment. The flow through circuit ring pipe 1 can be adjusted with ball valve KH 2. Due to this arrangement a continuous flow from the environment through circuit ring pipe1, through the bearing, through circuit ring pipe 2 to STENO is reached (Figure 4). The bearing is continuously flushed with fresh air (white arrows).

Referred to Figure 4, there is no connection ("air connection") from the right side, where STENO is connected to, to the left side of the bearing. Therefore an extraction flow is reached only at the right side. To collect the oil mist which is produced on the left side of the bearing a spot extraction (DN 80) has been installed underneath the

bearing. The flow from the spot extraction (blue arrows) can be adjusted with ball valve KH1.
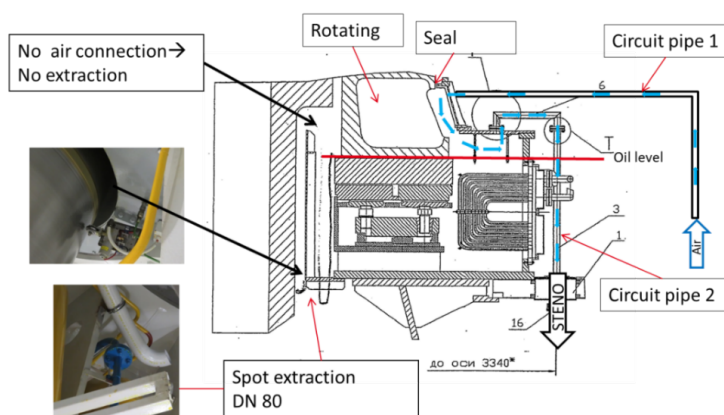
Figure 4: Schematic of flow in the bearing.

STENO has been installed at only one bearing instead of two bearings as discussed during the project planning phase.

Due to the fact that the sealing is very sensitive to vacuum pressure the connection at the bearing and to STENO has been done different as proposed.

After installing and checking the measurement equipment and setup several precise tests with different settings, the results of the tests showed that the oil is being condensed in the space between the generator carrying bearing and the turbine guide bearing, so it was necessary to connect the turbine guide bearing to STENO too.

Figure 5: Turbine guide bearing.

The final settings of STENO are shown in Table1.

Table 1: Final settings

Pressure before filter (pos. 11)	-5 mbar
Pressure at pos. 18	-2 mbar
Volume flow	≈200 m³/h
KH1	Open
KH2	Open

3   Proposal for turbine A2-A6

Based on the results of the measurements, the engineers proposed to use a STENO 300-S with a frequency converter. The capacity of this device is needed because of the recommended changes of piping and the possibility to connect the other bearings too.

3.1   Installation of piping / STENO

In the following chapters recommendations are stated to improve the systematic for oil mist collection. Regarding the condensed oil in the suction pipe to STENO it is not possible to avoid the condensation effects. The proposed changes will reduce this effect but not avoiding it. In addition, condensed oil in the room between generator carrying bearing and turbine guide bearing can be reduced but not avoided.

3.2   Changing flow direction through bearing

Because of the small distance between the current suction connection and the adjusted oil level due to rotating effects, the engineers proposed to change the flow direction through the bearing.
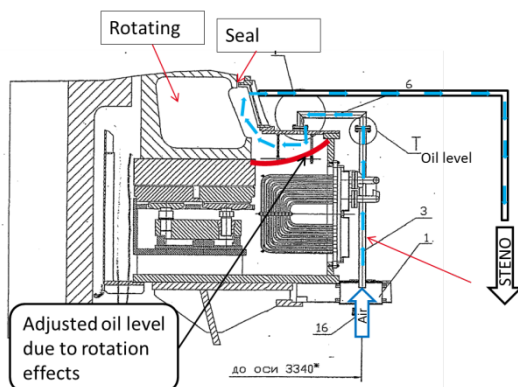
Figure 7: Modified flow direction in bearing.

3.3 Changing of the spot extraction

The efficiency of the spot extraction below the generator carrying bearing is assumed as low. To improve the efficiency, it is necessary to collect the produced oil mist on the left side of the bearing. In addition, close (seal) the gap between shaft and bearing housing (if possible) or decrease it. At least four extraction points distributed on the circumference are necessary. According to Figure 8, two possibilities for implementation are available. Possibility 1 represents a circuit ring pipe with four vertical pipes. With that solution it is possible to adjust the flow from the left side of the bearing. Possibility 2 is pipes which are installed in the bearing and connect the left air side with the right air side. No adjustment of the flow possible.
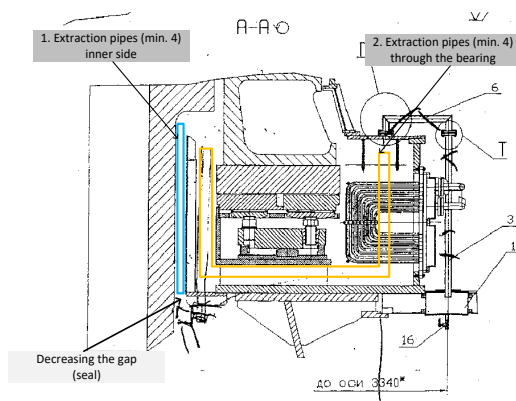
Figure 8: Changing spot extraction.
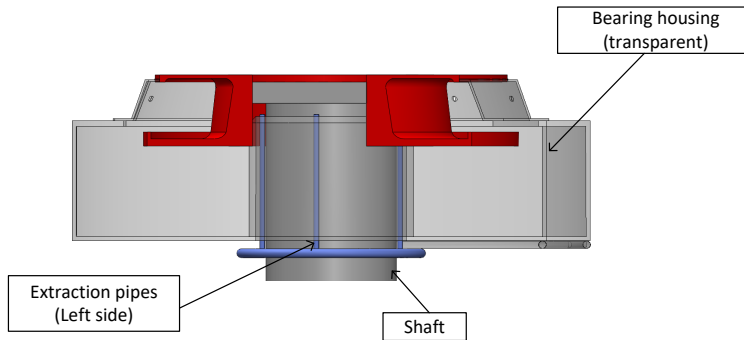
Figure 9: Circuit ring pipe inner side.

3.4 Air for flushing the bearing (optional)

The air for flushing the bearing is unfiltered now. To avoid dirt ingressions, it is possible to install breather filters or breather dryers. Two possibilities are shown in Figure 11: A and B. Position A would be at the end of the vertical pipes of circuit ring pipe 2. Position B would be at the top of the bearing with a maximum distance to the oil level.

3.5 Flow adjustment / adjustment of vacuum pressure for every suction point

To adjust the vacuum pressure, respectively the volume flow for every suction point / suction area it is necessary to have a ball valve on a pressure gauge for every junction as shown in Figure 11.

3.6 Pressure measuring / Pressure measuring at the bearing

The scale range of the installed pressure gauges is too great. Pressure gauges with a finer scale range e.g. 0 to -40 mbar shall be used.

In addition, for measuring the vacuum pressure in the bearing it would be advantageous to have a measuring connection at the bearing. An example is shown in Figure 10.
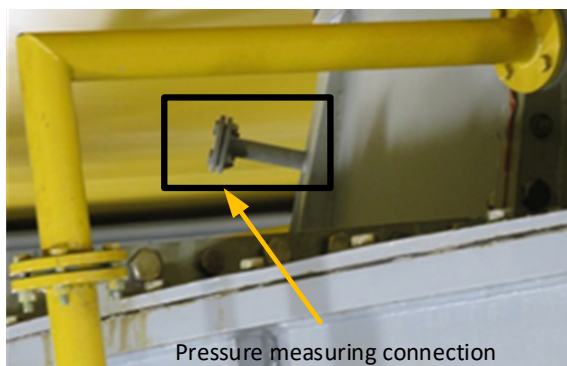
Figure 10: Pressure measuring connection at bearing (example).

3.7 Connection of turbine guide bearing (optional)

To decrease the oil condensation in the room between generator carrying bearing and turbine guide bearing it will be advantageous to connect the turbine guide bearing to STENO too.
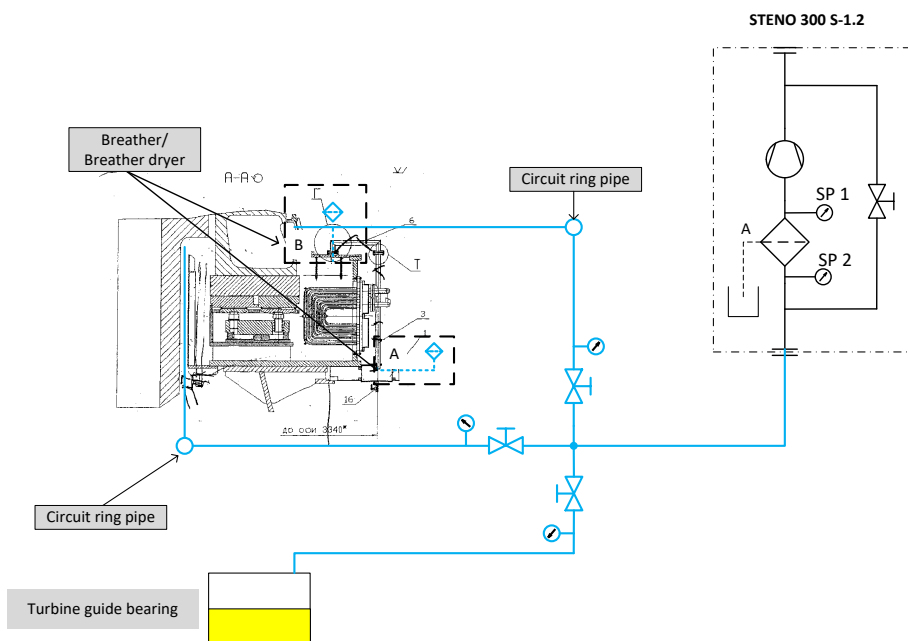
Figure 11: Schematic for changes of piping.

4   Conclusion

After the installation of STENO, the employees from the power plant are satisfied with the results. They used to clean the space around the bearing every 3-4 days, now they do this twice per month. The air is cleaner, with no dangerous oil droplets that have been inhaled before. This year, the HPP Djerdap made an offer for five more STENO devices and agreed to make some changes as being suggested by our engineers. Also, there are negotiations underway with the Romanian side of the hydropower plant.

Using devices for oil mist separation it is possible for over 99 % of the relevant oil droplets to be separated. This makes it possible to reduce the residual oil content to less than 10 mg/m³, even for high oil mist concentrations. This is due to mist separators performs two jobs - preventing oil mist from escaping and separating and recovering the lubricating oil.

References

[1]   N. N. Internal documentation of STENO

University of Maribor Press

Leakage Minimization in a Fuel Company

SANDI BABIČ & UROŠ OVEN

Abstract At a large fuel company, emerged the requirement to reduce the media loss due to leakage downstream. The root of the problem was in the valve operating range. Due to the value of the medium the scale of the problem was considered high and thus a replacement was required. Technicians and engineers are well aware of leakage problems but in the real world they tend to push them aside due to other concerns that may be bigger and because the effort tends to overweight the gain. Meaning too much work or thought is rarely spent in leakage. But with high medium value this gets easily reconsidered. An example on how the operating costs can eclipse the wrong valve choice and which valve was used to negate the leakage problem is presented in this paper. Explanation is also given, why a coaxial valve is a better choice in this example.

Keywords: • leakage • pressurized air • cost reduction • valves • liquid petrol gas •

_____
CORRESPONDENCE ADDRESS: Sandi Babič, TU-VAL d.o.o., Domžale, Slovenia, e-mail: sandi.babic@tu-val.si. Uroš Oven, TU-VAL d.o.o., Domžale, Slovenia, e-mail: uros.oven@tu-val.si.

1   Introduction

Generally, it is hard to convince someone, how important it is to consider the loss of the medium when designing a fluid system. This goes especially for compressed air. As soon as we start talking about higher value media, companies start to consider it more and more. But even with the considerate, some facts may escape the mind. For example, leakage downstream. Meaning when the medium leaks through the valve to the next department, even though the valve is closed.

A case of leakage downstream, presented a problem to our customer. A company working with Liquid Petrol Gas (LPG) needed to close of multiple compartments with similar or negligible pressure differences. Due to the required nominal pipe size, abbreviated DN which stands for "Diametre Nominal", and the high pressure-norm (PN), the customer decided to use pilot operated piston valves. The results did not satisfy though. The problem with pilot operated valves is that they require certain pressure difference to start functioning, meaning the valves were unsuitable for the application.

In this contribution we would like to present, how we reached an estimation of the media loss through the leakage, what we offered as a replacement and why we considered the replacement as the best choice.

2   Considerations and calculations

2.1   Valve as study sample

First a diaphragm valve was used in our case study. The differences were considered minimal and more conservative, which is the reason why we did not make a decision to invest into pilot operated piston valves.

Measured and estimated values of the used PN16, DN10 valve, are as following:

- – Diameter of the entry: 19 mm,
- – Diameter of the exit: 14 mm,

- Surface of chamber 1 (Figure 1) exit section: Limited by 2 diameters. Inner diameter of 14 mm and outer diameter of 27,5 mm, giving a surface area of about 440 mm²,
- Surface of chamber 2 effective section: about 640 mm²,
- Spring tension: about 90 g force per 1 mm compression,
- Pressure at the entry and exit of the valve can vary a lot (generally about 5 bar pressure, but may go up to 18 bar), but what we were truly interested in was the pressure difference between them. And even here, we are mostly interested in the range where the valve is not guaranteed to work properly. This being known as about 0,5 bar.
- Density of LPG: about 900 kg/m³,
- Area of leakage was determined by the diameter of the diameter, where the diaphragm covers the exit (being 12 mm) multiplied by the gap emerging through the flow at max 0,5 bar. This was measured as up to 0,24mm. Result being 27 mm².

2.2 Operation of the valve

At the normal operation of the valve, it undergoes the following steps [3]. The fluid enters at the chamber 1 (Figure 1).
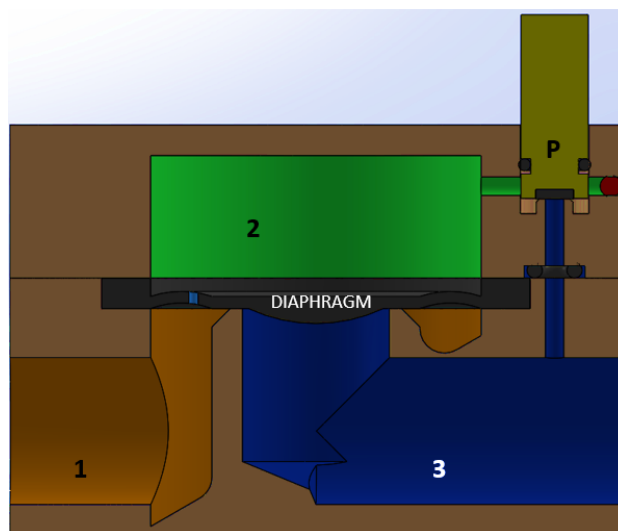
Figure 1: Design of a pilot operated diaphragm valve, presented chambers 1, 2 and 3.

As soon as the pressure rises to the minimum required working pressure, in both chambers, 1 and 2, the force from the upper side of the diaphragm exceeds the force from bellow. To open the valve, the plunger (P) needs to be pulled upwards with the help of an electromagnetic coil. As soon as this happens, the medium leaks through the newly formed orifice into chamber 3. This causes the force on the upper side of the diaphragm to decrease and bellow to increase, moving the diaphragm upwards.

Note, that during these phases minor leaks can already occur on the valve. For example, at the start, before the chamber 2 fills up with the medium, the force, bellow the diaphragm is higher than above, letting some of the medium escape through.

If the pressure difference is not above the required minimum, the diaphragm will not properly seal off chamber 3, allowing the medium to creep through. And to the contrary, if opened, there will not be enough differential pressure to push the diaphragm upwards and fully open the flow.

2.3   Calculations

The calculations were done as following. First the resistance of the spring and the differentials pressures that may emerge was compared. Our conclusion was that the tension of the spring is negligible. It just holds the diaphragm in place.

Bernoulli's equation was taken for the rough measurement of the diaphragm movement and went directly to the flow measurement [1].

$$p_1 + \frac{1}{2}\rho v_1^2 + \rho g h_1 = p_2 + \frac{1}{2}\rho v_2^2 + \rho g h_2 \tag{1}$$

Here we took out the potential energies as they are negligible in our case and joined p_1 and p_2 into Δp, as this is an information that we do have. We used another equation to consider the velocity of the fluid at entry. The volume flow rate equals the following:

$$R_v = a_1 v_1 = a_2 v_2, \tag{2}$$

which solves for:

$$v_1 = \frac{a_2}{a_1} v_2, \tag{3}$$

Considering that the area in the valve entry (a_1) is much larger than the leakage area (a_2) we can also neglect the entry velocity. Leaving us with the following equation:

$$\Delta p = \frac{1}{2}\rho v_2^2 \tag{4}$$

Solving for velocity we get the equation used:

$$v_2 = \sqrt{\frac{2\Delta p}{\rho}} \tag{5}$$

To get the volumetric flow we the surface of the leakage area:

$$R_v = a_2 v_2 \tag{6}$$

Inserting the values from section 2.1 we get a velocity of 10 m/s at the 0,5 bar differential pressure. This gives us a volumetric flow of 9×10^{-6} m³/s. The price of LPG in Slovenia was taken from a source [2], stating to be 0,64 USD/l or 0,576 EUR/l. This gives us a loss at $5,2\times10^{-3}$ EUR/s or as a more useful result 0,32 EUR/min. If this would leak for a full day at the calculated rate, the company would have a loss of 460 EUR daily. This is the worst-case scenario which is not expected to happen. Mostly because the pressure differentials would diminish over a much shorter time and then there is the time where the valves operate as normal. But we do get a good estimate with what we are dealing, when using this type of valves.

3   The alternative

3.1   Choosing the valve type

As an alternative we needed to take a valve that can operate at pressure ranges up to 18 bar, differential pressure needs to be without a low limit and the amount transferred needs to be relatively large, namely DN10. A majority of electrically operated valves gets here out of the question. Leaving us with either actuator operated valves or with coaxial valves. The bulkiness of the actuator operated valves did not bother the customer, but since the actuator operated valves require another medium to operate, being compressed air, the customer preferred the latter.

3.2   Coaxial valves

The coaxial valves benefit from the fact that they are pressure balanced [4]. The central pipe, moving back and forth in the valve hits the sealing in a way, that the fluid may reach the full frontal and rear face at all times. This makes the resistance to movement, emerging from pressure on both faces negligible. With this, close to zero, resistance we can operate the movement of the pipe, being actually a large modified plunger, with common power used on the coil. An additional benefit to this is the fact that the valve needs not to be so bulky. But again, this was not a deciding factor with this particular customer.

3.3   Long term gain - considerations

Due to the lack of certain information, like volumes of the compartments or flow from the downstream compartments, and due to high variables, like the actual pressures, it is nigh impossible to determine what the actual gain is in terms of saves. But when we consider the options that the customer wants or needs, we get down to these 2 valve types and as we can say that there is no notable leakage on the coaxial valves, it was the only other option to present to the customer.

4   Results

All we can present as a result at this point is a satisfied customer, who plans to use the same valve for future applications. But we also got a confirmation that the loss, which the customer was able to measure as it is just a "before and after" analysis, was reduced to pay for the alternative in a few weeks. Meaning that our considerations and calculations were accurate enough.

Table 1: The equation 6 with additional parameters. Gap is in mm², Δp is in bar and the results are in mm³/s

Δp\Gap	0.04	0.08	0.12	0.16	0.20	0.24
0.05	0.50	1.01	1.51	2.01	2.51	3.02
0.10	0.71	1.42	2.13	2.84	3.55	4.27
0.20	1.01	2.01	3.02	4.02	5.03	6.03
0.30	1.23	2.46	3.69	4.92	6.16	7.39
0.40	1.42	2.84	4.27	5.69	7.11	8.53
0.50	1.59	3.18	4.77	6.36	7.95	9.54

Figure 2: Coaxial valve MK10 in application.

Acknowledgments

References

[1]   Halliday, R., Resnick, R., Walker, J. (2010). Principles of Physics Extended, 9th edition international student version, ISBN: ES8-0-470-56158-4

[2]   GlobalPetrolPrices.com (2019). LPG prices, liter, 02-Sep-2019; Retrieved from https://www.globalpetrolprices.com/lpg_prices/

[3]   XHnotion Pneumatics. (2018). A Definitive Guide to Choose a Right Solenoid Valve (2018 update: include animation video and infographics); Retrieved from https://xpneumatic.com/blog/a-coverall-guide-to-choose-a-right-solenoid-valve/

[4]   Müller co-ax a.g. (V08/04-2016_e). Catalogue: Coax leading valve technology™

Conference sponsors

General sponsor
FESTO d.o.o.

Social event sponsor:
HAWE hidravlika d.o.o.

Conference organization has been sponsored by:

HYDAC d.o.o.

POCLAIN Hydraulics d.o.o.

OLMA d.o.o.

BECKHOFF Avtomatizacija d.o.o.

TESNILA Bogadi d.o.o.

PARKER Hannifin CEE s.r.o.

EXOR ETI d.o.o.

AS Teh d.o.o.

TID – Tinex industrijska diagnostika d.o.o.

TU-VAL d.o.o.

Media sponsors:

VENTIL   **UM Press**   **IRT3000**

We would like to thank all the sponsors for their support and contribution to the organization of the conference!

The right partner
for compact & efficient
hydraulic solutions.
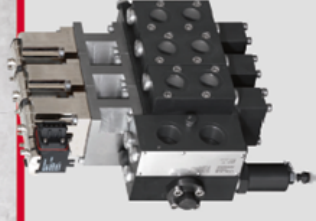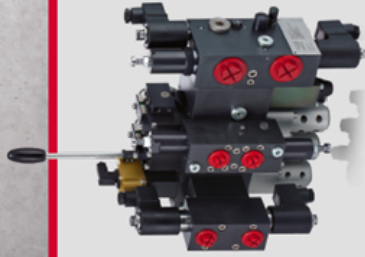
Solutions for a World under Pressure

HYDRAULIK

Izboljšan oprijem za večjo produktivnost in udobje

Enhanced traction for higher productivity and comfort

Ventil Addiflow
Omogoča zagon, izklop in prosti tek motorjev MF

AddiFlow control block
Manage MF motors engagement, disengagement and freewheeling sequences

Krmilnik SD-CT
Izvaja komunikacijo in krmiljenje funkcij

SD-CT ECU
Manage communication and extended functions

Črpalka PW
Poganja jo PTO motorja tovornjaka in zagotavlja hidravlično energijo za pogon sprednjih koles.

PW Pump
Driven by engine PTO; provide hydraulic power to the front motors
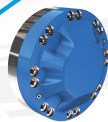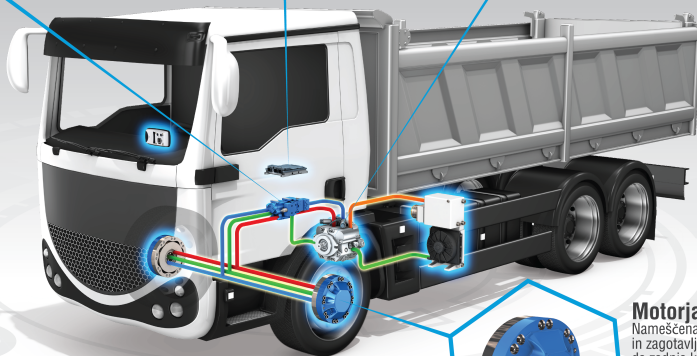
Motorja MF
Nameščena sta v sprednjih kolesih in zagotavljata pogon v primeru da zadnja kolesa zdrsnejo.

MF Motors
Located in the front wheels, they provide traction effort in case of loss of adherence in the rear axle

POCLAIN
Hydraulics

S pravim mazivom
ne spodrsava

Olma d.o.o., Poljska pot 2, 1000 Ljubljana,
tel.: (01) 58 73 600, e-pošta: komerciala@olma.si

OLMA
www.olma.si

Samo **ekonomsko** upravičeni, **tehnološko** zreli in **okolju prijazni** koncepti, so **resnično vzdržni**.

Zanesljivo, enostavno, učinkovito rešujemo vaše izzive

pritrdilna tehnika | industrijska pnevmatika | varjenje | rezkanje in struženje strojnih delov | meritve in lasersko graviranje

VENTILI

MÜLLER CO-AX AG že od leta 1960 predstavlja inovativnost, individualnost, zaupanje, kakovost, izkušnje in zanesljivost v tehnologiji izdelave ventilov.

Ventili so posebej primerni za uporabo v okolju,
kjer je prisotno veliko nečistoč (opilki,…).
Do **10x daljša življenjska doba**
kot pri običajnih ventilih.
Pretok možen v obe smeri.
Med **najhitrejšimi ventili na svetu**:
hitre, ponovljive operacije v manj kot 30 ms.

V naši ponudbi najdete tudi

Reducirne ventile	Varilne aparate	Avtomatizacijo	Cilindre

MMA
MAXITECH EVO 505

Vakuum

TU-VAL d.o.o., Breznikova ulica 26, 1230 Domžale, Slovenija
Telefon: +386 1 721 21 23, F: +386 1 721 27 46, E: tu-val@siol.net, www.tu-val.si

- Strokovni in znanstveni prispevki
- Iz prakse za prakso
- Ventil na obisku
- Novice - zanimivosti
- Aktualno iz industrije
- Novosti na trgu
- Podjetja predstavljajo
- Ali ste vedeli
- Dogodki

Spoštovani!

Ventil je znanstveno-strokovna revija in objavlja prispevke, ki obravnavajo razvojno in raziskovalno delo na Univerzi, inštitutih in v podjetjih s področja fluidne tehnike, avtomatizacije in mehat-ronike. Revija želi seznanjati strokovnjake z dosežki slovenskih podjetij, o njihovih izdelkih in dogodkih, ki so povezani z razvojem in s proizvodnjo na področjih, ki jih revija obravnava. Prav tako želi ustvariti povezavo med slovensko industrijo in razvojno in raziskovalno sfero ter med slovenskim in svetovnim proizvodnim, razvojnim in strokovnim prostorom. Naloga revije je tudi populari-zacija področij fluidne tehnike, avtomatizacije in mehatronike še posebno med mladimi. Skrbi tudi za strokovno izrazoslovje na omenjenih področjih.

Revija Ventil objavlja prispevke avtorjev iz Slovenije in iz tujine, v slovenskem in angleškem jeziku. Prispevkom v slovenskem jeziku je dodan povzetek v angleščini, prispevki v angleščini pa so objavljeni z daljšim povzetkom v slovenskem jeziku. Člani znanstveno strokovnega sveta so znanstveniki in strokovnjaki iz Slovenije in tujine. Revijo pošiljamo na več naslovov v tujini in imamo izmenjavo z drugimi revijami v Evropi. Revija je vodena v podatkovni bazi INSPEC.

Štiriindvajsetletno izhajanje revije Ventil pomeni, da je v prostoru neprecenljiva za razvoj stroke. Uredništvo si skupaj z znanstveno strokovnim svetom prizadeva za visokokvalitetno raven in relevan-tnost objav, ki bosta v prihodnosti vse napore usmerila v to, da bo kvalitetna raven še višja. V ta namen vključuje v znantveno stro-kovni svet priznane znanstvenike, raziskovalce in strokovnjake, ki s svojim znanjem vspodbujajo vsak na svojem področju objavljanje rezultatov razvojnega in raziskovalnega dela. Uredništvo spremlja razvoj stroke in znanstveno raziskovalno delo doma in vtujini preko konferenc, delavnic in seminarjev ter z izmenjavo tuje periodike.

Revija je priznana v tujini, še posebno na področju fluidne tehnike, kar želimo doseči tudi na področju mehatronike in avtomatizacije. Preko objav v reviji se promovirajo dosežki slovenske znanosti in industrijske proizvodnje. Revija je in bo tudi v prihodnje prostor za predstavljanje kvalitetnih razvojnih in raziskovalnih dosežkov slovenske industrije in raziskovalne sfere na področju fluidne tehnike, avtomatizacije in mehatronike.

Uredništvo

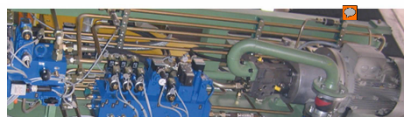University of Maribor Press

http://press.um.si/

University of Maribor Press

FIZIKALNO OZADJE
DELOVANJA HIDRAVLICNIH
SISTEMOV

DARKO LOVREC

UVOD V HIDRAVLIČNO
POGONSKO-KRMILNO
TEHNIKO

DARKO LOVREC

HIDRAVLIKA ZA
MEHATRONIKE

DARKO LOVREC

open
Open Access
Publishing in European Networks

doab
directory of
open access
books

Digitalna
Knjižnica
Univerze v
Mariboru
Univerza v Mariboru

dLib
DIGITALNA
KNJIŽNICA
SLOVENIJE

Clarivate
Analytics

http://press.um.si/

University of Maribor

Faculty of Mechanical Engineering

FT2019